Universidad de Concepción
Dirección de Postgrado
Facultad de Ciencias Físicas y Matemáticas
Programa de Doctoraro en Ciencias Aplicadas con mención en Ingeniería Matemática

Métodos de elementos virtuales para problemas Espectrales

Virtual element method for Spectral problem

Tesis para optar al grado de
Doctor en Ciencias Aplicadas con mención en Ingeniería Matemática

Gonzalo Alejandro Rivera Acuña
Concepción–Chile, Septiembre 2016

Virtual element method for Spectral problem

Gonzalo Rivera Acuña

Directores de Tesis: Prof. Rodolfo Rodríguez, Universidad de Concepción, Chile.
Prof. David Mora, Universidad del Bío-Bío, Chile.
Prof. Lourenço Beirão da Veiga, Università di Milano-Bicocca, Italy.

Director de Programa: Prof. Raimund Bürger, Universidad de Concepción, Chile

COMISIÓN EVALUADORA

Prof. Daniele Boffi, Università degli studi di Pavia, Italy
Prof. Richard S. Falk, Rutgers, The State University Of New Jersey, E.E.U.U.
Prof. Salim Meddahi, Universidad de Oviedo, España.
Prof. Pedro Morin, Universidad Nacional del Litoral, Argentina.

COMISIÓN EXAMINADORA

Firma: _____
Prof. Erwin Hernández, Universidad Técnica Federico Santa Maria, Chile.

Firma: _____
Prof. David Mora, Universidad del Bío-Bío, Chile.

Firma: _____
Prof. Pedro Morin, Universidad Nacional del Litoral, Argentina.

Firma: _____
Prof. Rodolfo Rodríguez, Universidad de Concepción, Chile.

Firma: _____
Prof. Pablo Venegas, Universidad del Bío-Bío, Chile.

Fecha Examen de Grado: _____

Calificación: _____

Concepción–Septiembre de 2016

Agradecimientos

Quisiera comenzar agradeciendo a mi director de tesis, Rodolfo Rodríguez, por su constante apoyo y confianza en mi trabajo, su paciencia y buena disposición para guiar mis ideas. Gran parte de mi formación académica que he logrado ha sido, sin duda, gracias al respaldo de Rodolfo.

A mi Codirector David Mora por aceptarme para realizar esta tesis doctoral bajo su dirección, por el continuo apoyo y consejos que me entrego, por su paciencia, disponibilidad y generosidad para compartir su experiencias, por su buena onda y ganas de trabajar.

A mi Codirector Lourenço Beirão da Veiga, por su importante aporte y participación activa en el desarrollo de esta tesis, pese a la distancia, por su hospitalidad, tiempo y paciencia de responder mis dudas y guiarme, en las dos estadías que hice en el Departamento de Matemática de la Universidad de Pavia, Italia,.

También agradezco a mis padres Jacqueline y Enrique, quienes siempre me brindaron su apoyo y a quienes les debo lo que soy. A mis hermanos Nataly y Gabriel por acompañarme y animarme cada vez que los necesite. En especial quiero agradecer a mi *tata* Raúl por enseñarme con el ejemplo que se puede ser un excelente abuelo, padre y esposo, gracias por inspirarnos a ser mejores personas, todos en la familia te amamos y respetamos.

A todos y cada uno de los profesores del Programa que me brindaron su tiempo y conocimiento, en especial al Director del Programa de Doctorado, Profesor Raimund Burger.

A mis compañeros del doctorado "clásicos " y "no-clásicos" a quienes les tengo un cariño muy grande, en especial a mi amigo Elvis, por enseñarme a ser más "empático" y a mi amiga Cinthya quien me soportó durante todo el doctorado, por tu infinita paciencia, buenos consejos y simpatía.

Quisiera agradecer al Centro de Investigación en Ingeniería Matemática CI^2MA, el cual me facilito sus instalaciones y recursos para trabajar adecuadamente durante mis estudios doctorales. A su Director, Profesor Gabriel Gatica y al personal del centro, por la hospitalidad y el trato cordial y afectuoso.

Agradezco también a las diferentes fuentes de financiamiento de este trabajo: CONICYT, Red Doctoral en Ciencias, Tecnología y Medio Ambiente de la Universidad de Concepción y a Becas Chile.

Resumen

El objetivo principal de esta tesis doctoral es el análisis matemático y numérico de la aplicación de los métodos de elementos virtuales en mallas con polígonos generales, a la solución de diversos problemas de valores propios y de flexión de placas moderadamente gruesas, con el propósito de obtener contribuciones originales y enriquecer el conocimiento existente en el área de los métodos de elementos virtuales. En particular se consideran el problema de valores propios de Steklov y el de vibraciones acústicas. En el primer caso también se propone un estimador a posteriori del error y un proceso adaptativo basado en este estimador.

Por otra parte, en esta tesis, también se propone y estudia un método de elementos virtuales para resolver el problema de flexión de placas modeladas por las ecuaciones de Reissner-Mindlin. En particular se propone un método de elementos virtuales para una formulación escrita en términos de las variables de la deformación de corte y la deflexión y se demuestra que no sufre de bloqueo.

En lo que se refiere al problema de valores propios de Steklov, el estudio se centra en la desarrollar un método de elementos virtuales apropiado para el estudio de la aproximación numérica de los autovalores del problema.

Para llevar a cabo este análisis, se propuso una discretización por medio de los elementos virtuales que se presentan en [L. Beirão da Veiga, *et al.*, Basic principles of virtual element methods, Models Methods Appl. Sci. 23 (2013) 199-214]. Bajo suposiciones estándar en el dominio computacional, se establece que el esquema resultante proporciona una aproximación correcta del espectro, y se demuestra que las estimaciones del error son de orden óptimo para las funciones propias y los valores propios. Adicionalmente, en esta primera parte, se demuestran estimaciones de un mejor orden para el cálculo del error de aproximación de las funciones propias en la frontera libre, que en algunos problemas de Steklov (por ejemplo, el calculo de los modos de "sloshing") son una cantidad de gran interés. Todas las estimaciones obtenidas en el análisis teórico, son corroboradas mediante ejemplos numéricos.

En la segunda parte se propone y desarrolla el análisis matemático y numérico de un estimador de error a posteriori del tipo residual para la aproximación por elementos virtuales del problema de valores propios de Steklov en dos dimensiones, aplicado a mallas poligonales muy generales. Dado que, los flujos normales de la solución virtual presentada en la primera parte no se pueden calcular explícitamente, estos son reemplazados por una proyección adecuada de ellos. Como consecuencia de esta sustitución, aparecen nuevos términos adicionales en el estimador, que representan la "inconsistencia virtual" de los métodos de elementos virtuales. De este modo

se obtiene un estimador del error a posteriori de tipo residual, que es totalmente calculable, ya que depende únicamente de las cantidades disponibles a partir de la solución virtual (sus grados de libertad y su proyección elíptica, local, sobre los polinomios), se establece que el estimador es equivalente al error salvo términos de orden superior. Finalmente, el estimador del error se utiliza para guiar el refinamiento de mallas adaptativas en una serie de problemas test, con diferentes regularidades de la solución exacta.

En la tercera parte de esta tesis se aborda el análisis matemático y numérico de la aproximación por elementos virtuales, para el problema de vibraciones acústicas. Para ello, se considera una formulación variacional del problema espectral en términos del desplazamiento del fluido. Inspirados en [*L. Beirão da Veiga, F. Brezzi, L. D. Marini and A. Russo*, Mixed virtual element methods for general second order elliptic problems on polygonal meshes, ESAIM Math. Model. Numer. Anal.(2016)], se propone una discretización virtual de $H(\mathrm{div})$ con rotor nulo. Bajo suposiciones estándar del dominio, se establece que el esquema resultante proporciona una aproximación correcta del espectro y se prueba que las estimaciones del error son óptimas para las funciones propias y los valores propios. Con este fin, se demuestran propiedades de aproximación para los elementos virtuales propuestos. Por último se presentan experimentos numéricos que corroboran los resultados teóricos obtenidos.

Finalmente, se estudia un método de elementos virtuales para el problema de deflexión de placas de Reissner-Mindlin. Con este objetivo, se comienza con una formulación variacional del problema escrito en términos de las variables de deformación de corte y deflexión, presentádos en [L. Beirão da Veiga, *et al.*, A locking-free model for Reissner-Mindlin plates: analysis and isogeometric implementation via NURBS and triangular NURPS, Models Methods Appl. Sci. 25(8) (2015) 1519–1551]. Se propone una formulación discreta conforme en $[H^1(\Omega)]^2 \times H^2(\Omega)$ para la deformación de corte y deflexión, respectivamente. Una característica distintiva de este enfoque es la aproximación directa de la deformación de corte. Por otra parte, las rotaciones se obtienen con un simple tratamiento de post-proceso de la deformación de corte y deflexión. Se prueba que las estimaciones del error son óptimas para todas las variables involucradas (en las normas naturales de la formulación adoptada), con constantes independientes del espesor de la placa. Por último, se presenta experimentos numéricos que permiten evaluar el desempeño del método, mostrando que es convergente y libre de bloqueo como lo predice la teoría.

Abstract

The main objective of this doctoral thesis is the mathematical and numerical analysis of the application of virtual element methods in general polygonal meshes to solve diverse eigenvalue problems and bending of moderately thick plates, with the aim of making an original contribution and enriching our understanding of virtual element methods. In particular, the Steklov eigenvalue and acoustic vibration problems are considered. In the first case an a posteriori error estimator and an adaptive process based on the estimator are proposed.

The thesis also proposes and explores a virtual element method to solve the problem of plate bending modeled by Reissner-Mindlin equations. In particular, a virtual element method is proposed for a formulation written in terms of shear strain and deflection variables, we shown that it does not suffer from locking. In relation to the Steklov eigenvalue problem, the study is focused on developing a virtual element method appropriate for the study of the numerical approximation of the eigenvalues of the problem.

Discretization by virtual elements, as presented in [L. Beirão da Veiga *et al.*, Basic principles of virtual element methods, Math. Models Methods Appl. Sci., 23 (2013), pp. 199–214] is proposed to carry out this analysis. Under the standard assumptions on the computational domain, the resulting scheme provides a correct approximation of the spectrum and the error estimations are of optimal order for the eigenfunctions and eigenvalues. Better order estimations are also shown for calculating the eigenfunctions errors in the free boundary, which with some Steklov problems (for example, calculation of sloshing modes) are a quantity of great interest (the free surface of a fluid). All the estimations obtained in the theoretical analysis are corroborated with numerical examples.

The second part of the thesis proposes and develops the mathematical and numerical analysis by virtual elements of a residual-type a posteriori error estimator to approximate the Steklov eigenvalue problem in two dimensions. Given that normal fluxes of the virtual solution presented in the first part cannot be calculated explicitly, they are replaced with an appropriate projection, As a consequence of this substitution, new terms appear in the estimator that represent the virtual inconsistency of the virtual element methods. In this way a residual-type a posteriori error estimator is obtained that is completely computable, given that it depends solely on quantities available based on the virtual solution. It is established that the estimator is equivalent to the error except for higher-order terms. Finally, the error estimator is used to guide the refinement of adaptive meshes in a series of test problems with different regularities of the exact solution.

The third part of the thesis addresses the mathematical and numerical analysis of the ap-

proximation by virtual elements of the acoustic vibration problem. A variational formulation of the spectral problem in terms of fluid displacements is considered. Based on [L. Beirão da Veiga *et al.*, Mixed virtual element methods for general second order elliptic problems on polygonal meshes, ESAIM Math. Model. Numer. Anal., DOI: http://dx.doi.org/10.1051/m2an/2015067 (2016)], virtual discretization of $H(\mathrm{div})$ with a null rotor is proposed. Under standard assumptions of the domain, the resulting scheme provides a correct approximation of the spectrum and the error estimations are optimal for the eigenfunctions and eigenvalues. With this end, we prove approximation properties of the proposed virtual element method. Finally, numerical experiments are presented to corroborate the theoretical results obtained.

Finally, a virtual element method is studied for the Reissner-Mindlin plate bending problem, beginning with a variational formulation written in terms of shear strain and deflection variables. A conforming discrete formulation is proposed in $[H^1(\Omega)]^2$ and $H^2(\Omega)$ for shear strain and deflection, respectively. A distinct characteristic of this approach is the direct approximation of shear strain. The rotations are obtained with a simple post-process treatment from shear strains and deflections. The estimation errors prove to be optimal for all the variables involved (in the natural norms of the adopted formulation), with constants independent of the thickness of the plate. Finally, numerical experiments are presented to evaluate the performance of the method, showing that it is convergent and locking-free as the theory predicts.

Tabla de Contenidos

Índice de Tablas

Índice de figuras

Capítulo 1

Introducción

1.1. Método de elementos virtuales

Las diferencias finitas miméticas (MFD) y en particular su marco matemático y esquemas, han ido evolucionando desde las diferencia finitas/volúmenes finitos, hacia un análisis más parecido al de elementos finitos. En su última presentación se podrían considerar como una forma de aproximación por los métodos de elementos finitos (FEM) en el que sólo se usan los grados de libertad (ya que las funciones de prueba no están disponibles en el interior de los elementos). Esto, sin embargo, permite que imiten (junto con varias leyes físicas fundamentales), la mayoría de los espacios de elementos finitos de distintos tipo de orden más bajo (desde los polinomios a trozos y continuos estándar, hasta los más sofisticados utilizados para formulaciones mixtas) en elementos con geometrías más generales (véase, por ejemplo, [62, 17, 53, 16, 52] y las referencias del último).

En los últimos años se han hecho algunos intentos para introducir MFD de orden superior, haciendo uso de grados de libertad más generales, tales como momentos en las caras, aristas y elementos (ver [32, 88, 27, 28]). Sin embargo, debido a la no existencia de funciones de prueba dentro de los elementos (o incluso dentro de las caras) la presentación de estos resultaba ser muy incómoda. Por lo tanto, se hizo evidente que el método sería más claro si los grados de libertad (incógnitas típicas para MFD) se unieran a las funciones de prueba dentro de los elementos, aunque estas funciones no necesariamente sean polinomios. Así, nacen los métodos de elementos virtuales (VEM) el cual toma las principales ideas de los esquemas miméticos modernos, pero sigue una discretización de Galerkin del problema y por lo tanto se puede interpretar plenamente como una generalización del método de elementos finitos (FEM) en polígonos, tales como los métodos de elementos finitos poligonales (PFEM, véase, por ejemplo, [109, 111]) o los FEM extendidos (ver [82] y sus referencias). Sin embargo, a diferencia de los métodos mencionados anteriormente, VEM intenta ser un método más sencillo, que preserva la capacidad de reproducir varias leyes físicas con exactitud (como MFD) y hacer frente a geometrías más complicadas (polígonos/poliedros). Al mismo tiempo, comparte las ventajas de las formulaciones de elementos finitos y la exactitud polinomial que se obtiene en los simplex, mientras se trabaja en los polígonos/poliedros.

Los métodos de elementos virtuales se introducen por primera ves en [18] para la ecuación de Laplace en $2D$ y en ella se presentan las ideas centrales del método las cuales se pueden resumir en:

- Los espacios locales están diseñados para contener polinomios de grado $\leq k$ (como en los elementos finitos clásicos). Lo que, en última instancia, es responsable de la exactitud del método. Pero los espacios locales también incluyen funciones más generales (por lo general definidas a través de un operador diferencial) cuyos valores puntuales no son calculables (de ahí el nombre "Virtual");

- Para producir formulaciones VEM totalmente calculables y precisas en mallas generales, los grados de libertad del método se eligen cuidadosamente de modo que las correspondientes proyecciones de las funciones de prueba locales en el sub-espacio de los polinomios, también locales, sean calculables.

Una consecuencia importante del enfoque de los VEM es que la solución calculada no está disponible en forma de una función (un elemento virtual). Por el contrario, la solución es representada a través de los valores de sus grados de libertad, a los que podemos acceder, por ejemplo, mediante la proyección polinomial a trozos de la función virtual en el elemento.

Como conclusión de este primer trabajo ([18]), los VEM resultaron ser apropiados para hacer frente a los requisitos de continuidad para ordenes superiores y permiten diseñar aproximaciones de tipo C^1 fácilmente. Así los VEM pueden ser extendidos a otro tipo de problemas. Posteriormente, VEM se aplicó a álgunos problemas simples de elasticidad en dos dimensiones (ver [19]) y a problemas de placas (ver [57]).

Una de las ideas básicas de los VEM es que incluso en un elemento K con una geometría general, se pueden, calcular integrales de polinomios, a través de fórmulas del tipo

$$\int_K x^r dK = \int_{\partial K} \frac{x^{r+1}}{r+1} dS,$$

mientras que el cálculo de las funciones no polinómicas (y sus integrales) requiere algún truco adicional (e incluso podría ser inviable en la práctica). En particular, con el fin de calcular la contribución de cada una de estas funciones no polinómicas a la matriz de rigidez local de un elemento K, primero se tiene que calcular un proyector local (por lo general denominado Π_K^∇) en el espacio de polinomios de grado $\leq k$. Estos son, en general, los proyectores en el producto escalar $H_0^1(K)$, con un ajuste adecuado de la parte constante (ver [18, 19, 57]).

En muchas aplicaciones, el conocer explícitamente el proyector Π_K^∇ es suficiente para completar el proceso de discretización y para realizar el análisis teórico. Sin embargo, hay casos en los que sería muy útil también conocer explícitamente el proyector ortogonal local (Π_K^0) de $L^2(K)$ en el espacio de polinomios de grado $\leq k$, junto al proyector Π_K^∇. Así, [3] muestra que, en un cierto número de casos, simplemente cambiando ligeramente la definición de las funciones locales no polinomiales (las cuales no se calculan), se puede obtener un espacio local en el que el operador Π_K^0 se puede calcular fácilmente, a partir del operador Π_K^∇ y los grados de libertad locales. Por lo tanto, una vez calculado explícitamente Π_K^∇ se puede conseguir Π_K^0 casi sin

ningún esfuerzo adicional. Este artículo ([3]) también incluye una extensión de los VEM al caso tridimensional, gracias al operador Π^0_K, el cual es mucho más barato de calcular que la versión que se obtiene en los MFD. Además se muestran algunos ejemplos de aplicaciones.

El siguiente paso en VEM fue entregar una guía para la implementación del método. En [22] se presentan todos los detalles de implementación de los VEM para un problema elíptico de segundo orden simple. En ese artículo, se enseñan los lineamientos para construir una matriz de rigidez local adecuada de manera de garantizar la consistencia y la estabilidad necesarias en VEM, junto a los detalles sobre cómo calcular el proyector elíptico Π^∇_K sobre los polinomios de grado $\leq k$, utilizando sólo los grados de libertad del espacio. Una vez conocido Π^∇_K, las matrices de rigidez local, se construyen fácilmente para problemas del tipo:

$$\begin{cases} \Delta u = f & \text{in } \Omega, \\ u = 0 & \text{on } \partial\Omega, \end{cases}$$

donde Ω es un dominio poligonal en $\mathbb{R}^2$. En la segunda parte de ese artículo ([22]), se introduce el proyector ortogonal Π^0_K de L^2 en el espacio de polinomios de grado $\leq k$, el cual se puede calcular sólo con cambiar la definición y la perspectiva de los espacios locales (pero no los grados de libertad ni la construcción del operador Π^∇_K). Una vez conocido Π^0_K, se ilustra la construcción de la matriz de masa y los términos de carga, así como los de orden cero que surgen debido a la presencia de un término de reacción o para problemas dependientes del tiempo. Además se discute el uso del operador Π^0_K en cada cara de un poliedro, lo que allana el camino para una implementación eficiente de los VEM en 3D. Por último, se entregan algunos comentarios para la ejecución de los VEM para formas débiles más generales.

Desde entonces VEM se ha extendido para problemas con regularidad arbitraria (ver [33]), problemas de cuarto orden (ver [67]), espacios no conformes (ver [14, 63, 1, 2]), problemas elípticos en general (ver [23, 21]), hiperbólicos (ver [114]), mixtos (ver [20, 23, 31, 54, 58]) (en particular el problema de Stokes (ver [6, 31, 58])), problemas de placas (ver [57, 35]), de elasticidad lineal y no lineal (ver [19, 30, 84, 83]), flujos de fluidos en medios fracturados (ver [37, 38]), problemas de Helmholtz (ver [101]). Además se han realizado trabajos en 3D (ver [61, 84, 83]), problemas evolutivos (ver [7]), estimaciones de error a posteriori y técnicas adaptativas (ver [34, 61]) y a problemas espectrales [97, 36]. Recientemente, se presentó un trabajo de implementación de los VEM en Matlab (ver [110]). También se han realizado algunos artículos en que se comparan los VEM con otros esquemas numéricos; (ver [64, 98, 99]).

Una característica interesante que comparten los métodos de elementos finitos clásicos (en rectángulos o cuadriláteros) y los VEM, es que ambos métodos comparten las mismas funciones de prueba y grados de libertad en los lados. Pero en lo que se refiere a los grados de libertad internos, en general los VEM resultan más caros que los FEM tradicionales. Por ejemplo, si k es el grado de precisión de aproximación, entonces los VEM en triángulos necesitan $k(k-1)/2$ grados de libertad internos (ver [18]), en lugar de los $(k-1)(k-2)/2$ utilizados por FEM. Esto también implica que la posibilidad de combinar FEM y VEM no es inmediata en tres dimensiones, incluso cuando la cara común es un triángulo. En cuadriláteros, VEM nuevamente utiliza $k(k-1)/2$ grados de libertad internos, que ahora resultan ser menos que los $(k-1)^2$

grados de libertad internos de $\mathbb{Q}_k$-finite elements, pero no que los $(k-2)(k-3)/2$ grados de libertad internos de los Serendipity FEM (en cuadriláteros).

Sin embargo, en los cuadriláteros no-afines los Elementos Finitos "Serendipity" sufren un grave deterioro de la precisión: (véase, por ejemplo [11, 12, 103]). Esto no ocurre en los VEM, los cuales tienen como una de sus ventajas más relevantes la robustez con respecto a la de distorsión del elemento.

Por otro lado, la mayor ventaja de los FEM clásicos es el hecho de que los valores de las funciones de prueba se pueden calcular fácilmente en cualquier punto, mientras que en VEM se calculan fácilmente sólo en los lados. La solución a dicho problema ya fue comentada ampliamente antes y consiste en calcular la proyección L^2 de las funciones de prueba sobre el espacio de los polinomios de grado r. Para los VEM presentados en [18] sólo se puede tomar $r = k-2$ (con una evidente falta de precisión). Sin embargo, para sus versiones avanzadas, como en [3], se puede llegar a $r = k$ con los mismos $k(k-1)/2$ grados de libertad internos. Sin embargo, en elementos simples como triángulos o tetraedros, VEM sigue siendo más costoso que FEM. En [24] se propone una nueva variante de los VEM que imita, en cierto sentido, el enfoque de los Serendipity FEM. Esta nueva variante hace que la cantidad de grados de libertad internos coincidan exactamente, con los de los elementos finitos tradicionales (en triángulos $(k-1)(k-2)/2$) y mantiene todos las buenas propiedades de los elementos finitos en cuadriláteros. En particular en paralelogramos, donde se utilizan $(k-2)(k-3)/2$ grados de libertad internos (como para Serendipity FEM). Además, los grados de libertad en la frontera son exactamente los mismos que para los elementos finitos. La propuesta de [24] es una combinación de ideas "Serendipity" para FEM y VEM mejorados como los presentados en [3]. En términos generales, en lugar de mantener entre los grados de libertad los momentos hasta el orden $k-2$ (como en los VEM original), se baja a $k-3$ y, usando los grados de libertad en la frontera y los $k-3$ momentos internos, se calcula un proyector del espacio VEM en $\mathbb{P}_k$. Ese mismo proyector se utiliza para definir los momentos hasta el grado k como un subproducto.

Por último en [25], se extienden la ideas básicas de [24], a un marco más general y se aplica la estrategia general al caso de los VEM conformes para $H(\mathrm{div})$ y $H(\mathrm{curl})$ en dos y tres dimensiones.

El objetivo de esta tesis es analizar la aplicación del método de los elementos virtuales en mallas con polígonos generales (incluso no conformes o no convexos), a la solución de diversos problemas de valores propios y de flexión de placas moderadamente gruesas.

La aproximación numérica de problemas de valores propios es objeto de gran interés, desde los puntos de vista práctico y teórico. Una referencia clásica para la solución computacional de este tipo es [15]. Por otra parte, [49] es una monografía más reciente en lo que se presenta el estado del arte en este tema. En nuestro caso proponemos analizar los VEM para distintos problemas de valores propios. En particular, consideramos el problema de Steklov y el de vibraciones acústicas. En el caso del primero propondremos también un estimador a posteriori del error y un proceso adaptativo basado en este estimador.

Por otra parte también se propone y estudia en esta tesis un VEM para resolver el problema de flexión de placas modeladas por las ecuaciones de Reissner-Mindlin. En particular se demuestra que el método propuesto no sufre de bloqueo como ocurre con los métodos estándar.

El objetivo es hacer una contribución original y enriquecer la literatura existente en el área

de los métodos de elementos virtuales. A continuación describiremos y resumiremos en qué consisten y cuales serán los aportes de nuestro estudio.

1.2. Problema de valores propios de Steklov.

El problema de valores propios de Steklov, se caracteriza por la presencia del valor propio en la condición de contorno. Este problema aparece en muchas aplicaciones interesantes, por ejemplo, podemos mencionar el estudio de los modos de vibración de una estructura en contacto con un fluido incompresible con una superficie libre (ver [45]), el análisis de la estabilidad de los osciladores mecánicos sumergidos en un medio viscoso (ver [72]), el estudio de ondas superficiales (ver [39]) entre otras. Una de sus principales aplicaciones surge en la dinámica de líquidos en recipientes, es decir, problemas de oscilaciones por gravedad de una superficie libre ("sloshing", ver[46, 59, 65, 68, 80, 117]). Entre las técnicas existentes para resolver este problema, se han introducido y analizado diversos métodos de elementos finitos, bajo un marco general. Por ejemplo, en [5, 50] se han considerado elementos finitos conformes para la discretización del problema, mientras que en [92, 120] se usan elementos finitos no conformes. Tradicionalmente, los métodos de elementos finitos se basan en forma triangulares (simplicial) o mallas de cuadriláteros. Sin embargo, en simulaciones complejas, puede ser conveniente utilizar mallas poligonales más generales.

Nosotros estamos interesados en desarrollar y analizar un método de elementos virtuales aplicado a mallas con polígonos generales (no necesariamente convexos), para la solución del problema de valores propios de Steklov en dos dimensiones.

En el Capítulo 2 de esta tesis se introduce y analiza un VEM para el problema de valores propios de Steklov, en el caso en que el dominio $\Omega \subset \mathbb{R}^2$ es acotado con frontera poligonal $\partial\Omega$. En primer lugar, y con el fin de caracterizar el espectro del problema, se introduce una formulación variacional primal del problema espectral y se define un operador solución adecuado, para luego establecer su caracterización espectral. Posteriormente, se propone una discretización virtual, basada en el enfoque introducido en [18] para la ecuación de Laplace y se describe el operador solución junto a su caracterización espectral discreta. Mediante el uso de la teoría de aproximación espectral abstracta (ver [15]) y bajo las suposiciones estándar sobre dominios computacionales, se establece que el esquema numérico resultante proporciona una aproximación espectral correcta y se demuestra un orden óptimo para las estimaciones de los errores para las funciones propias y los valores propios. También se demuestran estimaciones de mejor orden para el cálculo del error de las funciones propias en la frontera libre, que en algunos problemas de Steklov (por ejemplo, el calculo de los modos de "sloshing") son una cantidad de gran interés (la superficie libre del fluido). Por último, se presentan algunos ensayos numéricos que apoyan los resultados teóricos.

Los resultados contenidos en este capítulo se recoge en el artículo:

- D. Mora, G. Rivera and R. Rodríguez: *A virtual element method for Steklov eigenvalue problem*, Math. Models Methods Appl. Sci., **25(8)**, (2015), pp. 1421–1445.

1.3. Error a posteriori para el problema de valores propios de Steklov.

Dado que hemos desarrollado en [97] un VEM para el problema de valores propios de Steklov en dos dimensiones. Ahora estamos particularmente interesados en desarrollar y analizar un estimador del error a posteriori del tipo residual para la aproximación por VEM del problema de valores propios de Steklov (ver [97]) aplicado a mallas con polígonos generales (no necesariamente convexos).

La estrategia basada en un indicador de error a posteriori para el refinamiento de mallas adaptadas juega un papel relevante en la solución numérica de las ecuaciones diferenciales parciales en un sentido general. Por ejemplo, garantizan la convergencia de los métodos numéricos, especialmente en presencia de geometrías complejas. Varios enfoques han sido considerados para construir estimadores de error basados en las ecuaciones residuales (véase [4, 116] y sus referencias). En particular, para el problema de valores propios de Steklov que incluyendo un análisis de errores a posteriori FEM, podemos mencionar [9, 10, 73, 85, 119] y las referencias citadas en estos.

Una motivación del por qué desarrollar y analizar un estimador del error a posteriori del tipo residual para la aproximación por VEM del problema de valores propios de Steklov es que, debido a la gran flexibilidad de las mallas, a las que se puede aplicar VEM, la adaptabilidad de estas, se convierte en una característica atractiva para que la estrategia de refinamiento de mallas pueda ser implementado de manera muy eficiente. Puesto que VEM admite nodos colgantes, estos pueden ser introducidas de forma natural en la malla sin la necesidad de extender las zonas de refinamiento y así garantizar la conformidad de la malla. Como VEM admite células poligonales con formas muy generales, permite adoptar simples algoritmos de refinamiento de mallas.

Dada la naturaleza virtual de los VEM, el diseño y el análisis de cotas de error a posteriori para estos es una tarea complicada. Actualmente en la literatura [34, 61] son los únicos trabajos de error a posteriori para VEM, disponibles. En [34], se desarrolla y analiza un estimador del error a posteriori del tipo residual para la aproximación por VEM del tipo C^1-conformes, para el problema de Poisson en dos dimensiones. Mientras que en [61], se desarrolla y analiza un estimador del error a posteriori del tipo residual para los VEM C^0-conformes introducidos en [63] para la discretización de segundo orden, del problema elíptico lineal de difusión-convección-reacción, de dos y tres dimensiones con coeficientes no constantes.

En el Capitulo 3 de esta tesis se propone y desarrolla el análisis matemático y numérico del estimador del error a posteriori del tipo residual para la aproximación por VEM del problema de valores propios de Steklov. Primero se presentan las formulaciones continuas y discretas del problema de valores propios de Steklov junto con su caracterización espectral, a continuación, se resumen las estimaciones de error a priori para la aproximación por VEM obtenidas en [97]. Dado que, los flujos normales de la solución virtual presentada en [97] no se pueden calcular explícitamente, estos son reemplazados por una proyección adecuada de ellos. Como consecuencia de esta sustitución, aparecen nuevos términos adicionales en el estimador de error a posteriori, que representan la "inconsistencia virtual" de los VEM, estos términos también aparecen en otros documentos para error a posteriori de los VEM (ver [34, 61]). A continuación, se prueba

que el indicador de error es equivalente al error. Hacemos hincapié en que los nodos colgantes introducidos por el refinamiento de un elemento vecino, simplemente, son tratados como nodos nuevos, ya que es perfectamente aceptables que la interfaces entre dos elemento adyacentes no coincidan. Por último, se presentan un conjunto de experimentos numéricos que permiten evaluar el desempeño de tales estimador cuando se combina con una estrategia adaptativa en la resolución de una serie de problemas modelo.

Con los resultados obtenidos en este capítulo se esta preparando el siguiente artículo:

- D. Mora, G. Rivera and R. Rodríguez: *A posteriori error estimates by VEM for the Steklov eigenvalue problem.*

1.4. Problemas de vibraciones acústicas.

La aproximación numérica de problemas de valores propios para ecuaciones diferenciales parciales, derivados de las aplicaciones de ingeniería, es objeto de gran interés. En particular, nos centramos en el llamado problema de vibraciones acústicas; es decir, aquellos problemas en que se calculan los modos de vibración y las frecuencias naturales de un fluido compresible no viscoso dentro de una cavidad rígida (ver [121]). Una motivación del porque estudiar este problema es que constituye un primer paso hacia un objetivo más difícil, como lo es, el de diseñar un método de elementos virtuales para aproximaciones espectrales de los sistemas acoplados que implican la interacción fluido-estructura, que surge en muchos problemas de ingeniería. La formulación más simple de este problema es en términos de la variación de la presión lo que conduce a un problema de valores propios para el operador de Laplace ([121]). Sin embargo, para problemas acoplados, es conveniente utilizar una formulación dual en términos del desplazamiento del fluido (ver [91]). Una aproximación por elementos finitos estándar de este problema conduce a modos espurios (ver [89]). Esta polución espectral se puede evitar mediante el uso de elementos finitos conformes ("H(div)-conforming"), como los Raviart-Thomas (ver [40, 43, 44, 49, 105]). Para una discusión más a fondo de este tema ver [42].

Nuestro objetivo es proponer y analizar un VEM para $H(\mathrm{div})$ que se aplique a mallas con polígonos generales (no necesariamente convexos), para el problema de vibración acústica en dos dimensiones.

En el Capitulo 4 de esta tesis se aborda el análisis matemático y numérico del problema de vibraciones acústicas utilizando VEM. Se comienza con una formulación variacional del problema espectral basándose sólo en el desplazamiento del fluido, para luego definir un operador solución adecuado y establecemos su caracterización espectral. A continuación, se propone una discretización basada en los VEM mixtos para problemas elípticos generales de segundo orden introducidos en [23]. La teoría clásica de aproximación espectral abstracta (ver [15]) no se puede utilizar para el análisis de este problema. De hecho, en este caso, el núcleo de la forma bilineal del lado izquierdo de la formulación variacional, es de dimensión infinita. Aunque la estrategia de "shifteo" estándar permite obtener un operador solución bien definido, el cual no es compacto y en tal caso, su espectro esencial no trivial puede generar valores espurios del espectro discreto. Sin embargo, bajo suposiciones estándar sobre el dominio computacional, la teoría de

la aproximación espectral abstracta para operadores no compactos desarrollado en [74, 75] se puede adaptar adecuadamente. Así, haciendo las adaptaciones necesarias, se establece que el esquema resultante proporciona una aproximación correcta del espectro y se demuestra un orden óptimo de la estimación de los errores para las funciones propias y los valores propios. Adicionalmente se demuestran estimaciones óptimas de aproximación en los VEM para $H(\mathrm{div})$ con rotor nulo, resultado que podría ser útil también para otras aplicaciones. Estos resultados y sus correspondientes demostraciones se recoge en un apéndice al final del Capitulo 4. Por último, se presenta un par de ensayos numéricos que nos permiten evaluar las propiedades de convergencia del método, para confirmar que no hay polución por modos espurios y para comprobar que las tasas de convergencia experimentales están de acuerdo con las teóricas.

Los resultados contenidos en este capítulo se recoge en la siguiente pre-publicación:

- L. Beirão D. Mora, G. Rivera and R. Rodríguez: *A virtual element method for the acoustic vibration problem*. Preprint 2015-44, Centro de Investigación en Ingeniería Matemática (CI^{2}MA), Universidad de Concepción Chile, (2015).

1.5. Problemas de placas moderadamente gruesas.

La teoría de Reissner-Mindlin es el modelo más utilizado para aproximar la deformación de una placa elástica delgada o moderadamente gruesa. Hoy en día, es muy bien conocido que los elementos finitos estándar aplicados a este modelo conducen a resultados erróneos, debido al llamado fenómeno de bloqueo, que ocurre, cuando el espesor de la placa t es pequeño con respecto a las otras dimensiones de esta. Sin embargo, este fenómeno puede evitarse, por ejemplo, utilizando un método de integración reducida o una formulación técnica de interpolación mixta. De hecho, se ha demostrado rigurosamente que varias familias de métodos libres de bloqueo convergen de manera óptima. Por ejemplo, mencionamos [81, 94] para una descripción exhaustiva del estado del arte y otras referencias.

Recientemente, un nuevo enfoque para resolver el problema de la flexión de Reissner-Mindlin se ha presentado en [26] por Beirão da Veiga et al. (ver también [79, 93]). En este caso se considera una formulación variacional del problema de flexión de placas en términos de la deformación de corte y la deflexión, lo que permite evitar el fenómeno de "shear-locking". Se propone una discretización del problema por análisis isogeométricos y, bajo ciertos supuestos de regularidad de la solución exacta, se demuestra que las estimaciones del error son óptimas con constantes independientes del espesor de la placa.

Una de las ventajas de VEM es su fácil implementación para espacios discretos altamente regulares. De hecho, evitando la construcción explícita de las funciones de base locales, los VEM permiten manejar fácilmente polígonos/poliedros generales sin integraciones complejas sobre el elemento (ver [22] para más detalles sobre los aspectos de codificación del método).

Nuestro interés es desarrollar y analizar un método de elementos virtuales para la solución del problema de placas de Reissner-Mindlin, considerando una formulación variacional escrita en términos de deformación de corte y la deflexión que se presentó en [26].

En el Capitulo 3 se propone y desarrolla el análisis matemático y numérico de los VEM para el problema de placas de Reissner-Mindlin. Comenzamos con una formulación variacional del problema escrito en términos de las variables de deflexión y rotación. Luego se presenta una forma equivalente escrita en términos de las variables de deformación de corte y deflexión, presentados en [26]. A continuación, explotando la capacidad de los VEM para construir espacios discretos altamente regulares, se propone una formulación discreta conforme en $[H^1(\Omega)]^2 \times H^2(\Omega)$ para la deformación de corte y deflexión, respectivamente. Enseguida se demuestra que la forma bilineal resultante es continua y elíptica con respecto a normas t-dependientes apropiadas. Una característica distintiva de este enfoque, es que se aproxima directamente la deformación de corte. Por otra parte, las rotaciones se obtienen con un simple tratamiento de post-proceso de las deformaciones de corte y la deflexión.

Una vez probada la existencia de soluciones débiles para el problema discreto virtual y bajo ciertos supuestos de regularidad de la solución exacta, se demuestra que las estimaciones del error son óptimas para todas las variables involucradas (en las normas naturales de la formulación adoptada), con constantes independientes del espesor de la placa. Además, utilizando argumentos de dualidad, se presentan las estimaciones de error en normas más débiles. Por último, se hace notar que, a diferencia del método de elementos finitos donde la construcción de funciones globales de tipo $C^1(\Omega)$ es complicada, aquí el espacio de deflexión virtual puede ser construido con una construcción bastante simple debido a la flexibilidad del enfoque virtual. En resumen, las ventajas del método propuesto son la posibilidad de utilizar mallas poligonales generales y una mejor conformidad para el problema limite (placas Kirchhoff), derivada de la aproximación $H^2(\Omega)$ utilizada para la deflexión discreta. Por último, se presenta un par de ensayos numéricos que nos permiten evaluar las propiedades de convergencia del método.

Los resultados contenidos en este capítulo se recoge en la siguiente pre-publicación:

- L. Beirão D. Mora and G. Rivera: *A virtual element method for Reissner-Mindlin plates*.Preprint 2016-14, Centro de Investigación en Ingeniería Matemática (CI^{2}MA), Universidad de Concepción Chile, (2016).

Introduction

1.6. Virtual element method

Mimetic finite differences (MFD) and in particular their mathematical framework and schemes have been evolving from finite differences/finite volumes towards an analysis more like that of finite elements. They can be considered a form of approximation by finite element methods (FEM) in which only the degrees of freedom are used (given that the test functions are not available within the elements), which allows them to imitate (together with several fundamental physical laws) most types of finite element spaces of lower order (from continues piecewise polynomial and to more sophisticated ones used for mixed formulations) in elements with more general geometry (see for example [62, 17, 53, 16, 52] and the references therein).

There have been attempts in recent years to introduce higher-order MFD using more general degrees of freedom such as moments on the faces, edges and elements (see [32, 88, 27, 28]). However, because there are no test functions within the elements (or even within the face) the presentation of these results is very awkward. Consequently, it is evident that the method would be clearer if the degrees of freedom (typical unknowns for the MFD) were joined to the test functions inside the elements, although these functions are not necessarily polynomial. The virtual element method (VEM) thus emerged, which takes its main ideas from modern mimetic schemes, but follows Galerkin discretization of the problem and consequently can be interpreted as a generalization of the finite element method (FEM) on polygons, such as the polygonal finite element methods (PFEM, see for example [109, 111]) or the extended FEM (see [82] and references). However, in contrast to the methods mentioned above, VEM seeks to be a simpler method that preserves the capacity to reproduce several physical laws with exactitude (like MFD) and in dealing with more complicated geometry (polygons/polyhedrons). At the same time, it shares the advantages of finite element formulations and polynomial exactitude obtained in the simplex, while working in polygons and polyhedrons.

Virtual element methods were first introduced in [18] for the 2D Laplace equation with the central ideas of the method, which can be summarized as follows:

- The local spaces are designed to contain polynomials of degree $\leq k$ (as in classic finite elements), which in the final instance, are responsible for the exactitude of the method. However, the local spaces also include more general functions (generally defined through a differential operator) whose exact values are not computable (hence it is termed "virtual");
- To produce completely computable and precise VEM formulations in general meshes, the degrees of freedom of the method are chosen carefully so that the corresponding projections of the local test functions in the polynomial sub-space, also local, are computable.

An important consequence of the approach of VEM is that the computed solution is not available in the form of a function (a virtual element). In contrast, the solution is represented through the values of its degrees of freedom, which can be accessed for example through the piecewise polynomial projection of the virtual function in the element.

As a conclusion of this first work on this subject ([18]), VEM prove to be appropriate for dealing with higher order continuity requisites and allow for easily designing C^1-approximations. Thus, VEM can be extended to other types of problems. Subsequently, VEM have been applied to simple problems of elasticity in two dimensions (see [19]) and of plates ([57]).

One of the basic ideas of VEM is that even on an element K with a rather general geometry, it is possible to compute integrals of polynomials, through formulas such as

$$\int_K x^r dK = \int_{\partial K} \frac{x^{r+1}}{r+1} dS,$$

while the calculation of non-polynomial functions (and their integrals) requires an additional trick (and could also be practically unfeasible). In particular, in order to compute the contribution of each of these non-polynomial functions to the local stiffness matrix of an element K, a local projector must first be calculated (generally termed Π_K^∇) on the space of polynomials of degree $\leq k$. These are generally the projectors in the $H_0^1(K)$ scalar product, with an adequate adjustment of the constant part (see [18, 19, 57]).

Knowing explicitly the projector Π_K^∇ is sufficient in many applications to obtain a complete discretization and make the theoretical analysis. However, there are cases in which it would also be useful to explicitly know the local $L^2(K)$-orthogonal projector (Π_K^0) on the space of polynomials of degrees $\leq k$, together with the Π_K^∇. Thus, [3] shows that in a certain number of cases simply by slightly changing the definition of non-polynomial local functions (which are not calculated), a local space can be obtained in which the operator Π_K^0 can be calculated easily based on the operator Π_K^∇ and the local degrees of freedom. Consequently, once Π_K^∇ is explicitly calculated, Π_K^0 can be obtained almost without additional effort. This article ([3]) also includes an extension of VEM in the three-dimensional case, thanks to the operator Π_K^0, which is much less expensive to calculate than the version that is obtained by MFD. As well, some examples of applications are shown.

The following step for VEM was to provide a guide for employing the method. The details for employing VEM for a simple linear elliptic second-order problem are presented in [22]. This article sets out the lines for constructing an adequate local stiffness matrix to ensure the consistency and stability necessary of VEM, together with the details about how to calculate the elliptic projector Π_K^∇ on polynomials of degrees $\leq k$ using only the degrees of freedom of the space. Once Π_K^∇ is known, the local stiffness matrices are easily constructed for problems such as:

$$\begin{cases} \Delta u = f & \text{in } \Omega, \\ u = 0 & \text{on } \partial\Omega, \end{cases}$$

where Ω is a polygonal domain in $\mathbb{R}^2$. The second part of this article ([22]) introduces the local L^2-orthogonal projector (Π_K^0) on the space of polynomials of degree $\leq k$, which can only be calculated by changing the definition and perspective of the local spaces (but not the degrees of freedom and the construction of the operator Π_K^∇). Once Π_K^0 is known, the construction of the mass matrix and the load terms are illustrated, as well as the zero order that emerges owing to the presence of a reaction term or for time-dependent problems. Moreover, the use of the operator Π_K^0 on each face of the polyhedron is discussed, which sets the stage for the efficient

use of VEM in 3D. Finally, some comments are provided for executing VEM for more general weak forms.

VEM has been extended for problems of arbitrary regularity ([33]), fourth order ([67]), non-conforming spaces ([14, 63, 1, 2]), elliptic in general ([23, 21]), hyperbolic ([114]), mixed problems ([20, 23, 31, 54, 58])(in particular the Stokes problem [6, 31, 58]), plates ([57]) and linear and non-linear elasticity problems ([19, 30, 84, 83]), fluid flows inside a fractured medium ([37, 38]) and the Helmholtz problem ([101]). Works have also been carried out in 3D ([61, 84, 83]), evolutive problems ([7, 115]), a posteriori error estimation and adaptativity techniques ([34, 61]). A work was recently presented implementing VEM in Matlab ([110]). There have also been articles comparing VEM to other numerical schemes (see [64, 98, 99]).

An interesting characteristic that classic FEM (in rectangles and quadrilaterals) and VEM share are the same test functions and degrees of freedom on the edges. However, in relation to internal degrees of freedom, VEM are generally more costly than traditional FEM. For example, if k is the degree of approximation precision, so that with triangles VEM require $k(k-1)/2$ internal degrees of freedom (see [18]) instead of the $(k-1)(k-2)/2$ used by FEM. This also implies that it not easy to combine FEM and VEM in three dimensions, even when the common face is a triangle. With quadrilaterals, VEM again use $k(k-1)/2$ internal degrees of freedom, which now is less than the $(k-1)^2$ internal degrees of freedom of $\mathbb{Q}_k$-finite elements, but not less than the $(k-2)(k-3)/2$ internal degrees of freedom of the Serendipity FEM (on quadrilaterals). However, Serendipity FEM suffers a serious loss of precision with non-affine quadrilaterals (see [11, 12, 103]) that does not occur with VEM, this robustness in the relation to the distortion of the element being one of its more important advantages.

The major advantage of classic FEM is that test function values can be calculated easily at any point, while with VEM they can only be calculated easily on the edges. The solution to this problem has been widely commented on and consists of calculating the L^2-projection of the test functions on the space of polynomials of degrees r. The VEM presented in [18] can only take $r = k-2$ (with an evident lack of precision). However, its advanced versions, as in [3] can reach $r = k$ with the same $k(k-1)/2$ internal degrees of freedom. However, with simple elements like triangles or tetrahedrons, VEM is more costly than FEM. A new variant of VEM was proposed in [24] that in a certain sense mimics the Serendipity approach of FEM. This new variant makes that the number of internal degrees of freedom coincide exactly with those of the traditional finite elements (on triangles $(k-1)(k-2)/2$) and maintain all the good properties of finite elements on quadrilaterals, in particular on parallelograms where $(k-2)(k-3)/2$ internal degrees of freedom are used (such as for the Serendipity FEM). As well, the degrees of freedom on the edges are exactly the same as those for finite elements. The proposal of [24] is a combination of "Serendipity" for improved FEM and the advanced versions of VEM presented in [3]. In general terms, instead of maintaining the moments among the degrees of freedom up to the order of $k-2$ (as in the original VEM), it is lowered to $k-3$, and using boundary degrees of freedom and internal $k-3$ moments, to compute a projector from the VEM space onto $\mathbb{P}_k$. This same projector is used to define the moments up to the k degree as a byproduct.

Finally, [25], extended the basic ideas of [24] to a more general framework and applied the general strategy to the case of conforming VEM for $H(\mathrm{div})$ and $H(\mathrm{curl})$ in two and three

dimension.

The objective of this thesis is to analyze the application of the virtual element method with general polygonal meshes (including non-conforming and non-convex meshes) to solve diverse eigenvalue problems and bending problems moderately thick plates.

The numerical approximation of eigenvalue problems is the object of great practical and theoretical interest. A classical reference for the computational solution of this type is [15]. A more recent monograph [49] presents the state-of-the-art on this theme. In our case, we propose analyzing VEM for different eigenvalue problems, in particular the Steklov problem and that of acoustic vibrations. For the former we also propose an a posteriori error estimator and an adaptive process based on this estimator.

This thesis also proposes and studies a VEM to solve the Reissner-Mindlin plate problem. In particular, we show that the proposed method does not suffer from locking, as occurs with standard methods.

The objective is to make an original contribution and enrich the literature on virtual element methods. Below we summarize the content of our study.

1.7. Steklov eigenvalue problem.

The Steklov eigenvalue problem is characterized by the presence of the eigenvalue in the boundary condition. This problem appears in many interesting applications such as the study of vibration modes of a structure in contact with an incompressible fluid with a free surface (see [45]), the analysis of the stability of mechanical oscillators submerged in a viscous medium (see [72]), the study of surface waves ([39]), among others. One of its main applications is the dynamics of liquids in containers, that is, the problem of gravity oscillations on a free surface ("sloshing", see [46, 59, 65, 68, 80, 117]).

Among the techniques to solve this problem, diverse finite element methods have been introduced and analyzed under a general framework. For example, [5, 50] conforming finite element discretization have been considered, while [92, 120] used non-conforming finite elements. Traditionally, finite element methods are based on triangular (simplicial) or quadrilateral meshes. However, with complex simulations it might be more convenient to use more general polygonal meshes.

We are interested in developing and analyzing a virtual element method applied to general polygonal meshes (not necessarily convex) to solve the Steklov eigenvalue problem.

Chapter 2 of this thesis introduces and analyzes a VEM for the Steklov eigenvalue problem in the case in which the domain $\Omega \subset \mathbb{R}^2$ is bounded with polygonal boundary $\partial\Omega$. Firstly, and with the aim of characterizing the spectral problem, a primal variational formulation of spectral problem is introduced and a suitable solution operator is defined to then establish its spectral characterization. Subsequently, virtual discretization is proposed, based on the approach introduced in [18] for the Laplace equation and the operator solution is described and its discrete spectrum is characterized. Through the abstract spectral approximation theory (see [15]) and under the standard assumptions about computational domains, it is established that the resulting numerical scheme provides a correct spectral approximation and shows an optimal order for

the error estimations for the eigenfunctions and eigenvalues. Better order estimations are also shown for calculating the eigenfunctions errors in the free boundary, which with some Steklov problems (for example, calculation of sloshing modes) are a quantity of great interest (the free surface of a fluid). Finally, numerical essays are presented that support the theoretical results.

The results of this chapter are contained in the following article:

- D. Mora, G. Rivera and R. Rodríguez: *A virtual element method for Steklov eigenvalue problem*, Math. Models Methods Appl. Sci., **25(8)**, (2015), pp. 1421–1445.

1.8. A posteriori error by VEM for Steklov eigenvalue problem.

Based on [97], where a VEM for the Steklov eigenvalue problem in two dimensions is developed, we are now interested in developing and analyzing residual-type a posteriori error estimator to approximate by VEM the Steklov eigenvalue problem applied to general polygonal meshes (not necessarily convex).

The strategy based on an a posteriori error indicator for adapted meshes plays an important role in the numerical solution of partial differential equations in a general sense. For example, it ensures the convergence of numerical methods, especially in the presence of complex geometries. Several approaches have been considered to construct error estimators based on residual equations (see [4, 116] and their references). In particular, for Steklov eigenvalue problems, we note [9, 10, 73, 85, 119] and the references in these, for the analysis of a posteriori FEM errors.

One motive for developing and analyzing a residual-type a posteriori error estimator to approximate the Steklov eigenvalue problem by VEM is that the flexibility of the meshes to which VEM can be applied makes their adaptability attractive for the efficient employment of the mesh refinement strategy. Because VEM admits hanging nodes, these can be introduced naturally in the mesh without the need to extend the refinement zones and thus ensure the conformity of the mesh. As VEM admits polygonal cells with very general shapes, it allows for adopting simple mesh refinement strategies.

Given the virtual nature of VEM, the design and analysis of their a posteriori error estimators is complicated. Currently [34, 61] are the only works in the literature on a posteriori error for VEM. A residual-type a posteriori error estimator was developed in [34] to approximate by conforming C^1-type VEM the Poisson problem in two dimensions, while [61] developed a residual-type a posteriori error estimator for the C^0-conforming VEM introduced in [63] for the second order discretization of the linear elliptic diffusion-convection-reaction problem on two and three dimensions, with non-constant coefficients.

Chapter 3 of this thesis proposes and develops a mathematical and numerical analysis of a residual-type a posteriori error estimator to approximate the Steklov eigenvalue problem by VEM. First, the continuous and discrete formulations for the Steklov eigenvalue problem are presented together with its spectral characterization, followed by a summary of the a priori error estimations obtained by VEM in [97]. Given that the normal fluxed of the virtual solution presented in [97] cannot be explicitly calculated, they are replaced by an appropriate projection. As a result of the substitution, new terms appear in the a posteriori error estimator that represent

the "virtual inconsistency" of VEM. These terms also appear in other publications for a posteriori VEM error (see [34, 61]). The error indicator proved to be equivalent to the error up to higher order terms. We emphasize that the hanging nodes introduced by refining a neighboring element are simply treated as new nodes, given that it is perfectly acceptable that the interfaces between two adjacent elements do not coincide. Finally, a set of numerical experiments to evaluate the performance of such estimators when combined with an adaptive strategy, to solve a series of model problems is reported.

With the results obtained in this chapter, the following article is currently being developed:

- D. Mora, G. Rivera and R. Rodríguez: *A posteriori error estimates by VEM for the Steklov eigenvalue problem.*

1.9. Acoustic vibration problems.

We focus on the problem of acoustic vibrations, that is, the problem of calculating modes of vibration and the natural frequency of a compressible non-viscous fluid in a rigid container (see [121]). A reason for studying this problem is that it constitutes a first step toward a more difficult objective of designing a virtual element method for spectral approximations of coupled systems that imply fluid-structure interaction that arise in many engineering problems. The simplest formulation of this problem is in terms of the variation of the pressure, which leads to an eigenvalue problem for the Laplace operator ([121]). However, for coupled problems it is convenient to use a dual formulation in terms of fluid displacements (see [91]). An approximation of this problem by standard finite elements leads to spurious modes (see [89]). This spectral pollution can be avoided by using H(div)-conforming elements, like Raviart-Thomas elements (see [40, 43, 44, 49, 105]). For a more in-depth discussion of this theme see [42].

Our objective is to propose and analyze a VEM for $H(\mathrm{div})$ that is applied to meshes with general polygons (not necessarily convex) for the acoustic vibration problem.

Chapter 4 addresses the mathematical and numerical analysis of the acoustic vibration problem using VEM. It begins with a variational formulation of the spectral problem based on the displacements of the fluid. It then defines an adequate operator solution and establishes its spectral characterization. The chapter proposes a discretization based on mixed VEM for general second order elliptic problems based on that introduced in [23]. The classical theory of abstract spectral approximation (see [15]) cannot be used to analyze this problem. In fact, in this case the kernel of the bilinear form on the left side of the variational formulation has an infinite dimension. Although the standard shifting strategy yields a well-defined operator solution, this is not compact and, in such case, its essential non-trivial spectrum can generate spurious values of the discrete spectrum. Nevertheless, under standard assumptions about the computational domain, the theory of abstract spectral approximation for non-compact operators developed in [74, 75] can be adapted adequately. Making the necessary adaptations, it is thus established that the resulting scheme provides a correct approximation of the spectrum and an optimal order of the error estimation for the eigenfunctions and eigenvalues. As well, optimal VEM approximation estimations are proved for $H(\mathrm{div})$ with a null rotor, which can also be

useful for other application. These results and their corresponding proves are presented in the appendix at the end of Chapter 4. Finally, a pair of numerical tests is presented to evaluate the convergence properties of the method to confirm that there is no pollution by spurious modes and that the experimental convergence rates are in accordance with the theoretical ones.

The results contained in this chapter are in the following pre-print:

- L. Beirão D. Mora, G. Rivera and R. Rodríguez: *A virtual element method for the acoustic vibration problem*. Preprint 2015-44, Centro de Investigación en Ingeniería Matemática (CI^{2}MA), Universidad de Concepción Chile, (2015).

1.10. Moderately thick plates problem.

The Reissner-Mindlin theory is the most often used model to approximate the deformation of a thin or moderately thick elastic plate. It is well known that standard finite elements applied to this model lead to erroneous results owing to what is termed locking, which occurs when the thickness of the plate t is small compared to the other dimensions. However, this can be avoided by using a reduced integration or mixed interpolation technique. In fact, it has been rigorously proved several locking-free families converge optimally. For example, we note [81, 94] and other references for exhaustive descriptions of the state-of the-art.

A new focus for solving the Reissner-Mindlin bending problem was presented by Beirão da Veiga et al. [26], who considered a variational formulation of plate bending in terms of shear strain and deflection that avoids shear-locking. Discretization of the problem by isogeometric analysis is proposed and under certain assumptions of regularity of the exact solution it is shown that the error estimations are optimal, with constants independent of the plate thickness. One of the advantages of VEM is its easy use for highly regular discrete spaces. In fact, by avoiding the explicit construction of local basis functions, VEM allows for easily handling general polygons/polyhedrons without complex integrations on the element (see [22] for more details about the aspects of codification of the method).

Our intent is to develop and analyze a virtual element method to solve Reissner-Mindlin plate problem, considering a variational formulation written in terms of shear strain and deflection that is presented in [26].

A mathematical and numerical VEM analysis for the Reissner-Mindlin plate problem is proposed and developed in Chapter 3. We begin with a variational formulation of the problem written in terms of deflection and rotation variables, followed by an equivalent form written in terms of the shear strain and deflection variables presented in [26]. Taking advantage of the capacity of VEM to construct highly regular discrete spaces, a discrete conforming formulation is proposed in $[H^1(\Omega)]^2$ and $H^2(\Omega)$ for shear strain and deflection, respectively. The resulting bilinear form is continuous and elliptic in relation to suitable t-dependent norms. A distinctive characteristic of this approach is that the deformation is approximated directly by shear strain. The rotations can be obtained with a simple post-process treatment from shear strains and deflections.

Once the existence of weak solutions for the discrete virtual problem have been checked and under certain assumptions of the regularity of the exact solution, optimal error estimations are shown for all the variables involved (in the natural norms of the adopted formulation), with constants independent of the plate thickness. Using duality arguments, the error estimations are presented in weaker norms. Unlike the finite element method in which the construction of global $C^1(\Omega)$-type functions is complicated, here the virtual deflection space requires a very simple construction owing to the flexibility of the virtual approach. The advantages of the proposed method are the possibility of using general polygonal meshes and better conformity for the limit problem (Kirchhoff plates), derived from the $H^2(\Omega)$ approximation used for discrete deflection. Finally, a pair of numerical tests is presented to evaluate the convergence properties of the method.

The results contained in this chapter are in the following pre-print:

- L. Beirão D. Mora and G. Rivera: *A virtual element method for Reissner-Mindlin plates*.Preprint 2016-14, Centro de Investigación en Ingeniería Matemática (CI^{2}MA), Universidad de Concepción Chile, (2016).

Capítulo 2

A virtual element method for the Steklov eigenvalue problem

2.1. Introduction

Very recently, a new evolution of the *Mimetic Finite Difference Method* was proposed in Ref. [18] under the name of *Virtual Element Method* (VEM). This approach takes the steps from the main ideas of modern mimetic schemes but follows from a Galerkin discretization of the problem and therefore can be fully interpreted as a generalization of the finite element method. Thus, VEM couples the flexibility of mimetic methods with the theoretical and applicative background of finite elements. Since VEM is very recent, the current published literature is still very limited [3, 6, 18, 19, 22, 33, 57].

The present paper deals with the solution of an eigenvalue problems by means of VEM. In particular, we have chosen the Steklov eigenvalue problem, which involves the Laplace operator but is characterized by the presence of the eigenvalue in the boundary condition. The reason of this choice is that the analysis turns out simpler, since the right-hand side involves only boundary terms whose approximation by virtual elements can be seen as a classical interpolation.

The numerical approximation of eigenvalue problems is object of great interest from both, the practical and theoretical points of view. We refer to Ref. [48] and the references therein for the state of the art in this subject area. In particular, the Steklov eigenvalue problem appears in many applications. For instance, we mention the study of the vibration modes of a structure in contact with an incompressible fluid (see Ref. [45]) and the analysis of the stability of mechanical oscillators immersed in a viscous media (see Ref. [102]). One of its main applications arises from the dynamics of liquids in moving containers, i.e., sloshing problems (see Refs. [46, 59, 65, 68, 80, 117]).

Among the existing techniques to solve this problem, various finite element methods have been introduced and analyzed. For instance, conforming finite element discretization have been considered in Refs. [5, 50], while Refs. [120, 92] deal with nonconforming finite elements. Other numerical treatment for the Steklov eigenvalue problem, including a posteriori error analysis can be found in Refs. [9, 10, 73, 85, 119] and the references cited therein. Traditionally, finite

element methods rely on triangular (simplicial) or quadrilateral meshes. However, in complex simulations, it can be convenient to use more general polygonal meshes.

The aim of this paper is to introduce and analyze a virtual element method which applies to general polygonal (even non-convex) meshes for the solution of the two-dimensional Steklov eigenvalue problem. We begin with a variational formulation of the spectral problem. We propose a discretization based on the approach introduced in Ref. [18] for the Laplace equation. By using the abstract spectral approximation theory (see Ref. [15]), under rather mild assumptions on the polygonal meshes, we establish that the resulting scheme provides a correct approximation of the spectrum and prove optimal order error estimates for the eigenfunctions and a double order for the eigenvalues.

The outline of this article is as follows: We introduce in Section 2.2 the variational formulation of the Steklov eigenvalue problem, define a solution operator and establish its spectral characterization. In Section 2.3, we introduce the virtual element discrete formulation and describe the spectrum of a discrete solution operator. In Section 2.4, we prove that the numerical scheme provides a correct spectral approximation and establish optimal order error estimates for the eigenvalues and eigenfunctions. We also prove an improved error estimate for the eigenfunctions on the free boundary, which allows computing a quantity of typical interest in sloshing problems. Finally, in Section 2.5, we report a set of numerical experiments that allow us to assess the convergence properties of the method and to check whether the experimental rates of convergence agree with the theoretical ones.

Throughout the article we will use standard notations for Sobolev spaces, norms and seminorms. Moreover, we will denote by C a generic constant independent of the mesh parameter h, which may take different values in different occurrences.

2.2. The spectral problem

Let $\Omega \subset \mathbb{R}^2$ be a bounded domain with polygonal boundary $\partial\Omega$. Let Γ_0 and Γ_1 be disjoint open subsets of $\partial\Omega$ such that $\partial\Omega = \bar{\Gamma}_0 \cup \bar{\Gamma}_1$ and $|\Gamma_0| \neq 0$. We denote by n the outward unit normal vector to $\partial\Omega$ and by ∂_n the normal derivative.

We consider the following eigenvalue problem:

Find $(\lambda, w) \in \mathbb{R} \times H^1(\Omega)$, $w \neq 0$, such that

$$\begin{cases} \Delta w = 0 & \text{in } \Omega, \\ \partial_n w = \begin{cases} \lambda w & \text{on } \Gamma_0, \\ 0 & \text{on } \Gamma_1. \end{cases} \end{cases}$$

By testing the first equation above with $v \in H^1(\Omega)$ and integrating by parts, we arrive at the following equivalent weak formulation:

Problem 2.2.1 *Find $(\lambda, w) \in \mathbb{R} \times H^1(\Omega)$, $w \neq 0$, such that*

$$\int_\Omega \nabla w \cdot \nabla v = \lambda \int_{\Gamma_0} wv \qquad \forall v \in H^1(\Omega).$$

Since the bilinear form on the left-hand side is not $H^1(\Omega)$-elliptic, it is convenient to use a shift argument to rewrite this eigenvalue problem in the following form:

Problem 2.2.2 *Find* $(\lambda, w) \in \mathbb{R} \times H^1(\Omega)$, $w \neq 0$, *such that*

$$\widehat{a}(w, v) = (\lambda + 1)\, b(w, v) \qquad \forall v \in H^1(\Omega),$$

where

$$\begin{aligned} \widehat{a}(w, v) &:= a(w, v) + b(w, v), \qquad w, v \in H^1(\Omega), \\ a(w, v) &:= \int_\Omega \nabla w \cdot \nabla v, \qquad w, v \in H^1(\Omega), \\ b(w, v) &:= \int_{\Gamma_0} wv, \qquad w, v \in H^1(\Omega) \end{aligned}$$

are bounded bilinear symmetric forms.

Next, we define the solution operator associated with Problem 2.2.2:

$$\begin{aligned} T: \ H^1(\Omega) &\longrightarrow H^1(\Omega), \\ f &\longmapsto Tf := u, \end{aligned}$$

where $u \in H^1(\Omega)$ is the solution of the corresponding source problem:

$$\widehat{a}(u, v) = b(f, v) \qquad \forall v \in H^1(\Omega). \tag{2.1}$$

The following lemma allows us to establish the well-posedness of this source problem.

Lemma 2.2.1 *There exists a constant* $\alpha > 0$, *depending on* Ω, *such that*

$$\widehat{a}(v, v) \geq \alpha \|v\|_{1,\Omega}^2 \qquad \forall v \in H^1(\Omega).$$

Proof. The result follows immediately from the generalized Poincaré inequality. □

We deduce from Lemma 2.2.1 that the linear operator T is well defined and bounded. Notice that $(\lambda, w) \in \mathbb{R} \times H^1(\Omega)$ solves Problem 2.2.2 (and hence Problem 2.2.1) if and only if $Tw = \mu w$ with $\mu \neq 0$ and $w \neq 0$, in which case $\mu := \frac{1}{1+\lambda}$. Moreover, it is easy to check that T is self-adjoint with respect to the inner product $\widehat{a}(\cdot, \cdot)$ in $H^1(\Omega)$. Indeed, given $f, g \in H^1(\Omega)$,

$$\widehat{a}(Tf, g) = b(f, g) = b(g, f) = \widehat{a}(Tg, f) = \widehat{a}(f, Tg).$$

The following is an additional regularity result for the solution of problem (2.1) and consequently, for the eigenfunctions of T.

Lemma 2.2.2 *There exists* $r_\Omega > \frac{1}{2}$ *such that the following results hold:*

i) for all $f \in H^1(\Omega)$ *and for all* $r \in [\frac{1}{2}, r_\Omega)$, *the solution* u *of problem* (2.1) *satisfies* $u \in H^{1+r_1}(\Omega)$ *with* $r_1 := \min\{r, 1\}$ *and there exists* $C > 0$ *such that*

$$\|u\|_{1+r_1,\Omega} \leq C \|f\|_{1,\Omega};$$

ii) if w is an eigenfunction of Problem 2.2.1 with eigenvalue λ, for all $r \in [\frac{1}{2}, r_\Omega)$, $w \in H^{1+r}(\Omega)$ and there exists $C > 0$ (depending on λ) such that

$$\|w\|_{1+r,\Omega} \leq C \|w\|_{1,\Omega}.$$

Proof. The proof of (i) follows from the classical regularity result for the Laplace equation with Neumann boundary conditions (cf. Ref. [87]). The proof of (ii) follows from the same arguments and the fact that w is the solution of problem (2.1) with $f = \lambda w$, combined with a bootstrap trick. □

The constant $r_\Omega > \frac{1}{2}$ is the Sobolev exponent for the Laplace problem with Neumann boundary conditions. If Ω is convex, then $r_\Omega > 1$, whereas, otherwise, $r_\Omega := \frac{\pi}{\omega}$ with ω being the largest reentrant angle of Ω (see Ref. [87])). Hence, because of the compact inclusion $H^{1+r}(\Omega) \hookrightarrow H^1(\Omega)$, T is a compact operator. Therefore, we have the following spectral characterization result.

Theorem 2.2.1 *The spectrum of T decomposes as follows:* $\mathrm{sp}(T) = \{0, 1\} \cup \{\mu_k\}_{k\in\mathbb{N}}$, *where:*

i) $\mu = 1$ is an eigenvalue of T and its associated eigenspace is the space of constant functions in Ω;

ii) $\mu = 0$ is an infinite-multiplicity eigenvalue of T with associated eigenspace is $H^1_{\Gamma_0}(\Omega) := \{q \in H^1(\Omega) : \ q = 0 \text{ on } \Gamma_0\}$;

iii) $\{\mu_k\}_{k\in\mathbb{N}} \subset (0, 1)$ is a sequence of finite-multiplicity eigenvalues of T which converge to 0 and their corresponding eigenspaces lie in $H^{1+r}(\Omega)$.

Proof. Properties (i) and (ii) are easy to check. Property (iii) follows from the classical spectral characterization of compact operators and Lemma 2.2.2(ii). □

2.3. The discrete problem

In this section, first we recall the mesh construction and the assumptions considered in Ref. [18] for the virtual element method. Then, we will introduce a virtual element discretization of Problems 2.2.1 and 2.2.2 and provide a spectral characterization of the resulting discrete eigenvalue problems.

Let $\{\mathcal{T}_h\}_h$ be a sequence of decompositions of Ω into polygons K. Let h_K denote the diameter of the element K and h the maximum of the diameters of all the elements of the mesh, i.e., $h := \max_{K\in\Omega} h_K$.

For the analysis, we will make as in Ref. [18] the following assumptions.

- **A0.1.** Every mesh $\mathcal{T}_h$ consists of a finite number of *simple* polygons (i.e. open simply connected sets with non self intersecting polygonal boundaries).
- **A0.2.** There exists $\gamma > 0$ such that, for all meshes $\mathcal{T}_h$, each polygon $K \in \mathcal{T}_h$ is star-shaped with respect to a ball of radius greater than or equal to γh_K.

- **A0.3.** There exists $\widehat{\gamma} > 0$ such that, for all meshes $\mathcal{T}_h$, for each polygon $K \in \mathcal{T}_h$, the distance between any two of its vertices is greater than or equal to $\widehat{\gamma} h_K$.

We consider now a simple polygon K and, for $k \in \mathbb{N}$, we define

$$\mathbb{B}_k(\partial K) := \left\{ v \in C^0(\partial K) : v|_e \in \mathbb{P}_k(e) \text{ for all edges } e \subset \partial K \right\}.$$

We then consider the finite-dimensional space defined as follows:

$$V_k^K := \left\{ v \in H^1(K) : \ v|_{\partial K} \in \mathbb{B}_k(\partial K) \text{ and } \Delta v|_K \in \mathbb{P}_{k-2}(K) \right\},$$

where, for $k = 1$, we have used the convention that $\mathbb{P}_{-1}(K) := \{0\}$. We choose in this space the degrees of freedom introduced in Section 4.1 of Ref. [18]. Finally, for every decomposition $\mathcal{T}_h$ of Ω into simple polygons K and for a fixed $k \in \mathbb{N}$, we define

$$V_h := \left\{ v \in H^1(\Omega) : \ v|_K \in V_k^K \right\}.$$

In what follows, we will also use the broken H^1-seminorm

$$|v|_{1,h}^2 := \sum_{K \in \mathcal{T}_h} \|\nabla v\|_{0,K}^2 ,$$

which is well defined for every $v \in L^2(\Omega)$ such that $v|_K \in H^1(K)$ for all polygon $K \in \mathcal{T}_h$.

In order to construct the discrete scheme, we need some preliminary definitions. First, we split the bilinear form $\widehat{a}(\cdot, \cdot)$ as follows:

$$\widehat{a}(u, v) = \sum_{K \in \mathcal{T}_h} a^K(u, v) + b(u, v), \qquad u, v \in H^1(\Omega),$$

where

$$a^K(u, v) := \int_K \nabla u \cdot \nabla v, \qquad u, v \in H^1(\Omega). \tag{2.2}$$

To compute the local matrix a^K for $u, v \in V_h$, we must have into account that due to the implicit space definition, we would not know how to compute the bilinear form exactly. Nevertheless, the final output will be a local matrix on each element K whose associated bilinear form is exact whenever one of the two entries is a polynomial of degree k. This will allow us to retain the optimal approximation properties of the space V_h.

With this end, for any $K \in \mathcal{T}_h$ and for any sufficiently regular function φ, we define first

$$\overline{\varphi} := \frac{1}{N_K} \sum_{i=1}^{N_K} \varphi(P_i), \tag{2.3}$$

where P_i, $1 \leq i \leq N_K$, are the vertices of K. Now, we define the projector $\Pi_k^K : V_k^K \longrightarrow \mathbb{P}_k(K) \subseteq V_k^K$ for each $v \in V_k^K$ as the solution of

$$a^K\left(\Pi_k^K v, q\right) = a^K(v, q) \qquad \forall q \in \mathbb{P}_k(K), \tag{2.4a}$$

$$\overline{\Pi_k^K v} = \overline{v}. \tag{2.4b}$$

Remark 2.3.1 *Equation* (2.4b) *is only needed for the problem above to be well posed. However, it is not used at all on the forthcoming analysis. Therefore, it could be substituted by any other appropriate compatible average of* φ *on* ∂K*, for instance,*

$$\overline{\varphi} := \frac{1}{|\partial K|}\int_{\partial K}\varphi,$$

which makes sense for any $\varphi \in H^1(K)$*.*

On the other hand, let $S^K(\cdot,\cdot)$ be any symmetric positive definite bilinear form to be chosen as to satisfy

$$c_0\, a^K(v,v) \leq S^K(v,v) \leq c_1\, a^K(v,v) \qquad \forall v \in V_k^K \quad \text{with} \quad \Pi_k^K v = 0, \tag{2.5}$$

for some positive constants c_0 and c_1 independent of K. Then, set

$$a_h(u_h,v_h) := \sum_{K\in\mathcal{T}_h} a_h^K(u_h,v_h), \qquad u_h, v_h \in V_h,$$

where $a_h^K(\cdot,\cdot)$ is the bilinear form defined on $V_k^K \times V_k^K$ by

$$a_h^K(u,v) := a^K\big(\Pi_k^K u, \Pi_k^K v\big) + S^K\big(u - \Pi_k^K u, v - \Pi_k^K v\big), \qquad u, v \in V_k^K. \tag{2.6}$$

The following properties of the bilinear form $a_h^K(\cdot,\cdot)$ have been established in Theorem 4.1 of Ref. [18].

- *k-Consistency*:

$$a_h^K(p,v_h) = a^K(p,v_h) \qquad \forall p \in \mathbb{P}_k(K), \quad \forall v_h \in V_k^K.$$

- *Stability*: There exist two positive constants α_* and α^*, independent of K, such that:

$$\alpha_* a^K(v_h,v_h) \leq a_h^K(v_h,v_h) \leq \alpha^* a^K(v_h,v_h) \qquad \forall v_h \in V_k^K. \tag{2.7}$$

Now, we are in a position to write the virtual element discretization of Problem 2.2.1.

Problem 2.3.1 *Find* $(\lambda_h, w_h) \in \mathbb{R} \times V_h$*,* $w_h \neq 0$*, such that*

$$a_h(w_h,v_h) = \lambda_h b(w_h,v_h) \qquad \forall v_h \in V_h.$$

We use again a shift argument to rewrite this discrete eigenvalue problem in the following convenient equivalent form.

Problem 2.3.2 *Find* $(\lambda_h, w_h) \in \mathbb{R} \times V_h$*,* $w_h \neq 0$*, such that*

$$\widehat{a}_h(w_h,v_h) = (\lambda_h + 1)\, b(w_h,v_h) \qquad \forall v_h \in V_h,$$

where

$$\widehat{a}_h(w_h, v_h) := a_h(w_h, v_h) + b(w_h, v_h), \qquad w_h, v_h \in V_h.$$

We observe that by virtue of (2.7) and the trace theorem, the bilinear form $\widehat{a}_h(\cdot,\cdot)$ is bounded. Moreover, as shown in the following lemma, it is also uniformly elliptic.

Lemma 2.3.1 *There exists a constant $\beta > 0$, independent of h, such that*

$$\widehat{a}_h(v_h, v_h) \geq \beta \, \|v_h\|^2_{1,\Omega} \qquad \forall v_h \in V_h.$$

Proof. Thanks to (2.7) and Lemma 2.2.1, it is easy to check that the above inequality holds with $\beta := \alpha \, \min\{\alpha_*, 1\}$. □

The discrete version of the operator T is then given by

$$\begin{aligned} T_h : \; H^1(\Omega) &\longrightarrow H^1(\Omega), \\ f &\longmapsto T_h f := u_h, \end{aligned}$$

where $u_h \in V_h$ is the solution of the corresponding discrete source problem

$$\widehat{a}_h(u_h, v_h) = b(f, v_h) \qquad \forall v_h \in V_h.$$

Because of Lemma 2.3.1, the linear operator T_h is well defined and bounded uniformly with respect to h. Once more, as in the continuous case, $(\lambda_h, w_h) \in \mathbb{R} \times V_h$ solves Problem 2.3.2 (and hence Problem 2.3.1) if and only if $T_h w_h = \mu_h w_h$ with $\mu_h \neq 0$ and $w_h \neq 0$, in which case $\mu_h := \frac{1}{1+\lambda_h}$. Moreover, $T_h|_{V_h} : \; V_h \longrightarrow V_h$ is self-adjoint with respect to $\widehat{a}_h(\cdot,\cdot)$. Indeed, given $f, g \in V_h$,

$$\widehat{a}_h(T_h f, g) = b(f, g) = b(g, f) = \widehat{a}_h(T_h g, f) = \widehat{a}_h(f, T_h g).$$

As a consequence, we have the following spectral characterization.

Theorem 2.3.1 *The spectrum of $T_h|_{V_h}$ consists of $M_h := \dim(V_h)$ eigenvalues, repeated according to their respective multiplicities. It decomposes as follows:* $\mathrm{sp}(T_h|_{V_h}) = \{0, 1\} \cup \{\mu_{hk}\}_{k=1}^{N_h}$, *where:*

i) the eigenspace associated with $\mu_h = 1$ is the space of constant functions in Ω;

ii) the eigenspace associated with $\mu_h = 0$ is $Z_h := V_h \cap H^1_{\Gamma_0}(\Omega) = \{q_h \in V_h : \; q_h = 0 \text{ on } \Gamma_0\}$;

iii) $\{\mu_k\}_{k\in\mathbb{N}} \subset (0, 1)$, $k = 1, \ldots, N_h := M_h - \dim(Z_h) - 1$, are non-defective eigenvalues repeated according to their respective multiplicities.

2.4. Spectral approximation

To prove that T_h provides a correct spectral approximation of T, we will resort to the classical theory for compact operators (see Ref. [15]), which is based on the convergence in norm of T_h to T as $h \to 0$. With the aim of proving this, the first step is to establish the following result.

Lemma 2.4.1 *There exists $C > 0$ such that, for all $f \in H^1(\Omega)$, if $u = Tf$ and $u_h = T_h f$, then*

$$\|(T - T_h) f\|_{1,\Omega} = \|u - u_h\|_{1,\Omega} \leq C \left(\|u - u_I\|_{1,\Omega} + |u - u_\pi|_{1,h} \right),$$

for all $u_I \in V_h$ and for all $u_\pi \in L^2(\Omega)$ such that $u_\pi|_K \in \mathbb{P}_k(K)$ $\forall K \in \mathcal{T}_h$.

Proof. Let $f \in H^1(\Omega)$. For $u_I \in V_h$, we set $v_h := u_h - u_I$ and thanks to Lemma 2.3.1, the definitions (2.6) of a_h^K and those of T and T_h, we have

$$\begin{aligned}
\beta \|v_h\|_{1,\Omega}^2 \leq & \widehat{a}_h(v_h, v_h) = \widehat{a}_h(u_h, v_h) - \widehat{a}_h(u_I, v_h) \\
= & b(f, v_h) - \sum_{K \in \mathcal{T}_h} a_h^K(u_I, v_h) - b(u_I, v_h) \\
= & b(f, v_h) - b(u_I, v_h) \\
& - \sum_{K \in \mathcal{T}_h} \left(a_h^K(u_I - u_\pi, v_h) + a^K(u_\pi - u, v_h) + a^K(u, v_h) \right) \\
= & b(u - u_I, v_h) - \sum_{K \in \mathcal{T}_h} \left(a_h^K(u_I - u_\pi, v_h) + a^K(u_\pi - u, v_h) \right).
\end{aligned}$$

Therefore, from the trace theorem, (2.7) and the boundedness of $a_h^K(\cdot, \cdot)$ and $a^K(\cdot, \cdot)$,

$$\begin{aligned}
\beta \|v_h\|_{1,\Omega}^2 \leq & \|u - u_I\|_{0,\Gamma_0} \|v_h\|_{0,\Gamma_0} + \sum_{K \in \mathcal{T}_h} (\alpha^* |u_I - u_\pi|_{1,K} |v_h|_{1,K} + |u_\pi - u|_{1,K} |v_h|_{1,K}) \\
\leq & \|u - u_I\|_{1,\Omega} \|v_h\|_{1,\Omega} + \sum_{K \in \mathcal{T}_h} (\alpha^* |u_I - u|_{1,K} |v_h|_{1,K} + (\alpha^* + 1) |u - u_\pi|_{1,K} |v_h|_{1,K}) \\
\leq & C \left(\|u - u_I\|_{1,\Omega} + |u - u_\pi|_{1,h} \right) \|v_h\|_{1,\Omega}.
\end{aligned}$$

Hence, the proof follows from the triangular inequality. □

The next step is to find appropriate terms u_I and u_π that can be used in the above lemma to prove the claimed convergence. For the latter we have the following proposition, which is derived by interpolation between Sobolev spaces (see for instance Theorem I.1.4 in Ref. [86]) from the analogous result for integer values of s. In its turn, the result for integer values is stated in Proposition 4.2 of Ref. [18] and follows from the classical Scott-Dupont theory (see Ref. [51]).

Proposition 2.4.1 *If the assumption* **A0.2** *is satisfied, then there exists a constant C, depending only on k and γ, such that for every s with $0 \leq s \leq k$ and for every $v \in H^{1+s}(K)$, there exists $v_\pi \in \mathbb{P}_k(K)$ such that*

$$\|v - v_\pi\|_{0,K} + h_K |v - v_\pi|_{1,K} \leq C h_K^{1+s} \|v\|_{1+s,K}.$$

For the term $u_I \in V_h$ in Lemma 2.4.1, we have the following result which is an extension of Proposition 4.3 in Ref. [18] to less regular functions.

Proposition 2.4.2 *If the assumptions* **A0.2** *and* **A0.3** *are satisfied, then, for each s with $0 \leq s \leq k$, there exists a constant C, depending only on k, γ and $\widehat{\gamma}$, such that for every $v \in H^{1+s}(\Omega)$, there exists $v_I \in V_h$ that satisfies*

$$\|v - v_I\|_{0,\Omega} + h |v - v_I|_{1,\Omega} \leq C h^{1+s} \|v\|_{1+s,\Omega}.$$

Proof. Let $v \in H^{1+s}(\Omega)$, $0 \leq s \leq k$. Since we are assuming **A0.2**, let $v_\pi \in L^2(\Omega)$ be defined on each $K \in \mathcal{T}_h$ so that $v_\pi|_K \in \mathbb{P}_k(K)$ and the estimate of Proposition 2.4.1 holds true.

For each polygon $K \in \mathcal{T}_h$, consider the triangulation $\mathcal{T}_h^K$ obtained by joining each vertex of K with the midpoint of the ball with respect to which K is starred. Let $\widehat{\mathcal{T}}_h := \bigcup_{K\in\mathcal{T}_h} \mathcal{T}_h^K$. Since we are also assuming **A0.3**, $\left\{\widehat{\mathcal{T}}_h\right\}_h$ is a shape-regular family of triangulations of Ω.

Let v_c be the Clément interpolant of degree k of v over $\widehat{\mathcal{T}}_h$ (cf. Ref. [71]). Then, $v_\mathrm{c} \in H^1(\Omega)$ and the following error estimate follows by interpolation between Sobolev spaces from the analogous result for integer values of s (which in turn has been proved in Ref. [71]):

$$\|v - v_\mathrm{c}\|_{0,\Omega} + h\,|v - v_\mathrm{c}|_{1,\Omega} \leq Ch^{1+s}\,\|v\|_{1+s,\Omega}\,. \tag{2.8}$$

Now, for each $K \in \mathcal{T}_h$, we define $v_I|_K \in H^1(K)$ as the solution of the following problem:

$$\begin{cases} -\Delta v_I = -\Delta v_\pi & \text{in } K, \\ \quad v_I = v_\mathrm{c} & \text{on } \partial K. \end{cases}$$

Note that $v_I|_K \in V_k^K$. Moreover, although v_I is defined locally, since on the boundary of each element it coincides with v_c which belongs to $H^1(\Omega)$, we have that also v_I belongs to $H^1(\Omega)$ and, hence, $v_I \in V_h$.

According to the above definition we have that

$$\begin{cases} -\Delta(v_\pi - v_I) = 0 & \text{in } K, \\ \quad v_\pi - v_I = v_\pi - v_\mathrm{c} & \text{on } \partial K, \end{cases}$$

and, hence, it is easy to check that

$$|v_\pi - v_I|_{1,K} = \text{ínf}\left\{|z|_{1,K}\,,\ z \in H^1(K):\ z = v_\pi - v_\mathrm{c}\ \text{ on } \partial K\right\} \leq |v_\pi - v_\mathrm{c}|_{1,K}\,.$$

Therefore,

$$\begin{aligned} |v - v_I|_{1,K} \leq& |v - v_\pi|_{1,K} + |v_\pi - v_I|_{1,K} \leq |v - v_\pi|_{1,K} + |v_\pi - v_\mathrm{c}|_{1,K} \\ \leq& 2\,|v - v_\pi|_{1,K} + |v - v_\mathrm{c}|_{1,K}\,, \end{aligned}$$

which together with Proposition 2.4.1 and (2.8) lead to

$$|v - v_I|_{1,\Omega} \leq Ch^s\,\|v\|_{1+s,\Omega}\,. \tag{2.9}$$

On the other hand, for all $K \in \mathcal{T}_h$, each triangle $T \in \mathcal{T}_h^K$ has one edge on ∂K. Hence, since $v_I = v_\mathrm{c}$ on ∂K, a scaling argument and the classical Poincaré inequality yield

$$\|v_\mathrm{c} - v_I\|_{0,T} \leq Ch_K\,|v_\mathrm{c} - v_I|_{1,T}\,.$$

Thus, from the above inequality, (2.8) and (2.9), we have

$$\begin{aligned} \|v - v_I\|_{0,\Omega} &\leq \|v - v_\mathrm{c}\|_{0,\Omega} + \|v_\mathrm{c} - v_I\|_{0,\Omega} \leq \|v - v_\mathrm{c}\|_{0,\Omega} + Ch\,|v_\mathrm{c} - v_I|_{1,\Omega} \\ &\leq \|v - v_\mathrm{c}\|_{0,\Omega} + Ch\,|v - v_\mathrm{c}|_{1,\Omega} + Ch\,|v - v_I|_{1,\Omega} \\ &\leq Ch^{1+s}\,\|v\|_{1+s,\Omega}\,, \end{aligned}$$

which together with (2.9) allow us to conclude the proof. □

The following result yields the convergence in norm of T_h to T as $h \to 0$.

Lemma 2.4.2 *For all $r \in [\frac{1}{2}, r_\Omega)$, let $r_1 := \min\{r, 1\}$ as defined in Lemma 2.2.2(i). Then, there exists $C > 0$ such that*

$$\|(T - T_h) f\|_{1,\Omega} \leq C h^{r_1} \|f\|_{1,\Omega} \qquad \forall f \in H^1(\Omega).$$

Proof. The result follows from Lemma 2.4.1, Propositions 2.4.1 and 2.4.2, and Lemma 2.2.2(i). □

2.4.1. Error estimates

As a direct consequence of Lemma 2.4.2, standard results about spectral approximation (see Ref. [90], for instance) show that isolated parts of $\mathrm{sp}(T)$ are approximated by isolated parts of $\mathrm{sp}(T_h)$. More precisely, let $\mu \in (0, 1)$ be an isolated eigenvalue of T with multiplicity m and let $\mathcal{E}$ be its associated eigenspace. Then, there exist m eigenvalues $\mu_h^{(1)}, \ldots, \mu_h^{(m)}$ of T_h (repeated according to their respective multiplicities) which converge to μ. Let $\mathcal{E}_h$ be the direct sum of their corresponding associated eigenspaces.

We recall the definition of the *gap* $\widehat{\delta}$ between two closed subspaces $\mathcal{X}$ and $\mathcal{Y}$ of $H^1(\Omega)$:

$$\widehat{\delta}(\mathcal{X}, \mathcal{Y}) := \max\{\delta(\mathcal{X}, \mathcal{Y}), \delta(\mathcal{Y}, \mathcal{X})\},$$

where

$$\delta(\mathcal{X}, \mathcal{Y}) := \sup_{x \in \mathcal{X}:\ \|x\|_{1,\Omega}=1} \left(\inf_{y \in \mathcal{Y}} \|x - y\|_{1,\Omega} \right).$$

The following error estimates for the approximation of eigenvalues and eigenfunctions hold true.

Theorem 2.4.1 *There exists a strictly positive constant C such that*

$$\begin{aligned} \widehat{\delta}(\mathcal{E}, \mathcal{E}_h) &\leq C\gamma_h, \\ \left|\mu - \mu_h^{(i)}\right| &\leq C\gamma_h, \qquad i = 1, \ldots, m, \end{aligned}$$

where

$$\gamma_h := \sup_{f \in \mathcal{E}:\ \|f\|_{1,\Omega}=1} \|(T - T_h) f\|_{1,\Omega}.$$

Proof. As a consequence of Lemma 2.4.2, T_h converges in norm to T as h goes to zero. Then, the proof follows as a direct consequence of Theorems 7.1 and 7.3 from Ref. [15]. □

The theorem above yields error estimates depending on γ_h. The next step is to show an optimal order estimate for this term.

Theorem 2.4.2 *For all $r \in [\frac{1}{2}, r_\Omega)$ there exists a positive constant C such that*

$$\|(T - T_h) f\|_{1,\Omega} \leq C h^{\min\{r,k\}} \|f\|_{1,\Omega} \qquad \forall f \in \mathcal{E} \tag{2.10}$$

and, consequently,

$$\gamma_h \leq C h^{\min\{r,k\}}. \tag{2.11}$$

Proof. The proof is identical to that of Lemma 2.4.2, but using now the additional regularity from Lemma 2.2.2(ii). □

The error estimate for the eigenvalue $\mu \in (0,1)$ of T leads to an analogous estimate for the approximation of the eigenvalue $\lambda = \frac{1}{\mu} - 1$ of Problem 2.2.1 by means of the discrete eigenvalues $\lambda_h^{(i)} := \frac{1}{\mu_h^{(i)}} - 1$, $1 \leq i \leq m$, of Problem 2.3.1. However, the order of convergence in Theorem 2.4.1 is not optimal for μ and, hence, not optimal for λ either. Our next goal is to improve this order.

Theorem 2.4.3 *For all $r \in [\frac{1}{2}, r_\Omega)$, there exists a strictly positive constant C such that*

$$\left|\lambda - \lambda_h^{(i)}\right| \leq C h^{2\,\mín\{r,k\}}.$$

Proof. Let w_h be such that $(\lambda_h^{(i)}, w_h)$ is a solution of Problem 2.3.1 with $\|w_h\|_{1,\Omega} = 1$. According to Theorem 2.4.1, there exists a solution (λ, w) of Problem 2.2.1 such that

$$\|w - w_h\|_{1,\Omega} \leq C\gamma_h. \tag{2.12}$$

From the symmetry of the bilinear forms and the facts that $a(w,v) = \lambda b(w,v)$ for all $v \in H^1(\Omega)$ (cf. Problem 2.2.1) and $a_h(w_h, v_h) = \lambda_h^{(i)} b(w_h, v_h)$ for all $v_h \in V_h$ (cf. Problem 2.3.1), we have

$$\begin{aligned} a(w-w_h, w-w_h) - \lambda b(w-w_h, w-w_h) =& a(w_h, w_h) - \lambda b(w_h, w_h) \\ =& [a(w_h, w_h) - a_h(w_h, w_h)] \\ & - \left(\lambda - \lambda_h^{(i)}\right) b(w_h, w_h), \end{aligned}$$

from which we obtain the following identity:

$$\begin{aligned} \left(\lambda_h^{(i)} - \lambda\right) b(w_h, w_h) =& a(w-w_h, w-w_h) - \lambda b(w-w_h, w-w_h) \\ & + \left[a_h(w_h, w_h) - a(w_h, w_h)\right]. \end{aligned} \tag{2.13}$$

The next step is to bound each term on the right hand side above. The first and the second ones are easily bounded from the continuity of $a(\cdot,\cdot)$ and $b(\cdot,\cdot)$, the trace theorem, (2.12) and (2.11):

$$|a(w-w_h, w-w_h)| + \lambda\,|b(w-w_h, w-w_h)| \leq C h^{2\,\mín\{r,k\}}. \tag{2.14}$$

For the third term, we use (2.5) and (2.4a) to write:

$$
\begin{aligned}
&|a_h(w_h,w_h)-a(w_h,w_h)| \\
&= \left| \sum_{K\in\mathcal{T}_h} \left[a^K(\Pi_k^K w_h, \Pi_k^K w_h) + S^K\big(w_h-\Pi_k^K w_h, w_h-\Pi_k^K w_h\big)\right] - \sum_{K\in\mathcal{T}_h} a^K(w_h,w_h)\right| \\
&\leq \left| \sum_{K\in\mathcal{T}_h} \left[a^K\big(\Pi_k^K w_h, \Pi_k^K w_h\big) - a^K(w_h,w_h)\right]\right| \\
&\quad + \sum_{K\in\mathcal{T}_h} c_1\, a^K\big(w_h-\Pi_k^K w_h, w_h-\Pi_k^K w_h\big) \\
&= \sum_{K\in\mathcal{T}_h} \left[a^K\big(w_h-\Pi_k^K w_h, w_h-\Pi_k^K w_h\big)\right] + \sum_{K\in\mathcal{T}_h} c_1\, a^K(w_h-\Pi_k^K w_h, w_h-\Pi_k^K w_h) \\
&= \sum_{K\in\mathcal{T}_h} (1+c_1)\, a^K\big(w_h-\Pi_k^K w_h, w_h-\Pi_k^K w_h\big).
\end{aligned}
$$

Therefore, from the definition of $a^K(\cdot,\cdot)$ (cf. (2.2)) and the fact that Π_k^K is the projector defined by (2.4a), we obtain

$$
\begin{aligned}
|a_h(w_h,w_h)-a(w_h,w_h)| &\leq C \sum_{K\in\mathcal{T}_h} \left|w_h-\Pi_k^K w_h\right|_{1,K}^2 \\
&\leq C \sum_{K\in\mathcal{T}_h} \left|w_h-\Pi_k^K w\right|_{1,K}^2 \\
&\leq C \sum_{K\in\mathcal{T}_h} \Big(|w_h-w|_{1,K} + \left|w-\Pi_k^K w\right|_{1,K}\Big)^2.
\end{aligned}
$$

Now, also from (2.4a) it is immediate to check that

$$
\left|w-\Pi_k^K w\right|_{1,K} \leq |w-w_\pi|_{1,K} \qquad \forall w_\pi \in \mathbb{P}_k(K).
$$

Then, from the last two inequalities, Proposition 2.4.1, (2.12) and (2.11), we obtain

$$
|a_h(w_h,w_h)-a(w_h,w_h)| \leq C h^{2\,\mín\{r,k\}}.
$$

On the other hand, by virtue of Lemma 2.3.1 and the fact that $\lambda_h^{(i)} \to \lambda$ as h goes to zero, we know that there exists $C>0$ such that

$$
b(w_h,w_h) = \frac{\widehat{a}_h(w_h,w_h)}{\lambda_h^{(i)}+1} \geq \frac{\beta\,\|w_h\|_{1,\Omega}^2}{\lambda_h^{(i)}+1} \geq \frac{\beta}{C} > 0.
$$

By using this estimate to bound the left-hand side of (2.13) from below, together with the previous one and (2.14) for an upper bound of the right-hand side, we conclude that

$$
\left|\lambda-\lambda_h^{(i)}\right| \leq C h^{2\,\mín\{r,k\}}
$$

and we end the proof. □

2.4.2. Error estimates for the eigenfunctions on Γ_0.

Our next goal is to improve the error estimate for the trace of the eigenfunctions in the $L^2(\Gamma_0)$-norm. With this end, we will resort to a duality technique. Given $u \in H^1(\Omega)$ and $u_h \in V_h$, let $v \in H^1(\Omega)$ be the solution of the following problem:

$$\begin{cases} \Delta v = 0 \quad \text{in } \Omega, \\ \partial_n v + v = \begin{cases} u - u_h & \text{on } \Gamma_0, \\ 0 & \text{on } \Gamma_1. \end{cases} \end{cases}$$

By testing the first equation above with functions in $H^1(\Omega)$ and integrating by parts, we obtain

$$\widehat{a}(v,z) := \int_\Omega \nabla v \cdot \nabla z + \int_{\Gamma_0} vz = \int_{\Gamma_0} (u-u_h)z =: b(u-u_h, z) \qquad \forall z \in H^1(\Omega). \tag{2.15}$$

Therefore, $v = T(u-u_h)$, so that according to Lemma 2.2.2(i), for all $r \in [\frac{1}{2}, r_\Omega)$, $v \in H^{1+r_1}(\Omega)$ (recall that $r_1 := \min\{r, 1\}$) and

$$\|v\|_{1+r_1,\Omega} \le C \|u-u_h\|_{1,\Omega}. \tag{2.16}$$

The improved error estimate will be a consequence of the following result.

Lemma 2.4.3 *Let $f \in \mathcal{E}$ be an eigenfunction of the operator T. If $u = Tf$ and $u_h = T_h f$, then, for all $r \in [\frac{1}{2}, r_\Omega)$, there exists $C > 0$ such that*

$$\|(T - T_h)f\|_{0,\Gamma_0} = \|u - u_h\|_{0,\Gamma_0} \le C h^{r_1/2 + \min\{r,k\}} \|f\|_{1,\Omega}.$$

Proof. Let v be as defined above and $v_I \in V_h$ so that the estimate of Proposition 2.4.2 holds true. Testing (2.15) with $z = (u - u_h) \in H^1(\Omega)$, we obtain

$$\|u-u_h\|^2_{0,\Gamma_0} = \widehat{a}(u-u_h, v) = \widehat{a}(u-u_h, v-v_I) + \widehat{a}(u-u_h, v_I). \tag{2.17}$$

To bound the first term on the right-hand side above, we use the continuity of the bilinear form $\widehat{a}(\cdot,\cdot)$, Proposition 2.4.2 and (2.16):

$$\begin{aligned} \widehat{a}(u-u_h, v-v_I) &\le C \|u-u_h\|_{1,\Omega} \|v-v_I\|_{1,\Omega} \\ &\le C h^{r_1} \|u-u_h\|_{1,\Omega} \|v\|_{1+r_1,\Omega} \le C h^{r_1} \|u-u_h\|^2_{1,\Omega}. \end{aligned} \tag{2.18}$$

For the second term, we use that $\widehat{a}(u, v_h) = b(f, v_h) = \widehat{a}_h(u_h, v_h)$ for all $v_h \in V_h$ to write

$$\begin{aligned} \widehat{a}(u-u_h, v_I) =& \widehat{a}_h(u_h, v_I) - \widehat{a}(u_h, v_I) = \sum_{K \in \mathcal{T}_h} \left(a_h^K(u_h, v_I) - a^K(u_h, v_I) \right) \\ &= \sum_{K \in \mathcal{T}_h} \left(a^K(\Pi_k^K u_h, \Pi_k^K v_I) + S^K(u_h - \Pi_k^K u_h, v_I - \Pi_k^K v_I) - a^K(u_h, v_I) \right) \\ &= \sum_{K \in \mathcal{T}_h} \left(a^K(\Pi_k^K u_h - u_h, v_I - \Pi_k^K v_I) + S^K(u_h - \Pi_k^K u_h, v_I - \Pi_k^K v_I) \right), \end{aligned} \tag{2.19}$$

where we have used (2.4a) to derive the last equality.

Now, from the symmetry of $S^K(\cdot,\cdot)$, inequality (2.5) and the definition of $a^K(\cdot,\cdot)$, we have that $S^K(v_h, z_h) \leq c_1 \, |v_h|_{1,K} \, |z_h|_{1,K}$ for all $v_h, z_h \in V_k^K$ such that $\Pi_k^K v_h = \Pi_k^K z_h = 0$. We use this inequality to bound the second term on the right-hand side of (2.19):

$$\sum_{K\in\mathcal{T}_h} S^K(u_h - \Pi_k^K u_h, v_I - \Pi_k^K v_I) \leq c_1 \sum_{K\in\mathcal{T}_h} \left|u_h - \Pi_k^K u_h\right|_{1,K} \left|v_I - \Pi_k^K v_I\right|_{1,K}. \tag{2.20}$$

Using that Π_k^K is the projector defined by (2.4a), we have that

$$\begin{aligned}\left|u_h - \Pi_k^K u_h\right|_{1,K} &\leq \left|u_h - \Pi_k^K u\right|_{1,K} \\ &\leq |u_h - u|_{1,K} + |u - u_\pi|_{1,K} \qquad \forall u_\pi \in \mathbb{P}_k(K)\end{aligned}$$

and, analogously,

$$\left|v_I - \Pi_k^K v_I\right|_{1,K} \leq |v_I - v|_{1,K} + |v - v_\pi|_{1,K} \qquad \forall v_\pi \in \mathbb{P}_k(K).$$

Substituting these inequalities into (2.20) and using (2.10), Proposition 2.4.1 and Lemma 2.2.2(ii) (since $f \in \mathcal{E}$) for the former and Propositions 2.4.1 and 2.4.2 and (2.16) for the latter, we obtain

$$\sum_{K\in\mathcal{T}_h} S^K(u_h - \Pi_k^K u_h, v_I - \Pi_k^K v_I) \leq C h^{r_1+\min\{r,k\}} \|f\|_{1,\Omega} \|u - u_h\|_{1,\Omega}.$$

By repeating the same steps as above, we obtain a similar bound for the first term on the right hand side of (2.19):

$$\sum_{K\in\mathcal{T}_h} a^K(u_h - \Pi_k^K u_h, v_I - \Pi_k^K v_I) \leq C h^{r_1+\min\{r,k\}} \|f\|_{1,\Omega} \|u - u_h\|_{1,\Omega}.$$

Hence,

$$\widehat{a}(u - u_h, v_I) \leq C h^{r_1+\min\{r,k\}} \|f\|_{1,\Omega} \|u - u_h\|_{1,\Omega}.$$

The proof follows by substituting this inequality and (2.18) into (2.17) and using (2.10). □

The next step is to define a solution operator on the space $L^2(\Gamma_0)$:

$$\begin{aligned}\widetilde{T}: \; L^2(\Gamma_0) &\longrightarrow L^2(\Gamma_0), \\ \widetilde{f} &\longmapsto \widetilde{T}\widetilde{f} := u|_{\Gamma_0},\end{aligned}$$

where $u \in H^1(\Omega)$ is the solution of the following problem:

$$\widehat{a}(u, v) = \int_{\Gamma_0} \widetilde{f} v \qquad \forall v \in H^1(\Omega). \tag{2.21}$$

It is easy to check that the operator $\widetilde{T}$ is compact and self-adjoint. We also define the corresponding discrete solution operator:

$$\begin{aligned}\widetilde{T}_h: \; L^2(\Gamma_0) &\longrightarrow L^2(\Gamma_0), \\ \widetilde{f} &\longmapsto \widetilde{T}_h\widetilde{f} := u_h|_{\Gamma_0},\end{aligned}$$

where $u_h \in V_h$ is the solution of the discrete problem

$$\widehat{a}_h(u_h, v_h) = \int_{\Gamma_0} \widetilde{f} v_h \qquad \forall v_h \in V_h. \tag{2.22}$$

The spectra of T and $\widetilde{T}$ coincide. In fact, it is immediate to check that if $Tw = \mu w$, with $w \neq 0$ and $\mu \neq 0$, then $w|_{\Gamma_0} \neq 0$ and $\widetilde{T}(w|_{\Gamma_0}) = \mu w|_{\Gamma_0}$. Conversely, if $\widetilde{T}\widetilde{w} = \mu\widetilde{w}$, with $\widetilde{w} \neq 0$ and $\mu \neq 0$, then there exists $w \in H^1(\Omega)$, such that $Tw = \mu w$ and $w|_{\Gamma_0} = \widetilde{w}$. The same arguments allow us to show that the spectra of T_h and $\widetilde{T}_h$ also coincide and their respective eigenfunctions are related in the same way as those of T and $\widetilde{T}$.

To prove that the operators $\widetilde{T}_h$ converge in norm to $\widetilde{T}$, we will use the following additional regularity estimate analogous to that in Lemma 2.2.2 but that only involves $\|f\|_{0,\Gamma_0}$.

Lemma 2.4.4 *For all $s \in (0, \frac{1}{2})$, there exists $C > 0$ such that, for all $f \in L^2(\Gamma_0)$, the solution u of problem (2.21) satisfies $u \in H^{1+s}(\Omega)$ and*

$$\|u\|_{1+s,\Omega} \leq C \|f\|_{0,\Gamma_0}.$$

Proof. The proof is a consequence of Theorem 4 in Ref. [106]. □

Now, we are able to conclude the convergence in norm of $\widetilde{T}_h$ to $\widetilde{T}$.

Lemma 2.4.5 *For all $s \in (0, \frac{1}{2})$, there exists $C > 0$ such that*

$$\left\|(\widetilde{T} - \widetilde{T}_h)\widetilde{f}\right\|_{0,\Gamma_0} \leq Ch^s \left\|\widetilde{f}\right\|_{0,\Gamma_0}.$$

Proof. Given $\widetilde{f} \in L^2(\Gamma_0)$, let $u \in H^1(\Omega)$ and $u_h \in V_h$ be the solutions of problems (2.21) and (2.22), respectively, so that $\widetilde{T}\widetilde{f} = u|_{\Gamma_0}$ and $\widetilde{T}_h\widetilde{f} = u_h|_{\Gamma_0}$. The arguments used in the proof of Lemma 2.4.1 can be repeated in this case yielding

$$\|u - u_h\|_{1,\Omega} \leq C \left(\|u - u_I\|_{1,\Omega} + |u - u_\pi|_{1,h} \right),$$

with u_I and u_π as in that lemma. Thus, the result follows from Propositions 2.4.1 and 2.4.2, and Lemma 2.4.4. □

As a consequence of this lemma, a spectral convergence result analogous to Theorem 2.4.1 holds for $\widetilde{T}_h$ and $\widetilde{T}$. Moreover, we are in a position to establish the following estimate.

Theorem 2.4.4 *Let w_h be an eigenfunction of T_h associated with the eigenvalue $\mu_h^{(i)}$, $1 \leq i \leq m$, with $\|w_h\|_{0,\Gamma_0} = 1$. Then, there exists an eigenfunction w of T associated with μ such that, for all $r \in [\frac{1}{2}, r_\Omega)$, there exists $C > 0$ such that*

$$\|w - w_h\|_{0,\Gamma_0} \leq Ch^{r_1/2 + \min\{r,k\}}.$$

Proof. Thanks to Lemma 2.4.5, Theorem 7.1 from Ref. [15] yields spectral convergence of $\widetilde{T}_h$ to $\widetilde{T}$. In particular, because of the relation between the eigenfunctions of T and T_h with those of $\widetilde{T}$ and $\widetilde{T}_h$, respectively, we have that $w_h|_{\Gamma_0} \in \widetilde{\mathcal{E}}_h$ and there exists $w \in \mathcal{E}$ such that

$$\|w - w_h\|_{0,\Gamma_0} \leq C \sup_{\widetilde{f} \in \widetilde{\mathcal{E}}:\ \|\widetilde{f}\|_{0,\Gamma_0} = 1} \left\|(\widetilde{T} - \widetilde{T}_h)\widetilde{f}\right\|_{0,\Gamma_0}. \tag{2.23}$$

On the other hand, because of Lemma 2.4.3, for all $\widetilde{f} \in \widetilde{\mathcal{E}}$, if $f \in \mathcal{E}$ is such that $\widetilde{f} = f|_{\Gamma_0}$, then

$$\left\|(\widetilde{T} - \widetilde{T}_h)\widetilde{f}\right\|_{0,\Gamma_0} = \|(T - T_h)f\|_{0,\Gamma_0} \leq Ch^{r_1/2+\min\{r,k\}} \|f\|_{1,\Omega}.$$

Now, for $f \in \mathcal{E}$, $Tf = \mu f$. Hence, $\|f\|_{1,\Omega} = \frac{1}{\mu}\|Tf\|_{1,\Omega} \leq C\|f\|_{0,\Gamma_0}$ (cf. Lemma 2.4.4). Thus, substituting this expressions into the previous inequality, we have that

$$\left\|(\widetilde{T} - \widetilde{T}_h)\widetilde{f}\right\|_{0,\Gamma_0} \leq Ch^{r_1/2+\min\{r,k\}} \left\|\widetilde{f}\right\|_{0,\Gamma_0},$$

which together with (2.23) allow us to conclude the proof. □

Remark 2.4.1 *The result above is actually an improved error estimate in $L^2(\Gamma_0)$-norm as compared with the obviously one $\|w - w_h\|_{0,\Gamma_0} \leq Ch^{\min\{r,k\}}$ which follows from Theorems 2.4.1 and 2.4.2 and the trace Theorem.*

2.5. Numerical results

We report in this section some numerical examples which have allowed us to assess the theoretical results proved above. With this aim, we have implemented in a MATLAB code a lowest-order VEM ($k = 1$) on arbitrary polygonal meshes, by following the ideas proposed in Ref. [22].

To complete the choice of the VEM, we had to fix the bilinear forms $S^K(\cdot,\cdot)$ satisfying (2.5) to be used. To do this, we have proceeded as in Ref. [18]: for each polygon K with vertices $P_1, \ldots, P_{N_K}$, we have used

$$S^K(u,v) := \sigma_K \sum_{i=1}^{N_K} u(P_i)v(P_i), \qquad u, v \in V_1^K, \tag{2.24}$$

where σ_K is the so-called *stability constant* that can be chosen freely as far as it satisfy

$$0 < \sigma_* \leq \sigma_K \leq \sigma^*, \tag{2.25}$$

with the two constants σ_* and σ^* independent of h and the particular element K.

As stated in Section 4.6 of Ref. [18], under assumption **AO.3**, this choice of $S^K(\cdot,\cdot)$ satisfies (2.5).

2.5.1. Test 1: Sloshing in a square domain.

In this test, we have taken $\Omega := (0,1)^2$, with Γ_0 and Γ_1 as shown in Figure 2.1.

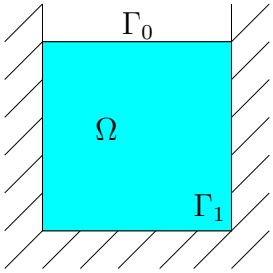

Figura 2.1: Sloshing in a square domain.

This problem corresponds to the computation of the sloshing modes of a two-dimensional fluid contained in Ω with a horizontal free surface Γ_0. The analytical solutions of this problem are

$$\lambda_n = n\pi \tanh(n\pi), \qquad w_n(x,y) = \cos(n\pi x)\sinh(n\pi y), \qquad n \in \mathbb{N}.$$

We have taken $\sigma_K = 1$ in (2.24). We have used three different families of meshes (see Figure 2.2):

- $\mathcal{T}_h^1$: triangular meshes, considering the middle point of each edge as a new degree of freedom;
- $\mathcal{T}_h^2$: trapezoidal meshes which consist of partitions of the domain into $N \times N$ congruent trapezoids, all similar to the trapezoid with vertexes $(0,0)$, $(\frac{1}{2},0)$, $(\frac{1}{2},\frac{2}{3})$, and $(0,\frac{1}{3})$;
- $\mathcal{T}_h^3$: meshes built from $\mathcal{T}_h^1$ with the edge midpoint moved randomly; note that these meshes contain non-convex elements.

The refinement parameter N used to label each mesh is the number of elements on each edge.

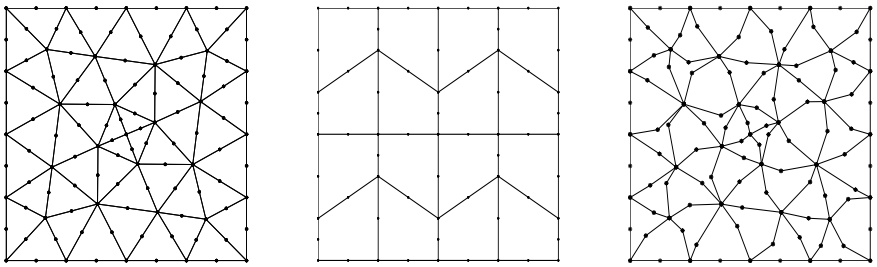

Figura 2.2: Test 1. Sample meshes: $\mathcal{T}_h^1$ (left), $\mathcal{T}_h^2$ (middle) and $\mathcal{T}_h^3$ (right) for $N = 4$.

We report in Table 2.1 the lowest eigenvalues λ_{hi} computed with this method. The table also includes the estimated orders of convergence. The exact eigenvalues are also reported in the last column to allow for comparison.

Cuadro 2.1: Test 1. Computed lowest eigenvalues λ_{hi}, $1 \leq i \leq 3$, on different meshes.

$\mathcal{T}_h$	λ_{hi}	$N = 16$	$N = 32$	$N = 64$	$N = 128$	Order	λ_i
$\mathcal{T}_h^1$	λ_{h1}	3.1330	3.1306	3.1301	3.1299	2.03	3.1299
	λ_{h2}	6.3095	6.2894	6.2846	6.2835	2.07	6.2831
	λ_{h3}	9.5183	9.4459	9.4298	9.4260	2.09	9.4248
$\mathcal{T}_h^2$	λ_{h1}	3.1424	3.1331	3.1307	3.1301	1.98	3.1299
	λ_{h2}	6.3765	6.3095	6.2900	6.2849	1.92	6.2831
	λ_{h3}	9.6929	9.5092	9.4475	9.4306	1.85	9.4248
$\mathcal{T}_h^3$	λ_{h1}	3.1331	3.1308	3.1301	3.1299	2.03	3.1299
	λ_{h2}	6.3105	6.2896	6.2847	6.2835	2.05	6.2831
	λ_{h3}	9.5193	9.4470	9.4300	9.4261	2.06	9.4248

It can be seen from Table 2.1 that the computed eigenvalues converge to the exact ones with an optimal quadratic order as predicted by the theory.

We report in Table 2.2 the $L^2(\Gamma_0)$-errors of the eigenfunctions corresponding to the lowest eigenvalue for each family of meshes and different refinement levels. We also include in this table the estimated orders of convergence.

Cuadro 2.2: Test 1. Errors $\|w - w_h\|_{0,\Gamma_0}$ of the vibration mode for the lowest eigenvalue λ_{h1} on different meshes.

$\mathcal{T}_h$	$N = 8$	$N = 16$	$N = 32$	$N = 64$	Order
$\mathcal{T}_h^1$	3.633e-3	8.715e-4	2.265e-4	5.567e-5	2.00
$\mathcal{T}_h^2$	2.507e-2	5.939e-3	1.445e-3	3.558e-4	2.05
$\mathcal{T}_h^3$	4.559e-3	9.943e-4	2.576e-4	6.592e-5	2.03

We observe from this table a clear quadratic order of convergence. Let us remark that this is the optimal order attainable with the virtual elements used, which is actually larger than the order $\mathcal{O}(h^{3/2})$ predicted by the theory.

Figure 2.3 shows the eigenfunctions on Γ_0 corresponding to the three lowest eigenvalues. Let us remark that, in the sloshing problem, this corresponds to the shape of the fluid free surface ($\partial_n w = \lambda w$) for each sloshing mode.

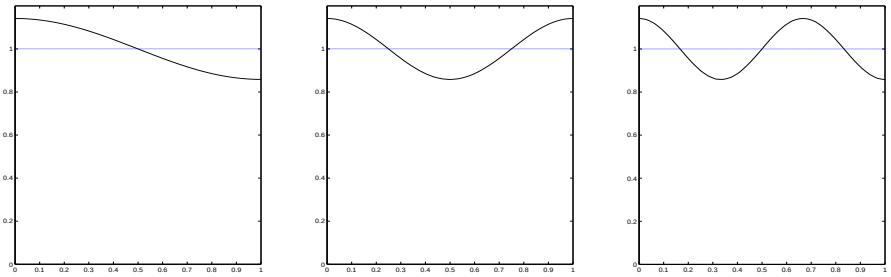

Figura 2.3: Test 1. Sloshing modes: w_{h1} (left), w_{h2} (middle) and w_{h3} (right) computed with $N = 256$.

2.5.2. Test 2: Effect of the stability.

The aim of this test is to analyze the influence of the *stability constant* σ_K in (2.24) on the computed spectrum. We will show that the introduction of the stability terms S_K in (2.6) leads to spurious eigenvalues. We will also show that these spurious eigenvalues can be driven by appropiately choosing the stability constant σ_K. If the same value of σ_K is chosen for all $K \in \mathcal{T}_h$ (as in the previous test), roughly speaking, the spurious eigenvalues will be proportional to this stability constant. This can be seen from Table 2.3, where we report the lowest eigenvalues computed by the method with varying values of σ_K on a fixed mesh $\mathcal{T}_h^1$ with refinement level $N = 8$ (see Figure 2.2, left).

The table also includes on the last column the three lowest exact eigenvalues. The computed eigenvalues into boxes correspond to approximations of these physical eigenvalues, whereas the rest correspond to spurious spectrum.

Cuadro 2.3: Test 2. Computed lowest eigenvalues for $\sigma_K = 4^{-k}$ with $-3 \leq k \leq 3$.

$\sigma_K = 1/64$	$\sigma_K = 1/16$	$\sigma_K = 1/4$	$\sigma_K = 1$	$\sigma_K = 4$	$\sigma_K = 16$	$\sigma_K = 64$	λ_i
1.517	3.078	3.101	3.142	3.175	3.189	3.193	3.1299
1.531	5.563	6.065	6.393	6.668	6.784	6.819	6.2831
1.587	5.646	8.716	9.788	10.755	11.181	11.309	9.4248
1.693	5.824	11.020	13.487	15.948	17.105	17.460	
1.715	5.903	12.878	17.494	22.298	24.551	25.235	
2.171	6.368	14.527	22.314	30.464	34.046	35.093	
2.180	6.537	15.731	27.513	39.415	43.831	45.055	
2.196	7.806	16.752	33.436	44.896	49.191	50.407	
2.214	8.134	18.433	41.706	113.899	405.657	1573.904	
3.071	8.251	19.318	49.196	141.263	501.449	1941.283	
5.834	8.409	21.881	61.343	183.830	655.050	2534.774	
8.037	8.607	23.403	72.371	231.747	844.138	3285.114	
9.645	10.182	27.705	85.040	282.392	1051.315	4119.669	
10.747	11.494	28.317	92.654	324.962	1237.860	4883.585	
11.080	12.064	29.445	99.697	358.294	1377.508	5448.886	
11.712	12.800	29.840	101.609	369.180	1426.727	5652.202	

For $\sigma_K \geq 1$ we observe that the lowest computed eigenvalues are correct approximations of the physical ones, whereas the largest are spurious and behave roughly speaking proportional to σ_K as claimed above. For values of $\sigma_K < 1$, the spurious eigenvalues appear interspersed among the correct ones, which makes it hard to distinguish spurious and physical eigenvalues. For very small values of σ_K, the spurious eigenvalues become even smaller than the physical ones, as can be seen on the first column of Table 2.3 for $\sigma_K = 1/64$.

The above analysis suggests to use sufficiently large σ_K in order to avoid the correct spectrum to be polluted. This phenomenon seems to contradict the theoretical analysis: spurious eigenvalues should not appear, when there is convergence in norm as was shown to happen in our case (see Lemma 2.4.2). However, this assertion is of an asymptotic nature: spurious eigenvalues will not appear interspersed among the correct spectrum for h small enough. In fact, this is what happens in our case as is shown in Table 2.4. In this table we report the eigenvalues computed only with the smallest σ_K of the previous experiment, but with increasingly refined meshes.

Cuadro 2.4: Test 2. Computed lowest eigenvalues for $\sigma_K = 1/64$.

$N = 4$	$N = 8$	$N = 16$	$N = 32$	$N = 64$	λ_i
0.747	1.517	2.929	3.126	3.129	3.1299
0.801	1.530	2.975	5.854	6.276	6.2831
0.874	1.587	3.033	5.901	9.399	9.4248
1.096	1.693	3.044	5.931	11.703	
1.098	1.715	3.056	5.981	11.752	
2.898	2.171	3.114	5.987	11.815	
4.760	2.180	3.150	5.990	11.857	
5.425	2.196	3.260	6.046	11.890	
	2.214	3.367	6.109	11.897	
	3.071	3.394	6.140	11.915	
	5.834	3.407	6.220	11.952	
	8.037	3.482	6.252	11.976	
	9.645	3.569	6.404	11.991	
	10.747	3.626	6.438	12.033	
	11.080	4.367	6.446	12.179	
	11.712	4.382	6.469	12.185	
		4.389	6.516	12.199	
		4.401	6.618	12.312	
		6.158	6.827	12.463	

The table shows that the spurious eigenvalues are also roughly speaking proportional to $1/h$, so that they blow up as the mesh is refined. For instance, for the most refined mesh reported in Table 2.4 (N=64), the three lowest correct eigenvalues are not polluted by the spurious ones.

This analysis suggests, that the user of VEM for spectral problems, has to be aware of the risk of spurious eigenvalue pollution. The way of minimizing this risk is to take a reasonably large σ_K (which will depend, in real problems, on the value of the physical constants) and sufficiently refined meshes. Moreover, the spurious character of an eigenvalue can be easily checked from its dependence on σ_K and the mesh.

2.5.3. Test 3: Circular Domain.

In this test, we have taken as domain the unit circle $\Omega := \left\{(x, y) \in \mathbb{R}^2 : x^2 + y^2 < 1\right\}$ with $\Gamma_0 = \partial\Omega$ and $\Gamma_1 = \emptyset$.

It is easy to check that any homogeneous harmonic polynomial of degree n satisfies $\partial_n w = nw$ on $\partial\Omega$. Therefore, for all $n \in \mathbb{N}$, $\lambda = n$ is an eigenvalue of this problem and the corresponding eigenspace is the set of homogeneous harmonic polynomials of degree n, whose dimension is 2.

We have taken $\sigma_K = 1$ in (2.24). We have used polygonal meshes created with Polymesher [113], as that shown in Figure 2.4. The refinement parameter N used to label each mesh is now the number of elements intersecting the boundary.

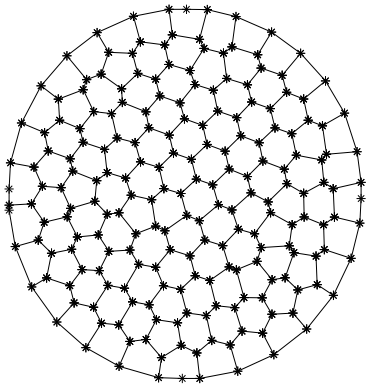

Figura 2.4: Test 3. Sample Polygonal mesh for $N = 29$.

We report in Table 2.5 the four lowest eigenvalues λ_{hi} computed with this method. The table also includes the estimated orders of convergence. The last column shows the exact eigenvalues.

Cuadro 2.5: Test 3. Computed lowest eigenvalues λ_{hi}, $1 \leq i \leq 4$.

λ_{hi}	$N = 8$	$N = 30$	$N = 104$	$N = 342$	Order	λ_i
λ_{h1}	0.9509	0.9960	0.9997	1.0000	1.97	1
λ_{h2}	0.9762	0.9971	0.9997	1.0000	1.81	1
λ_{h3}	1.9528	1.9957	1.9997	2.0000	1.91	2
λ_{h4}	2.0601	2.0002	1.9998	2.0000	1.89	2

Once more, a quadratic order of convergence can be clearly appreciated from Table 2.5. Finally, Figure 2.5 shows a plot of the eigenfunctions computed with the finest mesh.

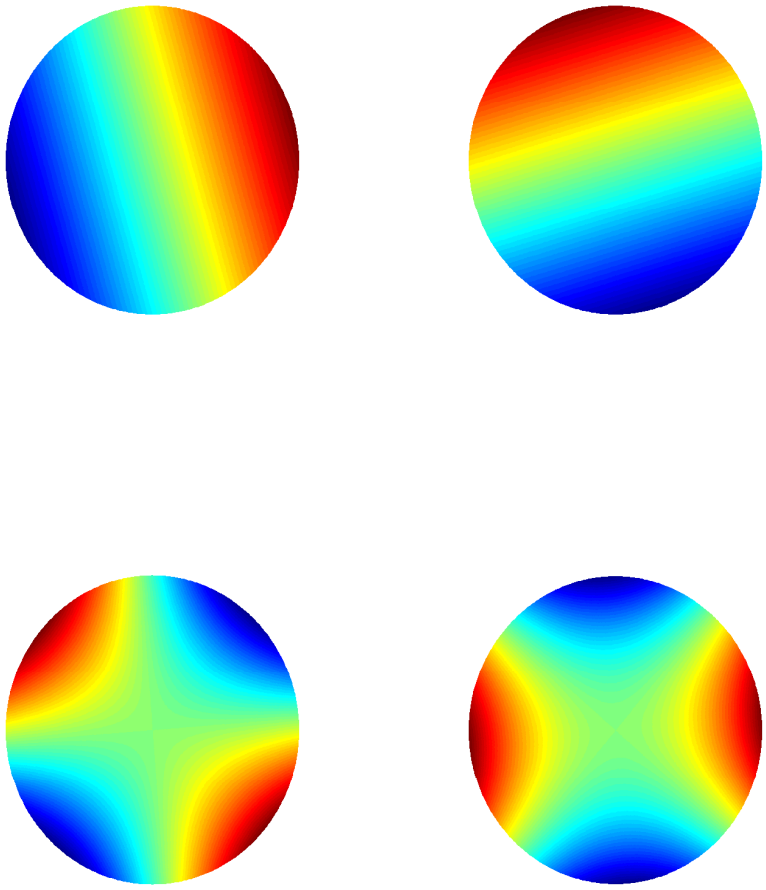

Figura 2.5: Test 3. Eigenfunctions: w_{h1} (upper left), w_{h2} (upper right), w_{h3} (lower left) and w_{h4} (lower right) computed with a very refined mesh ($N = 342$).

In order to compute the $L^2(\Gamma_0)$-errors, some special care had to be taken because of the double multiplicity of each eigenvalue. We focused on the eigenvalue $\lambda_3 = \lambda_4 = 2$, whose corresponding eigenspace is spanned by the eigenfunctions $w_3(x, y) = xy$ and $w_4(x, y) = x^2 - y^2$. As can be seem from Figure 2.5 (down), the computed eigenfunctions are not necessarily w_3 or w_4, but linear combination of these two. To isolate one particular eigenfunction, we took advantage of the symmetry of the domain and solved the problem in the quarter $x, y > 0$ of the unit circle. Thus, to compute $w_3(x, y) = xy$, which vanishes on $x = 0$ and $y = 0$, we imposed these values as homogeneous Dirichlet data of the problem. Proceeding in this way, we could ensure that the computed eigenfunction was actually an approximation of w_3.

Another difficulty of this test is that the curved domain is approximated by a polygonal one, so that the boundary values of these computed eigenfunctions are defined on the polygonal domain, whereas those of the exact eigenfunctions are given on the curved domain. To avoid these drawback, we projected the latter onto the polygonal domain.

We report in Table 2.6 the $L^2(\Gamma_0)$-errors computed as described above on the curved boundary of the quarter of circle by using again polygonal meshes obtained with Polymesher, similar to that shown in Figure 2.4, but for the quarter of circle. We also include in this table the computed order of convergence which, once more, is clearly quadratic.

Cuadro 2.6: Test 3. $L^2(\Gamma_0)$-errors of the eigenfunction $w_3(x, y) = xy$ on different polygonal meshes.

$N = 9$	$N = 37$	$N = 117$	$N = 379$	Order
3.485e-3	4.354e-4	2.970e-5	1.672e-6	2.06

Capítulo 3

A posteriori error estimates for a Virtual Elements Method for the Steklov eigenvalue problem.

3.1. Introduction

The *Virtual Element Method* (VEM), introduced in [18, 22], is a recent generalization of the Finite Element Method, which is characterized by the capability of dealing with very general polygonal/polyhedral meshes. The interest in numerical methods that can make use of general polytopal meshes has recently undergone a significant growth in the mathematical and engineering literature; among the large number of papers on this subject, we cite as a minimal sample [18, 29, 60, 76, 104, 109, 112]. Indeed, polytopal meshes can be very useful for a wide range of reasons including meshing of the domain, automatic use of hanging nodes, moving meshes and adaptivity. VEM has been applied successfully in a large range of problems; see for instance [3, 6, 14, 18, 22, 30, 35, 36, 38, 58, 84, 97, 100, 101].

The object of this paper is to introduce and analyze an a posteriori error estimator of residual type for the virtual element approximation of the Steklov eigenvalue problem. In fact, due to the large flexibility of the meshes to which the virtual element method is applied, mesh adaptivity becomes an appealing feature as mesh refinement strategies can be implemented very efficiently. For instance, hanging nodes can be introduced in the mesh to guarantee the mesh conformity without spreading the refined zones. In fact hanging nodes introduced by the refinement of a neighboring element are simply treated as new nodes since adjacent non matching element interfaces are perfectly acceptable. On the other hand, polygonal cells with very general shapes are admissible thus allowing us to adopt simple mesh coarsening algorithms.

The approximation of eigenvalue problems has been the object of great interest from both the practical and theoretical points of view, since they appear in many applications. We refer to [48] and the references therein for the state of art in this subject area. In particular, the Steklov eigenvalue problem, which involves the Laplace operator but is characterized by the presence of the eigenvalue in the boundary condition, appears in many applications; for example, the study

of the vibration modes of a structure in contact with an incompressible fluid (see [45]) and the analysis of the stability of mechanical oscillators immersed in a viscous media (see [102]). One of its main applications arises from the dynamics of liquids in moving containers, i.e., sloshing problems (see [46, 59, 65, 68, 80, 117]).

On the other hand, adaptive mesh refinement strategies based on a posteriori error indicators play a relevant role in the numerical solution of partial differential equations in a general sense. For instance, they guarantee achieving errors below a tolerance with a reasonable computer cost in presence of singular solutions. Several approaches have been considered to construct error estimators based on the residual equations (see [4, 78, 116] and the references therein). In particular, for the Steklov eigenvalue we mention [9, 10, 73, 85, 119]. On the other hand, the design and analyses of a posteriori error bounds for the VEM is a challenging task. References [34, 61] are the only a posteriori error analyses for VEM currently available in the literature. In [34], a posteriori error bounds for the C^1-conforming VEM for the two-dimensional Poisson problem are proposed. In [61], a posteriori error bounds for the C^0-conforming VEM introduced in [63] for the discretization of second order linear elliptic reaction-convection-diffusion problems with non constant coefficients in two and three dimensions are introduced.

We have recently developed in [97] a virtual element method for the Steklov eigenvalue problem. Under standard assumptions on the computational domain, we have established that the resulting scheme provides a correct approximation of the spectrum and proved optimal order error estimates for the eigenfunctions and a double order for the eigenvalues. In order to exploit the capability of VEM in the use of general polygonal meshes and its flexibility for the application of mesh adaptive strategies, we introduce and analyze an a posteriori error estimator for the virtual element approximation introduced in [97]. Since normal fluxes of the VEM solution are not computable, they will be replaced in the estimators by a proper projection. As a consequence of this replacement, new additional terms appear in the a posteriori error estimator, which represent the virtual inconsistency of VEM. Similar terms also appear in the other papers for a posteriori error estimates of VEM (see [34, 61]). We prove that the error estimator is equivalent to the error and use the corresponding indicator to drive an adaptive scheme.

The outline of this article is as follows: in Section 3.2 we present the continuous and discrete formulations of the Steklov eigenvalue problem together with the spectral characterization. Then, we recall the a priori error estimates for the virtual element approximation analyzed in [97]. In Section 3.3, we define the a posteriori error estimator and proved its reliability and efficiency. Finally, in Section 3.4, we report a set of numerical tests that allow us to assess the performance of the estimator when combined with an adaptive strategy. We have also made a comparison between the proposed estimator and the standard edge-residual error estimator for a finite element method.

Throughout the article we will use standard notations for Sobolev spaces, norms and semi-norms. Moreover, we will denote by C a generic constant independent of the mesh parameter h, which may take different values in different occurrences.

3.2. The Steklov eigenvalue problem and its virtual element approximation

Let $\Omega \subset \mathbb{R}^2$ be a bounded domain with polygonal boundary $\partial\Omega$. Let Γ_0 and Γ_1 be disjoint open subsets of $\partial\Omega$ such that $\partial\Omega = \bar{\Gamma}_0 \cup \bar{\Gamma}_1$ and $|\Gamma_0| \neq 0$. We denote by n the outward unit normal vector to $\partial\Omega$.

We consider the following eigenvalue problem:

Find $(\lambda, w) \in \mathbb{R} \times H^1(\Omega)$, $w \neq 0$, such that

$$\begin{cases} \Delta w = 0 \quad \text{in } \Omega, \\ \dfrac{\partial w}{\partial n} = \begin{cases} \lambda w & \text{on } \Gamma_0, \\ 0 & \text{on } \Gamma_1. \end{cases} \end{cases}$$

By testing the first equation above with $v \in H^1(\Omega)$ and integrating by parts, we arrive at the following equivalent weak formulation:

Problem 3.2.1 *Find $(\lambda, w) \in \mathbb{R} \times H^1(\Omega)$, $w \neq 0$, such that*

$$\int_\Omega \nabla w \cdot \nabla v = \lambda \int_{\Gamma_0} wv \qquad \forall v \in H^1(\Omega).$$

According to [97, Theorem 2.1], we know that the solutions (λ, w) of the problem above are:

- $\lambda_0 = 0$, whose associated eigenspace is the space of constant functions in Ω;
- a sequence of positive finite-multiplicity eigenvalues $\{\lambda_k\}_{k\in\mathbb{N}}$ such that $\lambda_k \to \infty$.

The eigenfunctions corresponding to different eigenvalues are orthogonal in $L^2(\Gamma_0)$. Therefore the eigenfunctions w^k corresponding to $\lambda_k > 0$ satisfy

$$\int_{\Gamma_0} w^k = 0. \tag{3.1}$$

We denote the bounded bilinear symmetric forms appearing in Problem 3.2.1 as follows:

$$a(w, v) := \int_\Omega \nabla w \cdot \nabla v, \qquad w, v \in H^1(\Omega),$$
$$b(w, v) := \int_{\Gamma_0} wv, \qquad w, v \in H^1(\Omega).$$

Let $\{\mathcal{T}_h\}_h$ be a sequence of decompositions of Ω into polygons K. Let h_K denote the diameter of the element K and h the maximum of the diameters of all the elements of the mesh, i.e., $h := \max_{K\in\mathcal{T}_h} h_K$.

For the analysis, we will make as in [18, 97] the following assumptions.

- **A1.** Every mesh $\mathcal{T}_h$ consists of a finite number of *simple* polygons (i.e., open simply connected sets with non self intersecting polygonal boundaries).

- **A2.** There exists $\gamma > 0$ such that, for all meshes $\mathcal{T}_h$, each polygon $K \in \mathcal{T}_h$ is star-shaped with respect to a ball of radius greater than or equal to γh_K.
- **A3.** There exists $\widehat{\gamma} > 0$ such that, for all meshes $\mathcal{T}_h$, for each polygon $K \in \mathcal{T}_h$, the distance between any two of its vertices is greater than or equal to $\widehat{\gamma} h_K$.

We consider now a simple polygon K and, for $k \in \mathbb{N}$, we define

$$\mathbb{B}_k(\partial K) := \left\{ v \in C^0(\partial K) : \ v|_\ell \in \mathbb{P}_k(\ell) \text{ for all edges } \ell \subset \partial K \right\}.$$

We then consider the finite-dimensional space defined as follows:

$$V_k^K := \left\{ v \in \mathrm{H}^1(K) : \ v|_{\partial K} \in \mathbb{B}_k(\partial K) \text{ and } \Delta v|_K \in \mathbb{P}_{k-2}(K) \right\}, \tag{3.2}$$

where, for $k = 1$, we have used the convention that $\mathbb{P}_{-1}(K) := \{0\}$. We choose in this space the degrees of freedom introduced in [18, Section 4.1]. Finally, for every decomposition $\mathcal{T}_h$ of Ω into simple polygons K and for a fixed $k \in \mathbb{N}$, we define

$$V_h := \left\{ v \in H^1(\Omega) : \ v|_K \in V_k^K \quad \forall K \in \mathcal{T}_h \right\}.$$

In what follows, we will use standard Sobolev spaces, norms and seminorms and also the broken H^1-seminorm

$$|v|_{1,h}^2 := \sum_{K \in \mathcal{T}_h} \|\nabla v\|_{0,K}^2 ,$$

which is well defined for every $v \in L^2(\Omega)$ such that $v|_K \in \mathrm{H}^1(E)$ for each polygon $K \in \mathcal{T}_h$.

We split the bilinear form $a(\cdot,\cdot)$ as follows:

$$a(u,v) = \sum_{K \in \mathcal{T}_h} a^K(u,v), \qquad u, v \in H^1(\Omega),$$

where

$$a^K(u,v) := \int_K \nabla u \cdot \nabla v, \qquad u, v \in \mathrm{H}^1(E).$$

Due to the implicit space definition, we must have into account that we would not know how to compute $a^K(\cdot,\cdot)$ for $u_h, v_h \in V_h$. Nevertheless, the final output will be a local matrix on each element K whose associated bilinear form can be exactly computed whenever one of the two entries is a polynomial of degree k. This will allow us to retain the optimal approximation properties of the space V_h.

With this end, for any $K \in \mathcal{T}_h$ and for any sufficiently regular function φ, we define first

$$\overline{\varphi} := \frac{1}{N_K} \sum_{i=1}^{N_K} \varphi(P_i),$$

where P_i, $1 \le i \le N_K$, are the vertices of K. Then, we define the projector $\Pi_k^K : V_k^K \longrightarrow \mathbb{P}_k(K) \subseteq V_k^K$ for each $v_h \in V_k^K$ as the solution of

$$\begin{aligned} a^K\left(\Pi_k^K v_h, q\right) &= a^K(v_h, q) \qquad \forall q \in \mathbb{P}_k(K), \\ \overline{\Pi_k^K v_h} &= \overline{v_h}. \end{aligned}$$

On the other hand, let $S^K(\cdot,\cdot)$ be any symmetric positive definite bilinear form to be chosen as to satisfy

$$c_0\, a^K(v_h, v_h) \leq S^K(v_h, v_h) \leq c_1\, a^K(v_h, v_h) \qquad \forall v_h \in V_k^K \text{ with } \Pi_k^K v_h = 0 \tag{3.4}$$

for some positive constants c_0 and c_1 independent of K. Then, set

$$a_h(u_h, v_h) := \sum_{K\in\mathcal{T}_h} a_h^K(u_h, v_h), \qquad u_h, v_h \in V_h,$$

where $a_h^K(\cdot,\cdot)$ is the bilinear form defined on $V_k^K \times V_k^K$ by

$$a_h^K(u_h, v_h) := a^K\big(\Pi_k^K u_h, \Pi_k^K v_h\big) + S^K\big(u_h - \Pi_k^K u_h, v_h - \Pi_k^K v_h\big), \qquad u_h, v_h \in V_k^K.$$

Notice that the bilinear form $S^K(\cdot,\cdot)$ has to be actually computable for $u_h, v_h \in V_k^K$.

The following properties of $a_h^K(\cdot,\cdot)$ have been established in [18, Theorem 4.1].

- *k-Consistency*:

$$a_h^K(p, v_h) = a^K(p, v_h) \qquad \forall p \in \mathbb{P}_k(K), \quad \forall v_h \in V_k^K. \tag{3.5}$$

- *Stability*: There exist two positive constants α_* and α^*, independent of K, such that:

$$\alpha_* a^K(v_h, v_h) \leq a_h^K(v_h, v_h) \leq \alpha^* a^K(v_h, v_h) \qquad \forall v_h \in V_k^K. \tag{3.6}$$

Now, we are in a position to write the virtual element discretization of Problem 3.2.1.

Problem 3.2.2 *Find* $(\lambda_h, w_h) \in \mathbb{R} \times V_h$, $w_h \neq 0$, *such that*

$$a_h(w_h, v_h) = \lambda_h b(w_h, v_h) \qquad \forall v_h \in V_h.$$

According to [97, Theorem 3.1] we know that the solutions (λ_h, w_h) of the problem above are:

- $\lambda_{h0} = 0$, whose associated eigenfunction are the constant functions in Ω.
- $\{\lambda_{hk}\}_{k=1}^{N_h}$, with $N_h := \dim\left(\{v_h|_{\Gamma_0},\, v_h \in V_h\}\right) - 1$, which are non-defective positive eigenvalues repeated according to their respective multiplicities.

Moreover, the eigenfunctions corresponding to different eigenvalues are orthogonal in $L^2(\Gamma_0)$. Therefore the eigenfunctions w_h^k corresponding to $\lambda_{hk} > 0$ satisfy

$$\int_{\Gamma_0} w_h^k = 0. \tag{3.7}$$

Let (λ, w) be a solution to Problem 3.2.1. We assume $\lambda > 0$ is a simple eigenvalue and we normalize w so that $\|w\|_{0,\Gamma_0} = 1$. Then, for each mesh $\mathcal{T}_h$, there exists a solution (λ_h, w_h) of

Problem 3.2.2 such that $\lambda_h \to \lambda$, $\|w_h\|_{0,\Gamma_0} = 1$ and $\|w - w_h\|_{1,\Omega} \to 0$ as $h \to 0$. Moreover, according to (3.1) and (3.7), we have that w and w_h belong to

$$V := \left\{ v \in H^1(\Omega) : \int_{\Gamma_0} v = 0 \right\}.$$

Let us remark that the following generalized Poincaré inequality holds true in this space: There exists $C > 0$ such that

$$\|v\|_{1,\Omega} \leq C|v|_{1,\Omega} \qquad \forall v \in V. \tag{3.8}$$

The following a priori error estimates have been proved in [97, Theorems 4.2–4.4]: There exists $C > 0$ such that for all $r \in [\frac{1}{2}, r_\Omega)$

$$\|w - w_h\|_{1,\Omega} \leq Ch^{\min\{r,k\}}, \tag{3.9}$$

$$|\lambda - \lambda_h| \leq Ch^{2\min\{r,k\}}, \tag{3.10}$$

$$\|w - w_h\|_{0,\Gamma_0} \leq Ch^{\min\{r,1\}/2+\min\{r,k\}}, \tag{3.11}$$

where the constant $r_\Omega > \frac{1}{2}$ is the Sobolev exponent for the Laplace problem with Neumann boundary conditions (if Ω is convex, then $r_\Omega > 1$; otherwise, $r_\Omega := \frac{\pi}{\omega}$, with ω being the largest re-entrant angle of Ω).

3.3. A posteriori error analysis

The aim of this section is to introduce a suitable residual-based error estimator for the Steklov eigenvalue problem which be completely computable, in the sense that it depends only on quantities available from the VEM solution. Then, we will show its equivalence with the error $\|w - w_h\|_{1,\Omega}$. For this purpose, we introduce the following definitions and notations.

For any polygon $K \in \mathcal{T}_h$, we denote by $\mathcal{E}_K$ the set of edges of K and let

$$\mathcal{E} := \bigcup_{K \in \mathcal{T}_h} \mathcal{E}_K.$$

We decompose $\mathcal{E} = \mathcal{E}_\Omega \cup \mathcal{E}_{\Gamma_0} \cup \mathcal{E}_{\Gamma_1}$, where $\mathcal{E}_{\Gamma_0} := \{\ell \in \mathcal{E} : \ell \subset \Gamma_0\}$, $\mathcal{E}_{\Gamma_1} := \{\ell \in \mathcal{E} : \ell \subset \Gamma_1\}$ and $\mathcal{E}_\Omega := \mathcal{E} \backslash (\mathcal{E}_{\Gamma_0} \cup \mathcal{E}_{\Gamma_1})$. For each inner edge $\ell \in \mathcal{E}_\Omega$ and for a sufficiently smooth function v, we define the jump of its normal derivative on ℓ by

$$\left[\!\left[\frac{\partial v}{\partial n} \right]\!\right]_\ell := \nabla(v|_K) \cdot n_K + \nabla(v|_{K'}) \cdot n_{K'},$$

where K and K' are the two elements in $\mathcal{T}_h$ sharing the edge ℓ and n_K and $n_{K'}$ are the respective outer unit normal vectors.

On the other hand, as a consequence of the mesh regularity assumptions, we have that each polygon $K \in \mathcal{T}_h$ admits a sub-triangulation $\mathcal{T}_h^K$ obtained by joining each vertex of K with the midpoint of the ball with respect to which K is starred. Let $\widehat{\mathcal{T}}_h := \bigcup_{K \in \mathcal{T}_h} \mathcal{T}_h^K$. Since we are also assuming **A3**, $\left\{\widehat{\mathcal{T}}_h\right\}_h$ is a shape-regular family of triangulations of Ω.

We introduce bubble functions on polygons as follows (see [61]). An interior bubble function $\psi_K \in H_0^1(K)$ for a polygon K can be constructed piecewise as the sum of the classical cubic bubble functions for each triangle of the sub-triangulation $\mathcal{T}_h^K$. On the other hand, an edge bubble function ψ_ℓ for $\ell \in \partial K$ is a piecewise quadratic function attaining the value 1 at the barycenter of ℓ and vanishing on the triangles $T \in \widehat{\mathcal{T}}_h$ that do not contain ℓ on its boundary.

The following results which establish standard estimates for bubble functions will be useful in what follows (see [4, 116]).

Lemma 3.3.1 (Interior bubble functions) *For any $K \in \mathcal{T}_h$, let ψ_K be the corresponding interior bubble function. Then, there exists a constant $C > 0$ independent of h_K such that*

$$C^{-1}\|q\|_{0,K}^2 \leq \int_K \psi_K q^2 \leq \|q\|_{0,K}^2 \qquad \forall q \in \mathbb{P}_k(K),$$
$$C^{-1}\|q\|_{0,K} \leq \|\psi_K q\|_{0,K} + h_K\|\nabla(\psi_K q)\|_{0,K} \leq C\|q\|_{0,K} \qquad \forall q \in \mathbb{P}_k(K).$$

Lemma 3.3.2 (Edge bubble functions) *For any $K \in \mathcal{T}_h$ and $\ell \in \mathcal{E}_K$, let ψ_ℓ be the corresponding edge bubble function. Then, there exists a constant $C > 0$ independent of h_K such that*

$$C^{-1}\|q\|_{0,\ell}^2 \leq \int_\ell \psi_\ell q^2 \leq \|q\|_{0,\ell}^2 \qquad \forall q \in \mathbb{P}_k(\ell).$$

Moreover, for all $q \in \mathbb{P}_k(\ell)$, there exists an extension of $q \in \mathbb{P}_k(K)$ (again denoted by q) such that

$$h_K^{-1/2}\|\psi_\ell q\|_{0,K} + h_K^{1/2}\|\nabla(\psi_\ell q)\|_{0,K} \leq C\|q\|_{0,\ell}.$$

Remark 3.3.1 *A possible way of extending q from $\ell \in \mathcal{E}_K$ to K so that Lemma 3.3.2 holds is as follows: first we extend q to the straight line $L \supset \ell$ using the same polynomial function. Then, we extend it to the whole plain through a constant prolongation in the normal direction to L. Finally, we restrict it to K.*

The following lemma provides an error equation which will be the starting points of our error analysis. From now on, we will denote by $e := (w - w_h) \in V$ the eigenfunction error and by

$$J_\ell := \begin{cases} \dfrac{1}{2}\left[\!\left[\dfrac{\partial(\Pi_k^K w_h)}{\partial n}\right]\!\right]_\ell & \ell \in \mathcal{E}_\Omega, \\ \lambda_h w_h - \dfrac{\partial(\Pi_k^K w_h)}{\partial n} & \ell \in \mathcal{E}_{\Gamma_0}, \\ -\dfrac{\partial(\Pi_k^K w_h)}{\partial n} & \ell \in \mathcal{E}_{\Gamma_1}, \end{cases} \tag{3.12}$$

the edge residuals that will appear in the error estimator. Notice that J_ℓ is actually computable since it only involves values of w_h on Γ_0 (which are computable in terms of the boundary degrees of freedom) and $\Pi_k^K w_h \in \mathbb{P}_k(K)$ which is also computable.

Lemma 3.3.3 *For any $v \in H^1(\Omega)$, we have the following identity:*

$$a(e,v) = \lambda b(w,v) - \lambda_h b(w_h,v) - \sum_{K\in\mathcal{T}_h} a^K(w_h - \Pi_k^K w_h, v) + \sum_{K\in\mathcal{T}_h} \left(\int_K \Delta(\Pi_k^K w_h) v + \sum_{\ell\in\mathcal{E}_K} \int_\ell J_\ell v \right).$$

Proof. Using that (λ, w) is a solution of Problem 3.2.1, adding and subtracting $\Pi_k^K w_h$ and integrating by parts, we obtain

$$\begin{aligned}
a(e,v) &= \lambda b(w,v) - a(w_h,v) \\
&= \lambda b(w,v) - \sum_{K\in\mathcal{T}_h} \left(a^K(w_h - \Pi_k^K w_h, v) + a^K(\Pi_k^K w_h, v) \right) \\
&= \lambda b(w,v) - \sum_{K\in\mathcal{T}_h} a^K(w_h - \Pi_k^K w_h, v) - \sum_{K\in\mathcal{T}_h} \left(-\int_K \Delta(\Pi_k^K w_h)\, v + \int_{\partial K} \frac{\partial(\Pi_k^K w_h)}{\partial n}\, v \right) \\
&= \lambda b(w,v) - \sum_{K\in\mathcal{T}_h} a^K(w_h - \Pi_k^K w_h, v) \\
&\quad + \sum_{K\in\mathcal{T}_h} \left(\int_K \Delta(\Pi_k^K w_h)\, v - \sum_{\ell\in\mathcal{E}_K\cap(\mathcal{E}_{\Gamma_0}\cup\mathcal{E}_{\Gamma_1})} \int_\ell \frac{\partial(\Pi_k^K w_h)}{\partial n}\, v + \frac{1}{2} \sum_{\ell\in\mathcal{E}_K\cap\mathcal{E}_\Omega} \int_\ell \left[\!\!\left[\frac{\partial(\Pi_k^K w_h)}{\partial n} \right]\!\!\right]_\ell v \right).
\end{aligned}$$

Finally, the proof follows by adding and subtracting the term $\lambda_h b(w_h, v)$. □

For all $K \in \mathcal{T}_h$, we introduce the local terms θ_K and R_K and the local error indicator η_K by

$$\begin{aligned}
\theta_K^2 &:= a_h^K(w_h - \Pi_k^K w_h, w_h - \Pi_k^K w_h), \\
R_K^2 &:= h_K^2 \|\Delta(\Pi_k^K w_h)\|_{0,K}^2, \\
\eta_K^2 &:= \theta_K^2 + R_K^2 + \sum_{\ell\in\mathcal{E}_K} h_K \|J_\ell\|_{0,\ell}^2.
\end{aligned}$$

We also introduce the global error estimator by

$$\eta := \left(\sum_{K\in\mathcal{T}_h} \eta_K^2 \right)^{1/2}.$$

Remark 3.3.2 *The indicators η_K include the terms θ_K which do not appear in standard finite element estimators. This term, which represent the virtual inconsistency of the method, has been introduced in [34, 61] for a posteriori error estimates of other VEM. Let us emphasize that it can be directly computed in terms of the bilinear form $S^K(\cdot,\cdot)$. In fact,*

$$\theta_K^2 = a_h^K(w_h - \Pi_k^K w_h, w_h - \Pi_k^K w_h) = S^K(w_h - \Pi_k^K w_h, w_h - \Pi_k^K w_h).$$

3.3.1. Reliability of the a posteriori error estimator

First, we provide an upper bound for the error.

Theorem 3.3.1 *There exists a constant $C > 0$ independent of h such that*

$$|w - w_h|_{1,\Omega} \leq C \left(\eta + \frac{\lambda + \lambda_h}{2} \|w - w_h\|_{0,\Gamma_0} \right).$$

Proof. Since $e = w - w_h \in V \subset H^1(\Omega)$, there exists $e_I \in V_h$ satisfying (see [97, Proposition 4.2])

$$\|e - e_I\|_{0,K} + h_K |e - e_I|_{1,K} \leq C h_K \|e\|_{1,K}. \tag{3.13}$$

Thanks to Lemma 3.3.3, we have that

$$\begin{aligned} |w - w_h|^2_{1,\Omega} &= a(w - w_h, e) \\ &= a(w - w_h, e - e_I) + a(w, e_I) - a_h(w_h, e_I) + a_h(w_h, e_I) - a(w_h, e_I) \\ &= \underbrace{\lambda b(w, e) - \lambda_h b(w_h, e)}_{T_1} + \underbrace{\sum_{K \in \mathcal{T}_h} \left(\int_K \Delta(\Pi_k^K w_h)(e - e_I) + \sum_{\ell \in \mathcal{E}_K} \int_\ell J_\ell (e - e_I) \right)}_{T_2} \\ &\quad - \underbrace{\sum_{K \in \mathcal{T}_h} a^K (w_h - \Pi_k^K w_h, e - e_I)}_{T_3} + \underbrace{a_h(w_h, e_I) - a(w_h, e_I)}_{T_4}. \end{aligned} \tag{3.14}$$

Next, we bound each term T_i separately.

For T_1, we use the definition of $b(\cdot, \cdot)$, the fact that $\|w\|_{0,\Gamma_0} = \|w_h\|_{0,\Gamma_0} = 1$, a trace theorem and (3.8) to write

$$T_1 = \lambda + \lambda_h - (\lambda + \lambda_h) \int_{\Gamma_0} w w_h = \frac{\lambda + \lambda_h}{2} \|e\|^2_{0,\Gamma_0} \leq C \frac{\lambda + \lambda_h}{2} \|e\|_{0,\Gamma_0} |e|_{1,\Omega}. \tag{3.15}$$

For T_2, first, we use a local trace inequality (see [36, Lemma 14]) and (3.13) to write

$$\|e - e_I\|_{0,\ell} \leq C(h_K^{-1/2} \|e - e_I\|_{0,K} + h_K^{1/2} |e - e_I|_{1,K}) \leq C h_K^{1/2} \|e\|_{1,K}.$$

Hence, using (3.13) again, we have

$$\begin{aligned} T_2 &\leq C \sum_{K \in \mathcal{T}_h} \left(\|\Delta(\Pi_k^K w_h)\|_{0,K} \|e - e_I\|_{0,K} + \sum_{\ell \in \mathcal{E}_K} \|J_\ell\|_{0,\ell} \|e - e_I\|_{0,\ell} \right) \\ &\leq C \sum_{K \in \mathcal{T}_h} \left(h_K \|\Delta(\Pi_k^K w_h)\|_{0,K} \|e\|_{1,K} + \sum_{\ell \in \mathcal{E}_K} h_K^{1/2} \|J_\ell\|_{0,\ell} \|e\|_{1,K} \right) \\ &\leq C \left(\sum_{K \in \mathcal{T}_h} \left(h_K^2 \|\Delta(\Pi_k^K w_h)\|^2_{0,K} + \sum_{\ell \in \mathcal{E}_K} h_K \|J_\ell\|^2_{0,\ell} \right) \right)^{1/2} |e|_{1,\Omega}, \end{aligned} \tag{3.16}$$

where for the last estimate we have used (3.8).

To bound T_3, we use the *stability* property (3.6) and (3.13) to write

$$T_3 \leq C \sum_{K\in\mathcal{T}_h} a_h^K(w_h - \Pi_k^K w_h, w_h - \Pi_k^K w_h)^{1/2}\|e\|_{1,K} \leq C \left(\sum_{K\in\mathcal{T}_h} \theta_K^2\right)^{1/2} |e|_{1,\Omega}, \tag{3.17}$$

where for the last estimate we have used (3.8) again.

Finally, to bound T_4, we add and subtract $\Pi_k^K w_h$ on each $K \in \mathcal{T}_h$ and use the *k-consistency* property (3.5):

$$\begin{aligned}
T_4 &= \sum_{K\in\mathcal{T}_h} \left(a_h^K(w_h - \Pi_k^K w_h, e_I) - a^K(w_h - \Pi_k^K w_h, e_I)\right) \\
&\leq \sum_{K\in\mathcal{T}_h} a_h^K(w_h - \Pi_k^K w_h, w_h - \Pi_k^K w_h)^{1/2} a_h^K(e_I, e_I)^{1/2} \\
&\quad + \sum_{K\in\mathcal{T}_h} a^K(w_h - \Pi_k^K w_h, w_h - \Pi_k^K w_h)^{1/2} a^K(e_I, e_I)^{1/2} \\
&\leq C \sum_{K\in\mathcal{T}_h} a_h^K(w_h - \Pi_k^K w_h, w_h - \Pi_k^K w_h)^{1/2} |e_I|_{1,K} \\
&\leq C \left(\sum_{K\in\mathcal{T}_h} \theta_K^2\right)^{1/2} |e|_{1,\Omega},
\end{aligned} \tag{3.18}$$

where we have used the *stability* property (3.6), (3.13) and (3.8) for the last two inequalities.

Thus, the result follows from (3.14)–(3.18). □

Although the virtual approximate eigenfunction is w_h, this function is not known in practice. Instead of w_h, what can be used as an approximation of the eigenfunction is $\Pi_h w_h$, where Π_h is defined for $v_h \in V_h$ by

$$(\Pi_h v_h)|_K := \Pi_k^K v_h \quad \forall K \in \mathcal{T}_h.$$

Notice that $\Pi_h w_h$ is actually computable. The following result shows that an estimate similar to that of Theorem 3.3.1 holds true for $\Pi_h w_h$.

Corollary 3.3.1 *There exists a constant $C > 0$ independent of h such that*

$$|w - w_h|_{1,\Omega} + |w - \Pi_h w_h|_{1,h} \leq C \left(\eta + \frac{\lambda + \lambda_h}{2}\|w - w_h\|_{0,\Gamma_0}\right).$$

Proof. For each polygon $K \in \mathcal{T}_h$, we have that

$$|w - \Pi_k^K w_h|_{1,K} \leq |w - w_h|_{1,K} + |w_h - \Pi_k^K w_h|_{1,K}.$$

Then, summing over all polygons we obtain

$$|w - \Pi_h w_h|_{1,h} \leq C \left(\sum_{K\in\mathcal{T}_h} |w - w_h|_{1,K}^2 + \sum_{K\in\mathcal{T}_h} |w_h - \Pi_k^K w_h|_{1,K}^2\right)^{1/2}.$$

Now, using (3.4) together with Remark 3.3.2, we have that

$$|w_h - \Pi_k^K w_h|_{1,K}^2 \leq \frac{1}{c_0} S^K(w_h - \Pi_k^K w_h, w_h - \Pi_k^K w_h) = \frac{1}{c_0}\theta_K^2 \leq \frac{1}{c_0}\eta_K^2.$$

Thus, the result follows from Theorem 3.3.1. □

In what follows, we prove a convenient upper bound for the eigenvalue approximation.

Corollary 3.3.2 *There exists a constant $C > 0$ independent of h such that*

$$|\lambda - \lambda_h| \leq C\left(\eta + \frac{\lambda + \lambda_h}{2}\|w - w_h\|_{0,\Gamma_0}\right)^2.$$

Proof. From the symmetry of the bilinear forms together with the facts that $a(w, v) = \lambda b(w, v)$ for all $v \in H^1(\Omega)$, $a_h(w_h, v_h) = \lambda_h b(w_h, v_h)$ for all $v_h \in V_h$ and $b(w_h, w_h) = 1$, we have

$$\begin{aligned}
|\lambda - \lambda_h| &= \frac{|a(w - w_h, w - w_h) - \lambda b(w - w_h, w - w_h) + a_h(w_h, w_h) - a(w_h, w_h)|}{b(w_h, w_h)} \\
&\leq C\left(|w - w_h|_{1,\Omega}^2 + \|w - w_h\|_{0,\Gamma_0}^2 + |a_h(w_h, w_h) - a(w_h, w_h)|\right) \\
&\leq C\left(|w - w_h|_{1,\Omega}^2 + |a_h(w_h, w_h) - a(w_h, w_h)|\right), \qquad (3.19)
\end{aligned}$$

where we have also used a trace theorem and (3.8). We now bound the last term on the right-hand side above. Using the definition of $a_h(\cdot, \cdot)$ and (3.4), we have

$$\begin{aligned}
&|a_h(w_h, w_h) - a(w_h, w_h)| \\
&= \left|\sum_{K\in\mathcal{T}_h}\left[a^K(\Pi_k^K w_h, \Pi_k^K w_h) + S^K\left(w_h - \Pi_k^K w_h, w_h - \Pi_k^K w_h\right)\right] - \sum_{K\in\mathcal{T}_h} a^K(w_h, w_h)\right| \\
&\leq \left|\sum_{K\in\mathcal{T}_h}\left[a^K\left(\Pi_k^K w_h, \Pi_k^K w_h\right) - a^K(w_h, w_h)\right]\right| + \sum_{K\in\mathcal{T}_h} c_1\, a^K\left(w_h - \Pi_k^K w_h, w_h - \Pi_k^K w_h\right) \\
&= \sum_{K\in\mathcal{T}_h}(1 + c_1)\, a^K\left(w_h - \Pi_k^K w_h, w_h - \Pi_k^K w_h\right) \\
&\leq (1 + c_1)\sum_{K\in\mathcal{T}_h}\left(|w_h - w|_{1,K}^2 + \left|w - \Pi_k^K w_h\right|_{1,K}^2\right).
\end{aligned}$$

Finally, from the above estimate and (3.19) we obtain

$$|\lambda - \lambda_h| \leq C\left(|w - w_h|_{1,\Omega}^2 + |w - \Pi_h w_h|_{1,h}^2\right). \qquad (3.20)$$

Hence, from Corollary 3.3.1, we conclude the proof. □

According to (3.9) and (3.11), the term $\|w - w_h\|_{0,\Gamma_0}$ in the estimate of Theorem 3.3.1 should be of higher order than $|w - w_h|_{1,\Omega}$ and hence asymptotically negligible. However this cannot be rigorously derived from (3.9) and (3.11), which are only upper error bounds. In fact, the actual error $|w - w_h|_{1,\Omega}$ could be in principle of higher order that the estimate (3.9).

Our next goal is to prove that the term $\|w - w_h\|_{0,\Gamma_0}$ is actually asymptotically negligible in the estimates of Corollaries 3.3.1 and 3.3.2, with this aim, we will modify the estimate (3.11) and prove that

$$\|w - w_h\|_{0,\Gamma_0} \leq Ch^{\min\{r,1\}/2} \left(|w - w_h|_{1,\Omega} + |w - \Pi_h w_h|_{1,h}\right). \tag{3.21}$$

This proof is based on the arguments used in Section 4 from [97]. To avoid repeating them step by step, in what follows we will only report the changes that have to be made in order to prove (3.21).

We define in $H^1(\Omega)$ the bilinear form $\widehat{a}(\cdot,\cdot) := a(\cdot,\cdot) + b(\cdot,\cdot)$, which is elliptic [97, Lemma 2.1]. Let $u \in H^1(\Omega)$ be the solution of

$$\widehat{a}(u,v) = b(w,v) \qquad \forall v \in H^1(\Omega).$$

Since $a(w,v) = \lambda b(w,v)$ we have that $u = w/(\lambda+1)$. We also define in V_h the bilinear form $\widehat{a}_h(\cdot,\cdot) := a_h(\cdot,\cdot) + b(\cdot,\cdot)$, which is elliptic uniformly in h [97, Lemma 3.1]. Let $u_h \in V_h$ be the solution of

$$\widehat{a}_h(u_h,v_h) = b(w,v_h) \qquad \forall v_h \in V_h. \tag{3.22}$$

The arguments in the proof of Lemma 4.3 from [97] can be easily modified to prove that

$$\|u - u_h\|_{0,\Gamma_0} \leq Ch^{\min\{r,1\}/2} \left(|u - u_h|_{1,\Omega} + |u - \Pi_h u_h|_{1,h}\right).$$

Now, using this estimate in the proof of [97, Theorem 4.4] yields

$$\|w - w_h\|_{0,\Gamma_0} \leq Ch^{\min\{r,1\}/2} \left(|u - u_h|_{1,\Omega} + |u - \Pi_h u_h|_{1,h}\right). \tag{3.23}$$

Now, since as stated above $u = w/(\lambda+1)$, we have that

$$|u - u_h|_{1,\Omega} \leq \frac{|w - w_h|_{1,\Omega}}{|\lambda+1|} + \left|\frac{1}{\lambda+1} - \frac{1}{\lambda_h+1}\right| |w_h|_{1,\Omega} + \left|\frac{w_h}{\lambda_h+1} - u_h\right|_{1,\Omega}. \tag{3.24}$$

For the second term on the right hand side above, we use (3.20) to write

$$\left|\frac{1}{\lambda+1} - \frac{1}{\lambda_h+1}\right| = \frac{|\lambda - \lambda_h|}{|\lambda+1||\lambda_h+1|} \leq C\left(|w - w_h|^2_{1,\Omega} + |w - \Pi_h w_h|^2_{1,h}\right). \tag{3.25}$$

To estimate the third term we recall first that

$$\widehat{a}_h(w_h,v_h) = (\lambda_h+1)b(w_h,v_h) \qquad \forall v_h \in V_h.$$

Then, subtracting this equation from (3.22) we have that

$$\widehat{a}_h\left(u_h - \frac{w_h}{\lambda_h+1}, v_h\right) = b(w - w_h, v_h) \qquad \forall v_h \in V_h.$$

Hence, from the uniform ellipticity of $\widehat{a}_h(\cdot,\cdot)$ in V_h, we obtain

$$\left\|u_h - \frac{w_h}{\lambda_h+1}\right\|^2_{1,\Omega} \leq C\|w - w_h\|_{0,\Gamma_0} \left\|u_h - \frac{w_h}{\lambda_h+1}\right\|_{0,\Gamma_0} \leq C\|w - w_h\|_{0,\Gamma_0} \left\|u_h - \frac{w_h}{\lambda_h+1}\right\|_{1,\Omega}.$$

Therefore

$$\left\| u_h - \frac{w_h}{\lambda_h + 1} \right\|_{1,\Omega} \leq C\|w - w_h\|_{0,\Gamma_0} \leq C\|w - w_h\|_{1,\Omega} \leq C|w - w_h|_{1,\Omega}, \tag{3.26}$$

the last inequality because of Poincaré inequality (3.8). Then, substituting (3.25) and (3.26) into (3.24) we obtain

$$|u - u_h|_{1,\Omega} \leq C\left(|w - w_h|_{1,\Omega} + |w - \Pi_h w_h|_{1,h}\right). \tag{3.27}$$

For the other term on the right hand side of (3.23) we have

$$|u - \Pi_h u_h|_{1,h} \leq |u - u_h|_{1,\Omega} + |u_h - \Pi_h u_h|_{1,h}, \tag{3.28}$$

whereas

$$\begin{aligned} |u_h - \Pi_h u_h|_{1,h} &\leq \left| u_h - \frac{w_h}{\lambda_h + 1} \right|_{1,\Omega} + \frac{|w_h - \Pi_h w_h|_{1,h}}{\lambda_h + 1} + \left| \Pi_h \left(\frac{w_h}{\lambda_h + 1} - u_h \right) \right|_{1,h} \\ &\leq 2 \left| u_h - \frac{w_h}{\lambda_h + 1} \right|_{1,\Omega} + \frac{|w - w_h|_{1,\Omega}}{\lambda_h + 1} + \frac{|w - \Pi_h w_h|_{1,h}}{\lambda_h + 1} \\ &\leq C\left(|w - w_h|_{1,\Omega} + |w - \Pi_h w_h|_{1,h}\right), \end{aligned}$$

where we have used (3.26) for the last inequality. Substituting this and estimate (3.27) into (3.28) we obtain

$$|u - \Pi_h u_h|_{1,h} \leq C\left(|w - w_h|_{1,\Omega} + |w - \Pi_h w_h|_{1,h}\right).$$

Finally, substituting the above estimate and (3.27) into (3.23), we conclude the proof of the following result.

Lemma 3.3.4 *There exists $C > 0$ independent of h such that*

$$\|w - w_h\|_{0,\Gamma_0} \leq C h^{\min\{r,1\}/2} \left(|w - w_h|_{1,\Omega} + |w - \Pi_h w_h|_{1,h}\right).$$

Using this result, now it easy to prove that the term $\|w - w_h\|_{0,\Gamma_0}$ in Corollaries 3.3.1 and 3.3.2 is asymptotically negligible. In fact, we have the following result.

Theorem 3.3.2 *There exist positive constants C and h_0 such that, for all $h < h_0$, there holds*

$$|w - w_h|_{1,\Omega} + |w - \Pi_h w_h|_{1,h} \leq C\eta; \tag{3.29}$$

$$|\lambda - \lambda_h| \leq C\eta^2. \tag{3.30}$$

Proof. From Lemma 3.3.4 and Corollary 3.3.1 we have

$$|w - w_h|_{1,\Omega} + |w - \Pi_h w_h|_{1,h} \leq C\left(\eta + h^{\min\{r,1\}/2}\left(|w - w_h|_{1,\Omega} + |w - \Pi_h w_h|_{1,h}\right)\right).$$

Hence, it is straightforward to check that there exists $h_0 > 0$ such that for all $h < h_0$ (3.29) holds true.

On the other hand, from Lemma 3.3.4 and (3.29) we have that for all $h < h_0$

$$\|w - w_h\|_{0,\Gamma_0} \leq C h^{\min\{r,1\}/2}\eta.$$

Then, for h small enough, (3.30) follows from Corollary 3.3.1 and the above estimate. □

3.3.2. Efficiency of the a posteriori error estimator

We will show in this section that the local error indicators η_K are efficient in the sense of pointing out which polygons should be effectively refined.

First, we prove an upper estimate of the volumetric residual term R_K.

Lemma 3.3.5 *There exists a constant $C > 0$ independent of h_K such that*

$$R_K \leq C\left(|w - w_h|_{1,K} + \theta_K\right).$$

Proof. For any $K \in \mathcal{T}_h$, let ψ_K be the corresponding interior bubble function. We define $v := \psi_K \Delta(\Pi_k^K w_h)$. Since v vanishes on the boundary of K, it may be extended by zero to the whole domain Ω. This extension, again denoted by v, belongs to $H^1(\Omega)$ and from Lemma 3.3.3 we have

$$a^K(e, v) = -a^K\big(w_h - \Pi_k^K w_h, \psi_K \Delta(\Pi_k^K w_h)\big) + \int_K \Delta(\Pi_k^K w_h)\psi_K \Delta(\Pi_k^K w_h).$$

Since $\Delta(\Pi_k^K w_h) \in \mathbb{P}_{k-2}(K)$, using Lemma 3.3.1 and the above equality we obtain

$$\begin{aligned} C^{-1}\|\Delta(\Pi_k^K w_h)\|_{0,K}^2 &\leq \int_K \psi_K \Delta(\Pi_k^K w_h)^2 \\ &= a^K\big(e, \psi_K \Delta(\Pi_k^K w_h)\big) + a^K\big(w_h - \Pi_k^K w_h, \psi_K \Delta(\Pi_k^K w_h)\big) \\ &\leq C\left(|e|_{1,K} + \left|w_h - \Pi_k^K w_h\right|_{1,K}\right)\left|\psi_K \Delta(\Pi_k^K w_h)\right|_{1,K} \\ &\leq C h_K^{-1}\left(|e|_{1,K} + \theta_K\right)\left\|\Delta(\Pi_k^K w_h)\right\|_{0,K}, \end{aligned} \tag{3.31}$$

where, for the last inequality, we have used again Lemma 3.3.1 and (3.4) together with Remark 3.3.2. Multiplying the above inequality by h_K allows us to conclude the proof. □

Next goal is to obtain an upper estimate for the local term θ_K.

Lemma 3.3.6 *There exists $C > 0$ independent of h_K such that*

$$\theta_K \leq C\left(|w - w_h|_{1,K} + |w - \Pi_k^K w_h|_{1,K}\right).$$

Proof. From the definition of θ_K together with Remark 3.3.2 and estimate (3.4) we have

$$\theta_K \leq C|w_h - \Pi_k^K w_h|_{1,K} \leq C\left(|w_h - w|_{1,K} + |w - \Pi_k^K w_h|_{1,K}\right).$$

The proof is complete. □

The following lemma provides an upper estimate for the jump terms of the local error indicator.

Lemma 3.3.7 *There exists a constant $C > 0$ independent of h_K such that*

$$h_K^{1/2}\|J_\ell\|_{0,\ell} \leq C\left(|w - w_h|_{1,K} + \theta_K\right) \qquad \forall \ell \in \mathcal{E}_K \cap \mathcal{E}_{\Gamma_1}, \tag{3.32}$$

$$h_K^{1/2}\|J_\ell\|_{0,\ell} \leq C(|w - w_h|_{1,K} + \theta_K + h_K^{1/2}\|\lambda w - \lambda_h w_h\|_{0,\ell}) \qquad \forall \ell \in \mathcal{E}_K \cap \mathcal{E}_{\Gamma_0}, \tag{3.33}$$

$$h_K^{1/2}\|J_\ell\|_{0,\ell} \leq C\sum_{K' \in \omega_\ell}\left(|w - w_h|_{1,K'} + \theta_{K'}\right) \qquad \forall \ell \in \mathcal{E}_K \cap \mathcal{E}_\Omega, \tag{3.34}$$

where $\omega_\ell := \{K' \in \mathcal{T}_h : \ell \in \mathcal{E}_{K'}\}$.

Proof. First, for $\ell \in \mathcal{E}_K \cap \mathcal{E}_{\Gamma_1}$, we extend $J_\ell \in \mathbb{P}_{k-1}(\ell)$ to the element K as in Remark 3.3.1. Let ψ_ℓ be the corresponding edge bubble function. We define $v := J_\ell \psi_\ell$. Then, v may be extended by zero to the whole domain Ω. This extension, again denoted by v, belongs to $H^1(\Omega)$ and from Lemma 3.3.3 we have that

$$a^K(e,v) = -a^K(w_h - \Pi_k^K w_h, J_\ell\psi_\ell) + \int_K \Delta\left(\Pi_k^K w_h\right) J_\ell\psi_\ell + \int_\ell J_\ell^2 \psi_\ell.$$

Since in this case $J_\ell \in \mathbb{P}_{k-1}(\ell)$, from Lemma 3.3.2 and the above equality we obtain

$$\begin{aligned}
\|J_\ell\|_{0,\ell}^2 &\leq \int_\ell J_\ell^2\psi_\ell \leq C\left(\left(|e|_{1,K} + |w_h - \Pi_k^K w_h|_{1,K}\right)|\psi_\ell J_\ell|_{1,K} + \left\|\Delta(\Pi_k^K w_h)\right\|_{0,K}\|J_\ell\psi_\ell\|_{0,K}\right)\\
&\leq C\left(\left(|e|_{1,K} + |w_h - \Pi_k^K w_h|_{1,K}\right) h_K^{-1/2}\|J_\ell\|_{0,\ell} + h_K^{-1}\left(\theta_K + |e|_{1,K}\right) h_K^{1/2}\|J_\ell\|_{0,\ell}\right)\\
&\leq C h_K^{-1/2}\|J_\ell\|_{0,\ell}\left(|e|_{1,K} + \theta_K\right),
\end{aligned}$$

where we have used again Lemma 3.3.2 together with estimate (3.31) from the proof of Lemma 3.3.5. Multiplying by $h_K^{1/2}$ the above inequality allows us to conclude (3.32).

Secondly, for $\ell \in \mathcal{E}_K \cap \mathcal{E}_{\Gamma_0}$, proceeding analogously to the previous case, we extended $v := J_\ell\psi_\ell$ to $H^1(\Omega)$. Taking into account that in this case $J_\ell \in \mathbb{P}_k(\ell)$ and ψ_ℓ is a quadratic bubble function in K, from Lemma 3.3.3 we obtain

$$a^K(e,v) = \lambda\int_\ell wJ_\ell\psi_\ell - \lambda_h\int_\ell w_h J_\ell\psi_\ell - a^K\left(w_h - \Pi_k^K w_h, J_\ell\psi_\ell\right) + \int_K \Delta\left(\Pi_k^K w_h\right) J_\ell\psi_\ell + \int_\ell J_\ell^2\psi_\ell.$$

Then, repeating the previous arguments we obtain

$$\left|\int_\ell J_\ell^2\psi_\ell\right| \leq C\left(\left|\lambda_h\int_\ell w_h J_\ell\psi_\ell - \lambda\int_\ell wJ_\ell\psi_\ell\right| + h_K^{-1/2}\|J_\ell\|_{0,\ell}\left(\theta_K + |e|_{1,K}\right)\right).$$

Hence, using Lemma 3.3.2 and a local trace inequality we arrive at

$$\begin{aligned}
\|J_\ell\|_{0,\ell}^2 &\leq C\left(\|\lambda w - \lambda_h w_h\|_{0,\ell}\|\psi_\ell J_\ell\|_{0,\ell} + h_K^{-1/2}\left(\theta_K + |e|_{1,K}\right)\|J_\ell\|_{0,\ell}\right)\\
&\leq C h_K^{-1/2}\|J_\ell\|_{0,\ell}\left(\theta_K + |e|_{1,K} + h_K^{1/2}\|\lambda w - \lambda_h w_h\|_{0,\ell}\right),
\end{aligned}$$

where we have used Lemma 3.3.2 again. Multiplying by $h_K^{1/2}$ the above inequality yields (3.33).

Finally, for $\ell \in \mathcal{E}_K \cap \mathcal{E}_\Omega$, let $\omega_\ell := \{K' \in \mathcal{T}_h : \ell \in \mathcal{E}_{K'}\}$. We extend $v := J_\ell\psi_\ell$ to $H^1(\Omega)$ again. Taking into account that $J_\ell \in \mathbb{P}_{k-1}(\ell)$ and ψ_ℓ is a quadratic bubble function in K, from Lemma 3.3.3 we obtain

$$a(e,v) = -\sum_{K'\in\omega_\ell} a^{K'}(w_h - \Pi_k^{K'} w_h, J_\ell\psi_\ell) + \sum_{K'\in\omega_\ell}\int_{K'} \Delta\left(\Pi_k^{K'} w_h\right) J_\ell\psi_\ell + \sum_{K'\in\omega_\ell}\int_\ell J_\ell^2\psi_\ell.$$

Then, proceeding analogously to the above case we obtain

$$\|J_\ell\|_{0,\ell}^2 \leq C h_K^{-1/2}\|J_\ell\|_{0,\ell}\left(\sum_{K'\in\omega_\ell}\left(|e|_{1,K'} + \theta_{K'}\right)\right).$$

Thus, the proof is complete. □

Now, we are in a position to prove an upper bound for the local error indicators η_K.

Theorem 3.3.3 *There exists $C > 0$ such that*

$$\eta_K^2 \leq C \left(\sum_{K' \in \omega_K} \left(|w - \Pi_k^{K'} w_h|_{1,K'}^2 + |w - w_h|_{1,K'}^2 + \sum_{\ell \in \mathcal{E}_K \cap \mathcal{E}_{\Gamma_0}} h_K \|\lambda w - \lambda_h w_h\|_{0,\ell}^2 \right) \right),$$

where $\omega_K := \{K' \in \mathcal{T}_h : K' \text{ and } K \text{ share an edge }\}$.

Proof. It follows immediately from Lemmas 3.3.5–3.3.7. □

According to the above theorem, the error indicators η_K^2 provide lower bounds of the error terms $\sum_{K' \in \omega_K} \left(|w - \Pi_k^{K'} w_h|_{1,K'}^2 + |w - w_h|_{1,K'}^2 \right)$ in the neighborhood ω_K of K. For those elements K with an edge on Γ_0, the term $h_K \|\lambda w - \lambda_h w_h\|_{0,\ell}^2$ also appears in the estimate. Let us remark that it is reasonable to expect that this terms be negligible. In fact, this is the case at least for the global estimator $\eta^2 = \sum_{K \in \mathcal{T}_h} \eta_K^2$ as is shown in the following result.

Corollary 3.3.3 *There exists a constant $C > 0$ such that*

$$\eta^2 \leq C \left(|w - w_h|_{1,\Omega}^2 + |w - \Pi_h w_h|_{1,h}^2 \right).$$

Proof. From Theorem 3.3.3 we have that

$$\eta^2 \leq C \left(|w - w_h|_{1,\Omega}^2 + |w - \Pi_h w_h|_{1,h}^2 + h \|\lambda w - \lambda_h w_h\|_{0,\Gamma_0}^2 \right).$$

The last term on the right hand side above is bounded as follows:

$$\|\lambda w - \lambda_h w_h\|_{0,\Gamma_0}^2 \leq 2\lambda^2 \|w - w_h\|_{0,\Gamma_0}^2 + 2|\lambda - \lambda_h|^2,$$

where we have used that $\|w_h\|_{0,\Gamma_0} = 1$. Now, by using a trace inequality and Poincaré inequality (3.8) we have

$$\|w - w_h\|_{0,\Gamma_0} \leq C |w - w_h|_{1,\Omega}.$$

On the other hand, using the estimate (3.20), we have

$$|\lambda - \lambda_h|^2 \leq (|\lambda| + |\lambda_h|)|\lambda - \lambda_h| \leq C \left(|w - w_h|_{1,\Omega}^2 + |w - \Pi_h w_h|_{1,h}^2 \right).$$

Therefore,

$$\eta^2 \leq C \left(|w - w_h|_{1,\Omega}^2 + |w - \Pi_h w_h|_{1,h}^2 \right)$$

and we conclude the proof. □

3.4. Numerical results

In this section, we will investigate the behavior of the error estimator in two numerical tests that differ in the shape of the computational domain Ω and, hence, in the regularity of the exact solution. With this aim, we have implemented in a MATLAB code a lowest-order VEM ($k = 1$) on arbitrary polygonal meshes following the ideas proposed in [22].

To complete the choice of the VEM, we have to choose the bilinear forms $S^K(\cdot,\cdot)$ satisfying (3.4). In this respect, we have proceeded as in [18, Section 4.6]: for each polygon K with vertices $P_1,\ldots,P_{N_K}$, we have used

$$S^K(u,v) := \sum_{r=1}^{N_K} u(P_r)v(P_r), \qquad u,v \in V_1^K.$$

In all our tests we have initiated the adaptive process with a coarse triangular mesh. In order to compare the performance of VEM with that of a the finite element method (FEM), we have used two different algorithms to refine the meshes. The first one is based on a classical FEM strategy for which all the subsequent meshes consist of triangles. In such a case, for $k = 1$, VEM reduces to FEM. The other procedure to refine the meshes is described in [34]. It consists of splitting each element into n quadrilaterals (n being the number of edges of the polygon) by connecting the barycenter of the element with the midpoint of each edge as shown in Figure 3.1 (see [34] for more details). Notice that although this process is initiated with a mesh of triangles, the successively created meshes will contain other kind of convex polygons as can be seen in Figure 3.3.

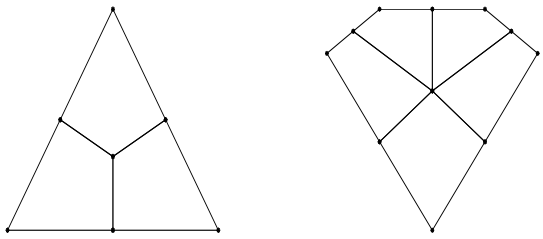

(a) Triangle K refined into 3 quadrilaterals.

(b) Pentagon K refined into 5 quadrilaterals.

Figura 3.1: Example of refined elements for VEM strategy.

Since we have chosen $k = 1$, according to the definition of the local virtual element space V_1^K (cf. (3.2)), the term $R_K^2 := h_K^2\|\Delta w_h\|_{0,K}^2$ vanishes. Thus, the error indicators reduce in this case to

$$\eta_K^2 = \theta_K^2 + \sum_{\ell\in\mathcal{E}_K} h_K\|J_\ell\|_{0,\ell}^2 \qquad \forall K \in \mathcal{T}_h.$$

Let us remark that in the case of triangular meshes, the term $\theta_K^2 := a_h^K(w_h - \Pi_k^K w_h, w_h - \Pi_k^K w_h)$ vanishes too, since $V_1^K = \mathbb{P}_1(K)$ and hence Π_k^K is the identity. By the same reason, the projection Π_k^K also disappears in the definition (3.12) of J_ℓ. Therefore, for triangular meshes, not only VEM reduces to FEM, but also the error indicator becomes the classical well-known edge-residual error

estimator (see [10]):

$$\eta_K^2 := \sum_{\ell \in \mathcal{E}_K} h_K \|J_\ell\|_{0,\ell}^2 \qquad \text{with} \qquad J_\ell := \begin{cases} \dfrac{1}{2}\left[\!\left[\dfrac{\partial w_h}{\partial n}\right]\!\right]_\ell & \ell \in \mathcal{E}_\Omega, \\ \lambda_h w_h - \dfrac{\partial w_h}{\partial n} & \ell \in \mathcal{E}_{\Gamma_0}, \\ -\dfrac{\partial w_h}{\partial n} & \ell \in \mathcal{E}_{\Gamma_1}. \end{cases}$$

In what follows, we report the results of a couple of tests. In both cases, we will restrict our attention to the approximation of the eigenvalues. Let us recall that according to Corollary 3.3.2, the global error estimator η^2 provides an upper bound of the error of the computed eigenvalue. In what follows, we will only report this error.

3.4.1. Test 1: Sloshing in a square domain.

The aim of this test is to assess the performance of adaptive schemes driven by the proposed error indicators. These schemes are based on the strategy of refining those elements K which satisfy

$$\eta_K \geq 0{,}5 \max_{K' \in \mathcal{T}_h} \{\eta_{K'}\}.$$

We have chosen for this test a problem with known analytical solution. It corresponds to the computation of the sloshing modes of a two-dimensional fluid contained in the domain $\Omega := (0,1)^2$ with a horizontal free surface Γ_0 as shown in Figure 3.2. The solutions of this problem are

$$\lambda_n = n\pi \tanh(n\pi), \qquad w_n(x,y) = \cos(n\pi x)\sinh(n\pi y), \qquad n \in \mathbb{N}.$$

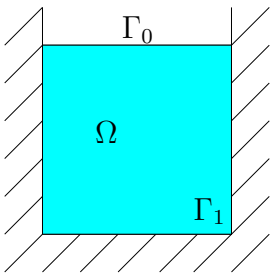

Figura 3.2: Test 1. Sloshing in a square domain.

Since the eigenfunctions are smooth, according to (3.9) we have that $|\lambda - \lambda_h| = \mathcal{O}(h^2)$. Therefore, in case of uniformly refined meshes, $|\lambda - \lambda_h| = \mathcal{O}\left(N^{-1}\right)$, where N denotes the number of degrees of freedom which is the optimal convergence rate that can be attained.

Figures 3.3 and 3.4 show the adaptatively refined meshes obtained with VEM and FEM procedures, respectively.

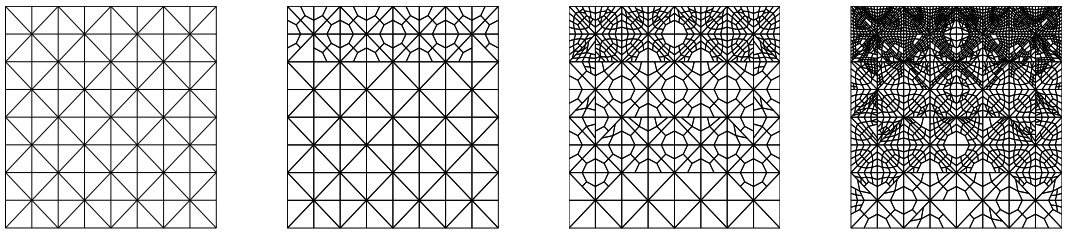

(a) Initial mesh. (b) Mesh after 1 adaptive refinement. (c) Mesh after 3 adaptive refinements. (d) Mesh after 6 adaptive refinements.

Figura 3.3: Test 1. Adaptively refined meshes for VEM scheme.

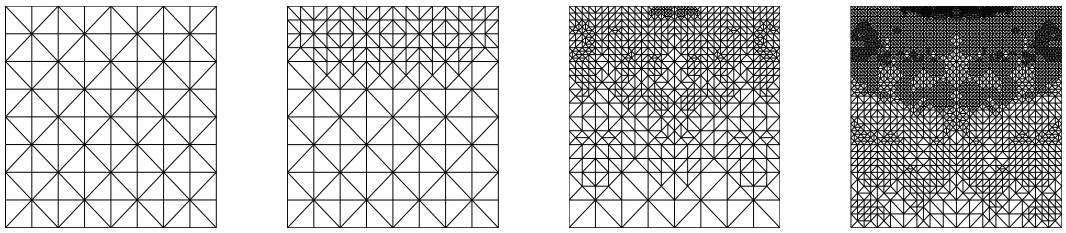

(a) Initial mesh. (b) Mesh after 1 adaptive refinement. (c) Mesh after 3 adaptive refinements. (d) Mesh after 6 adaptive refinements.

Figura 3.4: Test 1. Adaptively refined meshes for FEM scheme.

Figure 3.5 shows the error curves for the computed lowest eigenvalue on uniformly refined meshes and adaptively refined meshes with FEM and VEM schemes. The plot also includes a line of slope -1, which correspond to the optimal convergence rate of the method $\mathcal{O}\left(N^{-1}\right)$.

Figura 3.5: Test 1. Error curves of $|\lambda_1 - \lambda_{h1}|$ for uniformly refined meshes ("Uniform FEM"), adaptively refined meshes with FEM ("Adaptive FEM") and adaptively refined meshes with VEM ("Adaptive VEM").

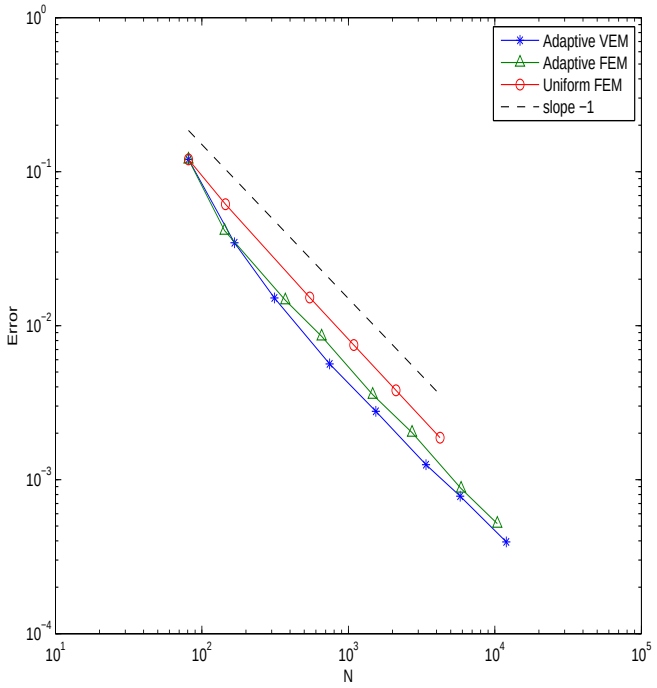

It can be seen from Figure 3.5 that the three refinement schemes lead to the correct convergence rate. Moreover, the performance of adaptive VEM is slightly better than that of adaptive FEM, while this is also better than uniform FEM.

We report in Table 3.1, the errors $|\lambda_1 - \lambda_{h1}|$ and the estimators η^2 at each step of the adaptive VEM scheme. We include in the table the terms $\theta^2 := \sum_{K\in\mathcal{T}_h} \theta_K^2$ which arise from the inconsistency of VEM and $J^2 := \sum_{K\in\mathcal{T}_h} \left(\sum_{\ell\in\mathcal{E}_K} h_K \|J_\ell\|^2_{0,\ell}\right)$ which arise from the edge residuals. We also include the effectivity indexes $|\lambda_1 - \lambda_{h1}|/\eta^2$.

Cuadro 3.1: Test 1. Components of the errors estimator and effectivity indexes on the adaptively refined meshes with VEM.

N	λ_{h1}	$\lvert\lambda_1 - \lambda_{h1}\rvert$	θ^2	J^2	η^2	$\frac{\lvert\lambda_1 - \lambda_{h1}\rvert}{\eta^2}$
38	3.2499	0.1200	0	0.8245	0.8245	0.1456
167	3.1644	0.0345	0.0111	0.2469	0.2580	0.1339
313	3.1450	0.0151	0.0117	0.1108	0.1225	0.1234
745	3.1355	0.0056	0.0054	0.0427	0.0481	0.1171
1540	3.1327	0.0028	0.0033	0.0216	0.0249	0.1113
3392	3.1311	0.0013	0.0015	0.0102	0.0117	0.1069
5806	3.1307	0.0008	0.0009	0.0064	0.0073	0.1069
11973	3.1303	0.0004	0.0005	0.0032	0.0037	0.1075

It can be seen from Table 3.1 that the effectivity indexes are bounded above and below far from zero and that the inconsistency and edge residual terms are roughly speaking of the same order, none of them being asymptotically negligible.

3.4.2. Test 2:

The aim of this test is to assess the performance of the adaptive scheme when solving a problem with a singular solution. In this test Ω consists of a unit square from which it is subtracted an equilateral triangle as shown in Figure 3.6. In this case Ω has a reentrant angle $\omega = \frac{5\pi}{3}$. Therefore, the Sobolev exponent is $r_\Omega := \frac{\pi}{\omega} = 3/5$, so that the eigenfunctions will belong to $H^{1+r}(\Omega)$ for all $r < 3/5$, but in general not to $H^{1+3/5}(\Omega)$. Therefore, according to (3.9), using quasi-uniform meshes, the convergence rate for the eigenvalues should be $|\lambda - \lambda_h| \approx \mathcal{O}\left(h^{6/5}\right) \approx \mathcal{O}\left(N^{-3/5}\right)$. An efficient adaptive scheme should lead to refine the meshes in such a way that the optimal order $|\lambda - \lambda_h| = \mathcal{O}\left(N^{-1}\right)$ could be recovered.

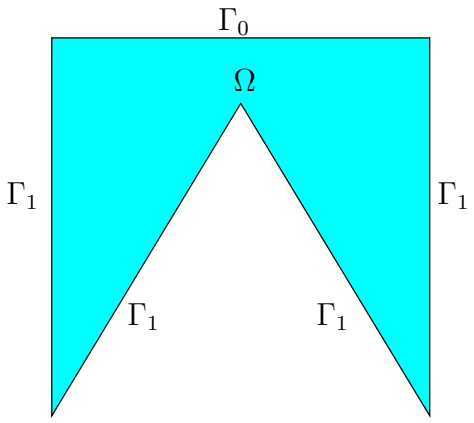

Figura 3.6: Test 2. Domain Ω.

Figures 3.7 and 3.8 shows the adaptively refined meshes for the VEM and FEM adaptive schemes, respectively.

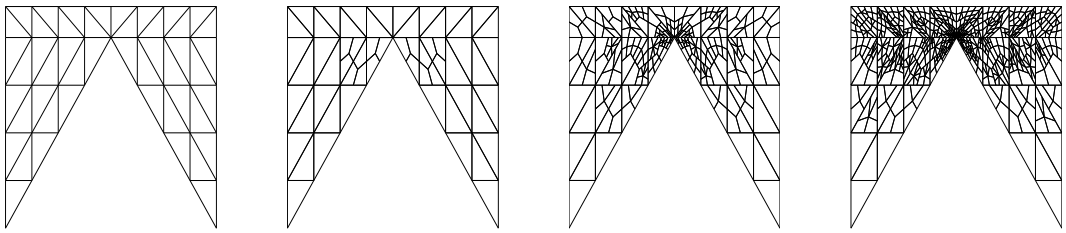

(a) Initial mesh. (b) Mesh after 1 adaptive refinement. (c) Mesh after 4 adaptive refinements. (d) Mesh after 6 adaptive refinements.

Figura 3.7: Test 2. Adaptively refined meshes for VEM scheme.

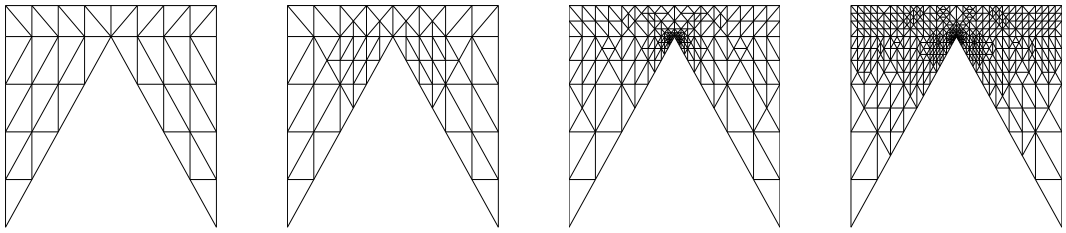

(a) Initial mesh. (b) Mesh after 1 adaptive refinement. (c) Mesh after 4 adaptive refinements. (d) Mesh after 6 adaptive refinements.

Figura 3.8: Test 2. Adaptively refined meshes for FEM scheme.

In order to compute the errors $|\lambda_1 - \lambda_{h1}|$, due to the lack of an exact eigenvalue, we have used an extrapolated approximation based on a least squares fitting of the computed values obtained with extremely refined meshes. Thus, we have obtained the value $\lambda_1 = 1{,}9288$, which has at least four correct significant digits.

We report in Tables 3.2–3.4 the lowest eigenvalue λ_{h1} computed with each of the three schemes. Each table includes the estimated convergence rate.

Cuadro 3.2: Test 2. Computed eigenvalue λ_{h1} on uniform meshes.

N	λ_{h1}
38	2.3083
123	2.0686
437	1.9828
1641	1.9505
6353	1.9377
14137	1.9341
24993	1.9325
38291	1.9316
55921	1.9310
75993	1.9306
99137	1.9303
125353	1.9301
154641	1.9299
187001	1.9298
222433	1.9297
Order	$\mathcal{O}\left(N^{-0,68}\right)$
λ_1	1.9288

Cuadro 3.3: Test 2. Computed eigenvalue λ_{h1} on the adaptive refined meshes with VEM.

N	λ_{h1}
38	2.3083
58	2.0721
106	1.9960
229	1.9592
350	1.9467
666	1.9384
909	1.9354
1340	1.9329
2141	1.9315
3438	1.9306
5172	1.9300
8014	1.9296
12365	1.9293
19153	1.9291
29403	1.9290
Order	$\mathcal{O}\left(N^{-1,10}\right)$
λ_1	1.9288

Cuadro 3.4: Test 2. Computed eigenvalue λ_{h1} on the adaptive refined meshes with FEM.

N	λ_{h1}
38	2.3083
60	2.1067
85	2.0362
148	1.9810
185	1.9678
280	1.9530
458	1.9427
646	1.9382
895	1.9356
1593	1.9325
2122	1.9315
3178	1.9306
5341	1.9298
7522	1.9295
11124	1.9292
Order	$\mathcal{O}\left(N^{-1,16}\right)$
λ_1	1.9288

It can be seen from Table 3.2, that the uniform refinement leads to a convergence rate close to that predicted by the theory $\mathcal{O}\left(N^{-3/5}\right)$. Instead, Tables 3.3 and 3.4 show that the adaptive VEM and FEM scheme allows to recover the optimal order of convergence $\mathcal{O}\left(N^{-1}\right)$. This can be clearly seen from Figure 3.9, where the three error curves are reported. The plot also includes lines of slopes -1 and $-3/5$, which correspond to the convergence rates of each scheme.

Figura 3.9: Test 2. Error curves of $|\lambda_1 - \lambda_{h1}|$ for uniformly refined meshes ("Uniform FEM"), adaptively refined meshes with FEM ("Adaptive FEM") and adaptively refined meshes with VEM ("Adaptive VEM").

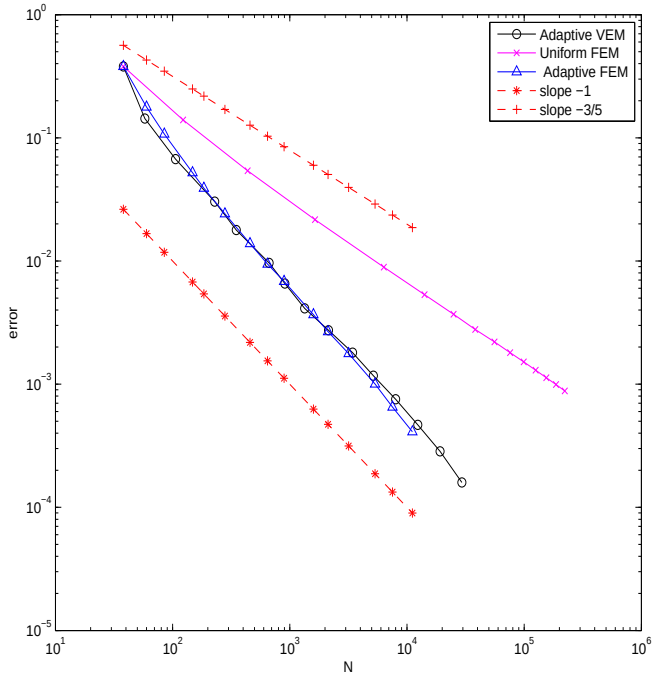

Finally, we report in Table 3.5 the same information as in Table 3.1 for this test. Similar conclusions as in the previous test follow from this table.

Cuadro 3.5: Test 2. Components of the error estimator and effectivity indexes on the adaptively refined meshes with VEM.

N	λ_{h1}	$\lvert\lambda_1 - \lambda_{h1}\rvert$	θ^2	J^2	η^2	$\frac{\lvert\lambda_1 - \lambda_{h1}\rvert}{\eta^2}$
38	2.3083	0.3795	0	2.3181	2.3181	0.1637
58	2.0721	0.1433	0.0379	0.8231	0.8609	0.1664
106	1.9960	0.0672	0.0368	0.4188	0.4556	0.1475
229	1.9592	0.0304	0.0216	0.1942	0.2158	0.1408
350	1.9467	0.0179	0.0164	0.1359	0.1522	0.1173
666	1.9384	0.0096	0.0094	0.0749	0.0844	0.1143
909	1.9354	0.0066	0.0068	0.0556	0.0624	0.1052
1340	1.9329	0.0041	0.0047	0.0408	0.0454	0.0907
2141	1.9315	0.0027	0.0032	0.0275	0.0308	0.0891
3438	1.9306	0.0018	0.0022	0.0178	0.0199	0.0904

Conclusions

We have derived an a posteriori error indicator for the VEM solution of the Steklov eigenvalue problem. We have proved that it is efficient and reliable. For lowest order elements on triangular meshes, VEM coincides with FEM and the a posteriori error indicators also coincide with the classical ones. However VEM allows using general polygonal meshes including hanging nodes, which is particularly interesting when designing an adaptive scheme. We have implemented such a scheme driven by the proposed error indicators. We have assessed its performance by means of a couple of tests which allow us to confirm that the adaptive scheme yields optimal order of convergence for regular as well as singular solutions.

Capítulo 4

A virtual element method for the acoustic vibration problem

4.1. Introduction

The *Virtual Element Method* (VEM) introduced in [18] is a recent generalization of the Finite Element Method which is characterized by the capability of dealing with very general polygonal/polyhedral meshes and the possibility to easily implement highly regular discrete spaces. Indeed, by avoiding the explicit construction of the local basis functions, the VEM can easily handle general polygons/polyhedrons without complex integrations on the element (see [22] for details on the coding aspects of the method). The interest in numerical methods that can make use of general polytopal meshes has recently undergone a significant growth in the mathematical and engineering literature; among the large number of papers on this subject, we cite as a minimal sample [8, 29, 60, 76, 77, 109, 112]. Regarding the VEM literature, we limit ourselves to the following few articles [3, 6, 14, 18, 22, 23, 30, 38, 54, 57, 84, 97, 101].

The numerical approximation of eigenvalue problems for partial differential equations derived from engineering applications, is object of great interest from both, the practical and theoretical points of view. We refer to [48, 49] and the references therein for the state of the art in this subject area. In particular, this paper focus on the so called acoustic vibration problem; namely, to compute the vibration modes and the natural frequencies of an inviscid compressible fluid within a rigid cavity [121]. One motivation for considering this problem is that it constitutes a stepping stone towards the more challenging goal of devising virtual element spectral approximations for coupled systems involving fluid-structure interaction, which arises in many engineering problems. The simplest formulation of this problem is obtained by using pressure variations which leads to an eigenvalue problem for the Laplace operator [121]. However, for coupled problems, it is convenient to use a dual formulation in terms of fluid displacements (see [91]). A standard finite element approximation of this problem leads to spurious modes (see [89]). Such a spectral pollution can be avoided by using H(div)-conforming elements, like Raviart-Thomas finite elements [40, 43, 44, 49, 105]. See [42] for a thorough discussion on this topic.

The aim of this paper is to introduce and analyze an H(div) VEM which applies to general polygonal (even non-convex) meshes for the two-dimensional acoustic vibration problem. We begin with a variational formulation of the spectral problem relying only on the fluid displacement. Then, we propose a discretization based on the mixed VEM introduced in [23] for general second order elliptic problems. The well-known abstract spectral approximation theory (see [15]) cannot be used to deal with the analysis of our problem. Indeed, the kernel of the bilinear form on the left-hand side of the variational formulation has in our case an infinite-dimensional kernel. Although the standard shift strategy allows a solution operator to be defined, this is not compact and its nontrivial essential spectrum may in such cases lead to spectral pollution at the discrete level. However, by appropriately adapting the abstract spectral approximation theory for non-compact operators developed in [74, 75], under rather mild assumptions on the polygonal meshes, we establish that the resulting scheme provides a correct approximation of the spectrum and prove error estimates for the eigenfunctions and a double order for the eigenvalues. As a by-product, we derive optimal approximation estimates for H(div) virtual elements with vanishing rotor, a result that could be useful also for other applications. These results and their corresponding proofs are collected in an appendix.

The outline of this article is as follows: We introduce in Section 4.2 the variational formulation of the acoustic vibration problem, define a solution operator and establish its spectral characterization. In Section 4.3, we introduce the virtual element discrete formulation, describe the spectrum of a discrete solution operator and establish some auxiliary results. In Section 4.4, we prove that the numerical scheme provides a correct spectral approximation and establish optimal order error estimates for the eigenvalues and eigenfunctions. In Section 4.5, we report a couple of numerical tests that allow us to assess the convergence properties of the method, to confirm that it is not polluted with spurious modes and to check that the experimental rates of convergence agree with the theoretical ones. Finally, we introduce in an appendix the proofs of the approximation results for the introduced virtual element interpolant.

Throughout the paper, Ω is a generic Lipschitz bounded domain of $\mathbb{R}^2$. For $s \geq 0$, $\|\cdot\|_{s,\Omega}$ stands indistinctly for the norm of the Hilbertian Sobolev spaces $\mathrm{H}^s(\Omega)$ or $[\mathrm{H}^s(\Omega)]^2$ with the convention $\mathrm{H}^0(\Omega) := L^2(\Omega)$. We also define the Hilbert space $\mathrm{H}(\mathrm{div};\Omega) := \left\{\boldsymbol{v} \in [L^2(\Omega)]^2 : \ \mathrm{div}\,\boldsymbol{v} \in L^2(\Omega)\right\}$, whose norm is given by $\|\boldsymbol{v}\|^2_{\mathrm{div},\Omega} := \|\boldsymbol{v}\|^2_{0,\Omega} + \|\mathrm{div}\,\boldsymbol{v}\|^2_{0,\Omega}$. Finally, we employ $\mathbf{0}$ to denote a generic null vector and C to denote generic constants independent of the discretization parameters, which may take different values at different places.

4.2. The spectral problem

We consider the free vibration problem for an acoustic fluid within a bounded rigid cavity $\Omega \subset \mathbb{R}^2$ with polygonal boundary Γ and outward unit normal vector $\boldsymbol{n}$:

$$\begin{cases} -\omega^2 \varrho \boldsymbol{w} = -\nabla p & \text{in } \Omega, \\ p = -\varrho c^2 \,\mathrm{div}\,\boldsymbol{w} & \text{in } \Omega, \\ \boldsymbol{w} \cdot \boldsymbol{n} = 0 & \text{on } \Gamma, \end{cases}$$

where $\boldsymbol{w}$ is the fluid displacement, p is the pressure fluctuation, ϱ the density, c the acoustic speed and ω the vibration frequency. Multiplying the first equation above by a test function

$$\boldsymbol{v} \in \boldsymbol{\mathcal{V}} := \{\boldsymbol{v} \in \mathrm{H}(\mathrm{div};\Omega) : \ \boldsymbol{v}\cdot\boldsymbol{n} = 0 \text{ on } \Gamma\},$$

integrating by parts, using the boundary condition and eliminating p, we arrive at the following weak formulation in which, for simplicity, we have taken the physical parameters ϱ and c equal to one and denote $\lambda = \omega^2$:

Problem 4.2.1 *Find* $(\lambda, \boldsymbol{w}) \in \mathbb{R} \times \boldsymbol{\mathcal{V}}$, $\boldsymbol{w} \neq 0$, *such that*

$$\int_\Omega \mathrm{div}\,\boldsymbol{w}\,\mathrm{div}\,\boldsymbol{v} = \lambda \int_\Omega \boldsymbol{w}\cdot\boldsymbol{v} \qquad \forall \boldsymbol{v} \in \boldsymbol{\mathcal{V}}.$$

Since the bilinear form on the left-hand side is not $\mathrm{H}(\mathrm{div};\Omega)$-elliptic, it is convenient to use a shift argument to rewrite this eigenvalue problem in the following equivalent form:

Problem 4.2.2 *Find* $(\lambda, \boldsymbol{w}) \in \mathbb{R} \times \boldsymbol{\mathcal{V}}$, $\boldsymbol{w} \neq 0$, *such that*

$$a(\boldsymbol{w},\boldsymbol{v}) = (\lambda+1)\, b(\boldsymbol{w},\boldsymbol{v}) \qquad \forall \boldsymbol{v} \in \boldsymbol{\mathcal{V}},$$

where the bilinear forms are defined for any $\boldsymbol{w}, \boldsymbol{v} \in \boldsymbol{\mathcal{V}}$ by

$$\begin{aligned} a(\boldsymbol{w},\boldsymbol{v}) &:= \int_\Omega \mathrm{div}\,\boldsymbol{w}\,\mathrm{div}\,\boldsymbol{v} + \int_\Omega \boldsymbol{w}\cdot\boldsymbol{v}, \\ b(\boldsymbol{w},\boldsymbol{v}) &:= \int_\Omega \boldsymbol{w}\cdot\boldsymbol{v}. \end{aligned}$$

We define the solution operator associated with Problem 4.2.2:

$$\begin{aligned} \mathbf{T} :\ \boldsymbol{\mathcal{V}} &\longrightarrow \boldsymbol{\mathcal{V}}, \\ \boldsymbol{f} &\longmapsto \mathbf{T}\boldsymbol{f} := \boldsymbol{u}, \end{aligned}$$

where $\boldsymbol{u} \in \boldsymbol{\mathcal{V}}$ is the solution of the corresponding source problem:

$$a(\boldsymbol{u},\boldsymbol{v}) = b(\boldsymbol{f},\boldsymbol{v}) \qquad \forall \boldsymbol{v} \in \boldsymbol{\mathcal{V}}.$$

Since the bilinear form $a(\cdot,\cdot)$ is $\mathrm{H}(\mathrm{div};\Omega)$-elliptic, the problem above is well posed. As an immediate consequence, we deduce that the linear operator $\mathbf{T}$ is well defined and bounded. Notice that $(\lambda, \boldsymbol{w}) \in \mathbb{R} \times \boldsymbol{\mathcal{V}}$ solves Problem 4.2.1 if and only if $(1/(1+\lambda), \boldsymbol{w})$ is an eigenpair of $\mathbf{T}$, i.e, if and only if

$$\mathbf{T}\boldsymbol{w} = \mu\boldsymbol{w}, \quad \text{with } \mu := \frac{1}{\lambda+1}.$$

Moreover, it is easy to check that $\mathbf{T}$ is self-adjoint with respect to the inner products $a(\cdot,\cdot)$ and $b(\cdot,\cdot)$ in $\boldsymbol{\mathcal{V}}$.

In what follows, we recall some results that can be found in [40] in the more general context of fluid-solid vibration problems. The proofs in [40] can be readily adapted to this case to obtain the following results. Let the space

$$\boldsymbol{\mathcal{K}} := \{\boldsymbol{v} \in \boldsymbol{\mathcal{V}} :\ \mathrm{div}\,\boldsymbol{v} = 0 \text{ in } \Omega\}.$$

Lemma 4.2.1 *The operator* $\mathbf{T}$ *admits the eigenvalue* $\mu = 1$ *with associated eigenspace* $\boldsymbol{\mathcal{K}}$.

The following result provides a simple characterization of the orthogonal complement of $\boldsymbol{\mathcal{K}}$ in $\boldsymbol{\mathcal{V}}$.

Lemma 4.2.2 *Let* $\boldsymbol{\mathcal{G}} := \left\{\nabla q : \ q \in H^1(\Omega)\right\}$. *Then,*

$$\boldsymbol{\mathcal{V}} = \boldsymbol{\mathcal{K}} \oplus (\boldsymbol{\mathcal{G}} \cap \boldsymbol{\mathcal{V}}),$$

is an orthogonal decomposition in both $[L^2(\Omega)]^2$ *and* $\mathrm{H}(\mathrm{div};\Omega)$.

Moreover, there exists $s \in (1/2, 1]$ *such that, for all* $\boldsymbol{v} \in \boldsymbol{\mathcal{V}}$, *if* $\boldsymbol{v} = \boldsymbol{\varphi} + \nabla q$ *with* $\boldsymbol{\varphi} \in \boldsymbol{\mathcal{K}}$ *and* $\nabla q \in \boldsymbol{\mathcal{G}} \cap \boldsymbol{\mathcal{V}}$, *then* $\nabla q \in [\mathrm{H}^s(\Omega)]^2$ *and* $\|\nabla q\|_{s,\Omega} \leq C \|\mathrm{div}\, \boldsymbol{v}\|_{0,\Omega}$.

From now on, we fix $s \in (1/2, 1]$ such that the above lemma holds true.

The following result shows that the subspace $\boldsymbol{\mathcal{G}} \cap \boldsymbol{\mathcal{V}}$ is invariant for $\mathbf{T}$.

Lemma 4.2.3 *There holds*

$$\mathbf{T}(\boldsymbol{\mathcal{G}} \cap \boldsymbol{\mathcal{V}}) \subset (\boldsymbol{\mathcal{G}} \cap \boldsymbol{\mathcal{V}}).$$

Smoothing properties of $\mathbf{T}$ as an operator from $\boldsymbol{\mathcal{G}} \cap \boldsymbol{\mathcal{V}}$ into itself are established in what follows.

Theorem 4.2.1 *There holds*

$$\mathbf{T}(\boldsymbol{\mathcal{G}} \cap \boldsymbol{\mathcal{V}}) \subset \left\{\boldsymbol{v} \in [\mathrm{H}^s(\Omega)]^2 : \ \mathrm{div}\, \boldsymbol{v} \in H^1(\Omega)\right\}$$

and there exists $C > 0$ *such that, for all* $\boldsymbol{f} \in \boldsymbol{\mathcal{G}} \cap \boldsymbol{\mathcal{V}}$, *if* $\boldsymbol{u} = \mathbf{T}\boldsymbol{f}$, *then*

$$\|\boldsymbol{u}\|_{s,\Omega} + \|\mathrm{div}\, \boldsymbol{u}\|_{1,\Omega} \leq C \|\boldsymbol{f}\|_{\mathrm{div},\Omega}.$$

Consequently, the operator $\mathbf{T}|_{\boldsymbol{\mathcal{G}}\cap\boldsymbol{\mathcal{V}}} : \ \boldsymbol{\mathcal{G}} \cap \boldsymbol{\mathcal{V}} \to \boldsymbol{\mathcal{G}} \cap \boldsymbol{\mathcal{V}}$ *is compact.*

Finally, the following result provides a spectral characterization of $\mathbf{T}$.

Theorem 4.2.2 *The spectrum of* $\mathbf{T}$ *decomposes as* $\mathrm{sp}(\mathbf{T}) = \{0, 1\} \cup \{\mu_k\}_{k\in\mathbb{N}}$, *where:*

i) $\mu = 1$ *is an infinite-multiplicity eigenvalue of* $\mathbf{T}$ *and its associated eigenspace is* $\boldsymbol{\mathcal{K}}$;

ii) $\{\mu_k\}_{k\in\mathbb{N}} \subset (0, 1)$ *is a sequence of finite-multiplicity eigenvalues of* $\mathbf{T}$ *which converge to* 0 *and if* $\boldsymbol{w}$ *is an eigenfunction of* $\mathbf{T}$ *associated with such an eigenvalue, then there exists* $\tilde{s} > 1/2$ *and* $C > 0$, *both depending on the eigenvalue, such that*

$$\|\boldsymbol{w}\|_{\tilde{s},\Omega} + \|\mathrm{div}\, \boldsymbol{w}\|_{1+\tilde{s},\Omega} \leq C \|\boldsymbol{w}\|_{\mathrm{div},\Omega};$$

iii) $\mu = 0$ *is not an eigenvalue of* $\mathbf{T}$.

4.3. The virtual elements discretization

We begin this section, by recalling the mesh construction and the assumptions considered to introduce a discrete virtual element space. Then, we will introduce a virtual element discretization of Problem 4.2.1 and provide a spectral characterization of the resulting discrete eigenvalue problem. Let $\{\mathcal{T}_h\}$ be a family of decompositions of Ω into polygons E. Let h_E denote the diameter of the element E and $h := \max_{E\in\Omega} h_E$.

For the analysis, we make the following assumptions on the meshes as in [23, 54]: there exists a positive real number $C_{\mathcal{T}}$ such that, for every $E \in \mathcal{T}_h$ and for every $\mathcal{T}_h$,

- $\mathbf{A_1}$: the ratio between the shortest edge and the diameter of E is larger than $C_{\mathcal{T}}$;
- $\mathbf{A_2}$: E is star-shaped with respect to every point of a ball of radius $C_{\mathcal{T}} h_E$.

For any subset $S \subseteq \mathbb{R}^2$ and any non-negative integer k, we indicate by $\mathbb{P}_k(S)$ the space of polynomials of degree up to k defined on S. To keep the notation simpler, we denote by $\boldsymbol{n}$ a generic normal unit vector; in each case, its precise definition will be clear from the context. We consider now a polygon E and, for any fixed non-negative integer k, we define the following finite dimensional space (inspired in [54, 23]):

$$\boldsymbol{\mathcal{V}}_h^E := \Big\{ \boldsymbol{v}_h \in \mathrm{H}(\mathrm{div}; E) : \ (\boldsymbol{v}_h \cdot \boldsymbol{n}) \in \mathbb{P}_k(e) \ \ \forall e \subset \partial E, \ \mathrm{div}\, \boldsymbol{v}_h \in \mathbb{P}_k(E), \ \mathrm{rot}\, \boldsymbol{v}_h = 0 \text{ in } E \Big\}.$$

Remark 4.3.1 *It is elementary to check that a vector field $\boldsymbol{v}_h \in \boldsymbol{\mathcal{V}}_h^E$ satisfying $\boldsymbol{v}_h \cdot \boldsymbol{n} = 0$ on ∂E and $\mathrm{div}\, \boldsymbol{v}_h = 0$ in E is identically zero. In fact, since a star-shaped polygon E is simply connected and $\mathrm{rot}\, \boldsymbol{v}_h = 0$ in E, there exists $\gamma \in \mathrm{H}^1(E)$ such that $\boldsymbol{v}_h = \nabla\gamma$. Then, $\Delta\gamma = \mathrm{div}\, \boldsymbol{v}_h = 0$ in E and $\partial\gamma/\partial\boldsymbol{n} = \boldsymbol{v}_h \cdot \boldsymbol{n} = 0$ on ∂E. Hence, $\boldsymbol{v}_h = \nabla\gamma = \boldsymbol{0}$ in E. This implies that $\boldsymbol{\mathcal{V}}_h^E$ is finite dimensional, the dimension being less or equal to $N_E\,(k+1) + (k+1)\,(k+2)\,/2 - 1$, where N_E is the number of edges of E.*

We define the following degrees of freedom for functions $\boldsymbol{v}_h$ in $\boldsymbol{\mathcal{V}}_h^E$:

$$\int_e (\boldsymbol{v}_h \cdot \boldsymbol{n})\, q\, ds \qquad \forall q \in \mathbb{P}_k(e), \quad \forall \text{ edge } e \subset \partial E; \tag{4.1}$$

$$\int_E \boldsymbol{v}_h \cdot \nabla q \qquad \forall q \in \mathbb{P}_k(E)/\mathbb{P}_0(E). \tag{4.2}$$

Proposition 4.3.1 *The degrees of freedom* (4.1)–(4.2) *are unisolvent in $\boldsymbol{\mathcal{V}}_h^E$.*

Proof. It is easy to check that the number of degrees of freedom (4.1)–(4.2) equals the dimension of $\boldsymbol{\mathcal{V}}_h^E$. Thus, we only need to show that if $\boldsymbol{v}_h$ in $\boldsymbol{\mathcal{V}}_h^E$ is such that

$$\int_e (\boldsymbol{v}_h \cdot \boldsymbol{n})\, q\, ds = 0 \qquad \forall q \in \mathbb{P}_k(e), \quad \forall \text{ edge } e \subset \partial E,$$

$$\int_E \boldsymbol{v}_h \cdot \nabla q = 0 \qquad \forall q \in \mathbb{P}_k(E)/\mathbb{P}_0(E),$$

then $\boldsymbol{v}_h = \mathbf{0}$. Since $\operatorname{div} \boldsymbol{v}_h \in \mathbb{P}_k(E)$, by taking $q := \operatorname{div} \boldsymbol{v}_h$ above, we have

$$\int_E (\operatorname{div} \boldsymbol{v}_h)^2 = \int_E \operatorname{div} \boldsymbol{v}_h \, q = -\int_E \boldsymbol{v}_h \cdot \nabla q + \int_{\partial E} (\boldsymbol{v}_h \cdot \boldsymbol{n}) \, q \, ds = 0.$$

Then, $\operatorname{div} \boldsymbol{v}_h = 0$. Similarly, for each edge $e \subset \partial E$, since $\boldsymbol{v}_h \cdot \boldsymbol{n} \in \mathbb{P}_k(e)$, by taking $q := \boldsymbol{v}_h \cdot \boldsymbol{n}$ we obtain

$$\int_e (\boldsymbol{v}_h \cdot \boldsymbol{n})^2 \, ds = 0.$$

Hence, $\boldsymbol{v}_h \cdot \boldsymbol{n} = 0$ on ∂E. Therefore, according to Remark 4.3.1, $\boldsymbol{v}_h = \mathbf{0}$ in E. □

Remark 4.3.2 *For the degrees of freedom* (4.2)*, we could integrate by parts and substitute them with*

$$\int_E \operatorname{div} \boldsymbol{v}_h \, q \qquad \forall q \in \mathbb{P}_k(E)/\mathbb{P}_0(E).$$

Needless to say, certain degrees of freedom will be more convenient when writing the code and the others might be more convenient when writing a proof.

For each decomposition $\mathcal{T}_h$ of Ω into polygons E, we define

$$\boldsymbol{\mathcal{V}}_h := \left\{ \boldsymbol{v}_h \in \boldsymbol{\mathcal{V}} : \ \boldsymbol{v}_h|_E \in \boldsymbol{\mathcal{V}}_h^E \right\}.$$

In agreement with the local choice, we choose the following global degrees of freedom:

$$\int_e (\boldsymbol{v}_h \cdot \boldsymbol{n}) \, q \, ds \qquad \forall q \in \mathbb{P}_k(e), \quad \text{for each internal edge } e \not\subset \Gamma;$$

$$\int_E \boldsymbol{v}_h \cdot \nabla q \qquad \forall q \in \mathbb{P}_k(E)/\mathbb{P}_0(E), \quad \text{for each element } E \in \mathcal{T}_h.$$

Remark 4.3.3 *The number of internal degrees of freedom of the Virtual Element Method here considered (VEM_k) is in general less than that of standard finite elements of the same order such as Raviart-Thomas (RT_k) or Brezzi-Douglas-Marini (BDM_k) elements, while the number of degrees of freedom per edge is the same. A count of the internal degrees of freedom gives*

$$RT_k : \ k\,(k+1)\,, \qquad BDM_k : \ (k+1)\,(k-1)\,, \qquad VEM_k : \ (k+1)\,(k+2)\,/2 - 1.$$

The proposed family may therefore be preferable to more standard finite elements even in the case of triangular meshes, especially for moderate-to-high values of k.

In order to construct the discrete scheme, we need some preliminary definitions. First, we split the bilinear form $a(\cdot,\cdot)$ introduced in the previous section as follows:

$$a(\boldsymbol{u}_h, \boldsymbol{v}_h) = \sum_{E \in \mathcal{T}_h} \left(\int_E \operatorname{div} \boldsymbol{u}_h \operatorname{div} \boldsymbol{v}_h + \int_E \boldsymbol{u}_h \cdot \boldsymbol{v}_h \right), \qquad \boldsymbol{u}_h, \boldsymbol{v}_h \in \boldsymbol{\mathcal{V}}_h.$$

The local matrices associated with the first term on the right hand side above are easily computable since $\operatorname{div} \boldsymbol{u}_h$ and $\operatorname{div} \boldsymbol{v}_h$ are polynomials in each element. We explicitly point out that, as

can be seem from (4.1)–(4.2), the divergence of any vector $\boldsymbol{v}_h \in \boldsymbol{\mathcal{V}}_h$ can be easily computed from knowledge of the degrees of freedom of $\boldsymbol{v}_h$. Instead, for the local matrices associated with the second term on the right hand side above, we must take into account that, due to the implicit space definition, it is not possible to compute exactly the integrals. Because of this, we will use an approximation of them. The final output will be a local matrix on each element E whose associated bilinear form is exact whenever one of the two entries is a gradient of a polynomial of degree $k+1$. This will allow us to retain the optimal approximation properties of the space $\boldsymbol{\mathcal{V}}_h$. With this aim, we define first for each element E the space

$$\widehat{\boldsymbol{\mathcal{V}}}_h^E := \nabla(\mathbb{P}_{k+1}(E)) \subset \boldsymbol{\mathcal{V}}_h^E.$$

Then, we define the $[\mathrm{L}^2(E)]^2$-orthogonal projector $\boldsymbol{\Pi}_h^E : [\mathrm{L}^2(E)]^2 \longrightarrow \widehat{\boldsymbol{\mathcal{V}}}_h^E$ by

$$\int_E \boldsymbol{\Pi}_h^E \boldsymbol{v} \cdot \widehat{\boldsymbol{u}}_h = \int_E \boldsymbol{v} \cdot \widehat{\boldsymbol{u}}_h \qquad \forall \widehat{\boldsymbol{u}}_h \in \widehat{\boldsymbol{\mathcal{V}}}_h^E. \tag{4.3}$$

We point out that $\boldsymbol{\Pi}_h^E \boldsymbol{v}_h$ is explicitly computable for every $\boldsymbol{v}_h \in \boldsymbol{\mathcal{V}}_h^E$ using only its degrees of freedom (4.1)–(4.2). In fact, it is easy to check that for all $\boldsymbol{v}_h \in \boldsymbol{\mathcal{V}}_h^E$ and for all $q \in \mathbb{P}_{k+1}(E)$,

$$\int_E \boldsymbol{\Pi}_h^E \boldsymbol{v}_h \cdot \nabla q = \int_E \boldsymbol{v}_h \cdot \nabla q = -\int_E \operatorname{div} \boldsymbol{v}_h \, q + \int_{\partial E} (\boldsymbol{v}_h \cdot \boldsymbol{n}) \, q \, ds.$$

Remark 4.3.4 *In particular, for $k = 0$, for all $\boldsymbol{v}_h \in \boldsymbol{\mathcal{V}}_h^E$ and for all $q \in \mathbb{P}_1(E)$, we have that*

$$\int_E \boldsymbol{\Pi}_h^E \boldsymbol{v}_h \cdot \nabla q = -\left(\frac{1}{|E|} \sum_{e \subset \partial E} \int_e \boldsymbol{v}_h \cdot \boldsymbol{n} \, ds \right) \left(\int_E q \right) + \sum_{e \subset \partial E} \int_e (\boldsymbol{v}_h \cdot \boldsymbol{n}) \, q \, ds.$$

On the other hand, let $S^E(\cdot,\cdot)$ be any symmetric positive definite (and computable) bilinear form to be chosen as to satisfy

$$c_0 \int_E \boldsymbol{v}_h \cdot \boldsymbol{v}_h \le S^E(\boldsymbol{v}_h, \boldsymbol{v}_h) \le c_1 \int_E \boldsymbol{v}_h \cdot \boldsymbol{v}_h \qquad \forall \boldsymbol{v}_h \in \boldsymbol{\mathcal{V}}_h^E, \tag{4.4}$$

for some positive constants c_0 and c_1 depending only on the constant $C_{\mathcal{T}}$ from mesh assumptions $\mathbf{A_1}$ and $\mathbf{A_2}$. Then, we define on each element E the bilinear form

$$b_h^E(\boldsymbol{u}_h, \boldsymbol{v}_h) := \int_E \boldsymbol{\Pi}_h^E \boldsymbol{u}_h \cdot \boldsymbol{\Pi}_h^E \boldsymbol{v}_h + S^E\big(\boldsymbol{u}_h - \boldsymbol{\Pi}_h^E \boldsymbol{u}_h, \boldsymbol{v}_h - \boldsymbol{\Pi}_h^E \boldsymbol{v}_h\big), \qquad \boldsymbol{u}_h, \boldsymbol{v}_h \in \boldsymbol{\mathcal{V}}_h^E, \tag{4.5}$$

and, in a natural way,

$$b_h(\boldsymbol{u}_h, \boldsymbol{v}_h) := \sum_{E \in \mathcal{T}_h} b_h^E(\boldsymbol{u}_h, \boldsymbol{v}_h), \qquad \boldsymbol{u}_h, \boldsymbol{v}_h \in \boldsymbol{\mathcal{V}}_h.$$

The following two properties of the bilinear form $b_h^E(\cdot,\cdot)$ are easily derived by repeating in our case the arguments from [54, Proposition 4.1].

- *Consistency*:

$$b_h^E(\widehat{\boldsymbol{u}}_h, \boldsymbol{v}_h) = \int_E \widehat{\boldsymbol{u}}_h \cdot \boldsymbol{v}_h \qquad \forall \widehat{\boldsymbol{u}}_h \in \widehat{\boldsymbol{\mathcal{V}}}_h^E, \quad \forall \boldsymbol{v}_h \in \boldsymbol{\mathcal{V}}_h^E, \quad \forall E \in \mathcal{T}_h. \tag{4.6}$$

- *Stability*: There exist two positive constants α_* and α^*, independent of E, such that:

$$\alpha_* \int_E \boldsymbol{v}_h \cdot \boldsymbol{v}_h \leq b_h^E(\boldsymbol{v}_h, \boldsymbol{v}_h) \leq \alpha^* \int_E \boldsymbol{v}_h \cdot \boldsymbol{v}_h \qquad \forall \boldsymbol{v}_h \in \boldsymbol{\mathcal{V}}_h^E, \quad \forall E \in \mathcal{T}_h. \tag{4.7}$$

Now, we are in a position to write the virtual element discretization of Problem 4.2.1.

Problem 4.3.1 *Find* $(\lambda_h, \boldsymbol{w}_h) \in \mathbb{R} \times \boldsymbol{\mathcal{V}}_h$, $\boldsymbol{w}_h \neq 0$, *such that*

$$\int_\Omega \operatorname{div} \boldsymbol{w}_h \operatorname{div} \boldsymbol{v}_h = \lambda_h b_h(\boldsymbol{w}_h, \boldsymbol{v}_h) \qquad \forall \boldsymbol{v}_h \in \boldsymbol{\mathcal{V}}_h.$$

We use again a shift argument to rewrite this discrete eigenvalue problem in the following convenient equivalent form.

Problem 4.3.2 *Find* $(\lambda_h, \boldsymbol{w}_h) \in \mathbb{R} \times \boldsymbol{\mathcal{V}}_h$, $\boldsymbol{w}_h \neq 0$, *such that*

$$a_h(\boldsymbol{w}_h, \boldsymbol{v}_h) = (\lambda_h + 1)\, b_h(\boldsymbol{w}_h, \boldsymbol{v}_h) \qquad \forall \boldsymbol{v}_h \in \boldsymbol{\mathcal{V}}_h,$$

where

$$a_h(\boldsymbol{w}_h, \boldsymbol{v}_h) := \int_\Omega \operatorname{div} \boldsymbol{w}_h \operatorname{div} \boldsymbol{v}_h + b_h(\boldsymbol{w}_h, \boldsymbol{v}_h) \qquad \forall \boldsymbol{w}_h, \boldsymbol{v}_h \in \boldsymbol{\mathcal{V}}_h.$$

We observe that by virtue of (4.7), the bilinear form $a_h(\cdot, \cdot)$ is bounded. Moreover, as is shown in the following lemma, it is also uniformly elliptic.

Lemma 4.3.1 *There exists a constant* $\beta > 0$, *independent of* h, *such that*

$$a_h(\boldsymbol{v}_h, \boldsymbol{v}_h) \geq \beta \, \|\boldsymbol{v}_h\|^2_{\operatorname{div},\Omega} \qquad \forall \boldsymbol{v}_h \in \boldsymbol{\mathcal{V}}_h.$$

Proof. Thanks to (4.7), the above inequality holds with $\beta := \min\{\alpha_*, 1\}$.
□

The next step is to introduce the discrete version of the operator $\mathbf{T}$:

$$\begin{aligned} \mathbf{T}_h : \ & \boldsymbol{\mathcal{V}}_h \longrightarrow \boldsymbol{\mathcal{V}}_h, \\ & \boldsymbol{f}_h \longmapsto \mathbf{T}_h \boldsymbol{f}_h := \boldsymbol{u}_h, \end{aligned}$$

where $\boldsymbol{u}_h \in \boldsymbol{\mathcal{V}}_h$ is the solution of the corresponding discrete source problem:

$$a_h(\boldsymbol{u}_h, \boldsymbol{v}_h) = b_h(\boldsymbol{f}_h, \boldsymbol{v}_h) \qquad \forall \boldsymbol{v}_h \in \boldsymbol{\mathcal{V}}_h.$$

We deduce from Lemma 4.3.1, (4.7) and the Lax-Milgram Theorem, that the linear operator $\mathbf{T}_h$ is well defined and bounded uniformly with respect to h.

Once more, as in the continuous case, $(\lambda_h, \boldsymbol{w}_h)$ solves Problem 4.3.1 if and only if $(1/(1 + \lambda_h), \boldsymbol{w}_h)$ is an eigenpair of $\mathbf{T}_h$, i.e, if and only if

$$\mathbf{T}_h \boldsymbol{w}_h = \mu_h \boldsymbol{w}_h, \quad \text{with } \mu_h := \frac{1}{\lambda_h + 1}.$$

Moreover, it is easy to check that $\mathbf{T}_h$ is self-adjoint with respect to $a_h(\cdot,\cdot)$ and $b_h(\cdot,\cdot)$. To describe the spectrum of this operator, we proceed as in the continuous case and decompose $\boldsymbol{\mathcal{V}}_h$ into a convenient direct sum. To this end, we define

$$\boldsymbol{\mathcal{K}}_h := \boldsymbol{\mathcal{V}}_h \cap \boldsymbol{\mathcal{K}} = \{\boldsymbol{v}_h \in \boldsymbol{\mathcal{V}}_h : \ \operatorname{div} \boldsymbol{v}_h = 0 \text{ in } \Omega\}$$

and notice that, here again, $\mathbf{T}_h|_{\boldsymbol{\mathcal{K}}_h} : \boldsymbol{\mathcal{K}}_h \longrightarrow \boldsymbol{\mathcal{K}}_h$ reduces to the identity. Moreover, we have the following result.

Proposition 4.3.2 *$\mu_h = 1$ is an eigenvalue of $\mathbf{T}_h$ and its eigenspace is $\boldsymbol{\mathcal{K}}_h$.*

Proof. We have that $\boldsymbol{w}_h \in \boldsymbol{\mathcal{V}}_h$ is an eigenfunction associated with the eigenvalue $\mu_h = 1$ if and only if $\int_E \operatorname{div} \boldsymbol{w}_h \operatorname{div} \boldsymbol{v}_h = 0 \ \forall \boldsymbol{v}_h \in \boldsymbol{\mathcal{V}}_h$, namely, if and only if $\boldsymbol{w}_h \in \boldsymbol{\mathcal{K}}_h$.
□

As a consequence of all this, we have the following spectral characterization of the discrete solution operator.

Theorem 4.3.1 *The spectrum of $\mathbf{T}_h$ consists of $M_h := \dim(\boldsymbol{\mathcal{V}}_h)$ eigenvalues, repeated according to their respective multiplicities. It decomposes as $\operatorname{sp}(\mathbf{T}_h) = \{1\} \cup \{\mu_{hk}\}_{k=1}^{N_h}$, where:*

i) the eigenspace associated with $\mu_h = 1$ is $\boldsymbol{\mathcal{K}}_h$;

ii) $\mu_{hk} \in (0,1)$, $k = 1, \ldots, N_h := M_h - \dim(\boldsymbol{\mathcal{K}}_h)$, are non-defective eigenvalues repeated according to their respective multiplicities.

In what follows, we derive several auxiliary results which will be used in the following section to prove convergence and error estimates for the spectral approximation.

First, we establish interpolation properties in the discrete space $\boldsymbol{\mathcal{V}}_h$. Although the $\boldsymbol{\mathcal{V}}_h$-interpolant can be defined for less regular functions, in our case it is enough to consider $\boldsymbol{v} \in \boldsymbol{\mathcal{V}}$ such that $\boldsymbol{v}|_E \in [\mathrm{H}^t(E)]^2$ for some $t > 1/2$ and for all $E \in \mathcal{T}_h$, so that we can easily take its trace on each individual edge. Then, we define its interpolant $\boldsymbol{v}_I \in \boldsymbol{\mathcal{V}}_h$ by fixing its degrees of freedom as follows:

$$\int_e (\boldsymbol{v} - \boldsymbol{v}_I) \cdot \boldsymbol{n} \, q \, ds = 0 \qquad \forall q \in \mathbb{P}_k(e), \quad \forall \text{ internal edge } e \not\subset \Gamma; \tag{4.8}$$

$$\int_E (\boldsymbol{v} - \boldsymbol{v}_I) \cdot \nabla q = 0 \qquad \forall q \in \mathbb{P}_k(E)/\mathbb{P}_0(E), \quad \forall E \in \mathcal{T}_h. \tag{4.9}$$

In what follows, we state two results about the approximation properties of this interpolant, whose proof we postpone to the Appendix. The first one concerns approximation properties of $\operatorname{div} \boldsymbol{v}_I$ and follows from a commuting diagram property for this interpolant, which involves the $L^2(\Omega)$-orthogonal projection

$$P_k : \ L^2(\Omega) \longrightarrow \left\{q \in L^2(\Omega) : q|_E \in \mathbb{P}_k(E) \quad \forall E \in \mathcal{T}_h\right\}.$$

Lemma 4.3.2 *Let $\boldsymbol{v} \in \boldsymbol{\mathcal{V}}$ be such that $\boldsymbol{v} \in [\mathrm{H}^t(\Omega)]^2$ with $t > 1/2$. Let $\boldsymbol{v}_I \in \boldsymbol{\mathcal{V}}_h$ be its interpolant defined by* (4.8)–(4.9)*. Then,*

$$\operatorname{div} \boldsymbol{v}_I = P_k(\operatorname{div} \boldsymbol{v}) \quad \text{in } \Omega.$$

Consequently, for all $E \in \mathcal{T}_h$, $\|\operatorname{div} \boldsymbol{v}_I\|_{0,E} \leq \|\operatorname{div} \boldsymbol{v}\|_{0,E}$ and, if $\operatorname{div} \boldsymbol{v}|_E \in \mathrm{H}^r(K)$ with $r \geq 0$, then

$$\|\operatorname{div} \boldsymbol{v} - \operatorname{div} \boldsymbol{v}_I\|_{0,E} \leq C h_E^{\min\{r,k+1\}} |\operatorname{div} \boldsymbol{v}|_{r,E}\,.$$

The second result concerns the $L^2(\Omega)$ approximation property of $\boldsymbol{v}_I$.

Lemma 4.3.3 *Let $\boldsymbol{v} \in \boldsymbol{\mathcal{V}}$ be such that $\boldsymbol{v} \in [\mathrm{H}^t(\Omega)]^2$ with $t > 1/2$. Let $\boldsymbol{v}_I \in \boldsymbol{\mathcal{V}}_h$ be its interpolant defined by* (4.8)–(4.9)*. Let $E \in \mathcal{T}_h$. If $1 \leq t \leq k+1$, then*

$$\|\boldsymbol{v} - \boldsymbol{v}_I\|_{0,E} \leq C h_E^t |\boldsymbol{v}|_{t,E}\,,$$

whereas, if $1/2 < t \leq 1$, then

$$\|\boldsymbol{v} - \boldsymbol{v}_I\|_{0,E} \leq C \left(h_E^t |\boldsymbol{v}|_{t,E} + h_E \|\operatorname{div} \boldsymbol{v}\|_{0,E} \right).$$

Let $\boldsymbol{\mathcal{K}}_h^\perp$ be the $[L^2(\Omega)]^2$-orthogonal complement of $\boldsymbol{\mathcal{K}}_h$ in $\boldsymbol{\mathcal{V}}_h$, namely,

$$\boldsymbol{\mathcal{K}}_h^\perp := \left\{ \boldsymbol{v}_h \in \boldsymbol{\mathcal{V}}_h : \int_\Omega \boldsymbol{v}_h \cdot \boldsymbol{\xi}_h = 0 \quad \forall \boldsymbol{\xi}_h \in \boldsymbol{\mathcal{K}}_h \right\}.$$

Note that $\boldsymbol{\mathcal{K}}_h$ and $\boldsymbol{\mathcal{K}}_h^\perp$ are also orthogonal in $\mathrm{H}(\operatorname{div};\Omega)$. The following lemma shows that, although $\boldsymbol{\mathcal{K}}_h^\perp \not\subset \boldsymbol{\mathcal{K}}^\perp = \boldsymbol{\mathcal{G}} \cap \boldsymbol{\mathcal{V}}$, the gradient part in the Helmholtz decomposition of a function in $\boldsymbol{\mathcal{K}}_h^\perp$ is asymptotically small.

Lemma 4.3.4 *Let $\boldsymbol{v}_h \in \boldsymbol{\mathcal{K}}_h^\perp$. Then, there exist $p \in H^{1+s}(\Omega)$ with $s \in (1/2, 1]$ as in Lemma 4.2.2 and $\boldsymbol{\psi} \in \boldsymbol{\mathcal{K}}$ such that $\boldsymbol{v}_h = \boldsymbol{\psi} + \nabla p$ and*

$$\|\nabla p\|_{s,\Omega} \leq C \|\operatorname{div} \boldsymbol{v}_h\|_{0,\Omega}\,, \tag{4.10}$$

$$\|\boldsymbol{\psi}\|_{0,\Omega} \leq C h^s \|\operatorname{div} \boldsymbol{v}_h\|_{0,\Omega}\,. \tag{4.11}$$

Proof. Let $\boldsymbol{v}_h \in \boldsymbol{\mathcal{K}}_h^\perp \subset \boldsymbol{\mathcal{V}}_h \subset \boldsymbol{\mathcal{V}}$. As a consequence of Lemma 4.2.2, we know that there exist $p \in H^{1+s}(\Omega)$ and $\boldsymbol{\psi} \in \boldsymbol{\mathcal{K}}$ such that $\boldsymbol{v}_h = \nabla p + \boldsymbol{\psi}$ and that $\|\nabla p\|_{s,\Omega} \leq C \|\operatorname{div} \boldsymbol{v}_h\|_{0,\Omega}$, which proves (4.10).

On the other hand, we have that

$$\|\boldsymbol{\psi}\|_{0,\Omega}^2 = \int_\Omega (\nabla p - \boldsymbol{v}_h) \cdot (\nabla p - (\nabla p)_I) + \int_\Omega (\nabla p - \boldsymbol{v}_h) \cdot ((\nabla p)_I - \boldsymbol{v}_h)\,.$$

Now, according to Lemma 4.3.2, $\operatorname{div}((\nabla p)_I) = P_k(\operatorname{div}(\nabla p))$. Therefore, since $\Delta p = \operatorname{div} \boldsymbol{v}_h$, we obtain

$$\operatorname{div}\left((\nabla p)_I - \boldsymbol{v}_h\right) = P_k\left(\Delta p\right) - \operatorname{div} \boldsymbol{v}_h = P_k\left(\operatorname{div} \boldsymbol{v}_h\right) - \operatorname{div} \boldsymbol{v}_h = 0,$$

where we have used that for $\boldsymbol{v}_h \in \boldsymbol{\mathcal{V}}_h$, $\operatorname{div} \boldsymbol{v}_h|_E \in \mathbb{P}_k(E)$. Therefore $((\nabla p)_I - \boldsymbol{v}_h) \in \boldsymbol{\mathcal{K}}_h \subseteq \boldsymbol{\mathcal{K}}$ and since $\nabla p \in \boldsymbol{\mathcal{G}} \cap \boldsymbol{\mathcal{V}} = \boldsymbol{\mathcal{K}}^\perp$ and $\boldsymbol{v}_h \in \boldsymbol{\mathcal{K}}_h^\perp$, we have that

$$\int_\Omega (\nabla p - \boldsymbol{v}_h) \cdot ((\nabla p)_I - \boldsymbol{v}_h) = 0.$$

Thus,

$$\|\boldsymbol{\psi}\|_{0,\Omega}^2 = \int_\Omega (\nabla p - \boldsymbol{v}_h) \cdot (\nabla p - (\nabla p)_I)$$

and, by using Cauchy-Schwarz inequality, Lemma 4.3.3 and (4.10), we obtain

$$\begin{aligned}
\|\boldsymbol{\psi}\|_{0,\Omega}^2 &\leq \sum_{E \in \mathcal{T}_h} \|\nabla p - \boldsymbol{v}_h\|_{0,E} \, \|\nabla p - (\nabla p)_I\|_{0,E} \\
&\leq C \sum_{E \in \mathcal{T}_h} \|\nabla p - \boldsymbol{v}_h\|_{0,E} \left(h_E^s \, \|\nabla p\|_{s,E} + h_E \, \|\operatorname{div}(\nabla p)\|_{0,E} \right) \\
&\leq C h^s \, \|\boldsymbol{\psi}\|_{0,\Omega} \, \|\operatorname{div} \boldsymbol{v}_h\|_{0,\Omega} \,,
\end{aligned}$$

which allows us to complete the proof.
□

To end this section, we prove the following result which will be used in the sequel. Let $\boldsymbol{\Pi}_h$ be defined in $\boldsymbol{\mathcal{V}}$ by

$$(\boldsymbol{\Pi}_h \boldsymbol{v})\,|_E := \boldsymbol{\Pi}_h^E(\boldsymbol{v}|_E) \quad \text{ for all } E \in \mathcal{T}_h \tag{4.12}$$

with $\boldsymbol{\Pi}_h^E$ defined by (4.3).

Lemma 4.3.5 *There exists a constant $C > 0$ such that, for every $p \in \mathrm{H}^{1+t}(\Omega)$ with $1/2 < t \leq k+1$, there holds*

$$\|\nabla p - \boldsymbol{\Pi}_h(\nabla p)\|_{0,\Omega} \leq C h^t \, \|\nabla p\|_{t,\Omega} \,.$$

Proof. The result follows from the fact that, since $\boldsymbol{\Pi}_h^E$ is the $[\mathrm{L}^2(E)]^2$-projection onto $\widehat{\boldsymbol{\mathcal{V}}}_h^E := \nabla(\mathbb{P}_{k+1}(E))$ (cf. (4.3)),

$$\left\|\nabla p - \boldsymbol{\Pi}_h^E(\nabla p)\right\|_{0,E} = \inf_{q \in \mathbb{P}_{k+1}(E)} \|\nabla p - \nabla q\|_{0,E} \leq C h_E^t \, \|\nabla p\|_{t,E} \,.$$

Let us remark that the last inequality is a consequence of standard approximation estimates for polynomials on polygons in case of integer t (see, for instance, [51, Lemma 4.3.8]) and standard Banach space interpolation results for non-integer t.
□

4.4. Spectral approximation and error estimates

To prove that $\mathbf{T}_h$ provides a correct spectral approximation of $\mathbf{T}$, we will resort to the theory developed in [74] for non-compact operators. To this end, we first introduce some notation. For any linear bounded operator $\mathbf{S} : \boldsymbol{\mathcal{V}} \longrightarrow \boldsymbol{\mathcal{V}}$, we define

$$\|\mathbf{S}\|_h := \sup_{\mathbf{0} \neq \boldsymbol{v}_h \in \boldsymbol{\mathcal{V}}_h} \frac{\|\mathbf{S}\boldsymbol{v}_h\|_{\operatorname{div},\Omega}}{\|\boldsymbol{v}_h\|_{\operatorname{div},\Omega}}.$$

We recall the definition of the *gap* $\widehat{\delta}$ between two closed subspaces $\boldsymbol{\mathcal{X}}$ and $\boldsymbol{\mathcal{Y}}$ of $\boldsymbol{\mathcal{V}}$:

$$\widehat{\delta}(\boldsymbol{\mathcal{X}},\boldsymbol{\mathcal{Y}}) := \max\left\{\delta(\boldsymbol{\mathcal{X}},\boldsymbol{\mathcal{Y}}),\delta(\boldsymbol{\mathcal{Y}},\boldsymbol{\mathcal{X}})\right\},$$

where

$$\delta(\boldsymbol{\mathcal{X}},\boldsymbol{\mathcal{Y}}) := \sup_{\substack{\boldsymbol{x}\in\boldsymbol{\mathcal{X}}\\ \|\boldsymbol{x}\|_{\mathrm{div},\Omega}=1}} \delta(\boldsymbol{x},\boldsymbol{\mathcal{Y}}) \qquad \text{with } \delta(\boldsymbol{x},\boldsymbol{\mathcal{Y}}) := \inf_{\boldsymbol{y}\in\boldsymbol{\mathcal{Y}}} \|\boldsymbol{x}-\boldsymbol{y}\|_{\mathrm{div},\Omega}.$$

The theory from [74] guarantees approximation of the spectrum of $\mathbf{T}$, provided the following two properties are satisfied:

- **P1**: $\|\mathbf{T}-\mathbf{T}_h\|_h \to 0$ as $h\to 0$;
- **P2**: $\forall \boldsymbol{v}\in\boldsymbol{\mathcal{V}} \quad \lim_{h\to 0}\delta(\boldsymbol{v},\boldsymbol{\mathcal{V}}_h)=0.$

Property **P2** follows immediately from the density of the smooth functions in $\boldsymbol{\mathcal{V}}$ and the approximation properties in Lemmas 4.3.2 and 4.3.3. Hence, there only remains to prove property **P1**. With this aim, first we note that since $\mathbf{T}|_{\boldsymbol{\mathcal{K}}_h}$ and $\mathbf{T}_h|_{\boldsymbol{\mathcal{K}}_h}$ both reduce to the identity, it is enough to estimate $\|(\mathbf{T}-\mathbf{T}_h)\,\boldsymbol{f}_h\|_{\mathrm{div},\Omega}$ for $\boldsymbol{f}_h\in\boldsymbol{\mathcal{K}}_h^{\perp}$.

Lemma 4.4.1 *There exists $C>0$ such that, for all $\boldsymbol{f}_h\in\boldsymbol{\mathcal{K}}_h^{\perp}$,*

$$\|(\mathbf{T}-\mathbf{T}_h)\,\boldsymbol{f}_h\|_{\mathrm{div},\Omega} \le C h^s \|\boldsymbol{f}_h\|_{\mathrm{div},\Omega}$$

with $s\in(1/2,1]$ as in Lemma 4.2.2.

Proof. Let $\boldsymbol{f}_h\in\boldsymbol{\mathcal{K}}_h^{\perp}$, $\boldsymbol{u}:=\mathbf{T}\boldsymbol{f}_h$ and $\boldsymbol{u}_h:=\mathbf{T}_h\boldsymbol{f}_h$. According to Lemma 4.2.2, we write $\boldsymbol{u}=\boldsymbol{\varphi}+\nabla q$ with $\boldsymbol{\varphi}\in\boldsymbol{\mathcal{K}}$, $\nabla q\in[\mathrm{H}^s(\Omega)]^2$ and $\|\nabla q\|_{s,\Omega}\le C\,\|\mathrm{div}\,\boldsymbol{u}\|_{0,\Omega}$. We have

$$\|(\mathbf{T}-\mathbf{T}_h)\,\boldsymbol{f}_h\|_{\mathrm{div},\Omega} \le \|\boldsymbol{u}-(\nabla q)_I\|_{\mathrm{div},\Omega} + \|\boldsymbol{u}_h-(\nabla q)_I\|_{\mathrm{div},\Omega}, \tag{4.13}$$

where $(\nabla q)_I$ is the $\boldsymbol{\mathcal{V}}_h$-interpolant of ∇q defined by (4.8)–(4.9). We define $\boldsymbol{v}_h:=\boldsymbol{u}_h-(\nabla q)_I\in\boldsymbol{\mathcal{V}}_h$. Thanks to Lemma 4.3.1, the definition (4.5) of $b_h^E(\cdot,\cdot)$ and those of $\mathbf{T}$ and $\mathbf{T}_h$, we have

$$\begin{aligned}
\beta\,\|\boldsymbol{v}_h\|_{\mathrm{div},\Omega}^2 &\le a_h(\boldsymbol{v}_h,\boldsymbol{v}_h) = a_h(\boldsymbol{u}_h,\boldsymbol{v}_h) - a_h((\nabla q)_I,\boldsymbol{v}_h)\\
&= b_h(\boldsymbol{f}_h,\boldsymbol{v}_h) - \int_\Omega \mathrm{div}((\nabla q)_I)\,\mathrm{div}\,\boldsymbol{v}_h - \sum_{E\in\mathcal{T}_h} b_h^E((\nabla q)_I,\boldsymbol{v}_h)\\
&= b_h(\boldsymbol{f}_h,\boldsymbol{v}_h) - \int_\Omega \boldsymbol{f}_h\cdot\boldsymbol{v}_h + \int_\Omega \mathrm{div}(\boldsymbol{u}-(\nabla q)_I)\,\mathrm{div}\,\boldsymbol{v}_h\\
&\quad - \sum_{E\in\mathcal{T}_h}\left(b_h^E\left((\nabla q)_I-\boldsymbol{\Pi}_h^E\boldsymbol{u},\boldsymbol{v}_h\right) + \int_E\left(\boldsymbol{\Pi}_h^E\boldsymbol{u}-\boldsymbol{u}\right)\cdot\boldsymbol{v}_h\right),
\end{aligned}$$

where for the last equality we have also used the consistency property (4.6). Since $\mathrm{div}((\nabla q)_I) = P_k(\mathrm{div}(\nabla q))$ (cf. Lemma 4.3.2), we have that $\int_\Omega \mathrm{div}(\boldsymbol{u}-(\nabla q)_I)\,\mathrm{div}\,\boldsymbol{v}_h=0$ for all $\boldsymbol{v}_h\in\boldsymbol{\mathcal{V}}_h$. Then,

$$\begin{aligned}
\beta\,\|\boldsymbol{v}_h\|_{\mathrm{div},\Omega}^2 \le \left(b_h(\boldsymbol{f}_h,\boldsymbol{v}_h) - \int_\Omega \boldsymbol{f}_h\cdot\boldsymbol{v}_h\right)\\
- \sum_{E\in\mathcal{T}_h}\left(b_h^E((\nabla q)_I-\boldsymbol{\Pi}_h^E\boldsymbol{u},\boldsymbol{v}_h) + \int_E\left(\boldsymbol{\Pi}_h^E\boldsymbol{u}-\boldsymbol{u}\right)\cdot\boldsymbol{v}_h\right).
\end{aligned} \tag{4.14}$$

The first term on the right hand side can be bounded as follows:

$$\begin{aligned} b_h(\boldsymbol{f}_h,\boldsymbol{v}_h) - \int_\Omega \boldsymbol{f}_h\cdot\boldsymbol{v}_h &= \sum_{E\in\mathcal{T}_h}\left(b_h^E(\boldsymbol{f}_h,\boldsymbol{v}_h) - \int_E \boldsymbol{f}_h\cdot\boldsymbol{v}_h\right)\\ &= \sum_{E\in\mathcal{T}_h}\left(\int_E \boldsymbol{\Pi}_h^E\boldsymbol{f}_h\cdot\boldsymbol{\Pi}_h^E\boldsymbol{v}_h + S^E\big(\boldsymbol{f}_h-\boldsymbol{\Pi}_h^E\boldsymbol{f}_h,\boldsymbol{v}_h-\boldsymbol{\Pi}_h^E\boldsymbol{v}_h\big) - \int_E \boldsymbol{f}_h\cdot\boldsymbol{v}_h\right)\\ &= \sum_{E\in\mathcal{T}_h}\int_E (\boldsymbol{\Pi}_h^E\boldsymbol{f}_h-\boldsymbol{f}_h)\cdot\boldsymbol{v}_h + \sum_{E\in\mathcal{T}_h} S^E\big(\boldsymbol{f}_h-\boldsymbol{\Pi}_h^E\boldsymbol{f}_h,\boldsymbol{v}_h-\boldsymbol{\Pi}_h^E\boldsymbol{v}_h\big), \end{aligned}$$

where we have used (4.3) to write the last equality. Now, from the symmetry of $S^E(\cdot,\cdot)$, (4.4), a Cauchy-Schwarz inequality and the fact that $\boldsymbol{\Pi}_h^E$ is an $\mathrm{L}^2(E)$-projection (cf. (4.3)), we have that

$$\sum_{E\in\mathcal{T}_h} S^E\big(\boldsymbol{f}_h-\boldsymbol{\Pi}_h^E\boldsymbol{f}_h,\boldsymbol{v}_h-\boldsymbol{\Pi}_h^E\boldsymbol{v}_h\big) \le \sum_{E\in\mathcal{T}_h} c_1\big\|\boldsymbol{f}_h-\boldsymbol{\Pi}_h^E\boldsymbol{f}_h\big\|_{0,E}\,\|\boldsymbol{v}_h\|_{0,E}\,.$$

Therefore, using Cauchy-Schwarz inequality again,

$$b_h(\boldsymbol{f}_h,\boldsymbol{v}_h) - \int_\Omega \boldsymbol{f}_h\cdot\boldsymbol{v}_h \le C\sum_{E\in\mathcal{T}_h}\big\|\boldsymbol{f}_h-\boldsymbol{\Pi}_h^E\boldsymbol{f}_h\big\|_{0,E}\,\|\boldsymbol{v}_h\|_{0,E}\,. \tag{4.15}$$

Substituting the above estimate in (4.14), from (4.7) and Cauchy-Schwarz inequality we obtain

$$\begin{aligned} \beta\,\|\boldsymbol{v}_h\|_{\mathrm{div},\Omega}^2 &\le C\sum_{E\in\mathcal{T}_h}\left(\big\|\boldsymbol{f}_h-\boldsymbol{\Pi}_h^E\boldsymbol{f}_h\big\|_{0,E} + \|\boldsymbol{u}-(\nabla q)_I\|_{0,E} + \big\|\boldsymbol{u}-\boldsymbol{\Pi}_h^E\boldsymbol{u}\big\|_{0,E}\right)\|\boldsymbol{v}_h\|_{0,E}\\ &\le C\left(\|\boldsymbol{f}_h-\boldsymbol{\Pi}_h\boldsymbol{f}_h\|_{0,\Omega} + \|\boldsymbol{u}-(\nabla q)_I\|_{0,\Omega} + \|\boldsymbol{u}-\boldsymbol{\Pi}_h\boldsymbol{u}\|_{0,\Omega}\right)\|\boldsymbol{v}_h\|_{\mathrm{div},\Omega}\,, \end{aligned}$$

with $\boldsymbol{\Pi}_h$ as defined in (4.12). Therefore, from (4.13),

$$\|(\mathbf{T}-\mathbf{T}_h)\,\boldsymbol{f}_h\|_{\mathrm{div},\Omega} \le C\left(\|\boldsymbol{f}_h-\boldsymbol{\Pi}_h\boldsymbol{f}_h\|_{0,\Omega} + \|\boldsymbol{u}-\boldsymbol{\Pi}_h\boldsymbol{u}\|_{0,\Omega} + \|\boldsymbol{u}-(\nabla q)_I\|_{\mathrm{div},\Omega}\right).$$

Thus, there only remains to estimate the three terms on the right-hand side above. For the first one we write $\boldsymbol{f}_h = \boldsymbol{\psi}+\nabla p$ with $\psi\in\boldsymbol{\mathcal{K}}$ and $p\in H^{1+s}(\Omega)$ as in Lemma 4.3.4. Hence, by using this and Lemma 4.3.5,

$$\begin{aligned} \|\boldsymbol{f}_h-\boldsymbol{\Pi}_h\boldsymbol{f}_h\|_{0,\Omega} &\le \|\boldsymbol{\psi}-\boldsymbol{\Pi}_h\boldsymbol{\psi}\|_{0,\Omega} + \|\nabla p-\boldsymbol{\Pi}_h(\nabla p)\|_{0,\Omega}\\ &\le C\left(\|\boldsymbol{\psi}\|_{0,\Omega} + \|\nabla p-\boldsymbol{\Pi}_h(\nabla p)\|_{0,\Omega}\right)\\ &\le Ch^s\,\|\mathrm{div}\,\boldsymbol{f}_h\|_{0,\Omega}\,. \end{aligned}$$

On the other hand, we have that $\boldsymbol{u} = \mathbf{T}(\boldsymbol{\psi}+\nabla p) = \boldsymbol{\psi}+\mathbf{T}(\nabla p)$ and, from Lemmas 4.2.3 and 4.2.2, $\mathbf{T}(\nabla p)=\nabla q$ and $\boldsymbol{\psi}=\boldsymbol{\varphi}$. Moreover, by virtue of Theorem 4.2.1, $q\in H^{1+s}(\Omega)$ and

$$\|\nabla q\|_{s,\Omega} \le C\,\|\nabla p\|_{\mathrm{div},\Omega} \le C\,\|\boldsymbol{f}_h\|_{\mathrm{div},\Omega}\,,$$

whereas estimate (4.11) still holds true for $\boldsymbol{\psi}$:

$$\|\boldsymbol{\psi}\|_{0,\Omega} \le Ch^s\,\|\mathrm{div}\,\boldsymbol{f}_h\|_{0,\Omega}\,.$$

Then, using that $\boldsymbol{\Pi}_h$ is an $[L^2(\Omega)]^2$-projection, from Lemmas 4.3.4 and 4.3.5 we have

$$\begin{aligned}\|\boldsymbol{u}-\boldsymbol{\Pi}_h\boldsymbol{u}\|_{0,\Omega} &\leq \|\boldsymbol{\psi}-\boldsymbol{\Pi}_h\boldsymbol{\psi}\|_{0,\Omega}+\|\nabla q-\boldsymbol{\Pi}_h(\nabla q)\|_{0,\Omega})\\ &\leq C\left(\|\boldsymbol{\psi}\|_{0,\Omega}+\|\nabla q-\boldsymbol{\Pi}_h(\nabla q)\|_{0,\Omega}\right)\\ &\leq Ch^s\,\|\mathrm{div}\,\boldsymbol{f}_h\|_{0,\Omega}+Ch^s\,\|\nabla q\|_{s,\Omega}\\ &\leq Ch^s\,\|\boldsymbol{f}_h\|_{\mathrm{div},\Omega}\,.\end{aligned}$$

Finally, using once more that $\boldsymbol{u}=\boldsymbol{\psi}+\nabla q$ and Lemmas 4.3.4, 4.3.3 and 4.3.2, we write

$$\begin{aligned}\|\boldsymbol{u}-(\nabla q)_I\|_{\mathrm{div},\Omega} &\leq \|\boldsymbol{\psi}\|_{\mathrm{div},\Omega}+\|\nabla q-(\nabla q)_I\|_{\mathrm{div},\Omega}\\ &\leq Ch^s\,\|\mathrm{div}\,\boldsymbol{f}_h\|_{0,\Omega}+\|\nabla q-(\nabla q)_I\|_{0,\Omega}+\|\mathrm{div}(\nabla q)-\mathrm{div}((\nabla q)_I)\|_{0,\Omega}\\ &\leq Ch^s\,\|\boldsymbol{f}_h\|_{\mathrm{div},\Omega}+C\left(h^s\,|\nabla q|_{s,\Omega}+h\,\|\mathrm{div}(\nabla q)\|_{0,\Omega}\right)+Ch\,|\mathrm{div}(\nabla q)|_{1,\Omega}\\ &\leq Ch^s\,\|\boldsymbol{f}_h\|_{\mathrm{div},\Omega}\,,\end{aligned}$$

where, we have used that $\nabla q=\mathbf{T}(\nabla p)$ and, hence, since $\nabla p\in\boldsymbol{\mathcal{G}}\cap\boldsymbol{\mathcal{V}}$, from Theorem 4.2.1 $\mathrm{div}(\nabla q)\in H^1(\Omega)$ and $\|\mathrm{div}(\nabla q)\|_{1,\Omega}\leq C\,\|\nabla p\|_{\mathrm{div},\Omega}\leq C\,\|\boldsymbol{f}_h\|_{\mathrm{div},\Omega}$.

Collecting the previous estimates, we obtain

$$\|(\mathbf{T}-\mathbf{T}_h)\,\boldsymbol{f}_h\|_{\mathrm{div},\Omega}\leq Ch^s\,\|\boldsymbol{f}_h\|_{\mathrm{div},\Omega}$$

and we end the proof.

□

Now, we are in a position to conclude property **P1**.

Corollary 4.4.1 *There exists $C>0$, independent of h, such that*

$$\|\mathbf{T}-\mathbf{T}_h\|_h\leq Ch^s.$$

Proof. Given $\boldsymbol{v}_h\in\boldsymbol{\mathcal{V}}_h$, we have that $\boldsymbol{v}_h=\boldsymbol{\psi}_h+\boldsymbol{f}_h$ with $\boldsymbol{\psi}_h\in\boldsymbol{\mathcal{K}}_h$ and $\boldsymbol{f}_h\in\boldsymbol{\mathcal{K}}_h^{\perp}$, then

$$\|(\mathbf{T}-\mathbf{T}_h)\,\boldsymbol{v}_h\|_{\mathrm{div},\Omega}=\|(\mathbf{T}-\mathbf{T}_h)\,\boldsymbol{f}_h\|_{\mathrm{div},\Omega}\leq Ch^s\,\|\boldsymbol{f}_h\|_{\mathrm{div},\Omega}\,,$$

where the last inequality follows from Lemma 4.4.1. The proof follows by noting that, since $\boldsymbol{v}_h=\boldsymbol{\psi}_h+\boldsymbol{f}_h$ is an orthogonal decomposition in $\mathrm{H}(\mathrm{div};\Omega)$, we have that $\|\boldsymbol{f}_h\|_{\mathrm{div},\Omega}\leq\|\boldsymbol{v}_h\|_{\mathrm{div},\Omega}$.

□

In order to establish spectral convergence and error estimates, we recall some other basic definitions from spectral theory.

Given a generic linear bounded operator $\mathbf{S}:\ \boldsymbol{\mathcal{V}}\longrightarrow\boldsymbol{\mathcal{V}}$ defined on a Hilbert space $\boldsymbol{\mathcal{V}}$, the spectrum of $\mathbf{S}$ is the set $\mathrm{sp}(\mathbf{S}):=\{z\in\mathbb{C}:\ (z\mathbf{I}-\mathbf{S})\ \text{is not invertible}\}$ and the resolvent set of $\mathbf{S}$ is its complement $\rho(\mathbf{S}):=\mathbb{C}\setminus\mathrm{sp}(\mathbf{S})$. For any $z\in\rho(\mathbf{S})$, $R_z(\mathbf{S}):=(z\mathbf{I}-\mathbf{S})^{-1}:\ \boldsymbol{\mathcal{V}}\longrightarrow\boldsymbol{\mathcal{V}}$ is the resolvent operator of $\mathbf{S}$ corresponding to z.

The following two results are consequence of property **P1**, see [74, Lemma 1 and Theorem 1].

Lemma 4.4.2 *Let us assume that* **P1** *holds true and let $F \subset \rho(\mathbf{T})$ be closed. Then, there exist positive constants C and h_0 independent of h, such that for $h < h_0$*

$$\sup_{\boldsymbol{v}_h \in \boldsymbol{\mathcal{V}}_h} \|R_z(\mathbf{T}_h)\boldsymbol{v}_h\|_{\mathrm{div},\Omega} \leq C \|\boldsymbol{v}_h\|_{\mathrm{div},\Omega} \qquad \forall z \in F.$$

Theorem 4.4.1 *Let $U \subset \mathbb{C}$ be an open set containing* $\mathrm{sp}(\mathbf{T})$*. Then, there exists $h_0 > 0$ such that* $\mathrm{sp}(\mathbf{T}_h) \subset U$ *for all $h < h_0$.*

An immediate consequence of this theorem and Corollary 4.4.1 is that the proposed virtual element method does not introduce spurious modes with eigenvalues interspersed among those with a physical meaning. Let us remark that such a spectral pollution could be in principle expected from the fact that the corresponding solution operator $\mathbf{T}$ has an infinite-dimensional eigenvalue $\mu = 1$ (see [40, 44, 48]).

By applying the results from [74, Section 2] to our problem, we conclude the spectral convergence of $\mathbf{T}_h$ to $\mathbf{T}$ as $h \to 0$. More precisely, let $\mu \in (0,1)$ be an isolated eigenvalue of $\mathbf{T}$ with multiplicity m and let $\mathcal{C}$ be an open circle in the complex plane centered at μ, such that μ is the only eigenvalue of $\mathbf{T}$ lying in $\mathcal{C}$ and $\partial\mathcal{C} \cap \mathrm{sp}(\mathbf{T}) = \emptyset$. Then, according to [74, Section 2], for h small enough there exist m eigenvalues $\mu_h^{(1)}, \ldots, \mu_h^{(m)}$ of $\mathbf{T}_h$ (repeated according to their respective multiplicities) which lie in $\mathcal{C}$. Therefore, these eigenvalues $\mu_h^{(1)}, \ldots, \mu_h^{(m)}$ converge to μ as h goes to zero.

Our next step is to obtain error estimates for the spectral approximation. The classical reference for this issue on non-compact operators is [75]. However, we cannot apply the results from this reference directly to our problem, because of the variational crimes in the bilinear forms used to define the operator $\mathbf{T}_h$. Therefore, we need to extend the results from this reference to our case. With this purpose, we follow an approach inspired by those of [41, 95].

Consider the eigenspace $\boldsymbol{\mathcal{E}}$ of $\mathbf{T}$ corresponding to μ and the $\mathbf{T}_h$-invariant subspace $\boldsymbol{\mathcal{E}}_h$ spanned by the eigenspaces of $\mathbf{T}_h$ corresponding to $\mu_h^{(1)}, \ldots, \mu_h^{(m)}$. As a consequence of Lemma 4.4.2, we have for h small enough

$$\|(z\mathbf{I} - \mathbf{T}_h)\,\boldsymbol{v}_h\|_{\mathrm{div},\Omega} \geq C \|\boldsymbol{v}_h\|_{\mathrm{div},\Omega} \qquad \forall \boldsymbol{v}_h \in \boldsymbol{\mathcal{V}}_h, \quad \forall z \in \partial\mathcal{C}. \tag{4.16}$$

Let $\mathbf{P}_h : \boldsymbol{\mathcal{V}} \longrightarrow \boldsymbol{\mathcal{V}}_h \hookrightarrow \boldsymbol{\mathcal{V}}$ be the projector with range $\boldsymbol{\mathcal{V}}_h$ defined by the relation

$$a(\mathbf{P}_h\boldsymbol{u} - \boldsymbol{u}, \boldsymbol{v}_h) = 0 \qquad \forall \boldsymbol{v}_h \in \boldsymbol{\mathcal{V}}_h.$$

In our case, the bilinear form $a(\cdot,\cdot)$ is the inner product of $\boldsymbol{\mathcal{V}}$, so that $\|\mathbf{P}_h\boldsymbol{u}\|_{\mathrm{div},\Omega} \leq \|\boldsymbol{u}\|_{\mathrm{div},\Omega}$ and

$$\|\boldsymbol{u} - \mathbf{P}_h\boldsymbol{u}\|_{\mathrm{div},\Omega} = \delta(\boldsymbol{u}, \boldsymbol{\mathcal{V}}_h) \qquad \forall \boldsymbol{u} \in \boldsymbol{\mathcal{V}}.$$

Now, we define $\widehat{\mathbf{T}}_h := \mathbf{T}_h\mathbf{P}_h : \boldsymbol{\mathcal{V}} \longrightarrow \boldsymbol{\mathcal{V}}_h$. Notice that $\mathrm{sp}(\widehat{\mathbf{T}}_h) = \mathrm{sp}(\mathbf{T}_h) \cup \{0\}$. Furthermore, we have the following result (cf. [75, Lemma 1]).

Lemma 4.4.3 *There exist $h_0 > 0$ and $C > 0$ such that*

$$\left\|R_z(\widehat{\mathbf{T}}_h)\right\|_{\mathrm{div},\Omega} \leq C \qquad \forall z \in \partial\mathcal{C}, \quad \forall h \leq h_0.$$

Proof. Since $\widehat{\mathbf{T}}_h$ is compact, it suffices to check that $\left\|(z\mathbf{I}-\widehat{\mathbf{T}}_h)\boldsymbol{v}\right\|_{\mathrm{div},\Omega} \geq C\,\|\boldsymbol{v}\|_{\mathrm{div},\Omega}\ \ \forall \boldsymbol{v}\in\boldsymbol{\mathcal{V}}$ and $\forall z\in\partial\mathcal{C}$. By using (4.16) and basic properties of the projector $\mathbf{P}_h$, we obtain

$$\begin{aligned}
\|\boldsymbol{v}\|_{\mathrm{div},\Omega} &\leq \|\mathbf{P}_h\boldsymbol{v}\|_{\mathrm{div},\Omega} + \|\boldsymbol{v}-\mathbf{P}_h\boldsymbol{v}\|_{\mathrm{div},\Omega}\\
&\leq C\,\|(z\mathbf{I}-\mathbf{T}_h)\,\mathbf{P}_h\boldsymbol{v}\|_{\mathrm{div},\Omega} + |z|^{-1}\,\|z\,(\boldsymbol{v}-\mathbf{P}_h\boldsymbol{v})\|_{\mathrm{div},\Omega}\\
&\leq C\left\|\left(z\mathbf{I}-\widehat{\mathbf{T}}_h\right)\mathbf{P}_h\boldsymbol{v}\right\|_{\mathrm{div},\Omega} + |z|^{-1}\left\|z\,(\boldsymbol{v}-\mathbf{P}_h\boldsymbol{v}) - \widehat{\mathbf{T}}_h\,(\boldsymbol{v}-\mathbf{P}_h\boldsymbol{v})\,\right\|_{\mathrm{div},\Omega}\\
&= C\left\|\mathbf{P}_h\left(z\mathbf{I}-\widehat{\mathbf{T}}_h\right)\boldsymbol{v}\right\|_{\mathrm{div},\Omega} + |z|^{-1}\left\|\,(\mathbf{I}-\mathbf{P}_h)\left(z\mathbf{I}-\widehat{\mathbf{T}}_h\right)\boldsymbol{v})\right\|_{\mathrm{div},\Omega}\\
&\leq C\left\|\left(z\mathbf{I}-\widehat{\mathbf{T}}_h\right)\boldsymbol{v}\right\|_{\mathrm{div},\Omega},
\end{aligned}$$

where we have used that the curve $\partial\mathcal{C}$ is bounded away from 0.
□

Next, we introduce the following spectral projectors (the second one, is well defined at least for h small enough):

- the spectral projector of $\mathbf{T}$ relative to μ: $\quad \mathbf{F} := \dfrac{1}{2\pi i}\displaystyle\int_{\partial\mathcal{C}} R_z(\mathbf{T})\,dz$;
- the spectral projector of $\widehat{\mathbf{T}}_h$ relative to $\mu_h^{(1)},\ldots,\mu_h^{(m)}$: $\quad \widehat{\mathbf{F}}_h := \dfrac{1}{2\pi i}\displaystyle\int_{\partial\mathcal{C}} R_z(\widehat{\mathbf{T}}_h)\,dz$.

We also introduce the quantities

$$\gamma_h := \delta(\boldsymbol{\mathcal{E}},\boldsymbol{\mathcal{V}}_h) \qquad \text{and} \qquad \eta_h := \sup_{\boldsymbol{w}\in\boldsymbol{\mathcal{E}}} \frac{\|\boldsymbol{w}-\boldsymbol{\Pi}_h\boldsymbol{w}\|_{0,\Omega}}{\|\boldsymbol{w}\|_{\mathrm{div},\Omega}}.$$

These two quantities are bounded as follows:

$$\gamma_h \leq Ch^{\mín\{\tilde{s},k+1\}} \qquad \text{and} \qquad \eta_h \leq Ch^{\mín\{\tilde{s},k+1\}}, \tag{4.17}$$

where $\tilde{s}>1/2$ is such that $\boldsymbol{\mathcal{E}}\subset[\mathrm{H}^{\tilde{s}}(\Omega)]^2$ (cf. Theorem 4.2.2). In fact, the first estimate follows from Lemmas 4.3.2 and 4.3.3 and Theorem 4.2.2(ii), whereas the latter follows from the fact that $\boldsymbol{\mathcal{E}}\subset\boldsymbol{\mathcal{G}}\cap\boldsymbol{\mathcal{V}}$, Lemma 4.3.5 and Theorem 4.2.2(ii) again.

The following estimate is a variation of Lemma 3 from [75]) that will be used to prove convergence of the eigenspaces.

Lemma 4.4.4 *There exist positive constants h_0 and C such that, for all $h<h_0$,*

$$\left\|(\mathbf{F}-\widehat{\mathbf{F}}_h)|_{\boldsymbol{\mathcal{E}}}\right\|_{\mathrm{div},\Omega} \leq C\left\|(\mathbf{T}-\widehat{\mathbf{T}}_h)|_{\boldsymbol{\mathcal{E}}}\right\|_{\mathrm{div},\Omega} \leq C\,(\gamma_h+\eta_h)\,.$$

Proof. The first inequality is proved using the same arguments of [75, Lemma 3] and Lemma 4.4.3. For the other estimate, let $\boldsymbol{f}\in\boldsymbol{\mathcal{E}}$, $\boldsymbol{w}:=\mathbf{T}\boldsymbol{f}$ and $\boldsymbol{w}_h := \widehat{\mathbf{T}}_h\boldsymbol{f} = \mathbf{T}_h\mathbf{P}_h\boldsymbol{f}$. Note that, by Theorem 4.2.2(ii), $\boldsymbol{f}\in\nabla(\mathrm{H}^{1+\tilde{s}}(\Omega))$, $\tilde{s}>1/2$. By using the first Strang lemma (see, for instance, [69, Theorem 4.1.1]), we have

$$\begin{aligned}
\|\boldsymbol{w}-\boldsymbol{w}_h\|_{\mathrm{div},\Omega} \leq C\Bigg(&\|\boldsymbol{w}-\mathbf{P}_h\boldsymbol{w}\|_{\mathrm{div},\Omega} + \sup_{\boldsymbol{v}_h\in\boldsymbol{\mathcal{V}}_h}\frac{|b(\mathbf{P}_h\boldsymbol{w},\boldsymbol{v}_h)-b_h(\mathbf{P}_h\boldsymbol{w},\boldsymbol{v}_h)|}{\|\boldsymbol{v}_h\|_{\mathrm{div},\Omega}}\\
&+\sup_{\boldsymbol{v}_h\in\boldsymbol{\mathcal{V}}_h}\frac{|b(\boldsymbol{f},\boldsymbol{v}_h)-b_h(\mathbf{P}_h\boldsymbol{f},\boldsymbol{v}_h)|}{\|\boldsymbol{v}_h\|_{\mathrm{div},\Omega}}\Bigg)
\end{aligned}$$

and by proceeding as in the proof of Lemma 4.4.1 to derive (4.15), we obtain

$$\begin{aligned}|b(\mathbf{P}_h\boldsymbol{w},\boldsymbol{v}_h)-b_h(\mathbf{P}_h\boldsymbol{w},\boldsymbol{v}_h)| &\le C\sum_{E\in\mathcal{T}_h}\left\|\mathbf{P}_h\boldsymbol{w}-\boldsymbol{\Pi}_h^E\mathbf{P}_h\boldsymbol{w}\right\|_{0,E}\|\boldsymbol{v}_h\|_{0,E}\\ &\le C\sum_{E\in\mathcal{T}_h}\left\|\left(\mathbf{I}-\boldsymbol{\Pi}_h^E\right)\left(\mathbf{P}_h\boldsymbol{w}-\boldsymbol{w}\right)+\left(\mathbf{I}-\boldsymbol{\Pi}_h^E\right)\boldsymbol{w}\right\|_{0,E}\\ &\le C\left(\|\boldsymbol{w}-\mathbf{P}_h\boldsymbol{w}\|_{0,\Omega}+\|\boldsymbol{w}-\boldsymbol{\Pi}_h\boldsymbol{w}\|_{0,\Omega}\right)\|\boldsymbol{v}_h\|_{\mathrm{div},\Omega}\,.\end{aligned}$$

On the other hand,

$$\begin{aligned}|b(\boldsymbol{f},\boldsymbol{v}_h)-b_h(\mathbf{P}_h\boldsymbol{f},\boldsymbol{v}_h)| &\le |b(\boldsymbol{f}-\mathbf{P}_h\boldsymbol{f},\boldsymbol{v}_h)|+|b(\mathbf{P}_h\boldsymbol{f},\boldsymbol{v}_h)-b_h(\mathbf{P}_h\boldsymbol{f},\boldsymbol{v}_h)|\\ &\le C\left(\|\boldsymbol{f}-\mathbf{P}_h\boldsymbol{f}\|_{0,\Omega}\|\boldsymbol{v}_h\|_{0,\Omega}\right)+|b(\mathbf{P}_h\boldsymbol{f},\boldsymbol{v}_h)-b_h(\mathbf{P}_h\boldsymbol{f},\boldsymbol{v}_h)|\\ &\le C\left(\|\boldsymbol{f}-\mathbf{P}_h\boldsymbol{f}\|_{0,\Omega}+\|\boldsymbol{f}-\boldsymbol{\Pi}_h\boldsymbol{f}\|_{0,\Omega}\right)\|\boldsymbol{v}_h\|_{\mathrm{div},\Omega}\,,\end{aligned}$$

where, for the last inequality, we have used the same argument as above. Then, we have

$$\begin{aligned}\|\boldsymbol{w}-\boldsymbol{w}_h\|_{\mathrm{div},\Omega} &\le C\Big(\|\boldsymbol{w}-\mathbf{P}_h\boldsymbol{w}\|_{\mathrm{div},\Omega}+\|\boldsymbol{w}-\boldsymbol{\Pi}_h\boldsymbol{w}\|_{0,\Omega}\\ &\qquad+\|\boldsymbol{f}-\mathbf{P}_h\boldsymbol{f}\|_{0,\Omega}+\|\boldsymbol{f}-\boldsymbol{\Pi}_h\boldsymbol{f}\|_{0,\Omega}\Big)\\ &\le C\left(\gamma_h+\|\boldsymbol{w}-\boldsymbol{\Pi}_h\boldsymbol{w}\|_{0,\Omega}+\|\boldsymbol{f}-\boldsymbol{\Pi}_h\boldsymbol{f}\|_{0,\Omega}\right)\\ &= C\big(\gamma_h+\left(1+\mu^{-1}\right)\|\boldsymbol{w}-\boldsymbol{\Pi}_h\boldsymbol{w}\|_{0,\Omega}\big)\\ &\le C\left(\gamma_h+\eta_h\right),\end{aligned}$$

where we have used that, for $\boldsymbol{f}\in\boldsymbol{\mathcal{E}}$, $\boldsymbol{w}:=\mathbf{T}\boldsymbol{f}=\mu\boldsymbol{f}$. Thus, we conclude the proof.
□

To prove an error estimate for the eigenspaces, we also need the following result.

Lemma 4.4.5 *Let*

$$\boldsymbol{\Lambda}_h:=\widehat{\mathbf{F}}_h|_{\boldsymbol{\mathcal{E}}}:\ \boldsymbol{\mathcal{E}}\longrightarrow\boldsymbol{\mathcal{E}}_h.$$

For h small enough, the operator $\boldsymbol{\Lambda}_h$ is invertible and there exists C independent of h such that

$$\left\|\boldsymbol{\Lambda}_h^{-1}\right\|\le C.$$

Proof. It follows by proceeding as in the proof of Lemma 2 from [75], by using Lemma 4.4.4 and the fact that $\gamma_h\to 0$ and $\eta_h\to 0$ as $h\to 0$ (cf. (4.17)).
□

The following theorem shows that the eigenspace of $\mathbf{T}_h$ (which coincides with that of $\widehat{\mathbf{T}}_h$) approximates the eigenspace of $\mathbf{T}$.

Theorem 4.4.2 *There exists $C>0$ such that,*

$$\widehat{\delta}(\boldsymbol{\mathcal{E}},\boldsymbol{\mathcal{E}}_h)\le C\left(\gamma_h+\eta_h\right).$$

Proof. It follows by arguing exactly as in the proof of Theorem 1 from [75] and using Lemmas 4.4.4 and 4.4.5.
□

Finally, we will prove a double-order error estimate for the eigenvalues. With this aim, let $\lambda := \dfrac{1}{\mu} - 1$ be the eigenvalue of Problem 4.2.1 with eigenspace $\boldsymbol{\mathcal{E}}$. Let $\lambda_h^i := \dfrac{1}{\mu_h^i} - 1$, $i = 1, \ldots, m$, be the eigenvalues of Problem 4.3.1 with invariant subspace $\boldsymbol{\mathcal{E}}_h$. We have the following result.

Theorem 4.4.3 *There exist positive constants C and h_0 independent of h, such that, for $h < h_0$,*

$$\left|\lambda - \lambda_h^{(i)}\right| \leq C\left(\gamma_h^2 + \eta_h^2\right), \qquad i = 1, \ldots, m.$$

Proof. Let $\boldsymbol{w}_h \in \boldsymbol{\mathcal{E}}_h$ be an eigenfunction corresponding to one of the eigenvalues $\lambda_h^{(i)}$ ($i = 1, \ldots, m$) with $\|\boldsymbol{w}_h\|_{\mathrm{div},\Omega} = 1$. According to Theorem 4.4.2, $\delta(\boldsymbol{w}_h, \boldsymbol{\mathcal{E}}) \leq C\,(\gamma_h + \eta_h)$. It follows that there exists $\boldsymbol{w} \in \boldsymbol{\mathcal{E}}$ such that

$$\|\boldsymbol{w} - \boldsymbol{w}_h\|_{\mathrm{div},\Omega} \leq C\,(\gamma_h + \eta_h)\,. \tag{4.18}$$

Moreover, it is easy to check that $\boldsymbol{w}$ can be chosen normalized in $\mathrm{H}(\mathrm{div};\Omega)$-norm.

From the symmetry of the bilinear forms and the facts that $\boldsymbol{w}$ and $\boldsymbol{w}_h$ are solutions of Problem 4.2.1 and 4.3.1, respectively, we have

$$\begin{aligned}\int_\Omega \mathrm{div}(\boldsymbol{w} - \boldsymbol{w}_h)^2 - \lambda \int_\Omega (\boldsymbol{w} - \boldsymbol{w}_h)^2 &= \lambda_h^{(i)} b_h(\boldsymbol{w}_h, \boldsymbol{w}_h) - \lambda\, b(\boldsymbol{w}_h, \boldsymbol{w}_h) \\ &= \lambda_h^{(i)}\left(b_h(\boldsymbol{w}_h, \boldsymbol{w}_h) - b(\boldsymbol{w}_h, \boldsymbol{w}_h)\right) + \left(\lambda_h^{(i)} - \lambda\right) b(\boldsymbol{w}_h, \boldsymbol{w}_h),\end{aligned}$$

from which we obtain the following identity:

$$\begin{aligned}\left(\lambda_h^{(i)} - \lambda\right) b(\boldsymbol{w}_h, \boldsymbol{w}_h) = &\int_\Omega \mathrm{div}(\boldsymbol{w} - \boldsymbol{w}_h)^2 - \lambda \int_\Omega (\boldsymbol{w} - \boldsymbol{w}_h)^2 \\ &- \lambda_h^{(i)}\left(b_h(\boldsymbol{w}_h, \boldsymbol{w}_h) - b(\boldsymbol{w}_h, \boldsymbol{w}_h)\right).\end{aligned} \tag{4.19}$$

The next step is to estimate each term on the right hand side above. The first and the second ones are easily bounded by using the Cauchy-Schwarz inequality and (4.18):

$$\left|\int_\Omega \mathrm{div}(\boldsymbol{w} - \boldsymbol{w}_h)^2 - \lambda \int_\Omega (\boldsymbol{w} - \boldsymbol{w}_h)^2\right| \leq C\,\|\boldsymbol{w} - \boldsymbol{w}_h\|_{\mathrm{div},\Omega}^2 \leq C\left(\gamma_h^2 + \eta_h^2\right). \tag{4.20}$$

For the third term, we use (4.4)–(4.5) to write

$$
\begin{aligned}
&|b_h(\boldsymbol{w}_h,\boldsymbol{w}_h)-b(\boldsymbol{w}_h,\boldsymbol{w}_h)|\\
&\quad=\left|\sum_{E\in\mathcal{T}_h}\left(\int_E\left(\boldsymbol{\Pi}_h^E\boldsymbol{w}_h\right)^2+S^E\left(\boldsymbol{w}_h-\boldsymbol{\Pi}_h^E\boldsymbol{w}_h,\boldsymbol{w}_h-\boldsymbol{\Pi}_h^E\boldsymbol{w}_h\right)\right)-\sum_{E\in\mathcal{T}_h}\int_E(\boldsymbol{w}_h)^2\right|\\
&\quad\leq\left|\sum_{E\in\mathcal{T}_h}\left(\left\|\boldsymbol{\Pi}_h^E\boldsymbol{w}_h\right\|_{0,E}^2-\|\boldsymbol{w}_h\|_{0,E}^2\right)\right|+\sum_{E\in\mathcal{T}_h}c_1\int_E\left(\boldsymbol{w}_h-\boldsymbol{\Pi}_h^E\boldsymbol{w}_h\right)^2\\
&\quad=\sum_{E\in\mathcal{T}_h}\left\|\boldsymbol{w}_h-\boldsymbol{\Pi}_h^E\boldsymbol{w}_h\right\|_{0,E}^2+c_1\sum_{E\in\mathcal{T}_h}\left\|\boldsymbol{w}_h-\boldsymbol{\Pi}_h^E\boldsymbol{w}_h\right\|_{0,E}^2\\
&\quad\leq C\left\|\boldsymbol{w}_h-\boldsymbol{\Pi}_h\boldsymbol{w}_h\right\|_{0,\Omega}^2\\
&\quad\leq C\left(\|\boldsymbol{w}_h-\boldsymbol{w}\|_{0,\Omega}^2+\|\boldsymbol{w}-\boldsymbol{\Pi}_h\boldsymbol{w}\|_{0,\Omega}^2+\|\boldsymbol{\Pi}_h(\boldsymbol{w}-\boldsymbol{w}_h)\|_{0,\Omega}^2\right).
\end{aligned}
$$

Then, from the last inequality, the definition of η_h, the fact that $\boldsymbol{\Pi}_h$ is an $[L^2(\Omega)]^2$-projection and (4.18), we obtain

$$|b(\boldsymbol{w}_h,\boldsymbol{w}_h)-b_h(\boldsymbol{w}_h,\boldsymbol{w}_h)|\leq C\big(\gamma_h^2+\eta_h^2\big). \tag{4.21}$$

On the other hand, from the stability property (4.7),

$$\|\mathrm{div}\,\boldsymbol{w}_h\|_{0,\Omega}^2=\lambda_h^{(i)}b_h(\boldsymbol{w}_h,\boldsymbol{w}_h)\leq\lambda_h^{(i)}\alpha^*\,\|\boldsymbol{w}_h\|_{0,\Omega}^2\,,$$

hence

$$\big(1+\lambda_h^{(i)}\alpha^*\big)\,\|\boldsymbol{w}_h\|_{0,\Omega}^2\geq\|\boldsymbol{w}_h\|_{\mathrm{div},\Omega}^2=1.$$

Therefore, since $\lambda_h^{(i)}\to\lambda$ as h goes to zero, the theorem follows from (4.19), (4.20), (4.21) and the inequality above.

□

As shown in Theorem 4.2.2(ii), the eigenfunctions satisfy additional regularity. The following result shows that this implies an optimal order of convergence for the numerical method.

Corollary 4.4.2 *If $\boldsymbol{\mathcal{E}}\subset[\mathrm{H}^{\tilde{s}}(\Omega)]^2$ with $\tilde{s}>1/2$, then*

$$\widehat{\delta}(\boldsymbol{\mathcal{E}},\boldsymbol{\mathcal{E}}_h)\leq Ch^{\mín\{\tilde{s},k+1\}}.$$

and

$$\big|\lambda-\lambda_h^{(i)}\big|\leq Ch^{2\,\mín\{\tilde{s},k+1\}},\qquad i=1,\ldots,m.$$

Proof. It follows from the above theorems and the estimates (4.17).

□

4.5. Numerical results

Following the ideas proposed in [22], we have implemented in a MATLAB code a lowest-order VEM ($k = 0$) on arbitrary polygonal meshes. We report in this section a couple of numerical tests which allowed us to assess the theoretical results proved above.

To complete the choice of the VEM, we had to fix the bilinear form $S^E(\cdot,\cdot)$ satisfying (4.4) to be used. To do this, we proceeded as in [18]. For each element $E \in \mathcal{T}_h$ with edges $e_1, \ldots, e_{N_E}$, let $\{\boldsymbol{\varphi}_1, \ldots, \boldsymbol{\varphi}_{N_E}\}$ be the dual basis of $\boldsymbol{\mathcal{V}}_h^E$ associated with the degrees of freedom (4.1); namely, $\boldsymbol{\varphi}_i \in \boldsymbol{\mathcal{V}}_h^E$ are such that

$$\int_{e_j} \boldsymbol{\varphi}_i \cdot \boldsymbol{n}\, ds = \delta_{ij}, \qquad i,j = 1, \ldots, N_E.$$

Therefore, $\|\boldsymbol{\varphi}_i\|_{\infty,E} \simeq \dfrac{1}{h_E}$, namely, there exists $C > 0$ such that

$$\frac{1}{Ch_E} \leq \|\boldsymbol{\varphi}_i\|_{\infty,E} \leq \frac{C}{h_E}, \qquad i = 1, \ldots, N_E.$$

Hence, a natural choice for $S^E(\cdot,\cdot)$ is given by

$$S^E(\boldsymbol{u}_h, \boldsymbol{v}_h) := \sigma_E \sum_{k=1}^{N_E} \left(\int_{e_k} \boldsymbol{u}_h \cdot \boldsymbol{n} \right) \left(\int_{e_k} \boldsymbol{v}_h \cdot \boldsymbol{n} \right), \qquad \boldsymbol{u}_h, \boldsymbol{v}_h \in \boldsymbol{\mathcal{V}}_h^E,$$

where σ_E is the so-called *stability constant* which will be taken of the order of unity (see for instance [18]).

4.5.1. Test 1: Rectangular acoustic cavity

In this test, the domain is a rectangle $\Omega := (0,a) \times (0,b)$, in which case the exact analytic solution is known. The non vanishing eigenvalues of Problem 4.2.1 are given by

$$\lambda_{nm} := \pi^2 \left(\left(\frac{n}{a}\right)^2 + \left(\frac{m}{b}\right)^2 \right), \qquad n,m = 0,1,2,\ldots, \quad n+m \neq 0,$$

while the corresponding eigenfunctions are

$$\boldsymbol{w}_{nm} := \begin{pmatrix} \dfrac{n}{a} \sin\dfrac{n\pi x}{a} \cos\dfrac{m\pi y}{b} \\ \dfrac{m}{b} \cos\dfrac{n\pi x}{a} \sin\dfrac{m\pi y}{b} \end{pmatrix}.$$

We have used $a = 1$ and $b = 1{,}1$. The stability constant has been taken $\sigma_E = 1$. We have used three different families of meshes (see Figure 4.1):

- $\mathcal{T}_h^1$: triangular meshes;
- $\mathcal{T}_h^2$: rectangular meshes;
- $\mathcal{T}_h^3$: hexagonal meshes.

The refinement parameter N used to label each mesh is the number of elements intersecting each edge.

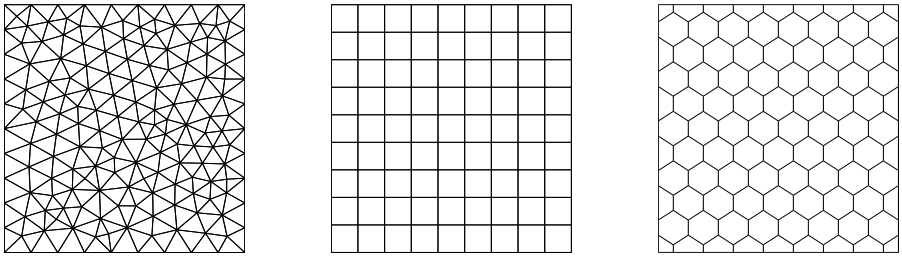

Figura 4.1: Sample meshes: $\mathcal{T}_h^1$ (left), $\mathcal{T}_h^2$ (middle) and $\mathcal{T}_h^3$ (right). In all of them $N = 9$.

Let us remark that for triangular and rectangular meshes like $\mathcal{T}_h^1$ and $\mathcal{T}_h^2$, respectively, the discrete spaces $\boldsymbol{\mathcal{V}}_h$ coincide with those of the standard lowest-order Raviart-Thomas discretization. However, the resulting discrete problems are not the same. In fact, the matrices corresponding to the left-hand side of Problem 4.3.1 also coincide, but this does not happen with the matrices corresponding to right-hand side.

We report in Table 4.1 the scaled lowest eigenvalues $\widehat{\lambda}_{hi} := \lambda_{hi}/\pi^2$ computed with the method analyzed in this paper. The table also includes estimated orders of convergence. The exact eigenvalues are also reported in the last column to allow for comparison.

It can be seen from Table 4.1 that the computed eigenvalues converge to the exact ones with an optimal quadratic order as predicted by the theory in almost all cases. The exception seems to be the computation of some of the eigenvalues with the hexagonal meshes. In this case, although the computed eigenvalues are as good approximations to the exact ones as those computed with the other families of meshes, the order of convergence deteriorates mildly. We have observed from our numerical experiments that this can be avoided by choosing a smaller stability constant σ_E.

This can be clearly seen by comparing the lowest part of Table 4.1 with Table 4.2, where we report the result obtained with a smaller value of σ_E and meshes $\mathcal{T}_h^3$. A more detailed discussion about the effect of the stability constant σ_E appears in the following test.

Figure 4.2 shows plots of the computed eigenfunctions $\boldsymbol{w}_{h1}$ and $\boldsymbol{w}_{h3}$ corresponding to the first and third lowest eigenvalues, respectively. The figure also includes the corresponding pressure fluctuation $p_{hi} = -\operatorname{div} \boldsymbol{w}_{hi}$, $i = 1, 3$. In both cases, the eigenfunctions have been computed on an hexagonal mesh $\mathcal{T}_h^3$ with $N = 27$ and stability constant $\sigma_E = 1$.

4.5.2. Test 2: Effect of the stability constant σ_E

As was shown in the previous test, in some cases the quality of the computation can be affected by the choice of the stability constant σ_E. A similar behavior was observed in other VEM for different eigenvalue problems. In particular, it was demonstrated in [97] that certain

Cuadro 4.1: Test 1. Computed lowest eigenvalues $\widehat{\lambda}_{hi}$, $1 \leq i \leq 5$, on different meshes with $\sigma_E = 1$.

$\mathcal{T}_h$	$\widehat{\lambda}_{hi}$	$N = 19$	$N = 35$	$N = 53$	$N = 71$	Order	λ_i
$\mathcal{T}_h^1$	$\widehat{\lambda}_{h1}$	0.8248	0.8259	0.8262	0.8263	2.01	0.82645
	$\widehat{\lambda}_{h2}$	0.9976	0.9993	0.9997	0.9998	2.00	1.00000
	$\widehat{\lambda}_{h3}$	1.8182	1.8240	1.8254	1.8259	2.01	1.82645
	$\widehat{\lambda}_{h4}$	3.2788	3.2978	3.3023	3.3039	2.02	3.30579
	$\widehat{\lambda}_{h5}$	3.9595	3.9883	3.9949	3.9972	2.03	4.00000
$\mathcal{T}_h^2$	$\widehat{\lambda}_{h1}$	0.8200	0.8245	0.8256	0.8260	1.99	0.82645
	$\widehat{\lambda}_{h2}$	0.9896	0.9969	0.9987	0.9992	1.99	1.00000
	$\widehat{\lambda}_{h3}$	1.8096	1.8214	1.8243	1.8252	1.99	1.82645
	$\widehat{\lambda}_{h4}$	3.2047	3.2754	3.2925	3.2983	1.98	3.30579
	$\widehat{\lambda}_{h5}$	3.8389	3.9512	3.9786	3.9880	1.97	4.00000
$\mathcal{T}_h^3$	$\widehat{\lambda}_{h1}$	0.8249	0.8260	0.8262	0.8263	1.98	0.82645
	$\widehat{\lambda}_{h2}$	0.9948	0.9982	0.9990	0.9993	1.56	1.00000
	$\widehat{\lambda}_{h3}$	1.8132	1.8220	1.8241	1.8249	1.63	1.82645
	$\widehat{\lambda}_{h4}$	3.2805	3.2979	3.3024	3.3039	1.98	3.30579
	$\widehat{\lambda}_{h5}$	3.9387	3.9823	3.9912	3.9946	1.84	4.00000

VEM discretizations of the Steklov eigenvalue problem introduces spurious eigenvalues which can be well separated from the physical spectrum by choosing appropriately the stability constant σ_E.

In the present case, no spurious eigenvalue was detected for any choice of the stability constant. However, for large values of σ_E, the eigenvalues computed with coarse meshes could be very poor. The aim of this test is to analyze the influence of the stability constant σ_E on the computed spectrum.

We report in Table 4.3 the lowest eigenvalue computed with varying values of σ_E on the family of meshes $\mathcal{T}_h^2$ (see Figure 2, middle). The table also includes the estimated order of convergence.

It can be seen from Table 4.3 that for values of the parameter $\sigma_E \leq 1$ the computed eigenvalues depend very mildly on this parameter. Moreover, this dependence becomes weaker, as the mesh is refined or σ_E is taken smaller. In fact, it can be seen from this table that even the value $\sigma_E = 0$ yields very accurate results, in spite of the fact that for such a value of the parameter the stability estimate and hence most of the proofs of the theoretical results do not hold. On the other hand, it can be seen from Table 4.3 that the numerical results depend much more significantly on this parameter σ_E when it is chosen larger. In such a case, the results for coarse meshes are poorer and more refined meshes are needed for the computed eigenvalues to lie close to the exact ones.

This analysis suggests that the user of H(div) VEM for this kind of spectral problems has to

Cuadro 4.2: Test 1. Computed lowest eigenvalues $\widehat{\lambda}_{hi}$, $1 \leq i \leq 5$, on meshes $\mathcal{T}_h^3$ with $\sigma_E = 2^{-4}$.

$\mathcal{T}_h$	$\widehat{\lambda}_{hi}$	$N = 19$	$N = 35$	$N = 53$	$N = 71$	Order	λ_i
$\mathcal{T}_h^3$	$\widehat{\lambda}_{h1}$	0.8294	0.8272	0.8268	0.8266	2.09	0.82645
	$\widehat{\lambda}_{h2}$	1.0032	1.0009	1.0004	1.0002	2.15	1.00000
	$\widehat{\lambda}_{h3}$	1.8389	1.8297	1.8278	1.8272	2.12	1.82645
	$\widehat{\lambda}_{h4}$	3.3539	3.3179	3.3112	3.3088	2.09	3.30579
	$\widehat{\lambda}_{h5}$	4.0536	4.0149	4.0063	4.0034	2.09	4.00000

be aware of the risk of degeneration of the eigenvalues for certain values of the stability constant σ_E. The way of minimizing this risk in this case is to take small values of σ_E (what "small" means in a real problem will of course depend on the value of the physical constants).

4.6. Appendix

We derive in this appendix optimal approximation properties for the H(div) virtual elements with vanishing rotor introduced in Section 4.3. The main goal of this appendix will be to prove the error estimates stated in Lemmas 4.3.2 and 4.3.3 for the $\boldsymbol{\mathcal{V}}_h$-interpolant defined by (4.8)–(4.9). Let us remark that these results could be useful for other applications as well.

Our first result, whose proof is quite straightforward, is a commuting diagram property and some consequences that follow from it. We recall that P_k denotes the $L^2(\Omega)$-orthogonal projection onto the subspace $\left\{q \in L^2(\Omega) : q|_E \in \mathbb{P}_k(E) \quad \forall E \in \mathcal{T}_h\right\}$.

Lemma 4.3.2 *Let $\boldsymbol{v} \in \boldsymbol{\mathcal{V}}$ be such that $\boldsymbol{v} \in [\mathrm{H}^t(\Omega)]^2$ with $t > 1/2$. Let $\boldsymbol{v}_I \in \boldsymbol{\mathcal{V}}_h$ be its interpolant defined by* (4.8)–(4.9)*. Then,*

$$\operatorname{div} \boldsymbol{v}_I = P_k(\operatorname{div} \boldsymbol{v}) \quad \text{in } \Omega.$$

Consequently, for all $E \in \mathcal{T}_h$, $\|\operatorname{div} \boldsymbol{v}_I\|_{0,E} \leq \|\operatorname{div} \boldsymbol{v}\|_{0,E}$ and, if $\operatorname{div} \boldsymbol{v}|_E \in \mathrm{H}^r(K)$ with $r \geq 0$, then

$$\|\operatorname{div} \boldsymbol{v} - \operatorname{div} \boldsymbol{v}_I\|_{0,E} \leq C h_E^{\min\{r,k+1\}} |\operatorname{div} \boldsymbol{v}|_{r,E}\,.$$

Proof. As a consequence of (4.8)–(4.9), for every element E and for every $q \in \mathbb{P}_k(E)$

$$\int_E \operatorname{div}(\boldsymbol{v} - \boldsymbol{v}_I)\, q = \int_E (\boldsymbol{v} - \boldsymbol{v}_I) \cdot \nabla q + \int_{\partial E} (\boldsymbol{v} - \boldsymbol{v}_I) \cdot \boldsymbol{n}\, q\, ds = 0.$$

Since $\operatorname{div} \boldsymbol{v}_I \in \mathbb{P}_k(E)$, we have that

$$\operatorname{div} \boldsymbol{v}_I = P_k(\operatorname{div} \boldsymbol{v}) \quad \text{in } E.$$

Therefore,

$$\|\operatorname{div} \boldsymbol{v}_I\|_{0,E} \leq \|\operatorname{div} \boldsymbol{v}\|_{0,E}\,.$$

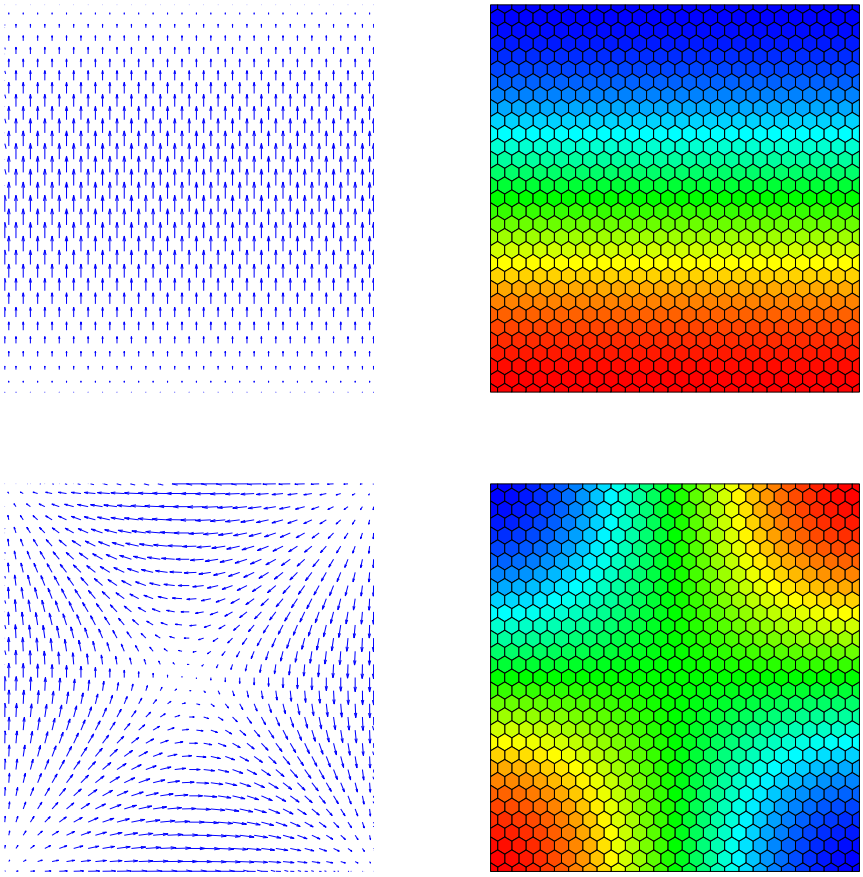

Figura 4.2: Eigenfunctions of the acoustic problem corresponding to the first and third lowest eigenvalues: displacement field $\boldsymbol{w}_{h1}$ (upper left), pressure fluctuation p_{h1},(upper right), displacement field $\boldsymbol{w}_{h3}$ (bottom left), pressure fluctuation p_{h3} (bottom right).

Additionally, if $\operatorname{div} \boldsymbol{v}|_E \in \mathrm{H}^r(K)$ with r a non-negative integer, as a consequence of [51, Lemma 4.3.8], we have that for every $E \in \mathcal{T}_h$

$$\|\operatorname{div} \boldsymbol{v} - \operatorname{div} \boldsymbol{v}_I\|_{0,E} \leq C h_E^{\min\{r,k+1\}} |\operatorname{div} \boldsymbol{v}|_{r,E} .$$

Thus, the second estimate of the lemma follows by standard Banach space interpolation.
□

In order to prove Lemma 4.3.3 about the $L^2(\Omega)$ approximation property of this interpolant, we need several previous results. We begin with the following local trace estimate on polygons.

Lemma 4.6.1 *Let $\boldsymbol{v} \in \boldsymbol{\mathcal{V}}$ and $E \in \mathcal{T}_h$ such that $\boldsymbol{v}|_E \in [\mathrm{H}^t(E)]^2$ with $t \in (1/2, 1]$. Then, there exists $C > 0$ such that*

$$\|\boldsymbol{v}\|_{0,\partial E} \leq C \left(h_E^{-1/2} \|\boldsymbol{v}\|_{0,E} + h_E^{t-1/2} |\boldsymbol{v}|_{t,E} \right) .$$

Cuadro 4.3: Test 2. The lowest eigenvalue $\widehat{\lambda}_{h1}$ for $\sigma_E = 0$ and $\sigma_E = 2^{-k}$ with $-6 \leq k \leq 6$.

N	$\sigma_E = 0$	$\sigma_E = 2^{-6}$	$\sigma_E = 2^{-5}$	$\sigma_E = 2^{-4}$	$\sigma_E = 2^{-3}$	$\sigma_E = 2^{-2}$	$\sigma_E = 2^{-1}$
8	0.8482	0.8472	0.8463	0.8444	0.8406	0.8332	0.8187
16	0.8318	0.8316	0.8313	0.8309	0.8300	0.8281	0.8245
32	0.8278	0.8277	0.8277	0.8275	0.8273	0.8269	0.8260
64	0.8268	0.8268	0.8268	0.8267	0.8267	0.8265	0.8263
128	0.8265	0.8265	0.8265	0.8265	0.8265	0.8265	0.8264
256	0.8265	0.8265	0.8265	0.8265	0.8265	0.8265	0.8264
Order	2.00	2.00	2.00	2.00	2.00	2.00	2.00
λ_1	0.82645	0.82645	0.82645	0.82645	0.82645	0.82645	0.82645
N	$\sigma_E = 2^0$	$\sigma_E = 2^1$	$\sigma_E = 2^2$	$\sigma_E = 2^3$	$\sigma_E = 2^4$	$\sigma_E = 2^5$	$\sigma_E = 2^6$
8	0.7912	0.7415	0.6586	0.5383	0.3943	0.2569	0.1513
16	0.8174	0.8034	0.7770	0.7289	0.6487	0.5317	0.3907
32	0.8242	0.8206	0.8135	0.7997	0.7735	0.7258	0.6463
64	0.8259	0.8250	0.8233	0.8196	0.8125	0.7988	0.7726
128	0.8263	0.8261	0.8256	0.8247	0.8229	0.8193	0.8123
256	0.8264	0.8264	0.8262	0.8260	0.8256	0.8247	0.8229
Order	1.99	1.97	1.94	1.90	1.82	1.70	1.55
λ_1	0.82645	0.82645	0.82645	0.82645	0.82645	0.82645	0.82645

Proof. Consider the triangulation $\mathcal{T}_h^E$ of the element E obtained by joining each vertex of E with the midpoint of the ball with respect to which E is star-shaped. Since we are assuming that the meshes satisfy $\mathbf{A_1}$ and $\mathbf{A_2}$, the triangles $T \in \mathcal{T}_h^E$ have a shape ratio (i.e., the quotient between outer and inner diameters) bounded above by a constant that only depends on $C_{\mathcal{T}}$. Moreover, each triangle $T \in \mathcal{T}_h^E$ has one edge on ∂E. Hence, a scaling argument and a trace inequality in the reference triangular element allow us to conclude the proof.
□

In order to prove an $L^2(\Omega)$ error estimate for the interpolant $\boldsymbol{v}_I$, we will introduce a basis of $\boldsymbol{\mathcal{V}}_h^E$ dual to the degrees of freedom (4.1)–(4.2).

Let $E \in \mathcal{T}_h$ with edges $e_1, \ldots, e_{N_E}$ and $F : E \longrightarrow \widehat{E}$ be an affine mapping of the form

$$F\begin{pmatrix} x \\ y \end{pmatrix} := \frac{1}{h_E}\begin{pmatrix} x - x_E \\ y - y_E \end{pmatrix} =: \begin{pmatrix} \widehat{x} \\ \widehat{y} \end{pmatrix},$$

where $\boldsymbol{x}_E = (x_E, y_E)^T$ is the center of the ball with respect to which E is star-shaped according to assumption $\mathbf{A_2}$. Note that $\widehat{E} := F(E)$ has diameter 1. Moreover, F maps the above mentioned ball onto a ball of radius $C_{\mathcal{T}}$ with $0 < C_{\mathcal{T}} \leq 1$ and $C_{\mathcal{T}}$ independent of h_E, Moreover, $\widehat{E}$ is star-shaped with respect to each point of this ball.

We define the following basis of $\mathbb{P}_k(E)$:

$$p_0(x,y) := 1,$$
$$p_s(x,y) := \frac{(x-x_E)^{\alpha_1}\,(y-y_E)^{\alpha_2}}{h_E^{\alpha_1+\alpha_2}} + C_s, \qquad \alpha_1,\alpha_2 \in \mathbb{N}, \quad 0 < \alpha_1+\alpha_2 \le k,$$

with the constant $C_s \in \mathbb{R}$ such that $\int_E p_s = 0$. We have associated above each $s = 1,\dots,\widetilde{N} := \dim(\mathbb{P}_k(E)) - 1$ with one particular couple (α_1,α_2), by fixing a particular ordering of these couples. Therefore, the set $\{p_0, p_1, \dots, p_{\widetilde{N}}\}$ is a basis for $\mathbb{P}_k(E)$ that satisfies $\int_E p_s = 0$ for $s = 1,\dots,\widetilde{N}$. Let now $\widehat{p}_s := p_s \circ F^{-1}$ be defined in $\widehat{E}$. Then, for the particular (α_1,α_2) associated with s, we have that $\widehat{p}_s(\widehat{x},\widehat{y}) = \widehat{x}^{\alpha_1}\widehat{y}^{\alpha_2} + C_s$. Moreover, since $|E| = h_E^2\big|\widehat{E}\big|$, we have

$$C_s = -\frac{1}{|E|}\int_E \frac{(x-x_E)^{\alpha_1}\,(y-y_E)^{\alpha_2}}{h_E^{\alpha_1+\alpha_2}}\,dx\,dy = -\frac{1}{\big|\widehat{E}\big|}\int_{\widehat{E}} \widehat{x}^{\alpha_1}\widehat{y}^{\alpha_2}\,d\widehat{x}\,d\widehat{y}.$$

As a consequence, note that $|C_s| \le 1$ and, hence, $\|p_s\|_{\infty,E} = \|\widehat{p}_s\|_{\infty,\widehat{E}} \le 2$, $s = 0,\dots,\widetilde{N}$.

For each edge e_l of E ($l = 1,\dots,N_E$), let T_l be the affine function mapping $\widehat{e} := [-1,1]$ onto e_l. We define $q_l^i := \widehat{q}^{\,i} \circ T_l^{-1}$ ($i = 1,\dots,k$) with $\widehat{q}^{\,i}$ being the Legendre polynomials on $[-1,1]$ normalized by $\widehat{q}^{\,i}(1) = 1$. Then, $\{q_l^0,\dots,q_l^k\}$ is a basis of $\mathbb{P}_k(e_l)$ which satisfies $q_l^0 = 1$, $\int_{e_l} q_l^i q_l^j\,ds = \delta_{ij}$, $i,j = 1,\dots,k$, and $\|q_l^i\|_{\infty,e_l} = 1$. Note that, in particular, $\int_{e_l} q_l^i\,ds = 0$, $i = 1,\dots,k$.

Therefore,

$$\{q_l^i\}_{i=0,\dots,k,\ l=1,\dots,N_E} \qquad \text{and} \qquad \{p_s\}_{s=1,\dots,\widetilde{N}}$$

are bases for the spaces of test functions appearing in the degrees of freedom (4.8) and (4.9), respectively. Next, we introduce a set of dual basis functions for $\boldsymbol{\mathcal{V}}_h^E$:

$$\{\boldsymbol{\varphi}_l^i\}_{i=0,\dots,k,\ l=1,\dots,N_E} \cup \{\widetilde{\boldsymbol{\varphi}}^s\}_{s=1,\dots,\widetilde{N}}. \tag{4.22}$$

The first ones, $\boldsymbol{\varphi}_l^i$, are the "boundary basis functions" determined by

$$\boldsymbol{\varphi}_l^i \in \boldsymbol{\mathcal{V}}_h^E, \tag{4.23}$$
$$\int_{e_m} (\boldsymbol{\varphi}_l^i \cdot \boldsymbol{n})\, q_m^j\,ds = \delta_{lm}\delta_{ij}, \qquad m = 1,\dots,N_E, \quad j = 0,\dots,k, \tag{4.24}$$
$$\int_E (\operatorname{div}\boldsymbol{\varphi}_l^i)\, p_r = 0, \qquad r = 1,\dots,\widetilde{N}. \tag{4.25}$$

Note that these boundary basis functions use two indexes, i and l, one for the moment and the other for the edge. On the other hand, note also that as a consequence of (4.23)–(4.24) $\boldsymbol{\varphi}_l^i \cdot \boldsymbol{n} = 0$ on $\partial E \backslash e_l$ The second kind of functions in (4.22), $\widetilde{\boldsymbol{\varphi}}^s$, are the "internal basis functions" determined by

$$\widetilde{\boldsymbol{\varphi}}^s \in \boldsymbol{\mathcal{V}}_h^E, \tag{4.26}$$
$$\widetilde{\boldsymbol{\varphi}}^s|_{\partial E} \cdot \boldsymbol{n} = 0, \tag{4.27}$$
$$\int_E (\operatorname{div}\widetilde{\boldsymbol{\varphi}}^s)\, p_r = \delta_{sr}, \qquad r = 1,\dots,\widetilde{N}. \tag{4.28}$$

Remark 4.6.1 *Since* $\operatorname{div}\boldsymbol{\varphi}_l^i \in \mathbb{P}_k(E) = \operatorname{span}\{1, p_1, \ldots, p_s\}$ *and* $\int_E p_s = 0$ *for* $s = 1, \ldots, \widetilde{N}$, *equation* (4.25) *implies that* $\operatorname{div}\boldsymbol{\varphi}_l^i$ *has to be constant. Therefore,*

$$\operatorname{div}\boldsymbol{\varphi}_l^i = \frac{1}{|E|}\int_E \operatorname{div}\boldsymbol{\varphi}_l^i = \frac{1}{|E|}\int_{\partial E} \boldsymbol{\varphi}_l^i \cdot \boldsymbol{n}\, ds.$$

Moreover, thanks to (4.24), *we have that*

$$\int_{\partial E} \boldsymbol{\varphi}_l^i \cdot \boldsymbol{n}\, ds = \sum_{m=1}^{N_E} \int_{e_m} \left(\boldsymbol{\varphi}_l^i \cdot \boldsymbol{n}\right) q_m^0\, ds = \sum_{m=1}^{N_E} \delta_{lm}\delta_{i0} = \delta_{i0}.$$

Then,

$$\operatorname{div}\boldsymbol{\varphi}_l^i = \frac{\delta_{i0}}{|E|}.$$

Next goal is to prove that all the functions in (4.22) are bounded uniformly in h. We begin with the boundary basis functions.

Lemma 4.6.2 *There exists* $C > 0$ *such that* $\left\|\boldsymbol{\varphi}_l^i\right\|_{0,E} \leq C$ *for* $l = 1, \ldots, N_E$ *and* $i = 0, \ldots, k$.

Proof. Since $\boldsymbol{\varphi}_l^i \in \boldsymbol{\mathcal{V}}_h^E$, we know that $\operatorname{rot}\boldsymbol{\varphi}_l^i = 0$. Therefore, there exists $\gamma \in \mathrm{H}^1(E)$ such that $\boldsymbol{\varphi}_l^i = \nabla\gamma$. Hence, from the remark above and (4.24), we have that γ is a solution of the following problem:

$$\begin{cases} \Delta\gamma = \dfrac{\delta_{i0}}{|E|} & \text{in } E, \\ \dfrac{\partial\gamma}{\partial\boldsymbol{n}} = \boldsymbol{\varphi}_l^i \cdot \boldsymbol{n} & \text{on } \partial E, \\ \displaystyle\int_E \gamma = 0. \end{cases}$$

It is easy to check that these Neumann problems are compatible. Therefore,

$$\int_E \nabla\gamma \cdot \nabla\zeta = \int_{\partial E} \left(\boldsymbol{\varphi}_l^i \cdot \boldsymbol{n}\right)\zeta\, ds - \int_E \frac{\delta_{i0}}{|E|}\zeta = \int_{e_l} \left(\boldsymbol{\varphi}_l^i \cdot \boldsymbol{n}\right)\zeta\, ds \qquad \forall \zeta \in \mathrm{H}^1(E) : \ \int_E \zeta = 0.$$

Now, taking $\zeta = \gamma$, we obtain

$$\begin{aligned} \left\|\boldsymbol{\varphi}_l^i\right\|_{0,E}^2 = \|\nabla\gamma\|_{0,E}^2 &\leq \left\|\boldsymbol{\varphi}_l^i \cdot \boldsymbol{n}\right\|_{0,e_l} \|\gamma\|_{0,e_l} \\ &\leq C\left\|\boldsymbol{\varphi}_l^i \cdot \boldsymbol{n}\right\|_{0,e_l} \left(h_E^{-1/2}\|\gamma\|_{0,E} + h_E^{1/2}\|\nabla\gamma\|_{0,E}\right) \\ &\leq C h_E^{1/2}\left\|\boldsymbol{\varphi}_l^i \cdot \boldsymbol{n}\right\|_{0,e_l} \|\nabla\gamma\|_{0,E}\,, \end{aligned}$$

where we have used Lemma 4.6.1 with $t = 1$, the generalized Poincaré inequality and a scaling argument. Now, because of (4.24) with $m = l$ and the orthogonality property of Legendre polynomials, $\boldsymbol{\varphi}_l^i \cdot \boldsymbol{n}\big|_{e_l} = \left(\int_{e_l} \left(q_l^i\right)^2\, ds\right)^{-1} q_l^i$. Therefore,

$$\left\|\boldsymbol{\varphi}_l^i \cdot \boldsymbol{n}\right\|_{0,e_l}^2 = \left(\int_{e_l} \left(q_l^i\right)^2\, ds\right)^{-1} = \frac{1}{h_E}\left(\int_{\widehat{e}} \left(\widehat{q}^{\,i}\right)^2\, d\widehat{s}\right)^{-1}.$$

Thus, from the last two estimates we derive that $\left\|\boldsymbol{\varphi}_l^i\right\|_{0,E} \leq C$ and we end the proof.
□

Next, we show a similar result for the internal basis functions.

Lemma 4.6.3 *There exists $C > 0$ such that $\|\widetilde{\boldsymbol{\varphi}}^s\|_{0,E} \leq C$ for $s = 1, \ldots, \widetilde{N}$.*

Proof. Since $\widetilde{\boldsymbol{\varphi}}^s \in \boldsymbol{\mathcal{V}}_h^E$, there exists $\gamma \in \mathrm{H}^1(E)$ such that $\widetilde{\boldsymbol{\varphi}}^s = \nabla\gamma$. Hence, by virtue of (4.27), we have that γ is a solution of the following well posed Neumann problem:

$$\begin{cases} \Delta\gamma = -\operatorname{div}\widetilde{\boldsymbol{\varphi}}^s & \text{in } E, \\ \dfrac{\partial\gamma}{\partial\boldsymbol{n}} = 0 & \text{on } \partial E, \\ \displaystyle\int_E \gamma = 0. \end{cases}$$

Therefore,

$$\int_E \nabla\gamma\cdot\nabla\zeta = -\int_E \psi^s\zeta \qquad \forall\zeta \in \mathrm{H}^1(E) : \ \int_E \zeta = 0,$$

where $\psi^s := \operatorname{div}\widetilde{\boldsymbol{\varphi}}^s$. Now, taking $\zeta = \gamma$ and using the generalized Poincaré inequality and a scaling argument, we have that

$$\|\widetilde{\boldsymbol{\varphi}}^s\|_{0,E}^2 = \|\nabla\gamma\|_{0,E}^2 \leq C\,\|\psi^s\|_{0,E}\,\|\gamma\|_{0,E} \leq Ch_E\,\|\psi^s\|_{0,E}\,\|\nabla\gamma\|_{0,E}\,.$$

Thus,

$$\|\widetilde{\boldsymbol{\varphi}}^s\|_{0,E} \leq Ch_E\,\|\psi^s\|_{0,E}\,. \tag{4.29}$$

On the other hand, since $\psi^s \in \mathbb{P}_k(E)$, it is easy to check that

$$h_E\,\|\psi^s\|_{0,E} \leq Ch_E^2\,\|\psi^s\|_{\infty,E} = Ch_E^2\,\left\|\widehat{\psi}^s\right\|_{\infty,\widehat{E}}, \tag{4.30}$$

where $\widehat{\psi}^s := (\psi^s \circ F^{-1}) \in \mathbb{P}_k(\widehat{E})$.

For $\widehat{\psi}^s \in \mathbb{P}_k(\widehat{E})$, we write $\widehat{\psi}^s = \sum_{i=1}^{\widetilde{N}} \beta_i^s\widehat{p}_i$ and, since $\|\widehat{p}_i\|_{\infty,\widehat{E}} \leq 2$, we have that

$$\left\|\widehat{\psi}^s\right\|_{\infty,\widehat{E}} \leq \max_{1\leq i\leq\widetilde{N}} |\beta_i^s| \sum_{i=1}^{\widetilde{N}} \|\widehat{p}_i\|_{\infty,\widehat{E}} \leq C \max_{1\leq i\leq\widetilde{N}} |\beta_i^s|\,. \tag{4.31}$$

Now, from (4.28), a change of variables from E to $\widehat{E}$ yields

$$\int_{\widehat{E}} \widehat{\psi}^s\widehat{p}_r = h_E^{-2}\delta_{sr}, \qquad r = 1, \ldots, \widetilde{N},$$

which can be written as

$$\sum_{i=1}^{\widetilde{N}} \beta_i^s \int_{\widehat{E}} \widehat{p}_i\widehat{p}_r = h_E^{-2}\delta_{sr}, \qquad r = 1, \ldots, \widetilde{N}. \tag{4.32}$$

Let

$$\mathbf{M} = \left(m_{ir}\right) \in \mathbb{R}^{\widetilde{N}\times\widetilde{N}} \qquad \text{with } m_{ir} := \int_{\widehat{E}} \widehat{p}_i \widehat{p}_r, \quad i,r = 1,\ldots,\widetilde{N}.$$

Therefore, from (4.32), if $\mathbf{M}$ is invertible, then $\boldsymbol{\beta}^s = \begin{pmatrix}\beta_1^s & \cdots & \beta_{\widetilde{N}}^s\end{pmatrix}^T$ is equal to h_E^{-2} times the s-th column of $\mathbf{M}^{-1}$.

Next, we will show that $\mathbf{M}$ is invertible and that its inverse is bounded uniformly in h. With this aim, note that the polygon $\widehat{E}$ is uniquely defined by the vector $((\widehat{x}_1,\widehat{y}_1),\ldots,(\widehat{x}_{N_E},\widehat{y}_{N_E})) \in \mathbb{R}^{2N_E}$ that collects the coordinates of its (ordered) vertexes. Let $U \subset \mathbb{R}^{2N_E}$, be the set of all possible values of these coordinates such that the mesh regularity assumptions $\mathbf{A_1}$ and $\mathbf{A_2}$ are satisfied. Since the diameter of $\widehat{E}$ is equal to 1, U is a bounded set. On the other hand, the constraints that arise from hypotheses $\mathbf{A_1}$ and $\mathbf{A_2}$ yield that U is a closed set. Therefore U is compact.

The function from U into $\mathbb{R}^{\widetilde{N}\times\widetilde{N}}$ that maps the coordinates of the vertexes of $\widehat{E}$ into the entries of the matrix $\mathbf{M}$ is a continuous function. Moreover, for any coordinates in U, $\widehat{E}$ satisfies $\mathbf{A_1}$ and $\mathbf{A_2}$ and, hence, it contains a ball of radius $C_{\mathcal{T}}$. Let us show that this implies that $\mathbf{M}$ has to be positive definite. In fact, given $\alpha \in \mathbb{R}^{\widetilde{N}}$, $\alpha^T\mathbf{M}\alpha = \int_{\widehat{E}} \left|\sum_{r=1}^{\widetilde{N}} \alpha_r \widehat{p}_r\right|^2 \geq 0$ and the equality holds only if $\sum_{r=1}^{\widetilde{N}} \alpha_r \widehat{p}_r$ vanishes a.e. in $\widehat{E}$, which in turn implies that α has to vanish (since $\widehat{E}$ contains a ball of radius $C_{\mathcal{T}} > 0$). Thus, $\mathbf{M}$ is positive definite and hence invertible. Therefore, taking also into account the continuity of the mapping $\mathbf{M} \longmapsto \mathbf{M}^{-1}$ for invertible matrices, we conclude that the mapping

$$U \ni ((\widehat{x}_1,\widehat{y}_1),\ldots,(\widehat{x}_{N_E},\widehat{y}_{N_E})) \longmapsto \mathbf{M}^{-1} \in \mathbb{R}^{\widetilde{N}\times\widetilde{N}}$$

is well defined and continuous and, hence, bounded above in the compact set U. Consequently, from (4.32),

$$\|\boldsymbol{\beta}^s\|_\infty \leq C h_E^{-2},$$

which recalling (4.31) yields

$$\left\|\widehat{\psi}^s\right\|_{\infty,\widehat{E}} \leq C h_E^{-2}. \tag{4.33}$$

Let us remark that, in principle, the constant C above depends on the number N_E of vertexes of E. However, by virtue of assumption $\mathbf{A_1}$, this number is bounded above in terms of $C_{\mathcal{T}}$. Therefore, N_E can take only a finite number of possible values and, hence, (4.33) holds true with C only depending on $C_{\mathcal{T}}$. Thus, we conclude the proof by combining (4.29), (4.30) and (4.33).

□

Now, we are in a position to prove $L^2(\Omega)$ error estimates for the $\boldsymbol{\mathcal{V}}_h$-interpolant.

Lemma 4.3.3 *Let $\boldsymbol{v} \in \boldsymbol{\mathcal{V}}$ be such that $\boldsymbol{v} \in [\mathrm{H}^t(\Omega)]^2$ with $t > 1/2$. Let $\boldsymbol{v}_I \in \boldsymbol{\mathcal{V}}_h$ be its interpolant defined by* (4.8)–(4.9)*. Let $E \in \mathcal{T}_h$. If $1 \leq t \leq k+1$, then*

$$\|\boldsymbol{v} - \boldsymbol{v}_I\|_{0,E} \leq C h_E^t \, |\boldsymbol{v}|_{t,E}\,, \tag{4.34}$$

whereas, if $1/2 < t \leq 1$, then

$$\|\boldsymbol{v} - \boldsymbol{v}_I\|_{0,E} \leq C \left(h_E^t \, |\boldsymbol{v}|_{t,E} + h_E \, \|\mathrm{div}\, \boldsymbol{v}\|_{0,E}\right). \tag{4.35}$$

Proof. First, we consider the case $1 \leq t \leq k+1$. The first step is to bound $\|\boldsymbol{v}_I\|_{0,E}$. Since $\boldsymbol{v}_I \in \boldsymbol{\mathcal{V}}_h^E$, thanks to (4.23)–(4.28) we write it in the basis (4.22) as follows:

$$\boldsymbol{v}_I = \sum_{l=1}^{N_E} \sum_{i=0}^{k} \left(\int_{e_l} (\boldsymbol{v} \cdot \boldsymbol{n})\, q_l^i \, ds \right) \boldsymbol{\varphi}_l^i + \sum_{s=1}^{\widetilde{N}} \left(\int_E (\operatorname{div} \boldsymbol{v})\, p_s \right) \widetilde{\boldsymbol{\varphi}}^s.$$

Therefore, from Lemmas 4.6.2 and 4.6.3 we have

$$\|\boldsymbol{v}_I\|_{0,E} \leq C \left(\sum_{l=1}^{N_E} \sum_{i=0}^{k} \left| \int_{e_l} (\boldsymbol{v} \cdot \boldsymbol{n})\, q_l^i \, ds \right| + \sum_{s=1}^{\widetilde{N}} \left| \int_E (\operatorname{div} \boldsymbol{v})\, p_s \right| \right).$$

Then, by using that $\left\|q_l^i\right\|_{\infty,e_l} = 1$ for $i = 1, \ldots, k$ and $l = 1, \ldots, N_E$, $\|p_s\|_{\infty,E} \leq C$ for $s = 1, \ldots, \widetilde{N}$, the Cauchy-Schwarz inequality and Lemma 4.6.1, we obtain

$$\begin{aligned} \|\boldsymbol{v}_I\|_{0,E} &\leq C \left(h_E^{1/2} \|\boldsymbol{v}\|_{0,\partial E} \left\|q_l^i\right\|_{\infty,e_l} + \widetilde{N} h_E \|\operatorname{div} \boldsymbol{v}\|_{0,E} \|p_s\|_{\infty,E} \right) \\ &\leq C \left(\|\boldsymbol{v}\|_{0,E} + h_E \, |\boldsymbol{v}|_{1,E} + h_E \|\operatorname{div} \boldsymbol{v}\|_{0,E} \right) \\ &\leq C \left(\|\boldsymbol{v}\|_{0,E} + h_E \, |\boldsymbol{v}|_{1,E} \right). \end{aligned} \tag{4.36}$$

Now, for all $\boldsymbol{v}_k \in [\mathbb{P}_k(E)]^2$ we note that $(\boldsymbol{v}_k)_I = \boldsymbol{v}_k$ and, hence, using the above estimate for $\boldsymbol{v} - \boldsymbol{v}_k$, we write

$$\|\boldsymbol{v} - \boldsymbol{v}_I\|_{0,E} = \|\boldsymbol{v} - \boldsymbol{v}_k - (\boldsymbol{v} - \boldsymbol{v}_k)_I\|_{0,E} \leq \|\boldsymbol{v} - \boldsymbol{v}_k\|_{0,E} + C \left(\|\boldsymbol{v} - \boldsymbol{v}_k\|_{0,E} + h_E \, |\boldsymbol{v} - \boldsymbol{v}_k|_{1,E} \right).$$

Thus, by choosing $\boldsymbol{v}_k$ as in [18, Proposition 4.2], we have that $\|\boldsymbol{v} - \boldsymbol{v}_k\|_{0,E} + h_E \, |\boldsymbol{v} - \boldsymbol{v}_k|_{1,E} \leq C h_E^t \, |\boldsymbol{v}|_{t,E}$, which together with the above inequality allow us to conclude (4.34).

Next, we consider the case $1/2 < t \leq 1$. Using the same arguments as above, we obtain in this case instead of (4.36),

$$\|\boldsymbol{v}_I\|_{0,E} \leq C \left(\|\boldsymbol{v}\|_{0,E} + h_E^t \, |\boldsymbol{v}|_{t,E} + h_E \|\operatorname{div} \boldsymbol{v}\|_{0,E} \right). \tag{4.37}$$

Therefore, repeating again the arguments above with $\boldsymbol{v}_0 \in [\mathbb{P}_0(E)]^2$ instead of $\boldsymbol{v}_k$, we have

$$\begin{aligned} \|\boldsymbol{v} - \boldsymbol{v}_I\|_{0,E} &\leq \|\boldsymbol{v} - \boldsymbol{v}_0 - (\boldsymbol{v} - \boldsymbol{v}_0)_I\|_{0,E} \\ &\leq \|\boldsymbol{v} - \boldsymbol{v}_0\|_{0,E} + C \left(\|\boldsymbol{v} - \boldsymbol{v}_0\|_{0,E} + h_E^t \, |\boldsymbol{v}|_{t,E} + h_E \|\operatorname{div} \boldsymbol{v}\|_{0,E} \right) \\ &\leq C \left(h_E^t \, |\boldsymbol{v}|_{t,E} + h_E \|\operatorname{div} \boldsymbol{v}\|_{0,E} \right), \end{aligned}$$

where we have used again [18, Proposition 4.2]. Thus, the proof is complete.
□

Remark 4.6.2 *Estimate* (4.35) *can be improved for* $k = 0$ *and* $1/2 < t \leq 1$. *In fact, in such a case, the interpolant* $\boldsymbol{v}_I \in \boldsymbol{\mathcal{V}}_h$ *is defined only by* (4.8). *Hence,*

$$\boldsymbol{v}_I = \sum_{l=1}^{N_E} \left(\int_{e_l} (\boldsymbol{v} \cdot \boldsymbol{n})\, q_l^0 \, ds \right) \boldsymbol{\varphi}_l^0$$

and repeating the arguments above we obtain

$$\|\boldsymbol{v}_I\|_{0,E} \leq C\left(\|\boldsymbol{v}\|_{0,E} + h_E^t\,|\boldsymbol{v}|_{t,E}\right),$$

instead of (4.37)*, which leads to*

$$\|\boldsymbol{v} - \boldsymbol{v}_I\|_{0,E} \leq C h_E^t\,|\boldsymbol{v}|_{t,E}\,.$$

Capítulo 5

A Virtual Element Method for Reissner-Mindlin plates

5.1. Introduction

The *Virtual Element Method* (VEM), introduced in [18, 22], is a recent generalization of the Finite Element Method which is characterized by the capability of dealing with very general polygonal/polyhedral meshes. The interest in numerical methods that can make use of general polytopal meshes has recently undergone a significant growth in the mathematical and engineering literature; among the large number of papers on this subject, we cite as a minimal sample [8, 18, 29, 60, 76, 104, 109, 112].

Indeed, polytopal meshes can be very useful for a wide range of reasons, including meshing of the domain (such as cracks) and data (such as inclusions) features, automatic use of hanging nodes, use of moving meshes, adaptivity. Moreover, the VEM presents the advantage to easily implement highly regular discrete spaces. Indeed, by avoiding the explicit construction of the local basis functions, the VEM can easily handle general polygons/polyhedrons without complex integrations on the element (see [22] for details on the coding aspects of the method). The Virtual Element Method has been applied successfully in a large range of problems, see for instance [3, 6, 14, 18, 22, 30, 36, 37, 38, 54, 57, 58, 84, 97, 100, 101, 118].

The Reissner–Mindlin theory is the most used model to approximate the deformation of a thin or moderately thick elastic plate. Nowadays, it is very well understood that the discretization of this problem poses difficulties due to the so called locking phenomenon when the thickness t is small with respect to the other dimensions of the plate. Nevertheless, adopting for instance a reduced integration or a mixed interpolation technique, this phenomenon can be avoided. Indeed, several families of methods have been rigorously shown to be free from locking and optimally convergent. We mention [81, 94] for a thorough description and further references.

Recently, a new approach to solve the Reissner–Mindlin bending problem has been presented in [26] by Beirão da Veiga et al. (see also [79, 93]). In this case a variational formulation of the plate bending problem is written terms of shear strain and deflection with the advantage that the "shear locking phenomenon" is avoided. A discretization of the problem by Isogeometric

Analysis is proposed. Under some regularity assumptions on the exact solution, optimal error estimates with constants independent of the plate thickness are proved.

The aim of this paper is on developing a Virtual Element Method which applies to general polygonal (even non-convex) meshes for Reissner-Mindlin plates. We consider a variational formulation written in terms of shear strain and deflection presented in [26]. Here, we exploit the capability of VEM to built highly regular discrete spaces and propose a conforming $[H^1(\Omega)]^2 \times H^2(\Omega)$ discrete formulation, respectively for the shear strain and deflections. The resulting bilinear form is continuous and elliptic with appropriate t-dependent norms. This method makes use of a very simple set of degrees of freedom, namely 5 degrees of freedom per vertex of the mesh plus the number of edges, and approximates directly the transverse shear strain, which is distinctive of this approach. Moreover, the rotations are obtained as a simple postprocess from the shear strain and deflection. Under some regularity assumptions on the exact solution, optimal error estimates (in the natural norms of the adopted formulation) with constants independent of the plate thickness are proved for all the involved variables. In addition, we present error estimates in weaker norms using a duality argument. Finally, we point out that, differently from the finite element method where building globally $C^1(\Omega)$ functions is complicated, here the virtual deflection space can be built with a rather simple construction due to the flexibility of the virtual approach. In a summary, the advantages of the proposed method are the possibility to use general polygonal meshes and a better conformity with the limit Kirchhoff problem, ensuing from the $H^2(\Omega)$ approximation used for the discrete deflection.

The outline of this article is as follows: we introduce in Section 5.2 the Reissner-Mindlin plate model, first in terms of deflection and rotations variables and then in an equivalent form in terms of deflection and transverse shear strain variable. In Section 5.3, we present the discrete spaces for the shear strain and deflection, together with their properties, next, we construct the discrete bilinear forms and the loading term. We end this section with the presentation of the virtual element discrete formulation. In Section 5.4, we present the error analysis of the virtual scheme. In Section 5.5, we report a couple of numerical tests that allow us to assess the convergence properties of the method.

Throughout the paper, Ω is a generic Lipschitz bounded domain of $\mathbb{R}^2$. For $s \geq 0$, $\|\cdot\|_{s,\Omega}$ stands indistinctly for the norm of the Hilbertian Sobolev spaces $\mathrm{H}^s(\Omega)$ or $[\mathrm{H}^s(\Omega)]^2$ with the convention $H^0(\Omega) := L^2(\Omega)$. Finally, we employ $\mathbf{0}$ to denote a generic null vector and we will denote with C a generic constant which may take different values in different occurrences, and which is independent of the mesh parameter h and the plate thickness t.

5.2. Continuous problem

Consider an elastic plate of thickness t, $0 < t \leq 1$, with reference configuration $\Omega \times (-t/2, t/2)$, where Ω is a convex polygonal domain of $\mathbb{R}^2$ occupied by the mid-section of the plate. The deformation of the plate is described by means of the Reissner-Mindlin model in terms of the rotations $\boldsymbol{\theta} = (\theta_1, \theta_2)$ of the fibers initially normal to the plate mid-surface and the deflection

w. We subdivide the boundary Γ of Ω in three disjoint parts such that,

$$\Gamma = \Gamma_c \cup \Gamma_s \cup \Gamma_f.$$

The plate is assumed to be clamped on Γ_c, simply supported on Γ_s and free on Γ_f. We assume that Γ_c has positive measure. We denote by $\boldsymbol{n}$ the outward unit normal vector to Γ, the following equations describe the plate response to a conveniently scaled transverse load g:

$$\begin{cases} -\mathbf{div}\boldsymbol{\mathcal{C}}\varepsilon(\boldsymbol{\theta}) - \lambda t^{-2}(\nabla w - \boldsymbol{\theta}) &= \mathbf{0} \quad in\ \ \Omega, \\ -\operatorname{div}(\lambda t^{-2}(\nabla w - \boldsymbol{\theta})) &= g \quad in\ \ \Omega, \\ \boldsymbol{\theta} = \mathbf{0}, \quad w = 0 & \quad on\ \ \Gamma_c, \\ \boldsymbol{\mathcal{C}}\varepsilon(\boldsymbol{\theta})\boldsymbol{n} = \mathbf{0}, \quad w = 0 & \quad on\ \ \Gamma_s, \\ \boldsymbol{\mathcal{C}}\varepsilon(\boldsymbol{\theta})\boldsymbol{n} = \mathbf{0}, \quad (\boldsymbol{\theta} - \nabla w) = \mathbf{0} & \quad on\ \ \Gamma_f, \end{cases} \tag{5.1}$$

where $\lambda := Ek/2(1+\nu)$ is the shear modulus, with E being the Young modulus, ν the Poisson ratio, and k a correction factor, $\varepsilon(\boldsymbol{\theta}) := \frac{1}{2}(\nabla\boldsymbol{\theta} + (\nabla\boldsymbol{\theta})^t)$ is the standard strain tensor, and $\boldsymbol{\mathcal{C}}$ is the tensor of bending moduli, given by (for isotropic materials)

$$\boldsymbol{\mathcal{C}}\boldsymbol{\sigma} := \frac{E}{12(1-\nu^2)}\left((1-\nu)\boldsymbol{\sigma} + \nu\operatorname{tr}(\boldsymbol{\sigma})\mathbf{I}\right), \qquad \boldsymbol{\sigma} \in [L^2(\Omega)]^{2\times 2},$$

where $\operatorname{tr}(\boldsymbol{\sigma})$ is trace of $\boldsymbol{\sigma}$ and $\mathbf{I}$ is the identity tensor.

Let us consider the space

$$\widetilde{\boldsymbol{X}} := \{(v, \boldsymbol{\eta}) \in H^1(\Omega) \times [H^1(\Omega)]^2 : v = 0 \text{ on } \Gamma_c \cup \Gamma_s, \boldsymbol{\eta} = \mathbf{0} \text{ on } \Gamma_c\}.$$

By testing the system (5.1) with $(v, \boldsymbol{\eta}) \in \widetilde{\boldsymbol{X}}$, integrating by parts and using the boundary conditions, we write the following variational formulation:

Problem 5.2.1 *Given $g \in L^2(\Omega)$, find $(w, \boldsymbol{\theta}) \in \widetilde{\boldsymbol{X}}$ such that*

$$a(\boldsymbol{\theta}, \boldsymbol{\eta}) + b(\boldsymbol{\theta} - \nabla w, \boldsymbol{\eta} - \nabla v) = (g, v)_{0,\Omega} \qquad \forall (v, \boldsymbol{\eta}) \in \widetilde{\boldsymbol{X}},$$

where $(\cdot,\cdot)_{0,\Omega}$ denotes the inner-product in $L^2(\Omega)$, and the bilinear forms are given by

$$a(\boldsymbol{\theta}, \boldsymbol{\eta}) := (\boldsymbol{\mathcal{C}}\varepsilon(\boldsymbol{\theta}), \varepsilon(\boldsymbol{\eta}))_{0,\Omega},$$
$$b(\boldsymbol{\theta}, \boldsymbol{\eta}) := \lambda t^{-2}(\boldsymbol{\theta}, \boldsymbol{\eta})_{0,\Omega}.$$

The following result states that the bilinear form appearing in Problem 5.2.1 is coercive (see [26, Proposition A.1]).

Lemma 5.2.1 *There exists a positive constant α depending only on the material constants and the domain Ω such that:*

$$a(\boldsymbol{\eta}, \boldsymbol{\eta}) + b(\boldsymbol{\eta} - \nabla v, \boldsymbol{\eta} - \nabla v) \geq \alpha\left(\|\boldsymbol{\eta}\|^2_{1,\Omega} + t^{-2}\|\boldsymbol{\eta} - \nabla v\|^2_{0,\Omega} + \|v\|^2_{1,\Omega}\right) \quad \forall (v, \boldsymbol{\eta}) \in \widetilde{\boldsymbol{X}}. \tag{5.2}$$

It is well known that the discretization of the Reissner-Mindlin equations have difficulties due to the so called locking phenomenon when the thickness t is small with respect to the other dimensions of the plate. To avoid this phenomenon we will introduce and analyze an alternative formulation of the problem that does not suffer from such a drawback. In order to simplify the notation, and without any loss of generality, we will assume $\lambda = 1$ in the following.

5.2.1. An equivalent variational formulation

The variational formulation that will be considered here, was introduced in the context of shells in [79, 93] and has been studied in [26] for Reissner-Mindlin plates using Isogeometric Analysis.

Now, we note that the equivalent formulation is derived by simply considering the following charge of variables:

$$(w, \boldsymbol{\theta}) \longleftrightarrow (w, \boldsymbol{\gamma}) \quad \text{with} \quad \boldsymbol{\theta} = \nabla w + \boldsymbol{\gamma}. \tag{5.3}$$

We note that the physical interpretation of the variable $\boldsymbol{\gamma}$ corresponds to the transverse shear strain.

The equivalent formulation will be obtained by using the change the variables (5.3) in Problem 5.2.1.

For the analysis we will consider the following t-dependent energy norm:

$$|||v, \boldsymbol{\tau}|||^2 := \|\boldsymbol{\tau} + \nabla v\|^2_{1,\Omega} + t^{-2}\|\boldsymbol{\tau}\|^2_{0,\Omega} + \|v\|^2_{1,\Omega}, \tag{5.4}$$

for all sufficiently regular functions $\boldsymbol{\tau} : \Omega \longrightarrow \mathbb{R}^2$ and $v : \Omega \longrightarrow \mathbb{R}$.

Now, we define the following variational spaces:

$$\widehat{\boldsymbol{X}} := \overline{C^\infty(\Omega) \times [C^\infty(\Omega)]^2}^{|||\cdot,\cdot|||};$$

$$\boldsymbol{X} := \{(v, \boldsymbol{\tau}) \in \widehat{\boldsymbol{X}} : v = 0 \text{ on } \Gamma_c \cup \Gamma_s, \nabla v + \boldsymbol{\tau} = \mathbf{0} \text{ on } \Gamma_c\}.$$

It is immediately verified that

$$H^2(\Omega) \times [H^1(\Omega)]^2 \subset \widehat{\boldsymbol{X}} \subset H^1(\Omega) \times [L^2(\Omega)]^2.$$

Moreover, note that the space $\boldsymbol{X}$ exactly corresponds to $\widetilde{\boldsymbol{X}}$ up to the change of variables (5.3).

Let us introduce the equivalent variational formulation for the Reissner-Mindlin model as follows:

Problem 5.2.2 *Given $g \in L^2(\Omega)$, find $(w, \boldsymbol{\gamma}) \in \boldsymbol{X}$ such that*

$$a(\nabla w + \boldsymbol{\gamma}, \nabla v + \boldsymbol{\tau}) + b(\boldsymbol{\gamma}, \boldsymbol{\tau}) = (g, v)_{0,\Omega} \qquad \forall (v, \boldsymbol{\tau}) \in \boldsymbol{X}.$$

We have that Problem 5.2.2 is equivalent to Problem 5.2.1 up to the change of variables (5.3). As a consequence, we have the following coercivity property for the bilinear form on the left hand side of Problem 5.2.2 (see (5.2)):

$$a(\nabla v + \boldsymbol{\tau}, \nabla v + \boldsymbol{\tau}) + b(\boldsymbol{\tau}, \boldsymbol{\tau}) \geq \alpha |||v, \boldsymbol{\tau}|||^2 \quad \forall (v, \boldsymbol{\tau}) \in \boldsymbol{X}, \tag{5.5}$$

with same constant α. Moreover, bilinear forms $a(\cdot, \cdot)$ and $b(\cdot, \cdot)$ are bounded uniformly in t.

Therefore, Problem 5.2.2 has a unique solution $(w, \boldsymbol{\gamma}) \in \boldsymbol{X}$ and

$$|||w, \boldsymbol{\gamma}||| \leq C\|g\|_{0,\Omega}.$$

5.3. Virtual element discretization

We begin this section, by recalling the mesh construction and the assumptions considered to introduce the discrete virtual element spaces for the shear strain and deflection, together with their properties, next, we will introduce discrete bilinear forms and the loading term. Finally, we end this section with the presentation of the virtual element discretization of Problem 5.2.2.

5.3.1. Mesh regularity assumption

Let $\{\mathcal{T}_h\}_h$ be a sequence of decompositions of Ω into polygons E. Let h_E denote the diameter of the element E and $h := \max_{E\in\mathcal{T}_h} h_E$.

For the analysis, we will make the following assumptions as in [18, 31, 36]: there exists a positive real number $C_{\mathcal{T}}$ such that, for every h and every $E \in \mathcal{T}_h$,

$\mathbf{A}_1$: the ratio between the shortest edge and the diameter h_E of E is larger than $C_{\mathcal{T}}$;

$\mathbf{A}_2$: $E \in \mathcal{T}_h$ is star-shaped with respect to every point of a ball of radius $C_{\mathcal{T}} h_E$.

For any subset $S \subseteq \mathbb{R}^2$ and nonnegative integer k, we indicate by $\mathbb{P}_k(S)$ the space of polynomials of degree up to k defined on S. To keep the notation simpler, we denote by $\boldsymbol{n}$ a general normal unit vector; in each case, its precise definition will be clear from the context and we denote by $\boldsymbol{t}$ the tangent unit vector $\boldsymbol{t}$ defined as the anticlockwise rotation of $\boldsymbol{n}$.

To continue the construction of the discrete scheme, we need some preliminary definitions. First, we split the bilinear forms $a(\cdot,\cdot)$ and $b(\cdot,\cdot)$ introduced in the previous section as follows:

$$a\left(\nabla w+\boldsymbol{\gamma}, \nabla v+\boldsymbol{\tau}\right) = \sum_{E\in\mathcal{T}_h} a^E\left(\nabla w+\boldsymbol{\gamma}, \nabla v+\boldsymbol{\tau}\right) \quad \forall (w,\boldsymbol{\gamma}),(v,\boldsymbol{\tau}) \in \boldsymbol{X}, \tag{5.6}$$

$$b\left(\boldsymbol{\gamma},\boldsymbol{\tau}\right) = \sum_{E\in\mathcal{T}_h} b^E(\boldsymbol{\gamma},\boldsymbol{\tau}) \qquad \forall \boldsymbol{\gamma},\boldsymbol{\tau} \in [H^1(\Omega)]^2, \tag{5.7}$$

with

$$a^E\left(\nabla w+\boldsymbol{\gamma}, \nabla v+\boldsymbol{\tau}\right) := \left(\boldsymbol{\mathcal{C}}\varepsilon(\nabla w+\boldsymbol{\tau}), \varepsilon(\nabla v+\boldsymbol{\gamma})\right)_{0,E}$$

and

$$b^E(\boldsymbol{\gamma},\boldsymbol{\tau}) := t^{-2}(\boldsymbol{\gamma},\boldsymbol{\tau})_{0,E}.$$

Finally, we define

$$\mathcal{A}((w,\boldsymbol{\gamma}),(v,\boldsymbol{\tau})) := a(\nabla w+\boldsymbol{\gamma}, \nabla v+\boldsymbol{\tau}) + b(\boldsymbol{\gamma},\boldsymbol{\tau}) = \sum_{E\in\mathcal{T}_h} \mathcal{A}^E((w,\boldsymbol{\gamma}),(v,\boldsymbol{\tau})) \quad \forall (w,\boldsymbol{\gamma}),(v,\boldsymbol{\tau}) \in \boldsymbol{X},$$

where

$$\mathcal{A}^E((w,\boldsymbol{\gamma}),(v,\boldsymbol{\tau})) = a^E\left(\nabla w+\boldsymbol{\gamma}, \nabla v+\boldsymbol{\tau}\right)) + b^E\left(\boldsymbol{\gamma},\boldsymbol{\tau}\right).$$

In order to construct the discrete scheme associated to Problem 5.2.2, in what follows, we will show that for each $h > 0$ it is possible to build the following:

1. a discrete virtual space $\boldsymbol{X}_h \subseteq \boldsymbol{X}$ such that

$$\boldsymbol{X}_h := \{(v_h, \boldsymbol{\tau}_h) \in (W_h \times \mathbf{V}_h) : v_h = 0 \text{ on } \Gamma_c \cup \Gamma_s, \nabla v_h + \boldsymbol{\tau}_h = \mathbf{0} \text{ on } \Gamma_c\},$$

in which the virtual spaces $W_h \subseteq H^2(\Omega)$ and $\mathbf{V}_h \subseteq [H^1(\Omega)]^2$;

2. a symmetric bilinear form $\mathcal{A}_h : \boldsymbol{X}_h \times \boldsymbol{X}_h \to \mathbb{R}$ which can be split as

$$\mathcal{A}_h((w_h, \boldsymbol{\gamma}_h), (v_h, \boldsymbol{\tau}_h)) := \sum_{E \in \mathcal{T}_h} \mathcal{A}_h^E((w_h, \boldsymbol{\gamma}_h), (v_h, \boldsymbol{\tau}_h)) \quad \forall (w_h, \boldsymbol{\gamma}_h), (v_h, \boldsymbol{\tau}_h) \in \boldsymbol{X}_h, \tag{5.8}$$

with $\mathcal{A}_h^E(\cdot, \cdot)$ local bilinear forms on $\boldsymbol{X}_h|_E \times \boldsymbol{X}_h|_E$;

3. an element $g_h \in \boldsymbol{X}_h'$ and a discrete duality pair $\langle \cdot, \cdot \rangle_h$ in such a way that the following discrete problem: Find $(w_h, \boldsymbol{\gamma}_h) \in \boldsymbol{X}_h$ such that

$$\mathcal{A}_h((w_h, \boldsymbol{\gamma}_h), (v_h, \boldsymbol{\tau}_h)) = \langle g_h, v_h \rangle_h \qquad \forall (v_h, \boldsymbol{\tau}_h) \in \boldsymbol{X}_h, \tag{5.9}$$

admits a unique solution $(w_h, \boldsymbol{\gamma}_h) \in \boldsymbol{X}_h$ and exhibits optimal approximation properties.

5.3.2. Discrete virtual spaces for shear strain and deflection

We introduce a pair of finite dimensional spaces for shear strain and deflection:

$$\mathbf{V}_h \subseteq [H^1(\Omega)]^2, \qquad W_h \subseteq H^2(\Omega).$$

First, we construct the shear strain virtual space $\mathbf{V}_h$, inspired from [6]. With this aim, we consider a simple polygon E and we define

$$\mathbb{B}_{\partial E} := \{\boldsymbol{\tau}_h \in [C^0(\partial E)]^2 : \boldsymbol{\tau}_h \cdot \boldsymbol{t}|_{\partial E} \in \mathbb{P}_2(e) \text{ and } \boldsymbol{\tau}_h \cdot \boldsymbol{n}|_{\partial E} \in \mathbb{P}_1(e) \ \ \forall e \in \partial E\}.$$

We then consider the finite dimensional space defined as follows:

$$\mathbf{V}_h^E := \{\boldsymbol{\tau}_h \in [\mathrm{H}^1(E)]^2 : \operatorname{rot} \boldsymbol{\tau}_h \in \mathbb{P}_0(E), \boldsymbol{\tau}_h|_{\partial E} \in \mathbb{B}_{\partial E}, \boldsymbol{\tau}_h \text{ minimizes the } H^1\text{-seminorm}\}.$$

Note that the space $\mathbf{V}_h^E$ is well defined. Indeed, given a (piecewise polynomial) boundary value $\boldsymbol{\tau}_h|_{\partial E} \in [H^{1/2}(\partial E)]^2$, the associated function $\boldsymbol{\tau}_h$ inside the element E is obtained by solving the following well-posed problem:

$$\begin{cases} -\Delta \boldsymbol{\tau}_h + \mathbf{rot}\, s = \mathbf{0} \text{ in } E, \\ \operatorname{rot} \boldsymbol{\tau}_h = f \text{ with } f \in \mathbb{P}_0(E), \\ \boldsymbol{\tau}_h \text{ assigned in } \partial E, \end{cases} \tag{5.10}$$

where

$$f = \operatorname{rot} \boldsymbol{\tau}_h|_E = \frac{1}{|E|} \int_E \operatorname{rot} \boldsymbol{\tau}_h = \frac{1}{|E|} \int_{\partial E} \boldsymbol{\tau}_h \cdot \boldsymbol{t}.$$

It is important to observe that, since the functions in $\mathbf{V}_h^E$ are uniquely identified by their boundary values, $\dim(\mathbf{V}_h^E) = \dim(\mathbf{V}_h^E|_{\partial E})$, i.e., $\dim(\mathbf{V}_h^E) = 3N_E$, with N_E being the number of edges of E. This leads to introducing the following $3N_E$ degrees of freedom for the space $\mathbf{V}_h^E$:

- $\mathcal{V}_E^h$: the values of $\boldsymbol{\tau}_h$ (vector) at the vertices of E.
- $\mathcal{E}_E^h$: the value of the
$$\frac{1}{|e|}\int_e \boldsymbol{\tau}_h \cdot \boldsymbol{t} \quad \forall \text{ edge } e \in \partial E.$$

Moreover, we note that as a consequence of the definition $\mathbf{V}_h^E$, the output values of the two sets of degrees of freedom $\mathcal{V}_E^h$ and $\mathcal{E}_E^h$ are sufficient to uniquely determine $\boldsymbol{\tau}_h \cdot \boldsymbol{t}$ and $\boldsymbol{\tau}_h \cdot \boldsymbol{n}$ on the boundary of E, for any $\boldsymbol{\tau}_h \in \mathbf{V}_h^E$. Finally, we note that clearly $[\mathbb{P}_1(E)]^2 \subset \mathbf{V}_h^E$.

For every decomposition $\mathcal{T}_h$ of Ω into simple polygons E, we define the global space $\mathbf{V}_h$ without boundary conditions.

$$\mathbf{V}_h := \{\boldsymbol{\tau}_h \in [H^1(\Omega)]^2 : \boldsymbol{\tau}_h|_E \in \mathbf{V}_h^E \quad \forall E \in \mathcal{T}_h\}.$$

In agreement with the local choice of the degrees of freedom, in $\mathbf{V}_h$ we choose the following degrees of freedom:

- $\mathcal{V}^h$: the values of $\boldsymbol{\tau}_h$ (vector) at the vertices of $\mathcal{T}_h$.
- $\mathcal{E}^h$: the value of the
$$\frac{1}{|e|}\int_e \boldsymbol{\tau}_h \cdot \boldsymbol{t} \quad \forall \text{ edge } e \in \mathcal{T}_h.$$

Now, we will introduce the discrete virtual space W_h for the deflection, see also [57, 6]. With this aim, we first define the following finite dimensional space:

$$\begin{aligned} W_h^E := \{v_h \in H^2(E) : \Delta^2 v_h = 0, v_h|_{\partial E} \in C^0(\partial E), v_h|_{\partial E} \in \mathbb{P}_3(e), \\ \nabla v_h|_{\partial E} \in [C^0(\partial E)]^2 \text{ and } \partial_{\boldsymbol{n}} v_h|_{\partial E} \in \mathbb{P}_1(e) \quad \forall e \in \partial E\}, \end{aligned}$$

where Δ^2 represents the biharmonic operator. We observe that any $v_h \in W_h^E$ satisfy the following conditions:

- the trace on the boundary of E is continuous and on each edge is a polynomial of degree 3;
- the gradient on the boundary is continuous and on each edge its normal (respectively tangential) component is a polynomial of degree 1 (respectively 2);
- inside E satisfy the biharmonic equation $\Delta^2 v_h = 0$;
- $\mathbb{P}_2(E) \subseteq W_h^E$.

We choose in W_h^E the degrees of freedom introduced in [7, Section 2.2], namely:

- $\mathcal{W}_E^h$: The values of v_h and ∇v_h at the vertices of E.

We note that as a consequence of the definition W_h^E, the degrees of freedom $\mathcal{W}_E^h$ are sufficient to uniquely determine v_h and ∇v_h on the boundary of E.

We now present the global virtual space for the deflection: for every decomposition $\mathcal{T}_h$ of Ω into simple polygons E, we define (without boundary conditions).

$$W_h := \{v_h \in H^2(\Omega) : v_h|_E \in W_h^E \quad \forall E \in \mathcal{T}_h\}.$$

In agreement with the local choice of the degrees of freedom, in W_h we choose the following degrees of freedom:

- $\mathcal{W}^h$: the values of v_h and ∇v_h at the vertices of $\mathcal{T}_h$.

As a consequence of the definition of local virtual spaces $\mathbf{V}_h^E$ and W_h^E, we have the following result which will be used in the forthcoming analysis.

Proposition 5.3.1 *Let E be a simple polygon with N_E edges. Then $\nabla W_h^E \subseteq \mathbf{V}_h^E$.*

Proof. Let $v_h \in W_h^E$, then we have that: $v_h \in H^2(E)$, $\Delta^2 v_h = 0$, $v_h|_e \in \mathbb{P}_3(e)$ and $\nabla v_h \cdot \boldsymbol{n}|_e \in \mathbb{P}_1(e)$ for all $e \in \partial E$. Hence, $\nabla v_h \in [\mathrm{H}^1(E)]^2$, $\nabla v_h \cdot \boldsymbol{t}|_e \in \mathbb{P}_2(e)$ and $\nabla v_h \cdot \boldsymbol{n}|_e \in \mathbb{P}_1(e)$ for all $e \in \partial E$, i.e, $\nabla v_h|_{\partial E} \in \mathbb{B}_{\partial E}$. Moreover, $\mathrm{rot}(\nabla v_h) = 0 \in \mathbb{P}_0(E)$. On the other hand, we have that

$$0 = \Delta^2 v_h = \Delta\left(\Delta v_h\right) = \Delta\left(\mathrm{div}(\nabla v_h)\right) = \mathrm{div}\left(\Delta(\nabla v_h)\right).$$

Since a star-shaped polygon E is simply connected, there exists $q \in \mathrm{H}^1(E)$ such that $\Delta(\nabla v_h) = \mathbf{rot}\, q$. Thus, ∇v_h satisfies (5.10) and therefore $\nabla v_h \in \mathbf{V}_h^E$. The proof is complete. □

Finally, once we have defined $\mathbf{V}_h$ and W_h, we are able to introduce our virtual element space $\boldsymbol{X}_h$.

$$\boldsymbol{X}_h := \{(v_h, \boldsymbol{\tau}_h) \in W_h \times \mathbf{V}_h\} \cap \boldsymbol{X}.$$

5.3.3. Bilinear forms and the loading term

In this section we will discuss the construction of the discrete version of the local bilinear forms $a^E(\cdot,\cdot)$ (cf (5.6)) and $b^E(\cdot,\cdot)$ (cf (5.7)), which will be used to built the local bilinear form appearing in (5.8). Moreover, we will discuss the construction of the loading term appearing in (5.9).

We define the projector $\Pi_\varepsilon^E : \mathbf{V}_h^E \longrightarrow [\mathbb{P}_1(E)]^2 \subset \mathbf{V}_h^E$ for each $\boldsymbol{\tau}_h \in \mathbf{V}_h^E$ as the solution of

$$\begin{cases} a^E(\boldsymbol{p}, \Pi_\varepsilon^E \boldsymbol{\tau}_h) = a^E(\boldsymbol{p}, \boldsymbol{\tau}_h) \quad \forall \boldsymbol{p} \in [\mathbb{P}_1(E)]^2, \\ \\ \left\langle\left\langle \boldsymbol{p}, \Pi_\varepsilon^E \boldsymbol{\tau}_h \right\rangle\right\rangle = \langle\langle \boldsymbol{p}, \boldsymbol{\tau}_h \rangle\rangle \quad \forall \boldsymbol{p} \in ker(a^E(\cdot,\cdot)), \end{cases} \tag{5.11}$$

where for all $\mathbf{r}_h, \mathbf{s}_h$ in $\mathbf{V}_h^E$

$$\langle\langle \mathbf{r}_h, \mathbf{s}_h \rangle\rangle := \frac{1}{N_E} \sum_{i=1}^{N_E} \mathbf{r}_h(v_i) \cdot \mathbf{s}_h(v_i), \quad v_i = \text{ vertices of } E,\ 1 \le i \le N_E.$$

We note that the second equation in (5.11) is needed for the problem to be well-posed. In fact, it is easy to check that it returns one (and only one) function $\Pi_\varepsilon^E \boldsymbol{\tau}_h \in [\mathbb{P}_1(E)]^2$. Moreover, we observe that the local degrees of freedom allow us to compute exactly the right hand side of (5.11). Indeed, for all $\boldsymbol{p} \in [\mathbb{P}_1(E)]^2$, we have

$$\begin{aligned} a^E(\boldsymbol{p}, \boldsymbol{\tau}_h) = \int_E \boldsymbol{\mathcal{C}}\varepsilon(\boldsymbol{p}) \colon \varepsilon(\boldsymbol{\tau}_h) &= -\int_E \mathbf{div}(\boldsymbol{\mathcal{C}}\varepsilon(\boldsymbol{p})) \cdot \boldsymbol{\tau}_h + \int_{\partial E} (\boldsymbol{\mathcal{C}}\varepsilon(\boldsymbol{p})\boldsymbol{n}) \cdot \boldsymbol{\tau}_h \\ &= \int_{\partial E} (\boldsymbol{\mathcal{C}}\varepsilon(\boldsymbol{p})\boldsymbol{n}) \cdot \boldsymbol{\tau}_h, \end{aligned}$$

where we have used that $\mathbf{div}(\boldsymbol{\mathcal{C}}\varepsilon(\boldsymbol{p})) = \mathbf{0}$. Therefore, since the functions $\boldsymbol{\tau}_h \in \mathbf{V}_h^E$ are known explicitly on the boundary, the right hand side of (5.11) can be computed exactly without knowing $\boldsymbol{\tau}_h$ in the interior of E. As a consequence, the projection operator Π_ε^E is computable solely on the basis of the degrees of freedom values.

Let $\Pi_0^E : \mathbf{V}_h^E \to [\mathbb{P}_0(E)]^2$ be the $[L^2(E)]^2$-projector, defined by

$$\int_E \Pi_0^E \boldsymbol{\tau}_h \cdot \boldsymbol{p}_0 = \int_E \boldsymbol{\tau}_h \cdot \boldsymbol{p}_0 \quad \forall \boldsymbol{p}_0 \in [\mathbb{P}_0(E)]^2.$$

We note that as before, the right hand side above is computable. In fact, we consider a simple polygon E with barycenter $\boldsymbol{x}_E = (x_E, y_E)^t$ and we have that any $\boldsymbol{p}_0 \in [\mathbb{P}_0(E)]^2$ can be written as $\boldsymbol{p}_0 = \alpha(1,0)^t + \beta(0,1)^t = \alpha\,\mathbf{rot}(y - y_E) + \beta\,\mathbf{rot}(x_E - x)$. Thus, for all $\boldsymbol{\tau}_h \in \mathbf{V}_h^E$ we have

$$\begin{aligned} \int_E \boldsymbol{\tau}_h \cdot (1,0)^t = \int_E \boldsymbol{\tau}_h \cdot \mathbf{rot}(y - y_E) &= \int_E \operatorname{rot} \boldsymbol{\tau}_h (y - y_E) - \int_{\partial E} (\boldsymbol{\tau}_h \cdot \boldsymbol{t})\,(y - y_E) \\ &= \operatorname{rot} \boldsymbol{\tau}_h \int_E (y - y_E) - \int_{\partial E} (\boldsymbol{\tau}_h \cdot \boldsymbol{t})\,(y - y_E) = -\int_{\partial E} (\boldsymbol{\tau}_h \cdot \boldsymbol{t})\,(y - y_E), \end{aligned}$$

where we have used that for $\boldsymbol{\tau}_h \in \mathbf{V}_h^E$, $\operatorname{rot} \boldsymbol{\tau}_h \in \mathbb{P}_0(E)$. Using the same arguments, we get

$$\int_E \boldsymbol{\tau}_h \cdot (0,1)^t = -\int_{\partial E} (\boldsymbol{\tau}_h \cdot \boldsymbol{t})\,(x_E - x),$$

which shows that $\Pi_0^E \boldsymbol{\tau}_h$ is computable solely on the basis of the degree of freedom values.

Let now $S^E(\cdot,\cdot)$ and $S_0^E(\cdot,\cdot)$ be any symmetric positive definite bilinear forms to be chosen as to satisfy

$$c_0 a^E(\boldsymbol{\tau}_h, \boldsymbol{\tau}_h) \le S^E(\boldsymbol{\tau}_h, \boldsymbol{\tau}_h) \le c_1 a^E(\boldsymbol{\tau}_h, \boldsymbol{\tau}_h) \quad \forall \boldsymbol{\tau}_h \in \mathbf{V}_h^E \ \text{ with } \Pi_\varepsilon^E \boldsymbol{\tau}_h = 0, \tag{5.12}$$

$$\tilde{c}_0 b^E(\boldsymbol{\tau}_h, \boldsymbol{\tau}_h) \le S_0^E(\boldsymbol{\tau}_h, \boldsymbol{\tau}_h) \le \tilde{c}_1 b^E(\boldsymbol{\tau}_h, \boldsymbol{\tau}_h) \quad \forall \boldsymbol{\tau}_h \in \mathbf{V}_h^E, \tag{5.13}$$

for some positive constants c_0, c_1, $\tilde{c}_0$ and $\tilde{c}_1$ depending only on the constant $C_{\mathcal{T}}$ from mesh assumptions $\mathbf{A}_1$ and $\mathbf{A}_2$. Then, we introduce on each element E the local (and computable) bilinear forms

$$\begin{aligned} a_h^E(\boldsymbol{\gamma}_h, \boldsymbol{\tau}_h) &:= a^E(\Pi_\varepsilon^E \boldsymbol{\gamma}_h, \Pi_\varepsilon^E \boldsymbol{\tau}_h) + S^E(\boldsymbol{\gamma}_h - \Pi_\varepsilon^E \boldsymbol{\gamma}_h, \boldsymbol{\tau}_h - \Pi_\varepsilon^E \boldsymbol{\tau}_h) \qquad \boldsymbol{\gamma}_h, \boldsymbol{\tau}_h \in \mathbf{V}_h^E, \\ b_h^E(\boldsymbol{\gamma}_h, \boldsymbol{\tau}_h) &:= b^E(\Pi_0^E \boldsymbol{\gamma}_h, \Pi_0^E \boldsymbol{\tau}_h) + S_0^E(\boldsymbol{\gamma}_h - \Pi_0^E \boldsymbol{\gamma}_h, \boldsymbol{\tau}_h - \Pi_0^E \boldsymbol{\tau}_h) \qquad \boldsymbol{\gamma}_h, \boldsymbol{\tau}_h \in \mathbf{V}_h^E. \end{aligned}$$

Now, we define in a natural way

$$a_h(\boldsymbol{\gamma}_h, \boldsymbol{\tau}_h) := \sum_{E \in \mathcal{T}_h} a_h^E(\boldsymbol{\gamma}_h, \boldsymbol{\tau}_h), \qquad b_h(\boldsymbol{\gamma}_h, \boldsymbol{\tau}_h) := \sum_{E \in \mathcal{T}_h} b_h^E(\boldsymbol{\gamma}_h, \boldsymbol{\tau}_h) \qquad \boldsymbol{\gamma}_h, \boldsymbol{\tau}_h \in \mathbf{V}_h.$$

The construction of $a_h^E(\cdot,\cdot)$ and $b_h^E(\cdot,\cdot)$ guarantees the usual consistency and stability properties of VEM, as noted in the Proposition below. Since the proof is simple and follows standard arguments in the Virtual Element literature, it is omitted.

Proposition 5.3.2 *The local bilinear forms $a_h^E(\cdot,\cdot)$ and $b_h^E(\cdot,\cdot)$ on each element E satisfy*

- *Consistency: for all $h > 0$ and for all $E \in \mathcal{T}_h$ we have that*

$$a_h^E(\boldsymbol{p}, \boldsymbol{\tau}_h) = a^E(\boldsymbol{p}, \boldsymbol{\tau}_h) \quad \forall \boldsymbol{p} \in [\mathbb{P}_1(E)]^2,\ \forall \boldsymbol{\tau}_h \in \mathbf{V}_h^E; \tag{5.14}$$

$$b_h^E(\boldsymbol{p}_0, \boldsymbol{\tau}_h) = b^E(\boldsymbol{p}_0, \boldsymbol{\tau}_h) \quad \forall \boldsymbol{p}_0 \in [\mathbb{P}_0(E)]^2,\ \forall \boldsymbol{\tau}_h \in \mathbf{V}_h^E. \tag{5.15}$$

- *Stability: there exist positive constants α_*, α^*, β_* and β^*, independent of h and E, such that*

$$\alpha_* a^E(\boldsymbol{\tau}_h, \boldsymbol{\tau}_h) \le a_h^E(\boldsymbol{\tau}_h, \boldsymbol{\tau}_h) \le \alpha^* a^E(\boldsymbol{\tau}_h, \boldsymbol{\tau}_h) \quad \forall \boldsymbol{\tau}_h \in \mathbf{V}_h^E, \quad \forall E \in \mathcal{T}_h, \tag{5.16}$$

$$\beta_* b^E(\boldsymbol{\tau}_h, \boldsymbol{\tau}_h) \le b_h^E(\boldsymbol{\tau}_h, \boldsymbol{\tau}_h) \le \beta^* b^E(\boldsymbol{\tau}_h, \boldsymbol{\tau}_h) \quad \forall \boldsymbol{\tau}_h \in \mathbf{V}_h^E, \quad \forall E \in \mathcal{T}_h. \tag{5.17}$$

We note that as a consequence of (5.16) and (5.17), the bilinear forms $a_h^E(\cdot,\cdot)$ and $b_h^E(\cdot,\cdot)$ are bounded with respect to the H^1 and L^2 norms, respectively.

We now discuss the construction of the loading term. For every $E \in \mathcal{T}_h$ we approximate the data g by a piecewise constant function g_h on each element E defined as the $L^2(E)$-projection of the load g (denoted by $\bar{g}_E$). Let the loading term

$$\langle g_h, v_h \rangle_h := \sum_{E \in \mathcal{T}_h} \bar{g}_E \sum_{i=1}^{N_E} v_h(v_i) \omega_E^i. \tag{5.18}$$

where $v_1, \ldots, v_{N_E}$ are the vertices of E and $\omega_E^1, \ldots, \omega_E^{N_E}$ are positive weights chosen to provide the exact integral on E when applied to linear functions.

5.3.4. Discrete problem

The results of the previous sections allow us to introduce the discrete VEM in shear strain-deflection formulation for the approximation of the continuous Reissner-Mindlin formulation presented in Problem 5.2.2.

With this aim, we first note that since $\nabla W_h^E \subset \mathbf{V}_h^E$ (see Proposition 5.3.1), the operator Π_ε^E can be also applied to ∇v_h for all $v_h \in W_h^E$. Hence, we introduce the following VEM discretization for the approximation of Problem 5.2.2.

Problem 5.3.1 *Find $(w_h, \boldsymbol{\gamma}_h) \in \boldsymbol{X}_h$ such that*

$$a_h(\nabla w_h + \boldsymbol{\gamma}_h, \nabla v_h + \boldsymbol{\tau}_h) + b_h(\boldsymbol{\gamma}_h, \boldsymbol{\tau}_h) = \langle g_h, v_h \rangle_h \qquad \forall (v_h, \boldsymbol{\tau}_h) \in \boldsymbol{X}_h. \tag{5.19}$$

The next lemma shows that the problem above is coercive in the $|||\cdot|||$ norm.

Lemma 5.3.1 *There exists $\beta > 0$, independent of h and t such that*

$$a_h(\nabla v_h + \boldsymbol{\tau}_h, \nabla v_h + \boldsymbol{\tau}_h) + b_h(\boldsymbol{\tau}_h, \boldsymbol{\tau}_h) \geq \beta \, |||(v_h, \boldsymbol{\tau}_h)|||^2 \qquad \forall (v_h, \boldsymbol{\tau}_h) \in \boldsymbol{X}_h.$$

Proof. Thanks to (5.16), (5.17) and (5.5), we have that

$$a_h(\nabla v_h+\boldsymbol{\tau}_h, \nabla v_h+\boldsymbol{\tau}_h)+b_h(\boldsymbol{\tau}_h, \boldsymbol{\tau}_h) \geq C_* \left(a(\nabla v_h + \boldsymbol{\tau}_h, \nabla v_h + \boldsymbol{\tau}_h) + b(\boldsymbol{\tau}_h, \boldsymbol{\tau}_h)\right) \geq \beta \, |||(v_h, \boldsymbol{\tau}_h)|||^2 ,$$

with $\beta := \min\{C_*, \alpha\}$. □ We deduce immediately from Lemma 5.3.1 that Problem 5.3.1 is well-posed.

Remark 5.3.1 *The solution of Problem 5.2.2 delivers the shear strain and deflection. In addition, it is possible to readily obtain the rotations $\boldsymbol{\theta}$ by recalling* (5.3)*. At the discrete level, this strategy corresponds to computing the rotations as a post-processing of the shear strain and deflection. If $(w_h, \boldsymbol{\gamma}_h) \in \boldsymbol{X}_h$ is the unique solutions of Problem 5.3.1, then the function*

$$\boldsymbol{\theta}_h = \nabla w_h + \boldsymbol{\gamma}_h,$$

is an approximation of the rotations. The accuracy of such approximation will be established in the following section.

5.4. Convergence analysis

In the present section, we develop an error analysis for the discrete virtual element scheme presented in Section 5.3.4. For the forthcoming analysis, we will assume that the mesh assumptions $\mathbf{A}_1$ and $\mathbf{A}_2$, introduced in Section 5.3.1, are satisfied.

For the analysis we will introduce the broken H^1-norm:

$$\|v\|^2_{1,h,\Omega} := \sum_{E \in \mathcal{T}_h} \|v\|^2_{1,E},$$

which is well defined for every $v \in L^2(\Omega)$ such that $v|_E \in \mathrm{H}^1(E)$ for all polygon $E \in \mathcal{T}_h$.

Moreover, we have the following propositions, which are derived by interpolation between Sobolev spaces (see for instance [86, Theorem I.1.5] from the analogous result for integer values of s. In its turn, the result for integer values is stated in [18, Proposition 4.2] and follows from the classical Scott-Dupont theory (see [51]).

Proposition 5.4.1 *There exists a constant $C > 0$, such that for every $v \in H^s(E)$ there exists $v_\Pi \in \mathbb{P}_k(E)$, $k \geq 0$ such that*

$$|v - v_\Pi|_{l,E} \leq C h_E^{s-l} |v|_{s,E} \quad 0 \leq s \leq k+1, l = 0, \ldots, s.$$

Proposition 5.4.2 *There exists a constant $C > 0$, such that for every $\boldsymbol{\tau} \in [H^s(E)]^2$ there exists $\boldsymbol{\tau}_\Pi \in [\mathbb{P}_k(E)]^2$, $k \geq 0$ such that*

$$|\boldsymbol{\tau} - \boldsymbol{\tau}_\Pi|_{l,E} \leq C h_E^{s-l} |\boldsymbol{\tau}|_{s,E} \quad 0 \leq s \leq k+1, l = 0, \ldots, s.$$

The first step is to establish the following result.

Lemma 5.4.1 *Let $(w,\boldsymbol{\gamma}) \in \boldsymbol{X}$ be the unique solution to the continuous Problem 5.2.2 and let $\boldsymbol{\theta} := \nabla w + \boldsymbol{\gamma}$. Let $(w_h,\boldsymbol{\gamma}_h) \in \boldsymbol{X}_h$ be the unique solution to the discrete Problem 5.3.1. Then, for any $(w_I,\boldsymbol{\gamma}_I) \in \boldsymbol{X}_h$ and $(\boldsymbol{\theta}_\Pi,\boldsymbol{\gamma}_\Pi,\boldsymbol{\gamma}_0) \in [L^2(\Omega)]^6$ such that $\boldsymbol{\theta}_\Pi|_E \in [\mathbb{P}_1(E)]^2$, $\boldsymbol{\gamma}_\Pi|_E \in [\mathbb{P}_1(E)]^2$ and $\boldsymbol{\gamma}_0|_E \in [\mathbb{P}_0(E)]^2$ for all $E \in \mathcal{T}_h$, there exists $C > 0$ independent of h and t such that*

$$|||w - w_h, \boldsymbol{\gamma} - \boldsymbol{\gamma}_h||| \leq C \left(t^{-1} \left(\|\boldsymbol{\gamma} - \boldsymbol{\gamma}_I\|_{0,\Omega} + \|\boldsymbol{\gamma}_0 - \boldsymbol{\gamma}\|_{0,\Omega} \right) + \|\boldsymbol{\gamma} - \boldsymbol{\gamma}_I\|_{1,\Omega} + h\|g\|_{0,\Omega} \right.$$
$$\left. + \|\boldsymbol{\theta} - \boldsymbol{\theta}_\Pi\|_{1,h,\Omega} + \|\nabla w - \nabla w_I\|_{1,\Omega} \right).$$

Proof. We set $\boldsymbol{\delta}_{\boldsymbol{\gamma}} := \boldsymbol{\gamma}_h - \boldsymbol{\gamma}_I$, $\delta_w := w_h - w_I$, $\boldsymbol{\theta}_h := \nabla w_h + \boldsymbol{\gamma}_h$, $\boldsymbol{\theta}_I := \nabla w_I + \boldsymbol{\gamma}_I$ and $\boldsymbol{\delta}_{\boldsymbol{\theta}} := \boldsymbol{\theta}_h - \boldsymbol{\theta}_I$. Thanks to Lemma 5.3.1 and equations (5.19), (5.14), (5.15) we have that

$$\begin{aligned}
\beta|||(w_h - w_I), (\boldsymbol{\gamma}_h - \boldsymbol{\gamma}_I)|||^2 &\leq a_h(\boldsymbol{\theta}_h - \boldsymbol{\theta}_I, \boldsymbol{\delta}_{\boldsymbol{\theta}}) + b_h(\boldsymbol{\gamma}_h - \boldsymbol{\gamma}_I, \boldsymbol{\delta}_{\boldsymbol{\gamma}}) \\
&= a_h(\nabla w_h + \boldsymbol{\gamma}_h, \boldsymbol{\delta}_{\boldsymbol{\theta}}) + b_h(\boldsymbol{\gamma}_h, \boldsymbol{\delta}_{\boldsymbol{\gamma}}) - (a_h(\boldsymbol{\theta}_I, \boldsymbol{\delta}_{\boldsymbol{\theta}}) + b_h(\boldsymbol{\gamma}_I, \boldsymbol{\delta}_{\boldsymbol{\gamma}})) \\
&= \langle g_h, \delta_w \rangle_h - \sum_{E \in \mathcal{T}_h} \left(a_h^E(\boldsymbol{\theta}_I - \boldsymbol{\theta}_\Pi, \boldsymbol{\delta}_{\boldsymbol{\theta}}) + a^E(\boldsymbol{\theta}_\Pi - \boldsymbol{\theta}, \boldsymbol{\delta}_{\boldsymbol{\theta}}) + a^E(\boldsymbol{\theta}, \boldsymbol{\delta}_{\boldsymbol{\theta}}) \right) \\
&\quad - \sum_{E \in \mathcal{T}_h} \left(b_h^E(\boldsymbol{\gamma}_I - \boldsymbol{\gamma}_0, \boldsymbol{\delta}_{\boldsymbol{\gamma}}) + b^E(\boldsymbol{\gamma}_0 - \boldsymbol{\gamma}, \boldsymbol{\delta}_{\boldsymbol{\gamma}}) + b^E(\boldsymbol{\gamma}, \boldsymbol{\delta}_{\boldsymbol{\gamma}}) \right) \\
&\leq T_1 + T_2 + T_3,
\end{aligned}$$

where

$$T_1 := \left| \langle g_h, \delta_w \rangle_h - (g, \delta_w)_{0,\Omega} \right|, \qquad T_2 := \left| \sum_{E \in \mathcal{T}_h} \left(a_h^E(\boldsymbol{\theta}_I - \boldsymbol{\theta}_\Pi, \boldsymbol{\delta}_{\boldsymbol{\theta}}) - a^E(\boldsymbol{\theta}_\Pi - \boldsymbol{\theta}, \boldsymbol{\delta}_{\boldsymbol{\theta}}) \right) \right|,$$

$$T_3 := \left| \sum_{E \in \mathcal{T}_h} \left(b_h^E(\boldsymbol{\gamma}_I - \boldsymbol{\gamma}_0, \boldsymbol{\delta}_{\boldsymbol{\gamma}}) - b^E(\boldsymbol{\gamma}_0 - \boldsymbol{\gamma}, \boldsymbol{\delta}_{\boldsymbol{\gamma}}) \right) \right|.$$

We now bound each term T_i, $i = 1, 2, 3$, with a constant C independent of h and t.

First, we bound the term T_2. Using (5.16), the fact that bilinear form $a(\cdot,\cdot)$ is bounded and finally adding and subtracting $\boldsymbol{\theta}$, we obtain

$$\begin{aligned}
T_2 &\leq \sum_{E \in \mathcal{T}_h} \left| a_h^E(\boldsymbol{\theta}_I - \boldsymbol{\theta}_\Pi, \boldsymbol{\delta}_{\boldsymbol{\theta}}) \right| + \sum_{E \in \mathcal{T}_h} \left| a^E(\boldsymbol{\theta}_\Pi - \boldsymbol{\theta}, \boldsymbol{\delta}_{\boldsymbol{\theta}}) \right| \\
&\leq \sum_{E \in \mathcal{T}_h} C(\|\boldsymbol{\theta}_I - \boldsymbol{\theta}_\Pi\|_{1,E} + \|\boldsymbol{\theta}_\Pi - \boldsymbol{\theta}\|_{1,E}) \|\boldsymbol{\delta}_{\boldsymbol{\theta}}\|_{1,E} \\
&\leq \sum_{E \in \mathcal{T}_h} C(\|\boldsymbol{\theta}_I - \boldsymbol{\theta}\|_{1,E} + \|\boldsymbol{\theta}_\Pi - \boldsymbol{\theta}\|_{1,E}) \|\boldsymbol{\delta}_{\boldsymbol{\theta}}\|_{1,E}.
\end{aligned}$$

For the term T_3, using (5.17), the definition of bilinear form $b(\cdot,\cdot)$, the Cauchy–Schwarz inequality, and finally adding and subtracting $\boldsymbol{\gamma}$, we obtain

$$T_3 \leq \sum_{E \in \mathcal{T}_h} C(\|\boldsymbol{\gamma}_I - \boldsymbol{\gamma}\|_{0,E} + \|\boldsymbol{\gamma}_0 - \boldsymbol{\gamma}\|_{0,E}) t^{-2} \|\boldsymbol{\delta}_{\boldsymbol{\gamma}}\|_{0,E}.$$

Now, we bound T_1. Using the definition (5.18), and adding and subtracting $\bar{g}_E$ we rewrite the term as follows

$$\begin{aligned} T_1 &= \left| \sum_{E\in\mathcal{T}_h} \left(\bar{g}_E \sum_{i=1}^{N_E} \delta_w(v_i)\omega_E^i \right) - \sum_{E\in\mathcal{T}_h} \int_E g\delta_w \right| \\ &= \left| \sum_{E\in\mathcal{T}_h} \left(\bar{g}_E \sum_{i=1}^{N_E} \delta_w(v_i)\omega_E^i - \int_E \bar{g}_E\delta_w \right) + \sum_{E\in\mathcal{T}_h} \left(\int_E (\bar{g}_E - g)(\delta_w - p) \right) \right|, \end{aligned}$$

for any $p \in \mathbb{P}_0(E)$, where we have used the definition of $\bar{g}_E$. Therefore,

$$T_1 \leq \left| \sum_{E\in\mathcal{T}_h} \left(\bar{g}_E \sum_{i=1}^{N_E} \delta_w(v_i)\omega_E^i - \int_E \bar{g}_E\delta_w \right) \right| + \sum_{E\in\mathcal{T}_h} \|g - \bar{g}_E\|_{0,E}\|\delta_w - p\|_{0,E} := T_1^a + T_1^b.$$

First, T_1^b is easily bounded. In fact, taking p as in Proposition 5.4.1, we obtain that

$$T_1^b \leq Ch\|g\|_{0,\Omega}\|\delta_w\|_{1,\Omega}.$$

In what follows we will manipulate the terms T_1^a: adding and subtracting $p_0 \in \mathbb{P}_0(E)$, and since the integration rule in (5.18) is exact for constant functions, we have

$$\begin{aligned} T_1^a &\leq \left| \sum_{E\in\mathcal{T}_h} \int_E \bar{g}_E(\delta_w - p_0) \right| + \left| \sum_{E\in\mathcal{T}_h} \left(\bar{g}_E \left(\sum_{i=1}^{N_E} (\delta_w - p_0)(v_i)\omega_E^i \right) \right) \right| \\ &\leq \|g\|_{0,\Omega} \left(\sum_{E\in\mathcal{T}_h} \|\delta_w - p_0\|_{0,E}^2 \right)^{1/2} + \sum_{E\in\mathcal{T}_h} |E|\bar{g}_E\|\delta_w - p_0\|_{L^\infty(\partial E)} \\ &\leq \|g\|_{0,\Omega} \left(\sum_{E\in\mathcal{T}_h} \|\delta_w - p_0\|_{0,E}^2 \right)^{1/2} + \|g\|_{0,\Omega} \left(\sum_{E\in\mathcal{T}_h} h_E^2\|\delta_w - p_0\|_{L^\infty(\partial E)}^2 \right)^{1/2}. \end{aligned}$$

We now recall that $\delta_w - p_0$ is a (continuous) piecewise polynomial on ∂E, and that the length of the edges of E is bounded from below in the sense of assumption $\mathbf{A}_1$. Therefore, we can apply Lemma 3.1 in [47], standard polynomial approximation estimates and a trace inequality to derive

$$\|\delta_w - p_0\|_{L^\infty(\partial E)} \leq C|\delta_w|_{1/2,\partial E} + h_E^{-1/2}\|\delta_w - p_0\|_{0,\partial E} \leq C|\delta_w|_{1/2,\partial E} \leq C|\delta_w|_{1,E}.$$

Hence, we obtain,

$$T_1^a \leq Ch\|g\|_{0,\Omega}|\delta_w|_{1,\Omega}.$$

Thus, since $|\delta_w|_{1,\Omega} \leq |||\delta_w, \boldsymbol{\delta_\gamma}|||$, we have that

$$T_1 \leq T_1^a + T_1^b \leq Ch\|g\|_{0,\Omega}|||\delta_w, \boldsymbol{\delta_\gamma}|||. \tag{5.20}$$

Therefore, by combining (5.20) with the above bounds for T_2 and T_3, we get

$$\begin{aligned}|||(w_h - w_I), (\boldsymbol{\gamma}_h - \boldsymbol{\gamma}_I)||| \leq & C\big(t^{-1}(\|\boldsymbol{\gamma} - \boldsymbol{\gamma}_I\|_{0,\Omega} + \|\boldsymbol{\gamma}_0 - \boldsymbol{\gamma}\|_{0,\Omega}) \\ & + \|\boldsymbol{\theta} - \boldsymbol{\theta}_I\|_{1,\Omega} + \|\boldsymbol{\theta}_\Pi - \boldsymbol{\theta}\|_{1,h,\Omega} + h\|g\|_{0,\Omega}\big).\end{aligned}$$

Hence, the proof follows from the bound above, the triangular inequality, the definition of $|||\cdot|||$ (see (5.4)), the definition of $\boldsymbol{\theta}_I$ and the inequality $\|\boldsymbol{\theta} - \boldsymbol{\theta}_I\|_{1,\Omega} \leq \|\nabla w - \nabla w_I\|_{1,\Omega} + \|\boldsymbol{\gamma} - \boldsymbol{\gamma}_I\|_{1,\Omega}$. In fact,

$$\begin{aligned}|||w - w_h, \boldsymbol{\gamma} - \boldsymbol{\gamma}_h||| \leq & |||w - w_I, \boldsymbol{\gamma} - \boldsymbol{\gamma}_I||| + |||w_I - w_h, \boldsymbol{\gamma}_I - \boldsymbol{\gamma}_h||| \\ \leq & C(t^{-1}\|\boldsymbol{\gamma} - \boldsymbol{\gamma}_I\|_{0,\Omega} + t^{-1}\|\boldsymbol{\gamma}_0 - \boldsymbol{\gamma}\|_{0,\Omega} + \|\boldsymbol{\gamma} - \boldsymbol{\gamma}_I\|_{1,\Omega} \\ & + h\|g\|_{0,\Omega} + \|\boldsymbol{\theta} - \boldsymbol{\theta}_\Pi\|_{1,h,\Omega} + \|\nabla w - \nabla w_I\|_{1,\Omega}).\end{aligned}$$

The proof is complete. □

The next step is to find appropriate terms $(w_I, \boldsymbol{\gamma}_I)$, $(w_\Pi, \boldsymbol{\gamma}_\Pi)$ and $\boldsymbol{\gamma}_0$ that can be used in Lemma 5.4.1 to prove the claimed convergence. As a preliminary construction, we introduce, for every vertex v of the mesh laying on $\partial\Omega$, the following function. Let e_v be any one of the two edges on $\partial\Omega$ sharing v, fixed once and for all; the only rule being that, if one of the two edges is in Γ_c and the other is not, then the one in Γ_c must be chosen. Then, we denote by $\boldsymbol{\varphi}_v$ the unique (vector valued) polynomial of degree 2 living on e_v such that

$$\int_{e_v} \mathbf{p} \cdot \boldsymbol{\varphi}_v = \mathbf{p}(v) \qquad \forall \mathbf{p} \in [\mathbb{P}_2(e_v)]^2. \tag{5.21}$$

Then, for the term $w_I \in W_h$, we have the following result.

Proposition 5.4.3 *There exists a positive constant C, such that for every $v \in H^3(\Omega)$ there exists $v_I \in W_h$ that satisfies*

$$|v - v_I|_{l,\Omega} \leq C h_E^{3-l} |v|_{3,\Omega}, \quad l = 0, 1, 2.$$

Proof. Given $v \in H^3(\Omega)$, we consider $v_\Pi \in L^2(\Omega)$ defined on each $E \in \mathcal{T}_h$ so that $v_\Pi|_E \in \mathbb{P}_2(E)$ and the estimate of Proposition 5.4.1 holds true.

For each polygon $E \in \mathcal{T}_h$, consider the triangulation $\mathcal{T}_h^E$ obtained by joining each vertex of E with the midpoint of the ball with respect to which E is starred. Let $\widehat{\mathcal{T}}_h := \bigcup_{E \in \mathcal{T}_h} \mathcal{T}_h^E$. Since we are assuming $\mathbf{A}_1$ and $\mathbf{A}_2$, $\{\widehat{\mathcal{T}}_h\}_h$ is a shape-regular family of triangulations of Ω.

Let v_c be the reduced Hsieh-Clough-Tocher triangle (see [69, 70]) interpolant of v over $\widehat{\mathcal{T}}_h$, slightly modified as follows. For the nodes on the boundary, the value of ∇v_c is given by

$$\nabla v_c(v) := \int_{e_v} \nabla v_c \cdot \boldsymbol{\varphi}_v,$$

see (5.21), while the values of the remaining degrees of freedom is the same as in the original version. This is a modification, in the spirit of the Scott-Zhang interpolation [107], of the standard nodal value; the motivation for such modification is not related directly to the present result (that would hold also with the original HCT interpolant) and will be clearer in the sequel. This

modified version still satisfies similar approximation properties with respect the original version [69, 70]; we omit the standard proof and simply state the result:

$$|v - v_{\rm c}|_{l,\Omega} \leq C h_E^{3-l} \, |v|_{3,\Omega} \quad l = 0, 1, 2. \tag{5.22}$$

Now, for each $E \in \mathcal{T}_h$, we define $v_I|_E \in H^2(E)$ as the solution of the following problem:

$$\begin{cases} -\Delta^2 v_I = -\Delta^2 v_\Pi \quad \text{in } E, \\ \qquad v_I = v_{\rm c} \quad \text{on } \partial E, \\ \qquad \partial_{\boldsymbol{n}} v_I = \partial_{\boldsymbol{n}} v_{\rm c} \quad \text{on } \partial E. \end{cases}$$

Note that $v_I|_E \in W_h^E$. Moreover, although v_I is defined locally, since on the boundary of each element it coincides with $v_{\rm c}$ which belongs to $H^2(\Omega)$, we have that also v_I belongs to $H^2(\Omega)$ and, hence, $v_I \in W_h$.

According to the above definition we have that

$$\begin{cases} -\Delta^2 (v_\Pi - v_I) = 0 \quad \text{in } E, \\ \qquad v_\Pi - v_I = v_\Pi - v_{\rm c} \quad \text{on } \partial E, \\ \qquad \partial_{\boldsymbol{n}} (v_\Pi - v_I) = \partial_{\boldsymbol{n}} (v_\Pi - v_{\rm c}) \quad \text{on } \partial E, \end{cases}$$

and, hence, it is easy to check that

$$\begin{aligned} |v_\Pi - v_I|_{2,E} &= \text{ínf} \left\{ |z|_{2,E} \,, \ z \in H^2(E) : \ z = v_\Pi - v_{\rm c} \ \text{ on } \partial E \text{ and } \ \partial_{\boldsymbol{n}} z = \partial_{\boldsymbol{n}} (v_\Pi - v_{\rm c}) \ \text{ on } \partial E \right\} \\ &\leq |v_\Pi - v_{\rm c}|_{2,E} \,. \end{aligned}$$

Therefore,

$$\begin{aligned} |v - v_I|_{2,E} &\leq |v - v_\Pi|_{2,E} + |v_\Pi - v_I|_{2,E} \\ &\leq |v - v_\Pi|_{2,E} + |v_\Pi - v_{\rm c}|_{2,E} \\ &\leq 2 \, |v - v_\Pi|_{2,E} + |v - v_{\rm c}|_{2,E} \,. \end{aligned}$$

By summing on all the elements and recalling (5.22) (plus standard approximation estimates for polynomials on polygons) we obtain

$$|v - v_I|_{2,\Omega} \leq C \big(|v - v_\Pi|_{2,\Omega} + |v - v_{\rm c}|_{2,\Omega} \big) \leq C h |v|_{3,\Omega}.$$

Moreover, from the above bound and (recalling that $\partial_{\boldsymbol{n}} (v_I - v_{\rm c}) = 0$ and $(v_I - v_{\rm c}) = 0$ on ∂E) a Poincaré-type inequality, we have

$$\begin{aligned} |v - v_I|_{1,E} &\leq |v - v_{\rm c}|_{1,E} + |v_{\rm c} - v_I|_{1,E} \leq |v - v_{\rm c}|_{1,E} + C h_E \, |v_{\rm c} - v_I|_{2,E} \\ &\leq |v - v_{\rm c}|_{1,E} + C h_E \, |v - v_{\rm c}|_{2,E} + C h_E \, |v - v_I|_{2,E} \,, \end{aligned}$$

so that, summing on all the elements and using the bounds above,

$$|v - v_I|_{1,\Omega} \leq C h^2 \, |v|_{3,\Omega} \,.$$

By an analogous argument one obtains

$$\|v - v_I\|_{0,\Omega} \leq C\big(\|v - v_{\mathrm{c}}\|_{0,\Omega} + h\,|v_{\mathrm{c}} - v_I|_{1,\Omega}\big) \leq Ch^3\,|v|_{3,\Omega}\,,$$

which allows us to complete the proof. □

Finally, we present the following result for the approximation properties of the space $\mathbf{V}_h$.

Proposition 5.4.4 *There exists $C > 0$ such that for every $\boldsymbol{\tau} \in [\mathrm{H}^s(\Omega)]^2$ with $s \in [1,2]$ there exists $\boldsymbol{\tau}_I \in \mathbf{V}_h$ that satisfies*

$$\|\boldsymbol{\tau} - \boldsymbol{\tau}_I\|_{0,\Omega} + h|\boldsymbol{\tau} - \boldsymbol{\tau}_I|_{1,\Omega} \leq Ch^s|\boldsymbol{\tau}|_{s,\Omega}.$$

Proof. We refer the reader to Section 5.3.2 for the definition of the degrees of freedom of $\mathbf{V}_h$ and define $\boldsymbol{\tau}_I$ as follows. All degrees of freedom associated to internal vertices are calculated as an integral average of $\boldsymbol{\tau}$ on the elements sharing the vertex (as in standard Clément interpolation). All the vertex boundary values are taken as (see (5.21))

$$\boldsymbol{\tau}_I(v) = \int_{e_v} \boldsymbol{\tau} \cdot \boldsymbol{\varphi}_v.$$

Finally, the edge degrees of freedom are computed directly by

$$\frac{1}{|e|}\int_e \boldsymbol{\tau}_I \cdot \boldsymbol{t} = \frac{1}{|e|}\int_e \boldsymbol{\tau} \cdot \boldsymbol{t} \quad \forall \text{ edge } e \in \mathcal{T}_h.$$

The rest of the proof is omitted since it follows repeating essentially the same argument used to establish [31, Proposition 4.1]. □

According to the above results, we are able to establish the convergence of the Virtual Element scheme presented in Problem 5.3.1.

Theorem 5.4.1 *Let $(w, \boldsymbol{\gamma}) \in \boldsymbol{X}$ and $(w_h, \boldsymbol{\gamma}_h) \in \boldsymbol{X}_h$ be the unique solutions of the continuous and discrete problems, respectively. Assume that $(w, \boldsymbol{\gamma}) \in (H^3(\Omega), [H^2(\Omega)]^2)$. Then, there exists $C > 0$ independent of h, g and t such that*

$$|||w - w_h, \boldsymbol{\gamma} - \boldsymbol{\gamma}_h||| \leq Ch\left(t^{-1}|\boldsymbol{\gamma}|_{1,\Omega} + |\boldsymbol{\theta}|_{2,\Omega} + |w|_{3,\Omega} + \|g\|_{0,\Omega}\right),$$

where $\boldsymbol{\theta} := \nabla w + \boldsymbol{\gamma}$.

Proof. The proof follows from Lemma 5.4.1 and Propositions 5.4.1, 5.4.2, 5.4.3 and 5.4.4. In fact,

$$\begin{aligned}
|||w - w_h, \boldsymbol{\gamma} - \boldsymbol{\gamma}_h||| \leq & C\Big(t^{-1}(\|\boldsymbol{\gamma} - \boldsymbol{\gamma}_I\|_{0,\Omega} + \|\boldsymbol{\gamma}_0 - \boldsymbol{\gamma}\|_{0,h,\Omega}) + \|\boldsymbol{\gamma} - \boldsymbol{\gamma}_I\|_{1,\Omega} \\
& + h\|g\|_{0,\Omega} + \|\boldsymbol{\theta} - \boldsymbol{\theta}_\Pi\|_{1,h,\Omega} + \|\nabla w - \nabla w_I\|_{1,\Omega}\Big) \\
\leq & Ch\left(t^{-1}|\boldsymbol{\gamma}|_{1,\Omega} + |\boldsymbol{\theta}|_{2,\Omega} + |w|_{3,\Omega} + \|g\|_{0,\Omega}\right),
\end{aligned}$$

where we have used that $\boldsymbol{\gamma} = \boldsymbol{\theta} - \nabla w$ so that $|\boldsymbol{\gamma}|_{2,\Omega} \leq |w|_{3,\Omega} + |\boldsymbol{\theta}|_{2,\Omega}$. Thus, we conclude the proof. □

Remark 5.4.1 *It is easy to check that the couple $(w_I, \boldsymbol{\gamma}_I)$ used in Theorem 5.4.1 (accordingly to the interpolants definition given in Propositions 5.4.3 and 5.4.4) does actually satisfy the boundary conditions and is thus in $\boldsymbol{X}_h$. Indeed, the condition $w_I = 0$ on $\Gamma_c \cup \Gamma_s$ follows immediately from the analogous one for w. The condition $\nabla w_I + \boldsymbol{\gamma}_I = \mathbf{0}$ on Γ_c can be easily derived from the analogous one for $(w, \boldsymbol{\gamma})$ combined with our choice for the boundary node interpolation and the definition of the discrete spaces.*

Remark 5.4.2 *We note that Theorem 5.4.1 provides also an error estimate for the rotations in $H^1(\Omega)$-norm.*

In what follows, we restrict our analysis considering clamped boundary conditions on the whole boundary, essentially to exploit the associated regularity properties of the continuous solution of the Reissner-Mindlin equations. Nevertheless, the analysis in what follows can be straightforwardly extended to other boundary conditions.

Now, we present the following result which establish an improve error estimate for rotations in $L^2(\Omega)$-norm and the deflection in $H^1(\Omega)$-norm.

Proposition 5.4.5 *Assume that the hypotheses of Theorem 5.4.1 hold. Moreover, assume that the domain Ω be either regular, or piecewise regular and convex, that $g \in H^1(E)$ for all $E \in \mathcal{T}_h$ and that $\Gamma_c = \Gamma$. Then, for any $(w_\Pi, \boldsymbol{\gamma}_\Pi, \boldsymbol{\gamma}_0) \in [L^2(\Omega)]^5$ such that $w_\Pi|_E \in \mathbb{P}_2(E)$, $\boldsymbol{\gamma}_\Pi|_E \in [\mathbb{P}_1(E)]^2$ and $\boldsymbol{\gamma}_0|_E \in [\mathbb{P}_0(E)]^2$ for all $E \in \mathcal{T}_h$, there exists $C > 0$ independent of h, g and t such that*

$$\|\boldsymbol{\theta} - \boldsymbol{\theta}_h\|_{0,\Omega} \leq C(h+t)\left(|||w - w_h, \boldsymbol{\gamma} - \boldsymbol{\gamma}_h||| + h\|g\|_{1,h,\Omega} + \|\nabla w - \nabla w_\Pi\|_{1,h,\Omega} + \|\boldsymbol{\gamma} - \boldsymbol{\gamma}_\Pi\|_{1,h,\Omega} + t^{-1}\|\boldsymbol{\gamma} - \boldsymbol{\gamma}_0\|_{0,\Omega}\right); \tag{5.23}$$

$$\|w - w_h\|_{1,\Omega} \leq C(\|\boldsymbol{\theta} - \boldsymbol{\theta}_h\|_{0,\Omega} + \|\boldsymbol{\gamma} - \boldsymbol{\gamma}_h\|_{0,\Omega}). \tag{5.24}$$

Proof. The core of the proof is based on a duality argument. We first establish (5.23). We begin by introducing the following well-posed auxiliary problem: Find $(\widetilde{w}, \widetilde{\boldsymbol{\gamma}}) \in \boldsymbol{X}$ such that

$$a(\nabla\widetilde{w} + \widetilde{\boldsymbol{\gamma}}, \nabla v + \boldsymbol{\tau}) + b(\widetilde{\boldsymbol{\gamma}}, \boldsymbol{\tau}) = (\boldsymbol{\theta} - \boldsymbol{\theta}_h, \nabla v + \boldsymbol{\tau})_{0,\Omega} \quad \forall (v, \boldsymbol{\tau}) \in \boldsymbol{X}. \tag{5.25}$$

The following regularity result for the solution of problem above holds (see [96, Theorem 2.1]):

$$\|\widetilde{w}^1\|_{3,\Omega} + t^{-1}\|\widetilde{w}^2\|_{2,\Omega} + t^{-1}\|\widetilde{\boldsymbol{\gamma}}\|_{1,\Omega} \leq C\|\boldsymbol{\theta} - \boldsymbol{\theta}_h\|_{0,\Omega}, \tag{5.26}$$

where $\widetilde{w}^1$ is the solution of the Kirchhoff limit problem and $\widetilde{w}^2 := \widetilde{w} - \widetilde{w}^1$. Let $(\widetilde{w}^1_I, \widetilde{\boldsymbol{\gamma}}_I) \in \boldsymbol{X}_h$ be the interpolant of $(\widetilde{w}^1, \widetilde{\boldsymbol{\gamma}})$ given by Propositions 5.4.3 and 5.4.4, respectively. Therefore, the above regularity result yield immediately:

$$\|\widetilde{w}^1 - \widetilde{w}^1_I\|_{1,\Omega} + h\|\widetilde{w}^1 - \widetilde{w}^1_I\|_{2,\Omega} + t^{-1}h\|\widetilde{\boldsymbol{\gamma}} - \widetilde{\boldsymbol{\gamma}}_I\|_{0,\Omega} \leq h^2\|\boldsymbol{\theta} - \boldsymbol{\theta}_h\|_{0,\Omega}, \tag{5.27}$$

$$\|\widetilde{w}^2\|_{2,\Omega} + \|\widetilde{\boldsymbol{\gamma}} - \widetilde{\boldsymbol{\gamma}}_I\|_{1,\Omega} \leq t\|\boldsymbol{\theta} - \boldsymbol{\theta}_h\|_{0,\Omega}. \tag{5.28}$$

Next, choosing $v := (w - w_h)$ and $\boldsymbol{\tau} = (\boldsymbol{\gamma} - \boldsymbol{\gamma}_h)$ in (5.25), so that $\nabla v + \boldsymbol{\tau} = \boldsymbol{\theta} - \boldsymbol{\theta}_h$, and then adding and subtracting the term $\nabla \widetilde{w}_I^1 + \widetilde{\boldsymbol{\gamma}}_I$, we obtain

$$\begin{aligned}\|\boldsymbol{\theta} - \boldsymbol{\theta}_h\|_{0,\Omega}^2 &= a(\boldsymbol{\theta} - \boldsymbol{\theta}_h, \nabla\widetilde{w} + \widetilde{\boldsymbol{\gamma}} - \nabla\widetilde{w}_I^1 + \widetilde{\boldsymbol{\gamma}}_I) + a(\boldsymbol{\theta} - \boldsymbol{\theta}_h, \nabla\widetilde{w}_I^1 + \widetilde{\boldsymbol{\gamma}}_I) \\ &\quad + b(\boldsymbol{\gamma} - \boldsymbol{\gamma}_h, \widetilde{\boldsymbol{\gamma}} - \widetilde{\boldsymbol{\gamma}}_I) + b(\boldsymbol{\gamma} - \boldsymbol{\gamma}_h, \widetilde{\boldsymbol{\gamma}}_I) \\ &\leq |||w - w_h, \boldsymbol{\gamma} - \boldsymbol{\gamma}_h||| \; |||\widetilde{w} - \widetilde{w}_I^1, \widetilde{\boldsymbol{\gamma}} - \widetilde{\boldsymbol{\gamma}}_I||| + \left|a(\boldsymbol{\theta} - \boldsymbol{\theta}_h, \nabla\widetilde{w}_I^1 + \widetilde{\boldsymbol{\gamma}}_I) + b(\boldsymbol{\gamma} - \boldsymbol{\gamma}_h, \widetilde{\boldsymbol{\gamma}}_I)\right|,\end{aligned} \tag{5.29}$$

where we have used that the bilinear forms are bounded uniformly in t with respect to the $|||\cdot|||$ norm. Now, we bound each term on the right hand side above. For the first term we have, using (5.27) and (5.28),

$$\begin{aligned}|||\widetilde{w} - \widetilde{w}_I^1, \widetilde{\boldsymbol{\gamma}} - \widetilde{\boldsymbol{\gamma}}_I|||^2 &\leq C\left(\|\widetilde{w} - \widetilde{w}_I^1\|_{2,\Omega}^2 + t^{-2}\|\widetilde{\boldsymbol{\gamma}} - \widetilde{\boldsymbol{\gamma}}_I\|_{0,\Omega}^2 + \|\widetilde{\boldsymbol{\gamma}} - \widetilde{\boldsymbol{\gamma}}_I\|_{1,\Omega}^2\right) \\ &\leq C\left(\|\widetilde{w}^1 - \widetilde{w}_I^1\|_{2,\Omega}^2 + \|\widetilde{w}^2\|_{2,\Omega}^2 + t^{-2}\|\widetilde{\boldsymbol{\gamma}} - \widetilde{\boldsymbol{\gamma}}_I\|_{0,\Omega}^2 + \|\widetilde{\boldsymbol{\gamma}} - \widetilde{\boldsymbol{\gamma}}_I\|_{1,\Omega}^2\right) \\ &\leq C(h^2 + t^2)\|\boldsymbol{\theta} - \boldsymbol{\theta}_h\|_{0,\Omega}^2.\end{aligned}$$

Therefore

$$|||\widetilde{w} - \widetilde{w}_I^1, \widetilde{\boldsymbol{\gamma}} - \widetilde{\boldsymbol{\gamma}}_I||| \leq C(h + t)\|\boldsymbol{\theta} - \boldsymbol{\theta}_h\|_{0,\Omega}. \tag{5.30}$$

For the second term on the right hand of (5.29), since $(\widetilde{w}_I^1, \widetilde{\boldsymbol{\gamma}}_I) \in \boldsymbol{X}$, we have that (see Problems 5.2.2 and 5.3.1),

$$\begin{aligned}&\left|a(\boldsymbol{\theta} - \boldsymbol{\theta}_h, \nabla\widetilde{w}_I^1 + \widetilde{\boldsymbol{\gamma}}_I) + b(\boldsymbol{\gamma} - \boldsymbol{\gamma}_h, \widetilde{\boldsymbol{\gamma}}_I)\right| = \left|(g, \widetilde{w}_I^1)_{0,\Omega} - a(\boldsymbol{\theta}_h, \nabla\widetilde{w}_I^1 + \widetilde{\boldsymbol{\gamma}}_I) - b(\boldsymbol{\gamma}_h, \widetilde{\boldsymbol{\gamma}}_I)\right| \\ &\quad = \left|(g, \widetilde{w}_I^1)_{0,\Omega} - \left\langle g_h, \widetilde{w}_I^1\right\rangle_h + a_h(\boldsymbol{\theta}_h, \nabla\widetilde{w}_I^1 + \widetilde{\boldsymbol{\gamma}}_I) + b_h(\boldsymbol{\gamma}_h, \widetilde{\boldsymbol{\gamma}}_I) - a(\boldsymbol{\theta}_h, \nabla\widetilde{w}_I^1 + \widetilde{\boldsymbol{\gamma}}_I) - b(\boldsymbol{\gamma}_h, \widetilde{\boldsymbol{\gamma}}_I)\right| \\ &\quad \leq B_1 + B_2,\end{aligned} \tag{5.31}$$

where

$$B_1 := \left|\left(g, \widetilde{w}_I^1\right)_{0,\Omega} - \left\langle g_h, \widetilde{w}_I^1\right\rangle_h\right|$$

and

$$B_2 := \left|a_h(\boldsymbol{\theta}_h, \nabla\widetilde{w}_I^1 + \widetilde{\boldsymbol{\gamma}}_I) - a(\boldsymbol{\theta}_h, \nabla\widetilde{w}_I^1 + \widetilde{\boldsymbol{\gamma}}_I) + b_h(\boldsymbol{\gamma}_h, \widetilde{\boldsymbol{\gamma}}_I) - b(\boldsymbol{\gamma}_h\widetilde{\boldsymbol{\gamma}}_I)\right|.$$

We now bound B_1 and B_2 uniformly in t.

We begin with the term B_1. First adding and subtracting $\widetilde{w}^1$ we have

$$\begin{aligned}B_1 &\leq \left|(g, \widetilde{w}_I^1 - \widetilde{w}^1)_{0,\Omega}\right| + \left|(g, \widetilde{w}^1)_{0,\Omega} - \left\langle g_h, \widetilde{w}^1\right\rangle_h\right| + \left|\left\langle g_h, \widetilde{w}_I^1 - \widetilde{w}^1\right\rangle_h\right| \\ &\leq h^2\|g\|_{0,\Omega}|\widetilde{w}^1|_{2,\Omega} + \left|(g, \widetilde{w}^1)_{0,\Omega} - \left\langle g_h, \widetilde{w}^1\right\rangle_h\right|,\end{aligned} \tag{5.32}$$

where we have used the Cauchy-Schwarz inequality and Proposition 5.4.3 to bound the first term; note moreover that the last term on the right hand side above vanish as a consequence of (5.18) and the definition of $\widetilde{w}_I^1$:

$$\left|\left\langle g_h, \widetilde{w}_I^1 - \widetilde{w}^1\right\rangle_h\right| = \left|\sum_{E\in\mathcal{T}_h}\left(\bar{g}_E\sum_{i=1}^{N_E}(\widetilde{w}_I^1 - \widetilde{w}^1)(v_i)\omega_E^i\right)\right| = 0.$$

Now, we bound the second term on the right hand side of (5.32) and we follow similar steps as in Lemma 5.4.1 to derive (5.20). In fact, using the definition (5.18), and adding and subtracting g_h we rewrite the term as follows

$$\begin{aligned}\left|(g,\widetilde{w}^1)_{0,\Omega}-\left\langle g_h,\widetilde{w}^1\right\rangle_h\right| &= \left|\sum_{E\in\mathcal{T}_h}\int_E g\widetilde{w}^1-\sum_{E\in\mathcal{T}_h}\left(\bar{g}_E\sum_{i=1}^{N_E}\widetilde{w}^1(v_i)\omega_E^i\right)\right| \\ &\leq \left|\int_E \bar{g}_E\widetilde{w}^1-\sum_{E\in\mathcal{T}_h}\left(\bar{g}_E\sum_{i=1}^{N_E}\widetilde{w}^1(v_i)\omega_E^i\right)\right|+\sum_{E\in\mathcal{T}_h}\|g-\bar{g}_E\|_{0,E}\|\widetilde{w}^1-p\|_{0,E},\end{aligned}$$

for any $p\in\mathbb{P}_0(E)$. Now, taking p as in Proposition 5.4.1 and using that $g|_E\in H^1(E)$ and [51, Lemma 4.3.8]. we have that

$$\left|(g,\widetilde{w}^1)_{0,\Omega}-\left\langle g_h,\widetilde{w}^1\right\rangle_h\right|\leq Ch^2\|g\|_{1,h,\Omega}\|\widetilde{w}^1\|_{1,\Omega}+\left|\int_E \bar{g}_E\widetilde{w}^1-\sum_{E\in\mathcal{T}_h}\left(\bar{g}_E\sum_{i=1}^{N_E}\widetilde{w}^1(v_i)\omega_E^i\right)\right|=B_1^1+B_1^2. \tag{5.33}$$

In what follows we will manipulate the terms B_1^2: adding and subtracting $p_1\in\mathbb{P}_1(E)$, and the fact that (5.18) is exact for linear functions, we have

$$\begin{aligned}B_1^2 &\leq \left|\sum_{E\in\mathcal{T}_h}\int_E \bar{g}_E(\widetilde{w}^1-p_1)\right|+\left|\sum_{E\in\mathcal{T}_h}\left(\bar{g}_E\left(\sum_{i=1}^{N_E}(\widetilde{w}^1-p_1)(v_i)\omega_E^i\right)\right)\right| \\ &\leq \|g\|_{0,\Omega}\left(\sum_{E\in\mathcal{T}_h}\|\widetilde{w}^1-p_1\|_{0,E}^2\right)^{1/2}+\|g\|_{0,\Omega}\left(\sum_{E\in\mathcal{T}_h}h_E^2\|\widetilde{w}^1-p_1\|_{\infty,E}^2\right)^{1/2}.\end{aligned} \tag{5.34}$$

By polynomial approximation results on star-shaped polygons we now have

$$\begin{aligned}\|\widetilde{w}^1-p_1\|_{0,E}&\leq Ch_E^2|\widetilde{w}^1|_{2,E},\\ \|\widetilde{w}^1-p_1\|_{\infty,E}&\leq Ch_E|\widetilde{w}^1|_{2,E},\end{aligned} \tag{5.35}$$

where the first bound follows from Proposition 5.4.1 and the second one can be derived, for instance, using the following brief guidelines. Let B be the ball with the same center appearing in $\mathbf{A}_2$, but radius h_E. It clearly holds $E\subset B$. One can then extend the function $\widetilde{w}^1$ to a function (still denoted by $\widetilde{w}^1$) in $H^2(B)$ with a uniform bound $\|\widetilde{w}^1\|_{2,B}\leq C\|\widetilde{w}^1\|_{2,E}$ (see for instance [108], where we use also that due to $\mathbf{A}_2$ all the elements E of the mesh family are uniformly Lipshitz continuous). Then, the result follows from the analogous known result on balls and some very simple calculations. Hence, from (5.34) and (5.35), we obtain

$$B_1^2\leq Ch^2\|g\|_{0,\Omega}|\widetilde{w}^1|_{2,\Omega}. \tag{5.36}$$

Finally, from (5.32), (5.33) and (5.36) we have the following bound for the term B_1:

$$B_1\leq Ch^2\|g\|_{1,h,\Omega}\|\widetilde{w}^1\|_{2,\Omega}\leq Ch^2\|g\|_{1,h,\Omega}\|\boldsymbol{\theta}-\boldsymbol{\theta}_h\|_{0,\Omega}\leq C(h+t)h\|g\|_{1,h,\Omega}\|\boldsymbol{\theta}-\boldsymbol{\theta}_h\|_{0,\Omega}.$$

Now, we bound the term B_2 in (5.31). First, we consider $(w_\Pi, \boldsymbol{\gamma}_\Pi, \boldsymbol{\gamma}_0) \in [L^2(\Omega)]^5$ such that $w_\Pi|_E \in \mathbb{P}_2(E)$, $\boldsymbol{\gamma}_\Pi|_E \in [\mathbb{P}_1(E)]^2$ and $\boldsymbol{\gamma}_0|_E \in [\mathbb{P}_0(E)]^2$. Moreover, we consider $\widetilde{w}^1_\Pi \in L^2(\Omega)$ with $\widetilde{w}^1_\Pi|_E \in \mathbb{P}_2(E)$ and define $\boldsymbol{\theta}_\Pi := \nabla w_\Pi + \boldsymbol{\gamma}_\Pi$. Thus, using the consistency property we rewrite the term as follows

$$
\begin{aligned}
B_2 = \Big| & \sum_{E\in\mathcal{T}_h} \left(a_h^E(\boldsymbol{\theta}_h, \nabla\widetilde{w}^1_I + \widetilde{\boldsymbol{\gamma}}_I - (\nabla\widetilde{w}^1_\Pi + \widetilde{\boldsymbol{\gamma}}_\Pi)) + a_h^E(\boldsymbol{\theta}_h, \nabla\widetilde{w}^1_\Pi + \widetilde{\boldsymbol{\gamma}}_\Pi)\right) \\
& - \sum_{E\in\mathcal{T}_h} \left(a^E(\boldsymbol{\theta}_h, \nabla\widetilde{w}^1_I + \widetilde{\boldsymbol{\gamma}}_I - (\nabla\widetilde{w}^1_\Pi + \widetilde{\boldsymbol{\gamma}}_\Pi)) + a^E(\boldsymbol{\theta}_h, \nabla\widetilde{w}^1_\Pi + \widetilde{\boldsymbol{\gamma}}_\Pi)\right) \\
& + \sum_{E\in\mathcal{T}_h} \left(b_h^E(\boldsymbol{\gamma}_h, \widetilde{\boldsymbol{\gamma}}_I - \widetilde{\boldsymbol{\gamma}}_0) + b_h^E(\boldsymbol{\gamma}_h, \widetilde{\boldsymbol{\gamma}}_0) - b^E(\boldsymbol{\gamma}_h, \widetilde{\boldsymbol{\gamma}}_I - \widetilde{\boldsymbol{\gamma}}_0) - b^E(\boldsymbol{\gamma}_h, \widetilde{\boldsymbol{\gamma}}_0)\right) \Big| \\
= \Big| & \sum_{E\in\mathcal{T}_h} \left(a_h^E(\boldsymbol{\theta}_h - \boldsymbol{\theta}_\Pi, \nabla\widetilde{w}^1_I + \widetilde{\boldsymbol{\gamma}}_I - (\nabla\widetilde{w}^1_\Pi + \widetilde{\boldsymbol{\gamma}}_\Pi)) - a^E(\boldsymbol{\theta}_h - \boldsymbol{\theta}_\Pi, \nabla\widetilde{w}^1_I + \widetilde{\boldsymbol{\gamma}}_I - (\nabla\widetilde{w}^1_\Pi + \widetilde{\boldsymbol{\gamma}}_\Pi))\right) \\
& + \sum_{E\in\mathcal{T}_h} \left(b_h^E(\boldsymbol{\gamma}_h - \boldsymbol{\gamma}_0, \widetilde{\boldsymbol{\gamma}}_I - \widetilde{\boldsymbol{\gamma}}_0) - b^E(\boldsymbol{\gamma}_h - \boldsymbol{\gamma}_0, \widetilde{\boldsymbol{\gamma}}_I - \widetilde{\boldsymbol{\gamma}}_0)\right) \Big|.
\end{aligned}
$$

Therefore, we have

$$
\begin{aligned}
B_2 &\leq C\left(\|\boldsymbol{\theta}_h - \boldsymbol{\theta}_\Pi\|_{1,h,\Omega} + t^{-1}\|\boldsymbol{\gamma}_h - \boldsymbol{\gamma}_0\|_{0,\Omega}\right) \times \\
&\qquad \left(\sum_{E\in\mathcal{T}_h} \|\nabla\widetilde{w}^1_I - \nabla\widetilde{w}^1_\Pi\|^2_{1,E} + \|\widetilde{\boldsymbol{\gamma}}_I - \widetilde{\boldsymbol{\gamma}}_\Pi\|^2_{1,E} + t^{-2}\|\widetilde{\boldsymbol{\gamma}}_I - \widetilde{\boldsymbol{\gamma}}_0\|^2_{0,E}\right)^{1/2} \\
&\leq C\left(\|\boldsymbol{\theta}_h - \boldsymbol{\theta}_\Pi\|_{1,h,\Omega} + t^{-1}\|\boldsymbol{\gamma}_h - \boldsymbol{\gamma}_0\|_{0,\Omega}\right)\left(h|\widetilde{w}^1|_{3,\Omega} + ht^{-1}|\widetilde{\boldsymbol{\gamma}}|_{1,\Omega} + |\widetilde{\boldsymbol{\gamma}}|_{1,\Omega}\right),
\end{aligned}
$$

where we have added and subtracted $\nabla\widetilde{w}^1$ and $\widetilde{\boldsymbol{\gamma}}$ and then we have used Propositions 5.4.3, 5.4.1, 5.4.4 and 5.4.2, respectively. Finally, using (5.26) and the triangular inequality we have

$$
B_2 \leq C(h+t)\|\boldsymbol{\theta} - \boldsymbol{\theta}_h\|_{0,\Omega}\left(|||w - w_h, \boldsymbol{\gamma} - \boldsymbol{\gamma}_h||| + \|\boldsymbol{\theta} - \boldsymbol{\theta}_\Pi\|_{1,h,\Omega} + t^{-1}\|\boldsymbol{\gamma} - \boldsymbol{\gamma}_0\|_{0,\Omega}\right).
$$

Hence, (5.23) follows from (5.29), combining the estimate (5.30), with the above bounds for B_1 and B_2 and the definition of $\boldsymbol{\theta}$. In fact, we obtain that

$$
\begin{aligned}
\|\boldsymbol{\theta} - \boldsymbol{\theta}_h\|_{0,\Omega} \leq C(h+t)\,(|||w - w_h, \boldsymbol{\gamma} - \boldsymbol{\gamma}_h||| + h\|g\|_{1,h,\Omega} + \|\nabla w - \nabla w_\Pi\|_{1,h,\Omega} \\
+ \|\boldsymbol{\gamma} - \boldsymbol{\gamma}_\Pi\|_{1,h,\Omega} + t^{-1}\|\boldsymbol{\gamma} - \boldsymbol{\gamma}_0\|_{0,\Omega}\big).
\end{aligned}
$$

Finally, bound (5.24) follows from the Poincaré inequality and the triangular inequality we have that

$$
\|w - w_h\|_{1,\Omega} \leq C\|\nabla w - \nabla w_h\|_{0,\Omega} = C\|\boldsymbol{\theta} - \boldsymbol{\gamma} - (\boldsymbol{\theta}_h - \boldsymbol{\gamma}_h)\|_{0,\Omega} \leq C(\|\boldsymbol{\theta} - \boldsymbol{\theta}_h\|_{0,\Omega} + \|\boldsymbol{\gamma} - \boldsymbol{\gamma}_h\|_{0,\Omega}).
$$

The proof is complete. □

Finally, we obtain the following result.

Corollary 5.4.1 *Assume that the hypotheses of Theorem 5.4.1 hold. Moreover, assume that the domain Ω be either regular, or piecewise regular and convex, that $g \in H^1(E)$ for all $E \in \mathcal{T}_h$ and that $\Gamma_c = \Gamma$. Then, there exists $C > 0$ independent of h, g and t such that*

$$\|\boldsymbol{\theta} - \boldsymbol{\theta}_h\|_{0,\Omega} + \|w - w_h\|_{1,\Omega} \leq C(h+t)h\left(t^{-1}|\boldsymbol{\gamma}|_{1,\Omega} + |\boldsymbol{\theta}|_{2,\Omega} + |w|_{3,\Omega} + \|g\|_{1,h,\Omega}\right).$$

Proof. The proof follows directly from Proposition 5.4.5, combining Theorem 5.4.1, Propositions 5.4.1, 5.4.2 and the fact that $\|\boldsymbol{\gamma} - \boldsymbol{\gamma}_h\|_{0,\Omega} \leq t|||w - w_h, \boldsymbol{\gamma} - \boldsymbol{\gamma}_h|||$. □

Remark 5.4.3 *We note that the shear strain variable in the present paper is given by $\boldsymbol{\gamma} = \nabla w - \boldsymbol{\theta}$ and it is related with the usual scaled shear strain used in other Reissner-Mindlin contributions in the literature as follows $Q = t^{-2}\boldsymbol{\gamma}$. Since $t^{-1}\boldsymbol{\gamma} = tQ$ is a quantity that is known to be uniformly bounded in the correct Sobolev norms (see, e.g [13, 56]). Therefore, the factors t^{-1} appearing in Theorem 5.4.1 and Corollary 5.4.1 are not a source of locking.*

Remark 5.4.4 *We note that in our convergence results, in order to obtain the full convergence rate in h (independently of the thickness t) we need $|w|_{3,\Omega}$ to be bounded uniformly in t. Even in the presence of regular data, this condition is not always assured due to the presence of layers at the boundaries of the plate. Such small limitation of the method is related to the adopted formulation and is, somehow, the drawback related to the advantage of having a method with C^1 deflections, that is therefore able to give (at the limit for vanishing thickness) a Kirchhoff conforming solution. We finally note that, in practice, this kind of difficulty can be effectively dealt with by an ad-hoc refinement of the mesh near the boundaries of the plate.*

5.5. Numerical results

We report in this section some numerical examples which have allowed us to assess the theoretical results proved above. We have implemented in a MATLAB code our method on arbitrary polygonal meshes, by following the ideas proposed in [22]. To complete the choice of the VEM, we have to fix the bilinear forms $S^E(\cdot,\cdot)$ and $S_0^E(\cdot,\cdot)$ satisfying (5.12) and (5.13), respectively. Proceeding as in [22], a natural choice for $S^E(\cdot,\cdot)$ is given by

$$S^E(\boldsymbol{\gamma}_h, \boldsymbol{\tau}_h) := \sum_{i=1}^{2N_E} \boldsymbol{\gamma}_h(v_i)\boldsymbol{\tau}_h(v_i) + \sum_{j=1}^{N_E} \left(\frac{1}{|e_j|}\int_{e_j} \boldsymbol{\gamma}_h \cdot \boldsymbol{t}\right)\left(\frac{1}{|e_j|}\int_{e_j} \boldsymbol{\tau}_h \cdot \boldsymbol{t}\right), \quad \boldsymbol{\gamma}_h, \boldsymbol{\tau}_h \in \mathbf{V}_h^E,$$

while a choice for $S_0^E(\cdot,\cdot)$ is given by

$$S_0^E(\boldsymbol{\gamma}_h, \boldsymbol{\tau}_h) := \frac{h_E^2}{t^2}\left(\sum_{i=1}^{2N_E} \boldsymbol{\gamma}_h(v_i)\boldsymbol{\tau}_h(v_i) + \sum_{j=1}^{N_E} \left(\frac{1}{|e_j|}\int_{e_j} \boldsymbol{\gamma}_h \cdot \boldsymbol{t}\right)\left(\frac{1}{|e_j|}\int_{e_j} \boldsymbol{\tau}_h \cdot \boldsymbol{t}\right)\right), \quad \boldsymbol{\gamma}_h, \boldsymbol{\tau}_h \in \mathbf{V}_h^E.$$

The choices above are standard in the Virtual Element literature, and correspond to a scaled identity matrix in the space of the degree of freedom values.

To test the convergence properties of the method, we introduce the following discrete L^2-like norm: for any sufficiently regular function $\boldsymbol{v}$,

$$\|\boldsymbol{v}\|_{0,\Omega}^2 := \sum_{E\in\mathcal{T}_h}\left(|E|\sum_{i=1}^{N_E}(\boldsymbol{v}(v_i))^2\right),$$

with $|E|$ being the area of element E. We also define the relative errors in discrete L^2-like norms (based on the vertex values):

$$(e_w)^2 := \frac{\displaystyle\sum_{E\in\mathcal{T}_h}\left(|E|\sum_{i=1}^{N_E}(w(v_i)-w_h(v_i))^2\right)}{\displaystyle\sum_{E\in\mathcal{T}_h}\left(|E|\sum_{i=1}^{N_E}(w(v_i))^2\right)},$$

and the obvious analogs for $e_{\nabla w}$ and $e_{\boldsymbol{\theta}}$. Finally, we introduce the relative error in the energy norm

$$(\boldsymbol{\mathcal{E}})^2 := \frac{\mathcal{A}_h((w-w_h,\boldsymbol{\gamma}-\boldsymbol{\gamma}_h),(w-w_h,\boldsymbol{\gamma}-\boldsymbol{\gamma}_h))}{\mathcal{A}_h((w,\boldsymbol{\gamma}),(w,\boldsymbol{\gamma}))},$$

where $\mathcal{A}_h(\cdot,\cdot)$ corresponds to the discrete bilinear form on the left hand side of Problem 5.3.1.

5.5.1. Test 1:

As a test problem we have taken an isotropic and homogeneous plate $\Omega := (0,1)^2$, clamped on the whole boundary, for which the analytical solution is explicitly known (see [66]).

Choosing the transversal load g as:

$$\begin{aligned} g(x,y) = \frac{E}{12(1-\nu^2)}\big[&12y(y-1)(5x^2-5x+1)(2y^2(y-1)^2+x(x-1)(5y^2-5y+1)\\ &+12x(x-1)(5y^2-5y+1)(2x^2(x-1)^2+y(y-1)(5x^2-5x+1)\big], \end{aligned}$$

the exact solution of the problem is given by:

$$\begin{aligned} w(x,y) = &\frac{1}{3}x^3(x-1)^3y^3(y-1)^3\\ &-\frac{2t^2}{5(1-\nu)}\left[y^3(y-1)^3x(x-1)(5x^2-5x+1)+x^3(x-1)^3y(y-1)(5y^2-5y+1)\right], \end{aligned}$$

$$\boldsymbol{\theta}(x,y) = \begin{bmatrix} y^3(y-1)^3x^2(x-1)^2(2x-1)\\ x^3(x-1)^3y^2(y-1)^2(2y-1)\end{bmatrix}.$$

The shear modulus λ is given by $\lambda := \dfrac{5E}{12(1+\nu)}$ (choosing 5/6 as shear correction factor), while the material constants have been chosen $E=1$ and $\nu=0$.

We have tested the method by using different values of the plate thickness: $t=0{,}1$, $t=0{,}01$ and $t=0{,}001$. Moreover, we have used different families of meshes (see Figure 5.1):

- $\mathcal{T}_h^1$: triangular meshes;
- $\mathcal{T}_h^2$: trapezoidal meshes which consist of partitions of the domain into $N \times N$ congruent trapezoids, all similar to the trapezoid with vertices $(0,0)$, $(\frac{1}{2},0)$, $(\frac{1}{2},\frac{2}{3})$ and $(0,\frac{1}{3})$;
- $\mathcal{T}_h^3$: triangular meshes, considering the middle point of each edge as a new degree of freedom but moved randomly; note that these meshes contain non-convex elements.

The refinement parameter h used to label each mesh is $h = \max_{E\in\mathcal{T}_h} h_E$.

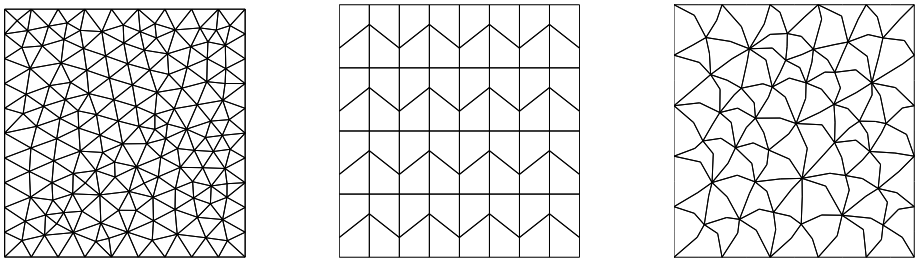

Figura 5.1: Sample meshes: $\mathcal{T}_h^1$ (left), $\mathcal{T}_h^2$ (middle) and $\mathcal{T}_h^3$ (right) with $h = 0{,}1189$, $h = 0{,}1719$ and $h = 0{,}11078$, respectively.

We report in Table 5.1, Table 5.2 and Table 5.3 the relative errors in the discrete L^2-norm of w, ∇w and $\boldsymbol{\theta}$, together with the relative errors in the energy norm, for each family of meshes and different refinement levels. We consider different thickness: $t = 1{,}0e-01$, $1{,}0e-02$ and $1{,}0e-03$, respectively. We also include in these table the experimental rate of convergence.

Cuadro 5.1: $\mathcal{T}_h^1$: Computed error in L^2-norm with $t = 1{,}0e-01$, $t = 1{,}0e-02$ and $t = 1{,}0e-03$, respectively.

error	$h = 0{,}1189$	$h = 0{,}05878$	$h = 0{,}03142$	$h = 0{,}01582$	$h = 0{,}008271$	Order
e_w	1.1084e-01	2.9410e-02	7.4232e-03	1.8414e-03	4.6791e-04	2.0627
$e_{\nabla w}$	1.3000e-01	4.1684e-02	1.3215e-02	4.2296e-03	1.5018e-03	1.6872
$e_{\boldsymbol{\theta}}$	8.8733e-02	2.2288e-02	5.4344e-03	1.3314e-03	3.3668e-04	2.1019
$\boldsymbol{\mathcal{E}}$	2.9935e-01	1.2776e-01	5.3946e-02	2.2765e-02	1.0702e-02	1.2625
e_w	1.0302e-01	2.6332e-02	6.4931e-03	1.5956e-03	4.0406e-04	2.0898
$e_{\nabla w}$	8.9532e-02	2.2548e-02	5.4769e-03	1.3430e-03	3.3972e-04	2.1023
$e_{\boldsymbol{\theta}}$	8.9247e-02	2.2442e-02	5.4452e-03	1.3345e-03	3.3748e-04	2.1036
$\boldsymbol{\mathcal{E}}$	1.7557e-01	8.5496e-02	4.1989e-02	2.0203e-02	1.0289e-02	1.0712
e_w	1.0296e-01	2.6311e-02	6.4884e-03	1.5960e-03	4.0430e-04	2.0893
$e_{\nabla w}$	8.9262e-02	2.2454e-02	5.4519e-03	1.3385e-03	3.3869e-04	2.1022
$e_{\boldsymbol{\theta}}$	8.9259e-02	2.2453e-02	5.4516e-03	1.3384e-03	3.3866e-04	2.1023
$\boldsymbol{\mathcal{E}}$	1.7332e-01	8.4751e-02	4.1677e-02	1.9984e-02	1.0143e-02	1.0719

Cuadro 5.2: $\mathcal{T}_h^2$: Computed error in L^2-norm with $t = 1{,}0e-01$, $t = 1{,}0e-02$ and $t = 1{,}0e-03$, respectively.

error	$h = 0{,}1719$	$h = 0{,}0859$	$h = 0{,}0430$	$h = 0{,}0215$	$h = 0{,}0122$	Order
e_w	3.8903e-01	1.1104e-01	2.9582e-02	7.6148e-03	1.8676e-03	1.9103
$e_{\nabla w}$	4.1467e-01	1.3705e-01	4.3810e-02	1.4053e-02	4.6530e-03	1.6097
$e_{\boldsymbol{\theta}}$	3.6466e-01	9.7423e-02	2.4805e-02	6.2472e-03	1.5348e-03	1.9574
$\boldsymbol{\mathcal{E}}$	6.2673e-01	3.1044e-01	1.3447e-01	5.8121e-02	2.5266e-02	1.1580
e_w	3.7958e-01	1.0366e-01	2.6508e-02	6.6562e-03	1.6079e-03	1.9554
$e_{\nabla w}$	3.6633e-01	9.8309e-02	2.5015e-02	6.2782e-03	1.5342e-03	1.9594
$e_{\boldsymbol{\theta}}$	3.6589e-01	9.8016e-02	2.4903e-02	6.2447e-03	1.5252e-03	1.9611
$\boldsymbol{\mathcal{E}}$	4.1994e-01	1.6745e-01	7.4795e-02	3.6193e-02	1.8249e-02	1.1154
e_w	3.7950e-01	1.0361e-01	2.6499e-02	6.6620e-03	1.6120e-03	1.9545
$e_{\nabla w}$	3.6591e-01	9.8030e-02	2.4914e-02	6.2538e-03	1.5283e-03	1.9603
$e_{\boldsymbol{\theta}}$	3.6590e-01	9.8027e-02	2.4913e-02	6.2534e-03	1.5282e-03	1.9604
$\boldsymbol{\mathcal{E}}$	4.1544e-01	1.6465e-01	7.3602e-02	3.5478e-02	1.7716e-02	1.1213

Cuadro 5.3: $\mathcal{T}_h^3$: Computed error in L^2-norm with $t = 1{,}0e-01$, $t = 1{,}0e-02$ and $t = 1{,}0e-03$, respectively.

error	$h = 0{,}1108$	$h = 0{,}05943$	$h = 0{,}02939$	$h = 0{,}01571$	$h = 0{,}007911$	Order
e_w	2.8478e-01	8.7688e-02	2.4214e-02	6.2665e-03	1.5694e-03	2.0614
$e_{\nabla w}$	3.1623e-01	1.2017e-01	4.0908e-02	1.3382e-02	4.4467e-03	1.6953
$e_{\boldsymbol{\theta}}$	2.5664e-01	7.4651e-02	1.9137e-02	4.7397e-03	1.1606e-03	2.1426
$\boldsymbol{\mathcal{E}}$	6.3713e-01	3.6532e-01	1.6896e-01	7.6472e-02	3.4702e-02	1.1691
e_w	2.6595e-01	7.4074e-02	1.9065e-02	4.7609e-03	1.1608e-03	2.1543
$e_{\nabla w}$	2.5677e-01	7.4955e-02	1.9117e-02	4.7777e-03	1.1667e-03	2.1435
$e_{\boldsymbol{\theta}}$	2.5625e-01	7.4605e-02	1.8981e-02	4.7359e-03	1.1552e-03	2.1466
$\boldsymbol{\mathcal{E}}$	3.7935e-01	1.9753e-01	9.5553e-02	4.8323e-02	2.3655e-02	1.1007
e_w	2.6642e-01	7.4576e-02	1.9021e-02	4.7417e-03	1.1613e-03	2.1801
$e_{\nabla w}$	2.5605e-01	7.4680e-02	1.9071e-02	4.7265e-03	1.1606e-03	2.1689
$e_{\boldsymbol{\theta}}$	2.5605e-01	7.4676e-02	1.9069e-02	4.7261e-03	1.1605e-03	2.1689
$\boldsymbol{\mathcal{E}}$	3.7438e-01	1.9044e-01	9.4471e-02	4.7568e-02	2.3429e-02	1.1081

It can be seen from Tables 5.1, 5.2 and 5.3 that the theoretical predictions of Section 5.4 are confirmed. In particular, we can appreciate a rate of convergence $O(h)$ for the energy norm $\boldsymbol{\mathcal{E}}$, that is equivalent to the $|||\cdot|||$ norm. This holds for all the considered meshes and thicknesses, thus also underlying the locking free nature of the scheme. Moreover, for sufficiently small t we also observe a clear rate of convergence $O(h^2)$ for for e_w, $e_{\nabla w}$ and $e_{\boldsymbol{\theta}}$, in accordance with Corollary 5.4.1.

5.5.2. Test 2:

As a second test, we investigate more in deep the locking-free character of the method, and also take the occasion for a comparison with the limit Kirchhoff model. It is well known (see [55]) that when t goes to zero the solution of the Reissner-Mindlin model converges to an identical Kirchhoff-Love solution: Find $w_0 \in H^2(\Omega)$ such that

$$\frac{E}{12(1-\nu^2)}\Delta^2 w_0 = g, \tag{5.37}$$

with the corresponding boundary conditions.

We have considered a rectangular plate $\Omega := (0,a)\times(0,b)$, simply supported on the whole boundary, and we have chosen the transversal load g as

$$g(x,y) = \sin\left(\frac{\pi}{a}x\right)\sin\left(\frac{\pi}{b}y\right).$$

Then, the analytical solution w_0 of problem (5.37) is given by

$$w_0(x,y) = \frac{12(1-\nu^2)}{E}\left(\pi^4\left(\frac{1}{a^2}+\frac{1}{b^2}\right)^2\right)^{-1}\sin\left(\frac{\pi}{a}x\right)\sin\left(\frac{\pi}{b}y\right).$$

The material constants have been chosen $E = 1$ and $\nu = 0{,}3$. Moreover, we have taken $a = 1$ and $b = 2$, and we have used three different families of meshes (see Figure 5.2):

- $\mathcal{T}_h^1$: triangular meshes;
- $\mathcal{T}_h^4$: hexagonal meshes;
- $\mathcal{T}_h^5$: Voronoi polygonal meshes.

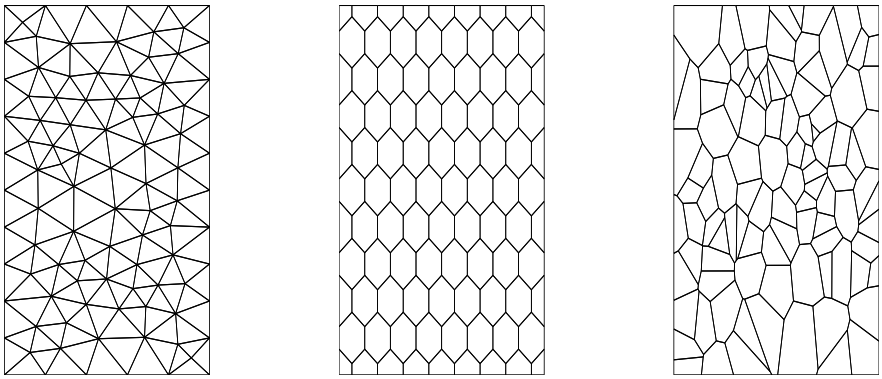

Figura 5.2: Sample meshes: $\mathcal{T}_h^1$ (left), $\mathcal{T}_h^4$ (middle) and $\mathcal{T}_h^5$ (right).

Tables 5.4, 5.5 and 5.6 show an analysis for various thicknesses in order to assess the locking-free nature of the proposed method. We show the relative errors in the discrete L^2-norm of the deflection w for each family of meshes and different refinement levels and considering different thickness: $t = 1{,}0e-01$, $t = 1{,}0e-02$, $t = 1{,}0e-03$, $t = 1{,}0e-04$ and $t = 1{,}0e-05$, respectively.

It can be clearly seen from these tables that the proposed method is locking-free, since even for corse meshes the solution does not lock but approximates (for small t) the Kirchhoff solution.

Cuadro 5.4: Computed error in e_w by $\mathcal{T}_h^1$.

$t\backslash h$	2.4495e-01	1.2706e-01	6.4686e-02	3.2407e-02	1.6166e-02
1.0e-01	8.6091e-03	4.0902e-02	6.0389e-02	7.1077e-02	7.5623e-02
1.0e-02	4.6875e-02	1.0335e-02	1.7984e-03	7.6646e-04	2.0123e-03
1.0e-03	4.7301e-02	1.0963e-02	2.7190e-03	6.6677e-04	1.3850e-04
1.0e-04	4.7305e-02	1.0969e-02	2.7284e-03	6.8234e-04	1.6637e-04
1.0e-05	4.7305e-02	1.0969e-02	2.7285e-03	6.8250e-04	1.6665e-04

Cuadro 5.5: Computed error in e_w by $\mathcal{T}_h^4$.

$t\backslash h$	2.7813e-01	1.3086e-01	6.7301e-02	4.4428e-02	3.3163e-02
1.0e-01	8.3939e-02	5.9358e-02	6.2558e-02	6.7150e-02	6.9098e-02
1.0e-02	4.9794e-02	1.0178e-02	4.0223e-03	2.4758e-03	2.0948e-03
1.0e-03	4.9428e-02	9.5752e-03	3.1448e-03	1.3334e-03	7.3806e-04
1.0e-04	4.9424e-02	9.5691e-03	3.1358e-03	1.3211e-03	7.2280e-04
1.0e-05	4.9424e-02	9.5691e-03	3.1357e-03	1.3210e-03	7.2265e-04

Cuadro 5.6: Computed error in e_w by $\mathcal{T}_h^5$.

$t\backslash h$	4.5918e-01	2.3481e-01	1.2942e-01	8.1744e-02	5.5071e-02
1.0e-01	2.7624e-02	4.0550e-02	4.6180e-02	6.5997e-02	6.9822e-02
1.0e-02	1.2695e-02	3.4544e-03	7.2182e-04	1.1407e-03	1.3932e-03
1.0e-03	1.2768e-02	3.0038e-03	3.8157e-04	6.4829e-05	4.5322e-05
1.0e-04	1.2768e-02	2.9994e-03	3.8727e-04	6.2480e-05	3.2567e-05
1.0e-05	1.2768e-02	2.9993e-03	3.8736e-04	6.2151e-05	3.1927e-05

Capítulo 6

Conclusiones y trabajo futuro

6.1. Conclusiones

Está tesis se desarrollo, con el propósito de estudiar la robustez y la flexibilidad de los VEM para adaptarse a diferente tipo de problemas que son de interés físico y teórico. Así la tesis recoge el análisis matemático y numérico de los métodos de elementos virtuales aplicado a los problemas de valores propios de Steklov y el de vibraciones acústicas y al problema de flexión de placas modeladas por las ecuaciones de Reissner-Mindlin. Para el problemas de valores propios de Steklov también se propuso un estimador a posteriori del tipo residual completamente calculable. A continuación se presentan las conclusiones mas relevantes de este trabajo.

1. En el Capitulo 2 se estudió el problema de valores propios de Steklov en dos dimensiones. Se propuso una discretización por medio de elementos virtuales para aproximar numéricamente el problema de autovalores y se estableció que el esquema resultante proporciona una aproximación correcta del espectro y se probó que las estimaciones de los errores son de orden óptimo para las funciones propias y los valores propios. Además, se demostró, una estimación de mejor orden para el el cálculo del error de las funciones propias en la frontera libre. Se desarrollaron códigos escritos en Matlab que permitieron validar los resultados teóricos. Adicionalmente se presentó un test numérico para verificar la influencia de la *constante de estabilización* σ_K en (2.24) en el espectro discreto calculado y se observó que la introducción de los términos de estabilidad S_K en (2.6) conduce a valores propios espurios, pero que estos valores propios espurios pueden ser controlados si se elige apropiadamente la constante de estabilidad σ_K.

   En el Capitulo 3 se desarrolló un estimador de error a posteriori del tipo residual para la aproximación por elementos virtuales del problema de valores propios de Steklov. Se observo que como consecuencia de utilizar VEM, aparecen nuevos términos adicionales en el estimador de error a posteriori, que representan la "inconsistencia virtual". Sin embargo el estimador es totalmente computable, ya que depende únicamente de las cantidades disponibles a partir de la solución VEM obtenida. Resultados numéricos confirmaron el buen rendimiento del esquema, además se observó que un residuo basado en un estimador

de error a posterior con VEM convergen con el mismo orden que los FEM para el problema de valores propios Steklov, sin embargo, el verdadero atractivo de este método es la flexibilidad de mallas que da la utilización de VEM, para la aplicación de estrategias de adaptación de malla.

2. En el Capitulo 4 se abordó el análisis matemático y numérico de la aproximación por elementos virtuales, para el problema de vibración acústica. Para ello, se introdujo una formulación variacional del problema espectral basándose sólo en el desplazamiento de fluido y se propuso una discretización mediante $H(\text{div})$ con elementos virtuales con rotor nulo y se demostró que el esquema virtual está bien planteado y que genera aproximaciones de orden óptimo. Con este fin, adicionalmente se probaron estimaciones óptimas de aproximación para los $H(\text{div})$–VEM con rotor nulo, este resultado podría ser útil también para otras aplicaciones. Tos los resultados teóricos obtenidos fueron validados numéricamente. Nuevamente, en la sección de resultados numéricos, se presenta un test numérico para verificar la influencia de la *constante de estabilización* σ_K. A diferencia del problema de Steklov, en este caso, no se detectan valores propios espurios para cualquier elección de la constante de estabilidad σ_K. Sin embargo, para valores grandes de σ_K , los valores propios calculados con mallas gruesas podrían ser muy pobre. Este análisis sugiere que al usar $H(\text{div})$-VEM para este tipo de problemas espectrales, se tiene que estar consciente del riesgo de la degeneración de los valores propios, para ciertos valores de la constante de estabilidad σ_K. La forma de minimizar este riesgo en este caso es tomar valores pequeños de σ_K (donde "pequeño.[en] un verdadero problema, dependerá de los valores de las constantes físicas).

3. En el Capitulo 5 se estudió un método de elementos virtuales para el problema de flexión de placas de Reissner-Mindlinse. La formulación variacional del problema se escribió en términos de las variables de la deformación de corte transversal y la deflexión y se propuso una formulación discreta conforme en $[H^1(\Omega)]^2 \times H^2(\Omega)$ para la deformación de corte y la deflexión, respectivamente. Se demostró que las estimaciones del error son óptimas para todas las variables involucradas (en las normas naturales de la formulación adoptada), con constantes independientes del espesor de la placa. Por último, se presentaron experimentos numéricos que nos permitieron evaluar el desempeño del método. Una característica distintiva de este enfoque es la aproximación directa de la deformación por esfuerzo cortante transversales. Por otra parte, las rotaciones se obtienen con un simple tratamiento de post-procesamiento de la deformación por esfuerzo cortante y la deflexión.

6.2. Trabajo futuro

1. Estudiar la aplicación de los VEM para el problema de los modos propios de cavidades electromagnéticas;

2. Estudiar la aplicación de los VEM para el problema de pandeo de placas delgadas utilizando los modelos de Kirkchhoff;

3. Derivar un estimador de error a posteriori residual, confiable y eficiente, para el problema de vibraciones acústicas presentados en el Capitulo 4;

4. Extender los resultados y técnicas introducidas en el Capitulo 4. Con el fin de diseñar un método de elementos virtuals de aproximaciones espectrales para los sistemas acoplados que implican la interacción entre fluido-estructura.

Conclusions and future work

6.3. Conclusions

The aim of this thesis was to study the robustness and flexibility of VEM to solve different types of problems of physical and theoretical interest. The thesis collects mathematical and numerical analysis of the virtual element methods applied to problems of Steklov eigenvalues, acoustic vibrations and plate bending modeled by Reissner-Mindlin equations. A computable residual type a posteriori estimator is also proposed for the Steklov eigenvalue problem. The most significant conclusions of this work are presented below.

1. Chapter 2 studies the Steklov eigenvalue problem in two dimensions. Discretization by virtual elements is proposed to numerically approximate the eigenvalue problem and it is established that the resulting scheme provides a correct spectral approximation and that the error estimations are of the optimal order for the eigenfunctions and eigenvalues. As well, a better order estimation is proved to calculate eigenfunctions errors on the free boundary. Codes written in Matlab were developed to validate the theoretical results. As well, a numerical test is presented to verify the influence of the *stability constant* in the calculated discrete spectrum and it is observed that the introduction of stability terms results in spurious eigenvalues, although these spurious eigenvalues can be controlled if the stability constant is appropriately chosen.

2. A residual type a posteriori error estimator was developed in Chapter 3 for the approximation by virtual elements of the Steklov eigenvalue problem. As a consequence of using VEM, new terms appear in the a posteriori error estimator that represents "virtual inconsistency". However, the estimator is completely computable, given that it depends solely on the quantities available from the VEM solution obtained. Reliability and efficiency estimates are proved to hold up to higher order terms. Numerical results confirm the good performance of the scheme.

3. The mathematical and numerical analysis of the approximation by virtual elements for acoustic vibration problem was addressed in Chapter 4. To do this, a variational formulation of the spectral problem based on fluid displacements and a virtual elements discretization of $H(\mathrm{div})$ with vanishing rotor was proposed. It was proved that the virtual scheme generates approximations of optimal order. All the theoretical results obtained were validated numerically. Once again, the numerical results section presents a numerical test to verify the influence of the *stability constant* . Unlike the Steklov problem, in this case no spurious eigenvalues were found for any chosen stability constant. However, for large values of it, the eigenvalues calculated with coarse meshes could be very poor. This analysis suggests that for the use of $H(\mathrm{div})$-VEM on this kind of spectral problems, it is necessary to be aware of the risk of degeneration of the eigenvalues for certain values of the stability constant. The way to minimize this risk in this case is to take small values of it (where "small", in a real problem, will of course depend on the values of the physicals

constants).

4. A virtual element method for the Reissner-Mindlinse bending problem was studied in Chapter 5. The variational formulation of the problem is written in terms of the shear strain and deflection variables and a discrete formulation in $[H^1(\Omega)]^2$ and $H^2(\Omega)$ was proposed. The error estimations are optimal for all the variables involved (in the natural norms of the adopted formulation), with constants independent of plate thickness. Finally, numerical experiments are presented to evaluate the performance of the method. A distinctive characteristic of this approach is the direct approximation of the deformation by shear strain. The rotations are obtained with a simple post-processing treatment from shear strains and deflections.

6.4. Future work

1. To study the solution by VEM of Maxwell eigenvalue problem;
2. To study the application of VEM to vibration and buckling problems of thin plates;
3. To derive a posteriori error estimators, reliable and efficient for the acoustic vibration problem;
4. To design VEM for coupled systems involving fluid-structure interaction.

Bibliografía

[1] D. Adak, E. Nataranjan. *Analysis of nonconforming Virtual element method for the convection diffusion reaction equation with polynomial coefficients*, Pre-print arXiv:1512.07359 [math.NA] (2015).

[2] D. Adak, E. Nataranjan. *Analysis of nonconforming Virtual element method for the convection diffusion reaction problem*, Pre-print arXiv:1601.01077 [math.NA] (2016).

[3] B. Ahmad, A. Alsaedi, F. Brezzi, L.D. Marini and A.Russo, *Equivalent Projectors for Virtual Element Methods*, Comput. Math. Appl. **66** (2013), pp. 376–391.

[4] M. Ainsworth and J.T. Oden, *A posteriori error estimate in finite element analysis*, Pure and Applied Mathematics (New York). Wiley-Interscience [Jhon Wiley and Sons] New York(2000).

[5] A.B. Andreev and T.D. Todorov, *Isoparametric finite-element approximation of a Steklov eigenvalue problem*, IMA J. Numer. Anal. **24** (2004), pp. 309–322.

[6] P.F. Antonietti, L. Beirão da Veiga, D. Mora and M. Verani, *A stream virtual element formulation of the Stokes problem on polygonal meshes*, SIAM J. Numer. Anal. **52** (2014), pp. 386–404.

[7] P. F. Antonietti, L. Beirão da Veiga, S. Scacchi and M. Verani, *A C^1 virtual element method for the Cahn–Hilliard equation with polygonal meshes*, SIAM J. Numer. Anal., **54(1)** (2016), pp. 36–56.

[8] P. F. Antonietti, P. Houston, M. Sarti and M. Verani, *Multigrid algorithms for hp-version interior penalty discontinuous Galerkin methods on polygonal and polyhedral meshes*, Preprint arXiv:1412.0913 [math.NA] (2014).

[9] M.G. Armentano, *The effect of reduced integration in the Steklov eigenvalue problem*, Math. Model. Numer. Anal. **38** (2004), pp. 27–36.

[10] M.G. Armentano and C. Padra, *A posteriori error estimates for the Steklov eigenvalue problem*, Appl. Numer. Math. **58** (2008), pp. 593–601.

[11] D.N. Arnold and G. Awanou, *The serendipity family of finite elements*, Found. Comput. Math. **11** (2011), no. 3, 337–344.

[12] D.N. Arnold, D. Boffi and R.S. Falk, *Approximation by quadrilateral finite elements*, Math. Comp **71** (2002), no. 239, 909–922 (electronic).

[13] D.N. Arnold and R.S. Falk, *A uniformly accurate finite element method for the Reissner-Mindlin plate*, SIAM J. Numer. Anal., **26** (1989), pp. 1276–1290.

[14] B. Ayuso de Dios, K. Lipnikov and G. Manzini, *The nonconforming virtual element method*, ESAIM Math. Model. Numer. Anal., **50(3)** (2016), pp. 879–904.

[15] I. Babuška and J. Osborn, *Eigenvalue problems*, in Handbook of Numerical Analysis, Vol. II, P.G. Ciarlet and J.L. Lions, eds., North-Holland, Amsterdam, 1991, 641–787.

[16] L. Beirão da Veiga, *A residual based error estimator for the mimetic finite difference method*, Numer. Math. **108** (2008), pp. 387–406.

[17] L. Beirão da Veiga, *A mimetic finite difference method for linear elasticity*, M2AN: Math. Model. Numer. Anal. **44** (2010), pp. 231–250.

[18] L. Beirão da Veiga, F. Brezzi, A. Cangiani, G. Manzini, L.D. Marini and A. Russo, *Basic principles of virtual element methods*, Math. Models Methods Appl. Sci. **23** (2013), pp. 199–214.

[19] L. Beirão da Veiga, F. Brezzi and L.D. Marini, *Virtual elements for linear elasticity problems*, SIAM J. Numer. Anal. **51** (2013), pp. 794–812.

[20] L. Beirão da Veiga, F. Brezzi, L. D. Marini and A. Russo, $H(\mathrm{div})$ *and* $H(\mathrm{curl})$*-conforming virtual element method*, Numer. Math. **123 no. 2** (2016), pp. 303–332.

[21] L. Beirão da Veiga, F. Brezzi, L. D. Marini and A. Russo, *Virtual element methods for general second order elliptic problems on polygonal meshes*, arXiv:1412.2646 [Math.NA], 2014, submitted.

[22] L. Beirão da Veiga, F. Brezzi, L. D. Marini and A. Russo, *The hitchhiker's guide to the virtual element method*, Math. Models Methods Appl. Sci. **24** (2014), pp. 1541–1573.

[23] L. Beirão da Veiga, F. Brezzi, L. D. Marini and A. Russo, *Mixed virtual element methods for general second order elliptic problems on polygonal meshes*, ESAIM Math. Model. Numer. Anal., DOI: http://dx.doi.org/10.1051/m2an/2015067 (2016).

[24] L. Beirão da Veiga, F. Brezzi, L.D. Marini and A. Russo *Serendipity Nodal VEM spaces*, Pre-print arXiv:1510.08477 [math.NA] (2015).

[25] L. Beirão da Veiga, F. Brezzi, L.D. Marini and A. Russo *Serendipity face and edge VEM spaces*, Pre-print arXiv:1606.01048 [math.NA] (2016).

[26] L. Beirão da Veiga, T.J.R. Hughes, J. Kiendl, C. Lovadina, J. Niiranen, A. Reali and H. Speleers, *A locking-free model for Reissner-Mindlin plates: analysis and isogeometric implementation via NURBS and triangular NURPS*, Math. Models Methods Appl. Sci., **25(8)** (2015), pp. 1519–1551.

[27] L. Beirão da Veiga, K. Lipnikov and G. Manzini, *Convergence analysis of the high- order mimetic finite difference method*, Numer. Math. **113** (2009), pp. 325–356.

[28] L. Beirão da Veiga, K. Lipnikov and G. Manzini, *Arbitrary-order nodal mimetic dis- cretizations of elliptic problems on polygonal meshes*, SIAM J. Numer. Anal. **49** (2011), pp. 1737–1760.

[29] L. Beirão da Veiga, K. Lipnikov and G. Manzini, *The Mimetic Finite Difference Method for Elliptic Problems*, Springer, MS&A, vol. **11**, 2014.

[30] L. Beirão da Veiga, C. Lovadina and D. Mora, *A virtual element method for elastic and inelastic problems on polytope meshes*, Comput. Methods Appl. Mech. Engrg., **295** (2015), pp. 327–346.

[31] L. Beirão da Veiga, C. Lovadina and G. Vacca, *Divergence free Virtual Elements for the Stokes problem on polygonal meshes*, ESAIM Math. Model. Numer. Anal., DOI: http://dx.doi.org/10.1051/m2an/2016032 (2016).

[32] L. Beirão da Veiga and G. Manzini, *A higher-order formulation of the mimetic finite difference method*, SIAM J. Sci. Comput. **31** (2008), pp. 732–760.

[33] L. Beirão da Veiga and G. Manzini, *A virtual element method with arbitrary regularity*, IMA J. Numer. Anal. **34** (2014), pp. 759–781.

[34] L. Beirão da Veiga and G. Manzini, *Residual a posteriori error estimation for the virtual element method for elliptic problems*, ESAIM Math. Model. Number. Anal., **49** (2015), pp. 577–599.

[35] L. Beirão da Veiga, D. Mora and G. Rivera, *A virtual element method for Reissner-Mindlin plates*, CI^{2}MA preprint 2016-14, available from http://www.ci2ma.udec.cl.

[36] L. Beirão da Veiga, D. Mora, G. Rivera and R, Rodríguez, *A virtual element method for the acoustic vibration problem*, CI^{2}MA preprint 2015-44, available from http://www.ci2ma.udec.cl.

[37] M. F. Benedetto, S. Berrone, A. Borio, S. Pieraccini and S. Scialò, *A hybrid mortar virtual element method for discrete fracture network simulations*, J. Comput. Phys., **306** (2016), pp. 148–166.

[38] M. F. Benedetto, S. Berrone, S. Pieraccini and S. Scialò, *The virtual element method for discrete fracture network simulations*, Comput. Methods Appl. Mech. Engrg., **280** (2014), pp. 135–156.

[39] S. Bergmann and M. Schiffer, *Kernel functions and Elliptic Differential Equations in Mathematical Physics*, Academic Press, New York. (1953).

[40] A. Bermúdez, R. Durán, M.A. Muschietti, R. Rodríguez and J. Solomin, *Finite element vibration analysis of fluid-solid systems without spurious modes*, SIAM J. Numer. Anal. **32** (1995), pp. 1280–1295 .

[41] A. Bermúdez, R. Durán, R. Rodríguez and J. Solomin, *Finite element analysis of a quadratic eigenvalue problem arising in dissipative acoustics*, SIAM J. Numer. Anal. **38** (2000), pp. 267–291 .

[42] A. Bermúdez, P. Gamallo, L. Hervella-Nieto, R. Rodríguez and D. Santamarina, *Fluid-structure acoustic interaction. In: Marburg, S., Nolte, B. (eds.) Computational Acoustics of Noise Propagation in Fluids. Finite and Boundary Element Methods.* Springer, Chap. 9, pp. 253–286 (2008).

[43] A. Bermúdez, L. Hervella-Nieto and R. Rodríguez, *Finite element computation of three-dimensional elastoacoustic vibrations*, J. Sound Vibration. **219** (1999), pp. 279–306.

[44] A. Bermúdez and R. Rodríguez, *Finite element computation of the vibration modes of a fluid-solid system*, Comput. Methods Appl. Mech. Engrg. **119** (1994), pp. 355–370 .

[45] A. Bermúdez, R. Rodríguez and D. Santamarina, *A finite element solution of an added mass formulation for coupled fluid-solid vibrations*, Numer. Math. **87** (2000), pp. 201–227.

[46] A. Bermúdez, R. Rodríguez and D. Santamarina, *Finite element computation of sloshing modes in containers with elastic baffle plates*, Internat. J. Numer. Methods Engrg. **56** (2003), pp. 447–467.

[47] S. Bertoluzza, *Substructuring preconditioners for the three fields domain decomposition method*, Math. Comp. **73** (2004), pp. 659–689.

[48] D. Boffi, *Finite element approximation of eigenvalue problems*, Acta Numerica. **19** (2010), pp. 1–120.

[49] D. Boffi, F. Gardini and L. Gastaldi, *Some remarks on eigenvalue approximation by finite elements. In: Frontiers in Numerical Analysis–Durham 2010. Lect. Notes Comput. Sci. Eng.* Springer, Heidelberg **85** (2012), pp. 1–77.

[50] J.H. Bramble and J.E. Osborn, *Approximation of Steklov eigenvalues of non-selfadjoint second order elliptic operators*, in The Mathematical Foundations of the Finite Element Method with Applications to Partial Differential Equations, A. K. Aziz, ed., Academic Press, New York, 1972, 387–408.

[51] S.C. Brenner and R.L. Scott, *The Mathematical Theory of Finite Element Methods*, (Springer, New York, 2008).

[52] F. Brezzi, and A. Buffa, *Innovative mimetic discretizations for electromagnetic problems*, J. Comput. Appl. Math. **234** (2010), 1980–1987.

[53] F. Brezzi, A. Buffa and K. Lipnikov, *Mimetic finite differences for elliptic problems*, M2AN: Math. Model. Numer. Anal. **43** (2009), 277–295.

[54] F. Brezzi, R. S. Falk and L. D. Marini, *Basic principles of mixed virtual element methods*, ESAIM Math. Model. Numer. Anal. **48** (2014), pp. 1227–1240.

[55] F. Brezzi and M. Fortin, *Mixed and Hybrid Finite Element Methods*, Springer-Verlag, New York (1991).

[56] F. Brezzi, M. Fortin and R. Stenberg, *Error analysis of mixed-interpolated elements for Reissner-Mindlin plates*, Math. Models Meth. Appl. Sci., **1** (1991), pp. 125–151.

[57] F. Brezzi and L.D. Marini, *Virtual elements for plate bending problems*, Comput. Methods Appl. Mech. Engrg. **253** (2012), pp. 455–462.

[58] E. Caceres and G.N. Gatica, *A mixed virtual element method for the pseudostress-velocity formulation of the Stokes problem*, IMA J. Numer. Anal., DOI:10.1093/imanum/drw002 (2016).

[59] J. Canavati and A. Minsoni, *A discontinuous Steklov problem with an application to water waves*, J. Math. Anal. Appl. **69** (1979), pp. 540–558.

[60] A. Cangiani, E. H. Georgoulis and P. Houston, *hp-version discontinuous Galerkin methods on polygonal and polyhedral meshes*, Math. Models Methods Appl. Sci., **24(10)** (2014), pp. 2009–2041.

[61] A. Cangiani, E.H. Georgoulis, T. Pryer and O.J. Sutton, *A Posteriori error estimates for the Virtual element method*, arXiv:1603.05855v.1.

[62] A. Cangiani and G. Manzini, *Flux reconstruction and pressure post-processing in mimetic finite difference methods*, Comput. Methods Appl. Mech. Engrg. **197** (2008), pp. 933–945.

[63] A. Cangiani, G. Manzini and O.J. Sutton, *Conforming and nonconforming virtual element methods for elliptic problems*, arXiv:1507.03543 (July 2015).

[64] L. Chen, *Equivalence of Weak Galerkin Methods and Virtual Element Methods for Elliptic Equations*, Pre-print arXiv:1503.04700 [math.NA] (2015).

[65] M. Chiba, *Non-linear hydroelastic vibrations of a cylindrical tank with an elastic bottom containing liquid; Part II: linear axisymmetric vibration analysis*, J. Fluids Struct. **7** (1993), pp. 57–73.

[66] C. Chinosi and C. Lovadina, *Numerical analysis of some mixed finite element methods for Reissner-Mindlin plates*, Comput. Mech., **16(1)** (1995), pp. 36–44.

[67] C. Chinosi and L. D. Marini. *Virtual Element Method for fourth order problems: L^2-estimates*, Pre-print arXiv:1601.07484 [math.NA] (2016).

[68] Y.S. Choun and C.B. Yun, *Sloshing characteristics in rectangular tanks with a submerged block*, Comput. Struct. **61** (1996), pp. 401–413.

[69] P. G. Ciarlet, *The Finite Element Method for Elliptic Problems*, SIAM, 2002.

[70] P. G. Ciarlet, *Interpolation error estimates for the reduced Hsieh–Clough–Tocher triangle*, Math. Comp., **32(142)** (1978), pp. 335–344.

[71] P. Clément, *Approximation by finite element functions using local regularization*, RAIRO Anal. Numér. **9** (1975), pp. 77–84.

[72] C. Conca, J. Planchard and M. Vanninathan, *Fluid and Periodic Structures*, J. Wiley and Sons, New York, 1995.

[73] A. Dello Russo and A. Alonso, *A posteriori error estimates for nonconforming approximations of Steklov eigenvalue problems*, Comput. Math. Appl. **62** (2011), pp. 4100–4117.

[74] J. Descloux, N. Nassif and J. Rappaz, *On spectral approximation. Part 1: The problem of convergence*, RAIRO Anal. Numér. **12** (1978), pp. 97–112.

[75] J. Descloux, N. Nassif and J. Rappaz, *On spectral approximation. Part 2: Error estimates for the Galerkin method*, RAIRO Anal. Numér. **12** (1978), pp.113–119.

[76] D. Di Pietro and A. Ern, *A hybrid high-order locking-free method for linear elasticity on general meshes*, Comput. Methods Appl. Mech. Eng., **283** (2015), pp. 1–21.

[77] D. Di Pietro and A. Ern, *Hybrid high-order methods for variable-diffusion problems on general meshes*, C. R. Acad. Sci., Paris I, **353**(1) (2015), pp. 31–34.

[78] R. Durán, C. Padra and R. Rodríguez, *A posteriori error estimates for the finite element approximation of eigenvalue problem*, Math. Models Method Appl. Sci., **13**(8) (2003), pp. 1219–1229.

[79] R. Echter, B. Oesterle and M. Bischoff, *A hierarchic family of isogeometric shell finite elements*, Comput. Methods Appl. Mech. Engrg., **254** (2013), pp. 170–180.

[80] D.V. Evans and P. McIver, *Resonance frequencies in a container with a vertical baffle*, J. Fluid Mech. **175** (1987), pp. 295–307.

[81] R. Falk, *Finite elements for the Reissner-Mindlin plate*, D. Boffi and L. Gastaldi, editors, Mixed finite elements, compatibility conditions, and applications, Springer, Berlin, 2008, pp. 195–232.

[82] T.-P. Fries and T. Belytschko, *The extended/generalized finite element method: An overview of the method and its applications*, Int. J. Numer. Methods Engrg. **84** (2010), pp. 253–304.

[83] A.L. Gain, G.H. Paulino, L. Duarte and I.F.M. Menezes *Topology Optimization Using Polytopes*, Comput Methods Appl Mech Eng. **293** (2015), pp. 411–430.

[84] A. L. Gain, C. Talischi and G.H. Paulino, *On the virtual element method for three-dimensional linear elasticity problems on arbitrary polyhedral meshes*, Comput. Methods Appl. Mech. Engrg., **282** (2014), pp. 132–160.

[85] E.M. Garau and P. Morin, *Convergence and quasi-optimality of adaptive FEM for Steklov eigenvalue problems*, IMA J. Numer. Anal. **31** (2011), pp. 914–946.

[86] V. Girault and P.A. Raviart, *Finite Element Methods for Navier-Stokes Equations*, (Springer-Verlag, Berlin, 1986).

[87] P. Grisvard, *Elliptic Problems in Non-Smooth Domains*, (Pitman, Boston, 1985).

[88] V. Gyrya and K. Lipnikov, *High-order mimetic finite difference method for diffusion problems on polygonal meshes*, J. Comput. Phys. **227** (2008), pp. 8841–8854.

[89] M. Hamdi, Y. Ousset and G. Verchery, *A displacement method for the analysis of vibrations of coupled fluid-structure systems*, Internat. J. Numer. Methods Engrg. **13** (1978), pp. 139–150.

[90] T. Kato, *Perturbation Theory for Linear Operators*, (Springer Verlag, Berlin, 1995).

[91] L. Kiefling and G. C. Feng, *Fluid-structure finite element vibrational analysis*, AIAA J. **14** (1976), pp.199–203.

[92] Q. Li, Q. Lin and H. Xie, *Nonconforming finite element approximations of the Steklov eigenvalue problem and its lower bound approximations*, Appl. Math. **58** (2013), pp. 129–151.

[93] Q. Long, P. B. Bornemann and F. Cirak, *Shear-flexible subdivision shells*, Internat. J. Numer. Methods Engrg., **90(13)** (2012), pp. 1549–1577.

[94] C. Lovadina, *A brief overview of plate finite element methods*, Integral methods in science and engineering. Vol. 2, 261–280, Birkhäuser Boston, Inc., Boston, MA, 2010.

[95] C. Lovadina, D. Mora and Rodríguez, R, *Approximation of the buckling problem for Reissner-Mindlin plates*, SIAM J. Numer. Anal. **48** (2010), pp. 603–632.

[96] M. Lyly, J. Niiranen and R. Stenberg, *A refined error analysis of MITC plate elements*, Math. Models Methods Appl. Sci., **16** (2006), pp. 967–977.

[97] D. Mora, G. Rivera and R. Rodríguez, *A virtual element method for the Steklov eigenvalue problem*, Math. Models Methods Appl. Sci., **25(8)** (2015), pp. 1421–1445.

[98] S. Nataranjan. S. PA Bordas and E.T. Ooid. *On the equivalence between the cell-based smoothed finite element method and the virtual element method* , Pre-print arXiv:1407.1909 [math.NA] (2014).

[99] H. Nilsen, J. Nordbotten and X. Raynaud *Comparison between cell-centered and nodal based discretization schemes for linear elasticity*, Pre-print arXiv:1064.08410 [math.NA] (2016).

[100] G. H. Paulino and A. L. Gain, *Bridging art and engineering using Escher-based virtual elements*, Struct. Multidiscip. Optim., **51(4)** (2015), pp. 867–883.

[101] I. Perugia, P. Pietra and A. Russo, *A plane wave virtual element method for the Helmholtz problem*, ESAIM Math. Model. Numer. Anal., **50(3)** (2016), pp. 783–808.

[102] J. Planchard and J.M. Thomas, *On the dynamic stability of cylinders placed in cross-flow*, J. Fluids Struct. **7** (1993), pp. 321–339.

[103] A. Rand, A. Gillette and C. Bajaj, *Quadratic serendipity finite elements on polygons using generalized barycentric coordinates*, Math. Comp **83** (2014), pp. 2691–2716.

[104] S. Rjasanow and S. Weißer, *Higher order BEM-based FEM on polygonal meshes*, SIAM J. Numer. Anal., **50(5)** (2012), pp. 2357–2378.

[105] R. Rodríguez and J. Solomin, *The order of convergence of eigenfrequencies in finite element approximations of fluid-structure interaction problems*, Math. Comp. **65** (1996), pp. 1463–1475.

[106] G. Savaré, *Regularity Results for Elliptic Equations in Lipschitz Domains*, J. Funct. Anal. **152** (1998), pp. 176–201.

[107] L. R. Scott and S. Zhang, *Finite element interpolation of nonsmooth functions satisfying boundary conditions*, Math. Comp. **54** (1990), pp. 483–493.

[108] E. M. Stein, *Singular integrals and differentiability properties of functions*, volume 2. Princeton University Press, 1970.

[109] N. Sukumar and A. Tabarraei, *Conforming polygonal finite elements*, Internat. J. Numer. Methods Engrg. **61** (2004), pp. 2045–2066.

[110] O. J. Sutton. *Virtual Element Method in 50 lines of MATLAB*, Pre-print arXiv:1604.06021 [math.NA] (2016).

[111] A. Tabarraei and N. Sukumar, *Extended finite element method on polygonal and quadtree meshes*, Comput. Methods Appl. Mech. Engrg. **197** (2007), pp. 425–438.

[112] C. Talischi, G. H. Paulino, A. Pereira and I. F. M. Menezes, *Polygonal finite elements for topology optimization: A unifying paradigm*, Internat. J. Numer. Methods Engrg., **82(6)** (2010), pp. 671–698.

[113] C. Talischi, G. H. Paulino, A. Pereira and I.F.M. Menezes, *PolyMesher: a general-purpose mesh generator for poygonal elements written in Matlab*, Struct. Multidisc. Optim. **45** (2012), pp. 309–328.

[114] G. Vacca. *Virtual Element Method for hyperbolic problems on polygonal meshes*, Pre-print arXiv:1602.05781 [math.NA] (2016).

[115] G. Vacca and L. Beirão da Veiga, *Virtual Element Method for parabolic problems on polygonal meshes*, Wiley Online Library (wileyonlinelibrary.com). DOI 10.1002/num.21982, (2015)

[116] R. Verfurth, *A review of a posteriori error estimate and adaptative mesh-refinement techniques*, Advanced Numerical Mathematics. Wiley-Teubner, (1996).

[117] E.B.B. Watson and D.V. Evans, *Resonance frequencies of a fluid in containers with internal bodies*, J. Eng. Math. **25** (1991), pp. 115–135.

[118] P. Wriggers, W. T. Rust and B. D. Reddy, *A virtual element method for contact*, Submitted for publication.

[119] H. Xie, *A type of multilevel method for the Steklov eigenvalue problem*, IMA J. Numer. Anal. **34** (2014), pp. 592–608.

[120] Y. Yang, Q. Li and S. Li, *Nonconforming finite element approximations of the Steklov eigenvalue problem*, Appl. Numer. Math. **59** (2009), pp. 2388–2401.

[121] O. C. Zienkiewicz and R. L. Taylor, *The Finite Element Method*, Vol. 2, McGraw-Hill, London (1991)